universität
wien

DISSERTATION

Titel der Dissertation

Einfluss der Koordination von Metallionen auf die
antiproliferative Aktivität von
α-N-heterozyklischen Thiosemicarbazonen

angestrebter akademischer Grad

Doktor der Naturwissenschaften (Dr. rer. nat.)

Verfasser:	Mag. Christian R. Kowol
Matrikel-Nummer:	0007567
Dissertationsgebiet (lt. Studienblatt):	Chemie (A 091 419)
Betreuer:	O. Univ.-Prof. DDr. Bernhard Keppler (Ao. Univ.-Prof. Dr. Vladimir Arion)

Wien, am 28. Mai 2009

Ph.D. Thesis

Effect of Metal Ion Complexation on the Antiproliferative Activity of α-N-Heterocyclic Thiosemicarbazones

Written by:

Christian R. Kowol

Vienna, May 2009

This Ph.D. thesis is based on the following papers and manuscripts, which are presented in the original format or as the submitted manuscripts:

Gallium(III) and Iron(III) Complexes of α-N-Heterocyclic Thiosemicarbazones: Synthesis, Characterization, Cytotoxicity, and Interaction with Ribonucleotide Reductase
Kowol, C. R.; Berger, R.; Eichinger, R.; Roller, A.; Jakupec, M. A.; Schmidt, P. P.; Arion, V. B.; Keppler, B. K.
J. Med. Chem. **2007**, *50*, 1254–1265.

Effect of Metal Ion Complexation and Chalcogen Donor Identity on the Antiproliferative Activity of 2-Acetylpyridine N,N-Dimethyl(chalcogen)semicarbazones
Kowol, C. R.; Eichinger, R.; Jakupec, M. A.; Galanski, M.; Arion, V. B.; Keppler, B. K.
J. Inorg. Biochem. **2007**, *101*, 1946–1957.

An Electrochemical Study of Antineoplastic Gallium, Iron and Ruthenium Complexes with Redox Noninnocent α-N-Heterocyclic Chalcogensemicarbazones
Kowol, C. R.; Reisner, E.; Chiorescu, I.; Arion, V. B.; Galanski, M.; Deubel, D. V.; Keppler, B. K.
Inorg. Chem. **2008**, *47*, 11032–11047.

Impact of Metal Coordination on Cytotoxicity of 3-Aminopyridine-2-carboxaldehyde Thiosemicarbazone (Triapine) and Novel Insights on Terminal Dimethylation
Kowol, C. R.; Trondl, R.; Heffeter, P.; Arion, V. B.; Jakupec, M. A.; Roller, A.; Galanski, M.; Berger, W.; Keppler, B. K.
J. Med. Chem., submitted.

Fluorescence Properties and Cellular Distribution of the Investigational Anti-cancer Drug Triapine (3-Aminopyridine-2-carboxaldehyde Thiosemicarbazone) and its Zinc(II) Complex
Kowol, C. R.; Trondl, R.; Arion, V. B.; Jakupec, M. A.; Lichtscheidl, I.; Keppler, B. K.
Angew. Chem. Int. Ed., submitted.

Acknowledgement

I would like to thank all persons who have supported me during this Ph.D. Thesis and in particular:

Abstract

The work presented in this Ph.D. thesis is focussed on the synthesis of novel metal complexes of α-N-heterocyclic thiosemicarbazones and the effect of metal complexation on the antiproliferative activity of this class of organic compounds. α-N-heterocyclic thiosemicarbazones are tridentate ligands with a NNS donor set and since several decades are known to possess antineoplastic properties. Currently the most promising drug candidate of this class of compounds is Triapine (3-aminopyridine-2-carboxaldehyde thiosemicarbazone, 3-AP), which entered several phase I and II clinical trials as an antitumor chemotherapeutic agent. α-N-heterocyclic thiosemicarbazones are potent inhibitors of the enzyme ribonucleotide reductase, which is a suitable and well established target in cancer chemotherapy, because of faster proliferation of tumor cells as compared to healthy cells and therefore higher expression of ribonucleotide reductase.

The influence of gallium(III) and iron(III) on the antiproliferative activity of the metal-free ligands was studied in this work by comparison of the cytotoxic activity of five different terminally dimethylated thiosemicarbazones and their metal complexes in two human cancer cell lines. The strategy behind the combination of gallium(III) and thiosemicarbazones is that both are directed to the same molecular target, each in its own way, namely the ribonucleotide reductase and therefore potentially provide a synergistic way of action. For selected compounds the inhibition potency towards purified ribonucleotide reductase was investigated. Subsequently the influence of changing the chalcogen donor atom from sulfur to oxygen or selenium in 2-acetylpyridine N,N-dimethyl(chalcogen)semicarbazone and their gallium(III) and ruthenium(III) complexes on cytotoxic activity was studied.

Cyclic voltammetry experiments of iron(III) and gallium(III) complexes showed that in addition to the metal-centred iron(III)/(II) redox couple several ligand-centred reductions take place. These reductions were studied in detail in organic solvents to locate the ligand-centred reduction site and the results are supported by quantum chemical studies.

In addition a novel straightforward synthetic procedure of Triapine was developed, permitting for the first time the isolation of metal complexes of this investigational anticancer drug. Furthermore it was discovered that Triapine possesses intrinsic fluorescence when light-irradiated at around $\lambda_{ex} = 360$ nm. This enabled for the first time to monitor the uptake and intra-cellular distribution of an α-N-heterocyclic thiosemicarbazone in living human cancer cells by fluorescence microscopy.

Zusammenfassung

Die vorliegende Dissertation beschäftigt sich mit der Synthese neuartiger Metallkomplexe mit α-N-heterozyklischen Thiosemicarbazonen als Liganden und dem Effekt der Komplexierung auf die antiproliferative Aktivität dieser Klasse von organischen Verbindungen. α-N-heterozyklische Thiosemicarbazone sind dreizähnige Liganden mit den Donoratomen NNS und seit mehreren Jahrzehnten ist bekannt, dass diese Verbindungen antineoplastische Aktivität aufweisen. Derzeit ist die vielversprechendste Verbindung dieser Klasse Triapine (3-Aminopyridin-2-carboxaldehyd Thiosemicarbazon, 3-AP), welches in mehreren Phase I und II klinischen Studien als Krebstherapeutikum untersucht wurde. α-N-heterozyklische Thiosemicarbazone sind als starke Inhibitoren des Enzyms Ribonukleotid Reduktase bekannt. Dieses Enzym ist ein geeignetes und viel erforschtes Target in der Krebstherapie, weil durch die schnellere Proliferation von Tumorzellen im Vergleich zu gesunden Zellen die Ribonukleotid Reduktase verstärkt exprimiert wird.

In dieser Dissertation wurde der Einfluss von Gallium(III) und Eisen(III) auf die antiproliferative Aktivität der freien Liganden durch Vergleich der Zytotoxizitäten von fünf verschiedenen terminal dimethylierten Thiosemicarbazonen und deren Komplexen in humanen Krebszelllinien untersucht. Die zugrundeliegende Idee hinter der Kombination von Gallium(III) und Thiosemicarbazonen ist die Tatsache, dass beide auf unterschiedliche Weise die Ribonukleotid Reduktase inhibieren und demzufolge potenziell synergistisch wirken. Für ausgewählte Verbindungen wurde die Inhibierungsstärke bezüglich isolierter Ribonukleotid Reduktase bestimmt. Anschließend wurde der Einfluss des Austausches von Schwefel gegen Sauerstoff und Selen in 2-Acetylpyridin N,N-Dimethyl(chalcogen)semicarbazon und deren Gallium(III) und Ruthenium(III) Komplexen auf die Zytotoxizität untersucht.

Untersuchungen von Eisen(III) und Gallium(III) Komplexen mittel zyklischer Voltammetrie zeigten neben der erwarteten metall-zentrierten Eisen(III)/(II) Redoxreaktion mehrere liganden-zentrierte Reduktionen. Diese wurden im Detail in organischen Lösungsmitteln untersucht und der Ort der Reduktion am Liganden bestimmt. Die Ergebnisse wurden von quantenchemischen Rechnungen untermauert.

Des Weiteren wurde in dieser Arbeit eine neue vereinfachte Synthese für Triapine entwickelt, was erstmalig die Isolierung von Metallkomplexen von Triapine ermöglichte. Zusätzlich wurde entdeckt, dass Triapine intrinsische Fluoreszenz besitzt wenn es bei $\lambda_{ex} = 360$ nm angeregt wird. Dies ermöglichte erstmals die Beobachtung der Aufnahme und der zellulären Verteilung eines α-N-heterozyklischen Thiosemicarbazons in lebenden humanen Krebszellen mittels Fluoreszenzmikroskopie.

Table of Contents

1 Introduction

1.1   Platinum based anti-cancer drugs – an overview

Cisplatin [*cis*-diamminedichloridoplatinum(II)] (Fig. 1) was first reported in 1844 by Michele Peyrone.[1] In 1969, more than one century later, the anticancer properties of cisplatin were accidentally discovered by Barnett Rosenberg[2,3] during his investigations on the influence of an electric field on the growth of *Escherichia coli* bacteria.[4]
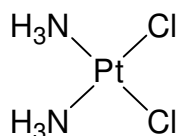
Figure 1. Structure of cisplatin.

Today cisplatin is one of the best selling anti-cancer drugs used in nearly 50% of all tumor chemotherapies and is one of few anticancer drugs with curative potential (cure rates of more than 90% in the case of testicular cancer).[5] The clinical success of cisplatin stimulated the search for novel even more effective drugs. To date thirty-eight platinum complexes from a few thousand prepared, entered phase I clinical trials and only two of them have received worldwide clinical approval so far. These are carboplatin[6] (*cis*-diammine-(1,1-cyclobutanedicarboxylato)platinum(II)) and oxaliplatin[7] ((*trans-R,R*-cyclohexan-1,2-diamine)oxalatoplatinum(II)) (Fig. 2). Carboplatin shows a tumor inhibiting profile which is very similar to that of cisplatin, but is less toxic than cisplatin and can therefore be administered at higher doses. Oxaliplatin displays tumor inhibiting properties different from those of cisplatin and carboplatin and is used in a combination therapy against metastatic colorectal cancer.[8]
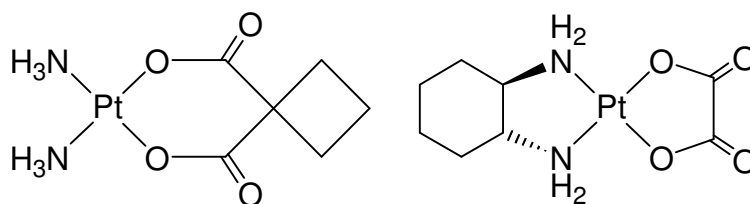
Figure 2. Structures of carboplatin (left) and oxaliplatin (right)

In addition to these complexes, other three platinum-based drugs have gained regionally limited approval: nedaplatin (Japan), lobaplatin (China) and heptaplatin (South Korea) (Fig. 3).
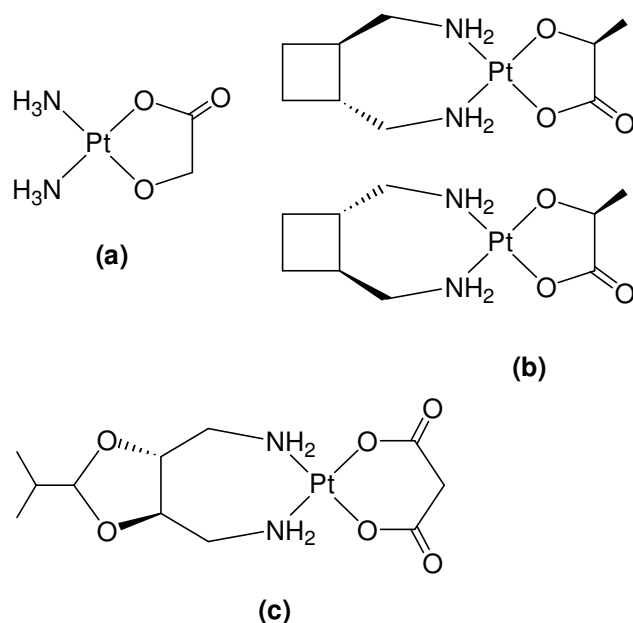
Figure 3. Platinum complexes with regionally limited approval: nedaplatin (a), lobaplatin (b) and heptaplatin (c).

Although cisplatin was approved for clinical use 30 years ago, the mode of action of cisplatin and analogous compounds is not fully understood. Nevertheless it is generally accepted that DNA is the critical target of cisplatin (and its analogues)[9] and that the active species is the aquated form of cisplatin cis-$[Pt(NH_3)_2Cl(OH_2)]^+$.[10] The electrophilic Pt(II) binds preferably to nitrogen atoms of the DNA bases, mainly the N7 of guanine. Initially, monofunctional DNA adducts are formed, but most of them react further to produce intrastrand cross-links of the type 1,2-d(GpG) and 1,2-d(ApG).[11] These adducts formed lead to serious conformational changes in the DNA, eventually resulting in programmed cell death (apoptosis). However, it should be mentioned that only about 1% of the intravenously administered cisplatin binds to DNA. So the main amount of cisplatin reacts with proteins and low molecular weight biomolecules, especially with those containing sulphur.[12]

The disadvantages of cisplatin and related compounds are: (a) they can only be used against a limited number of tumors, (b) they have severe side effects and (c) the development of drug resistance during treatment.

In summary cisplatin and closely related platinum antitumor agents show excellent activity in some tumors, but there is an increasing demand for novel anti-cancer drugs (Figure 4) which show reduced side effects, higher selectivity towards tumor cells, and a broader spectrum of responsive tumors, implying the ability to circumvent the problems of resistance to platinum compounds. This stimulated investigations in the field of non-platinum metal complexes with antitumor properties.
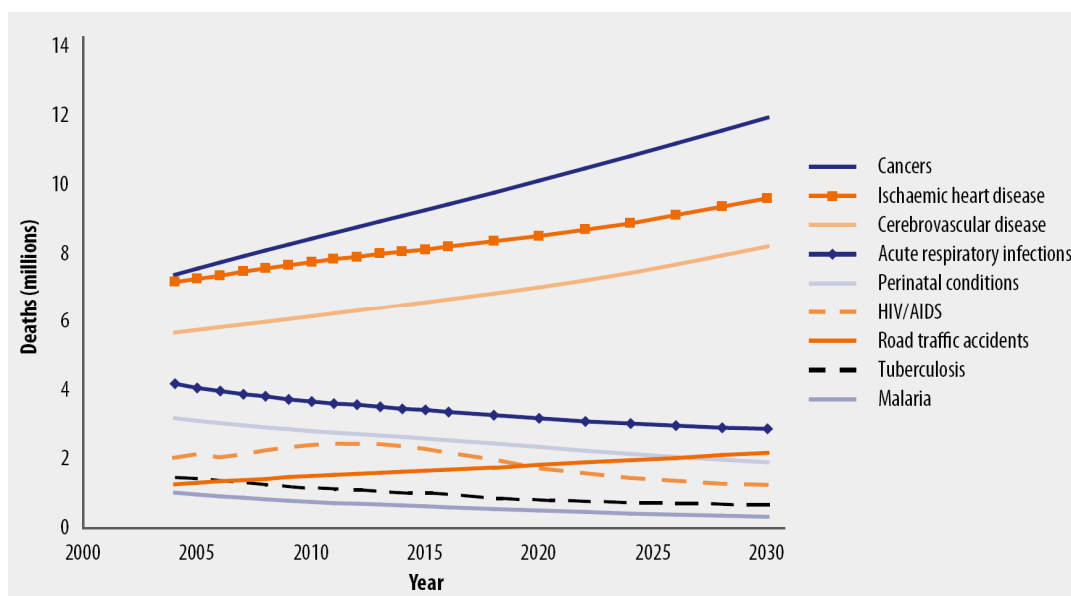
Figure 4. WHO prognosis (2004−2030) of the development of the main causes of death. The picture is taken from reference 13.

1.2   Non-platinum based anticancer drugs

Possible advantages of metal ions other than platinum(II) are (a) additional coordination sites, (b) changes in the oxidation state, (c) altered ligand affinity and substitution kinetics and accordingly a different mode of action.[14] The antitumor properties of a number of metal ions and complexes are under research, but only a few non-platinum metal based drugs are currently in clinical studies, the most promising of which are those containing ruthenium and gallium.[15]

1.2.1 Ruthenium

The two leading ruthenium compounds are $(H_2ind)[trans\text{-}RuCl_4(Hind)_2]$ (KP1019, Hind = indazole)[16], and $(H_2im)[trans\text{-}RuCl_4(Him)(DMSO)]$ (NAMI-A, Him = imidazole, DMSO = S-

bonded dimethyl sulfoxide)[17] which were the first ruthenium-based anticancer drugs in phase I clinical studies (Figure 5).
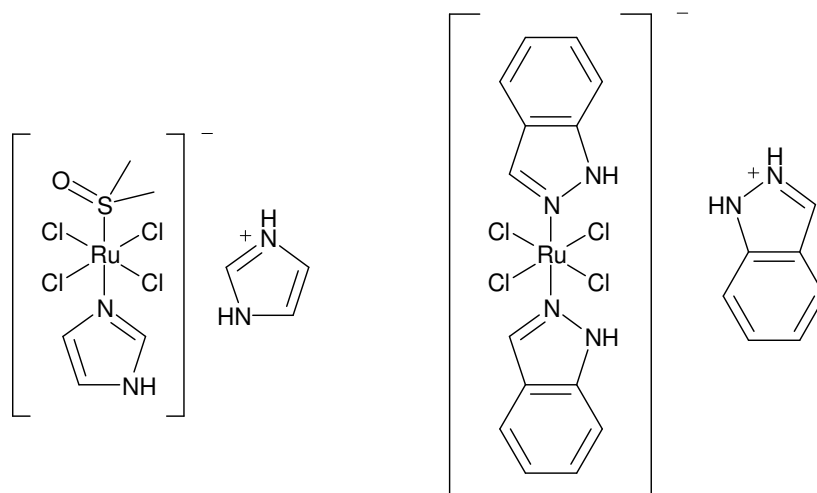
Figure 5. Ruthenium antitumor complexes: NAMI-A (left), KP1019 (right)

NAMI-A showed only efficacy against metastases in preclinical models,[18] whereas KP1019 exhibits excellent activity especially in an autochthonous colorectal tumor model that resembles human colon tumors in its histological appearance and behavior against chemotherapeutics.[19] A 70 to 90% average reduction of tumor growth or even complete remission was observed by using doses which do not lead to any signs of toxic side effects. Furthermore in this model KP1019 showed, higher tumor-inhibiting activity than the standard chemotherapeutic agent 5-fluoruracil. Remarkably cisplatin is completely inactive in this model which impressively shows the possible advantages of non-platinum based drugs in cancer chemotherapy.

1.2.2 Gallium[20]

Simple gallium salts, such as gallium(III) nitrate and gallium(III) chloride, have been studied for their applicability as antineoplastic drugs for more than 30 years, and the therapeutic potential of intravenous gallium nitrate has been extensively studied in clinical trials since 1976.[21] But the clinical experience has shown unfavourable pharmacokinetic and toxicological properties. Trials to improve the pharmacological effects by changing the mode of administration failed because of the low intestinal absorption.[22] Hence there were not sufficient reasons for the further development of gallium salts as anticancer drugs. (It has to be

mentioned that the "simple gallium salts" actually were administered as citrate containing solutions to prevent the precipitation of gallium as hydroxides. Citrate can coordinate to the gallium ion forming complexes of different stoichiometry, but it has been found that in the blood stream, gallium binds very fast to the stronger chelator transferrin[23] and model calculations suggest that less than 1% exists as citrate complex under equilibrium conditions.[24])
To circumvent the limitations arising when using "simple gallium salts", and to increase the intestinal absorption, gallium complexes with more lipophilic ligands, increased stability against hydrolysis and enhanced membrane penetration ability were prepared. Based on experience with a ferric maltol complex, which is known to provide iron in a soluble and readily absorbable form, an analogous gallium maltolate, *tris*(3-hydroxy-2-methyl-4H-pyran-4-onato)gallium(III) (Figure 6) has been developed.[25] This was the first gallium complex which entered clinical trials.
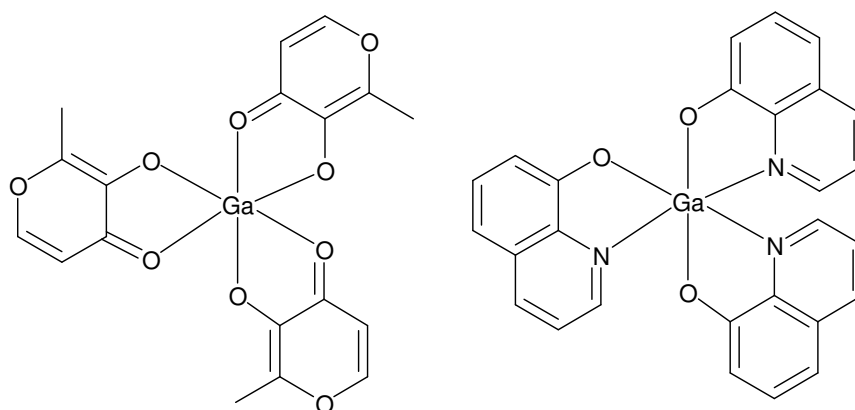
Figure 6. Structure of gallium maltolate (left) and KP46 (right)

A pharmacokinetic study in healthy humans has demonstrated high bioavailability and minor urinary excretion.[26] The mean maximum plasma gallium concentration obtained with a single administration of gallium maltolate was about five times higher than that from gallium chloride. Gallium maltolate was well tolerated in a phase I clinical trial, and the maximally tolerated dose was not reached.[27]
The second gallium complex that entered clinical phase I studies is *tris*(8-quinolinolato)gallium(III) (KP46) developed by Keppler et al.[28] (Figure 6). The complex shows improved bioavailability as compared to gallium chloride resulting in sufficient plasma concentrations in mice. The phase I clinical study included seven patients and the dose of KP46 was escalated from 30 mg/m^2/day up to 480 mg/m^2/day without dose-limiting toxicities.[29]

1.2.2.1 (Bio)chemical aspects of gallium[30]

The solution behavior and coordination chemistry of gallium(III) resemble that of iron(III). For example the electronegativity (Ga: 1.81; Fe: 1.83), the ionic radius for octahedral complexes (Ga: 0.620 Å; Fe: 0.645 Å) and tetrahedral complexes (Ga: 0.47 Å; Fe: 0.49 Å), as well as the electron affinity (Ga: 30.71 eV; Fe: 30.65 eV) are very similar. In contrast the electrochemical behavior of gallium(III) and iron(III) is totally different; iron(III) can be easily reduced and reoxidized under physiological conditions, whereas gallium(III) cannot change the oxidation state under similar conditions.

Because of the high charge-to-radius ratio gallium(III) is a hard Lewis acid and reacts therefore very readily with hard Lewis bases such as OH^-. In neutral aqueous solutions the hydrated Ga^{3+} ion hydrolyses nearly completely to highly insoluble, amorphous $Ga(OH)_3$, which slowly converts to nearly insoluble $GaO(OH)$, whereas at high pH values the soluble $[Ga(OH)_4]^-$ is formed. At pH 7.4 and 25 °C the total aqueous solubility of gallium is only around 1 μM and the dissolved gallium consists of 98.4% $[Ga(OH)_4]^-$ and 1.6% $Ga(OH)_3$. In comparison iron(III) is totally insoluble ($\sim 10^{-18}$ M) under these conditions and forms polymers of the form $[FeO(OH)]$. Thus gallium is slightly soluble in a physiological environment whereas iron is not and needs some proteins or chelates as a vehicle for its transport.

The biodistribution of gallium, especially the transport in blood and the cellular acquisition from blood, is markedly influenced by its similarities to iron. Studies showed that after administration of trace amounts of gallium nearly all is bound to the iron transport protein transferrin,[23] although in the blood there are thousands of other dissolved components. Gallium binds to both iron-binding sites of human serum apotransferrin (apotransferrin is the metal-free transferrin) with effective stability constants of $\log K_1 = 20.03$ and $\log K_2 = 19.3$ at a serum bicarbonate concentration of 27 mM and pH 7.4, in comparison to $\log K_1 = 22.8$ and $\log K_2 = 21.5$ for iron(III).[31] Thus gallium(III) has a lower affinity than iron(III) for binding to apotransferrin. However, iron normally occupies only around 30% of the apotransferrin binding sites, so there are enough unoccupied binding sites for gallium. The stability of the gallium/apotransferrin complex is pH dependent and it is lowered in acidic solution. Therefore gallium can be released in the tumor tissues, where the pH is more acidic than in normal tissues.[32]

After uptake of gallium into the cell by transferrin, it is able to bind to iron(III) dependent enzymes such as ribonucleotide reductase, where it is incorporated instead of iron and inhibits the function of the enzyme due to the inability to change the oxidation state, this is also the reason why gallium is not able to bind to iron(II) containing proteins like haemoglobin or cytochromes.

1.3   Ribonucleotide Reductase

The enzyme ribonucleotide reductase is responsible for the reduction of ribonucleotides to deoxyribonucleotides, which is the rate-limiting step in DNA synthesis, and it is the only way for the cell to synthesize deoxyribonucleotides. Thus ribonucleotide reductase is highly activated in proliferating tumor cells and therefore an excellent target for tumor chemotherapy.[33]

Ribonucleotide reductase consists of two non-identical dimeric subunits called R1 and R2. The R1 subunit harbours the substrate binding site, whereas R2 contains an iron center and a tyrosyl radical in both polypeptide chains. The radical in R2 is essential for the reduction of ribonucleotides, but it is located far away from the substrate binding site. The radical has to be transferred at least 35 Å, where it generates a thiyl radical of a cysteine residue which starts the substrate turnover cycle (Figure 7). In the first step the thiyl radical abstracts the 3´-hydrogen atom from ribose and thereby generates a substrate radical. Subsequently the 2´-OH group is protonated and leaves as a water molecule forming a 2´-ketyl radical (state 3). Then one hydrogen atom from a cysteine moves to the substrate radical and generates a disulfide radical anion, which is transferred to the substrate 3´-position (state 5). In the last step this substrate radical abstracts the hydrogen atom from the cysteine residue which started the turnover cycle and thereby regenerates the thiyl radical, which is transferred back to the R2 subunit to form the tyrosyl radical.[34] To complete the cycle the generated disulfide bridge has to be reduced, and the electron for this reduction is provided from thioredoxin or glutaredoxin, which itself is kept in the reduced state by the NADPH dependent protein thioredoxin reductase. A possible explanation for the radical transfer back from the cysteine to the R2 subunit is that the reduction of the disulfide bridge by thioredoxin or glutaredoxin would be disturbed.
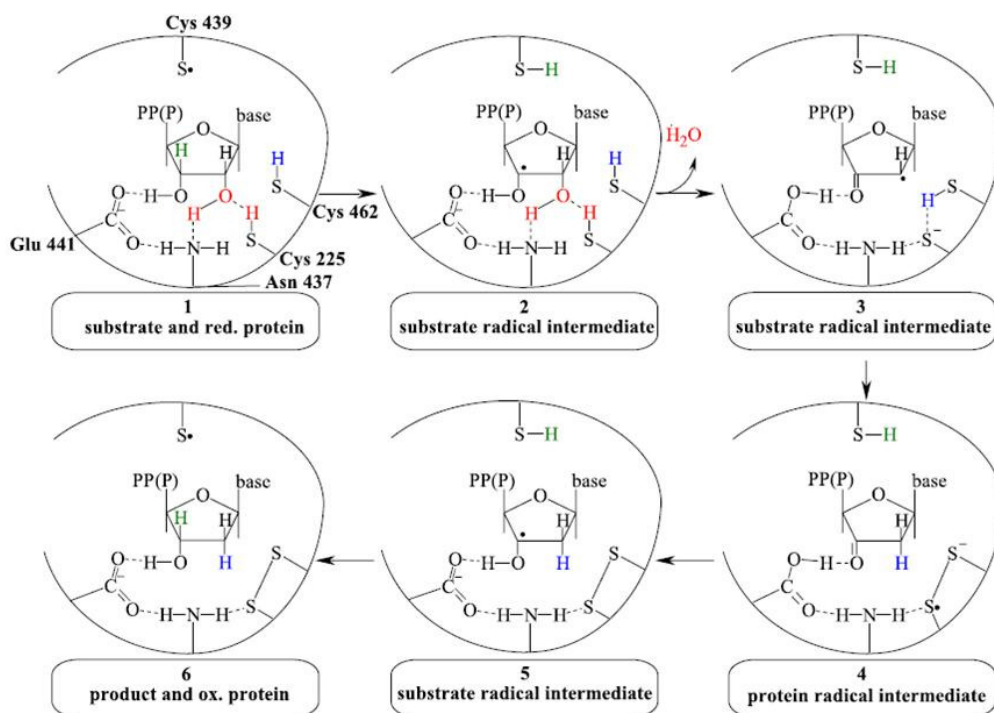
Figure 7. The postulated reaction mechanism for the reduction of a ribonucleotide (the involved amino acid residues are given with the *E. coli* numbering). The picture is taken from reference 34.

Inhibitors of ribonucleotide reductase can be divided into several classes depending on their mode of action:[35]

- Radical scavengers which directly destroy the tyrosyl radical. The most prominent representative of this class of compounds is hydroxyurea, which was the first ribonucleotide reductase inhibitor in clinical use.

- Chelating molecules such as pyridoxal isonicotinoyl hydrazone (PIH) or desferrioxamine (DFO) that remove iron or prevent the incorporation of iron into the metal binding site and thereby inhibit the formation of a stable tyrosyl radical.

- Nucleoside analogues such as gemcitabine and cytarabine are modified at the 2´-position of the sugar and are primarily intracellularly converted into the analogous nucleotides. In that form, they block the substrate binding site of ribonucleotide reductase and/or are incorporated into DNA, which causes a stop of DNA synthesis. These substances have received worldwide approval against various tumors, such as acute myeloid leukemia, non-small cell lung cancer and pancreatic cancer.

- Gallium salts and complexes which inhibit the activity of the R2 subunit by competing with iron for its binding site and hence destabilising the tyrosyl radical due to the inability to change the oxidation state.[36]
- α-*N*-Heterocyclic thiosemicarbazones, which are the strongest known inhibitors of ribonucleotide reductase (for more details see below).

1.4 α-N-Heterocyclic Thiosemicarbazones

The antineoplastic activity of thiosemicarbazones was discovered in 1956, with the observation that 2-formylpyridine thiosemicarbazone [Figure 8, (a)] showed antileukemic activity in mice.[37] In that study it was also reported that the analogous compounds 3-formylpyridine thiosemicarbazone (b) and 4-formylpyridine thiosemicarbazone (c) as well as thiosemicarbazones derived from 2-furandehyde, 2-thiophenaldehyde and 2-pyrrolaldehyde show no significant effect on the life span of the mice, (d). Further studies on thiosemicarbazones with different formyl heterocycles confirmed the assumption that all compounds with other donor set than *N,N,S* are inactive.[38] Hence the minimum requirement for biological activity is a heterocyclic nitrogen in α-position to the thiosemicarbazide side chain.
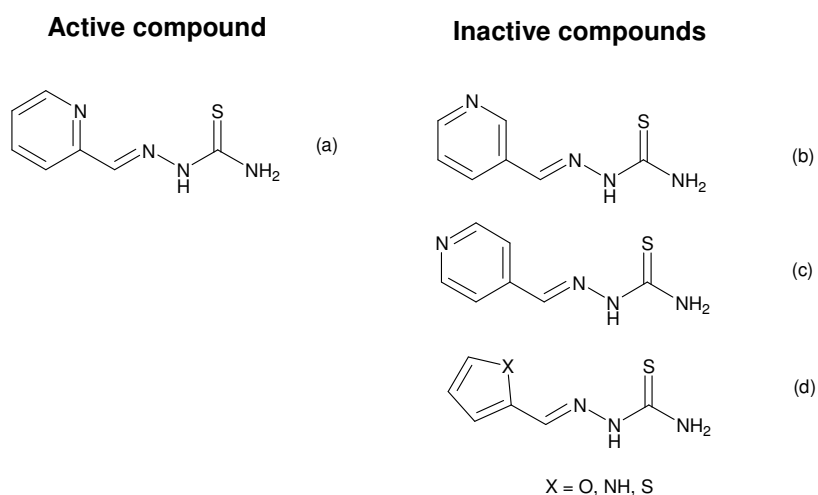
Figure 8. Structure of thiosemicarbazones which are active/inactive against L1210 leukemia in mice

Further structure-activity relationships of a series of 1-formylisoquinoline thiosemicarbazone derivatives [Figure 9, (A)] in mice bearing Sarcoma 180 ascites cells showed that replacement of the thiosemicarbazide side chain by semicarbazide (D), ^{2}N-methyl thiosemicarbazide (E),

11

S-methylisothiosemicarbazide (F) or 1-(picolinoyl) thiosemicarbazide (G) results in the loss of activity (Figure 8).[39] 1-acetylisoquinoline thiosemicarbazone (B) and 1-formylisoquinoline guanylhydrazone (C) are the most active derivatives, but with reduced tumor-inhibiting potency as compared to 1-formylisoquinoline thiosemicarbazone.

Active compounds **Inactive compounds**
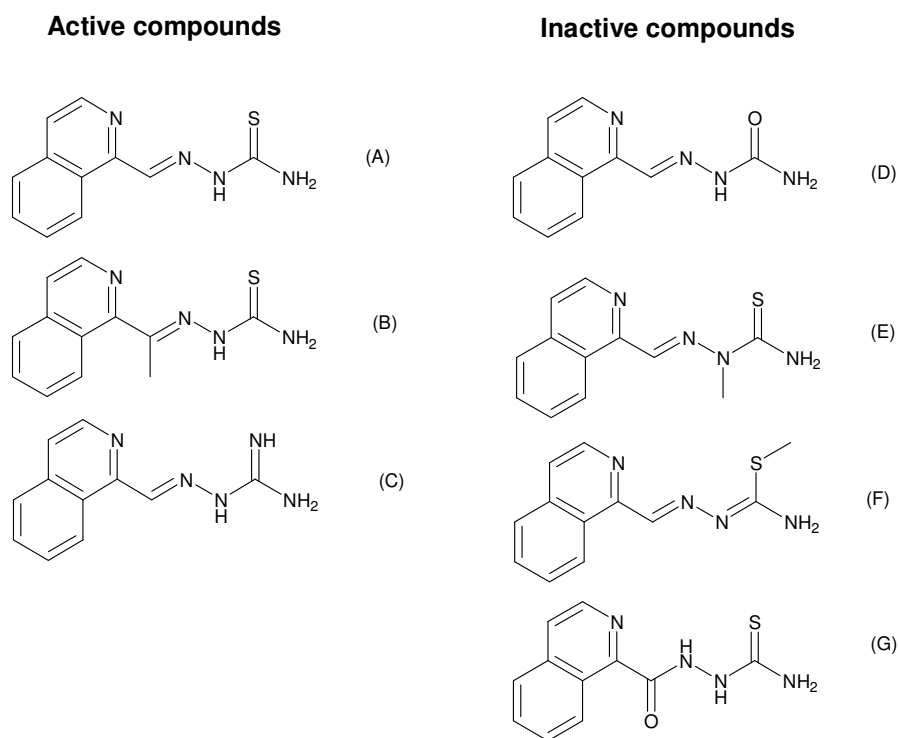
Figure 9. Effect of modifications in the side chain of 1-formylisoquinoline thiosemicarbazone on the tumor-inhibiting potency in mice bearing Sarcoma 180 ascites cells

These structure-activity studies led to the development of novel 2-formylpyridine and 1-isoquinoline thiosemicarbazones. Extensive studies by French et al.[40,41,42] showed that the most promising candidate is 5-hydroxy-2-formylpyridine thiosemicarbazone (Figure 10), which was further evaluated in clinical trials. However because of severe side effects and fast inactivation by glucoronidation it has been withdrawn.[43,44] To overcome these problems Sartorelli et. al. synthesized about 20 years later a panel of 4-methyl, 3-amino, 5-amino and 5-nitro substituted derivatives.[45,46] Compared to 5-hydroxy-2-formylpyridine thiosemicarbazone the amino substituted compounds showed higher activity in mice bearing L1210 leukemia, and 3-aminopyridine-2-carboxaldehyde thiosemicarbazone (Triapine, 3-AP) was selected for further evaluation in clinical trials (Figure 10).[46]
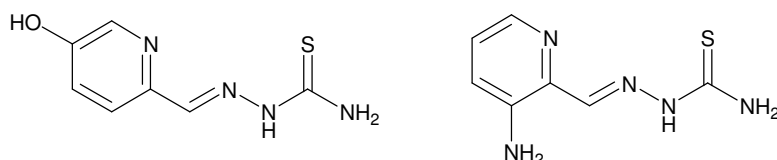
Figure 10. Structure of 5-HP (left) and Triapine (right)

The results of phase I and II clinical trials of Triapine as well as active or recruiting trials are summarized in Tables 1–3.

Table 1. Summary of the phase I clinical trials of Triapine.

Drug(s)	Patients/Cancer	Results	Ref.
Triapine	7 patients	1 patient with stable disease for 18 weeks.	47
Triapine	27 patients with advanced cancer	8 patients experienced stabilization of their disease for 2–4 months. No objective tumor responses were observed.	48
Triapine	24 patients with refractory leukemia	No objective responses occurred. Over 70% of the patients had a >50% reduction in white blood cell counts.	48
Triapine + Cisplatin	24 patients	No partial or complete responses were observed. 4 patients achieved stable disease for 2-6 treatment cycles.	49
Triapine	32 patients with advanced cancer	No partial or complete responses were observed.	48
Triapine + Gemcitabine	26 patients with progressive metastatic or locally advanced cancer	1 patient with complete response and 2 patients with partial responses. An additional patient had prolonged stabilization of a large liver metastasis.	48
Triapine	21 patients with advanced or metastatic cancer	No partial or complete responses were observed. 2 patients remained progression-free for 6 and >10 months, respectively. 4 other patients achieved stable disease for 3-4 months.	48
Triapine + Cytarabine	31 patients with refractory acute leukemia and high-risk myelodysplastic syndromes	4 patients achieved a complete response after the first cycle. No partial response.	48
Triapine + Irinotecan	10 patients with refractory tumors	1 patient achieved partial response.	50
Triapine + Doxorubicin	14 patients	No objective tumor responses were observed. 2 patients with stable disease.	51
Triapine	25 patients with advanced hematologic malignancies	No partial or complete responses were observed. 76% of patients had a >50% reduction in white blood cell counts.	52
Triapine + Fludarabine	33 patients with refractory acute leukemias and aggressive myeloproliferative disorders	2 patients achieved complete responses. 3 patients achieved partial responses.	53
Triapine + high dose Cytarabine	25 patients with relapsed or refractory myeloid leukemia	2 patients with complete responses. 1 patient with partial response.	54
Triapine + Cisplatin + Paclitaxel	Patients with advanced or metastatic cancer	Not reported	55

13

Table 2. Summary of the **phase II** clinical trials of Triapine.

Drug(s)	Patients/Cancer	Results	Ref.
Triapine	9 patients with metastatic breast cancer	3 patients achieved stable disease.	56
Triapine + Gemcitabine	60 patients with unresectable or metastatic pancreatic cancer	8 patients (15%) achieved partial responses, and 32 patients (60%) had stable disease. Median survival time was 8 months. 13% were alive after 1 year. Thus Triapine + Gemcitabine shows activity in pancreatic cancer.	57
Triapine + Gemcitabine	18 patients as 2nd line treatment of non-small cell lung cancer	No objective responses were observed. 5 patients had stable disease (till 135 days).	58
Triapine	19 patients with recurrent or metastatic renal cell carcinoma	1 patient achieved partial response over 4 months. Seven patients had stable disease (3.4–8.2 months). The study was stopped after the first stage.	59
Triapine + Gemcitabine	26 patients with advanced pancreatic carcinoma	No objective responses were observed. 11 patients had stable disease. 5 of them had stable disease for more than 6 months. The study was stopped after the first stage.	60
Triapine + Gemcitabine	12 patients with metastatic non-small cell lung cancer	No objective response was seen. 4 patients achieved stable disease. The study was stopped after the first stage.	61
Triapine	14 patients with advanced pancreatic cancer	There were no responses. 2 patients achieved stable disease.	62
Triapine + Cisplatin	Patients With Recurrent or Persistent Platinum-Resistant Ovarian Epithelial or Primary Peritoneal Cancer	Not reported	55

Table 3. Active or recruiting clinical phase I or II trials of Triapine[55]

Phase	Drug(s)	Cancer
Phase I	Triapine + (Cisplatin) + Radiation Therapy	External-beam radiation therapy with or without cisplatin in treating patients with gynecological cancer
Phase I	Triapine + Radiation Therapy	Radiation therapy in patients with stage III pancreatic cancer that cannot be removed by surgery
Phase II	Triapine + Cisplatin	Patients with recurrent or metastatic adenocarcinoma of the esophagus or gastroesophageal junction
Phase II	Triapine + Gemcitabine	Patients with unresectable or metastatic biliary duct or gallbladder cancer
Phase II	Triapine + Fludarabine	Patients with myeloproliferative disorders, chronic myelomonocytic leukemia, or accelerated phase or blastic phase chronic myelogenous leukemia

In conclusion, in six of seven phase II clinical trials containing Triapine only one patient with a renal cell carcinoma achieved partial response over 4 months.[59] The only clinical trial where Triapine in combination with Gemcitabine showed activity was a study in unresectable or metastatic pancreatic cancer.[57] From 60 patients which were treated 15% achieved partial response and 60% had stable disease. The median survival time was 8 months and after one

year 13% of the patients were still alive. In comparison, the standard therapy for pancreatic cancer is gemcitabine alone, approved in 1997 by the FDA (Food and Drug Administration) after a clinical trial[63] with a median survival time of 5.7 months and 18% survival rate after one year.

1.4.1 Iron Complexes of α-N-Heterocyclic Thiosemicarbazones and the Biochemical Mechanism of Action

As already mentioned in chapter 1.3, the principal target of α-*N*-heterocyclic thiosemicarbazones is the enzyme ribonucleotide reductase. In addition, the observation that the *N,N,S* donor set is essential for antitumor activity[38] of thiosemicarbazones led to the assumption that the activity originates from the capability of these compounds to form stable metal complexes. Thus the mechanism of the ribonucleotide reductase inhibition was primarily explained by simple chelation of the iron necessary for the activity of the R2 subunit. But this mechanism was ruled out by studies with 1-formylisoquinoline thiosemicarbazone, which demonstrated that the inhibition of the purified enzyme was not reversed by addition of iron and that the 50% inhibitory concentration was only about 0.1% of the standard iron concentration.[64] It was then assumed that the α-N-heterocyclic thiosemicarbazones directly bind to the iron in the R2 subunit of ribonucleotide reductase.[64] However, addition of a large excess of iron does not reverse the inhibitory capacity of 1-formylisoquinoline thiosemicarbazone.[65] Thus it was supposed that the active form of the inhibitor is the iron complex itself. This was confirmed by Thelander and Gräslund, who showed that the preformed iron(III) complex of 1-formylisoquinoline thiosemicarbazone in the presence of dithiothreitol is reduced to the iron(II) complex. The latter reacts with molecular oxygen, leading to the destruction of the tyrosyl radical (see below).[66] That iron is essential for effective ribonucleotide reductase inhibition was also reported for Triapine. The inhibition was found to be increased for both the iron(II) and iron(III) complex by a factor of 25 and 35, respectively as compared to metal free Triapine.[67] In addition metal-free Triapine had no significant effect on the EPR signal of the tyrosyl radical of the isolated ribonucleotide reductase R2 subunit, whereas the iron(II) complex very efficiently quenched the tyrosyl radical.[68] Furthermore spin trapping experiments showed that the iron(II) complex in contrast to Triapine alone or its iron(III) complex is able to produce reactive oxygen species (ROS) by

activation of molecular oxygen via a Fenton-like reaction, which are then quenching the tyrosyl radical.

$$Fe(II)–Triapine + O_2 \rightarrow Fe(III)–Triapine + O_2^{-}$$
$$Fe(II)–Triapine + O_2^{-} + 2H^{+} \rightarrow Fe(III)–Triapine + H_2O_2$$
$$Fe(II)–Triapine + H_2O_2 \rightarrow Fe(III)–Triapine + OH\cdot + OH^{-}$$
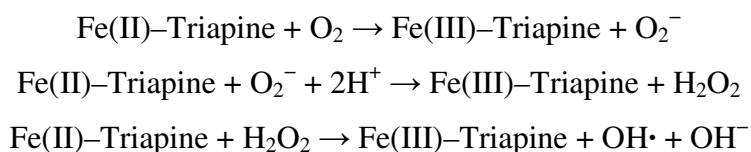
That the reactive oxygen species are associated with the antiproliferative activity in cells was shown by addition of the antioxidant catalase, resulting in a decrease of the IC_{50} value of Triapine by a factor of 10. The ROS can also explain the formation of DNA strand breaks observed with 5-hydroxy-2-formylpyridine thiosemicarbazone,[69] 1-formylisoquinoline thiosemicarbazones[70] and Triapine[71]. *In vivo* the ROS were linked with severe side effects such as methaemoglobinemia and hypoxia frequently observed in clinical phase I/II trials of Triapine.[52,54,59]

The mechanism of action described above is only valid for [4]N-unsubstituted α-N-heterocyclic thiosemicarbazones such as 5-hydroxy-2-formylpyridine thiosemicarbazones (5-HP) [Figure 11, (A)]. A study of various [4]*N*-disubstituted analogues of 5-HP [for example: Figure 11, (B, C)] showed that they have similar anticancer activity in mice, but a markedly decreased inhibitory activity on ribonucleotide reductase compared to 5-HP.[72]
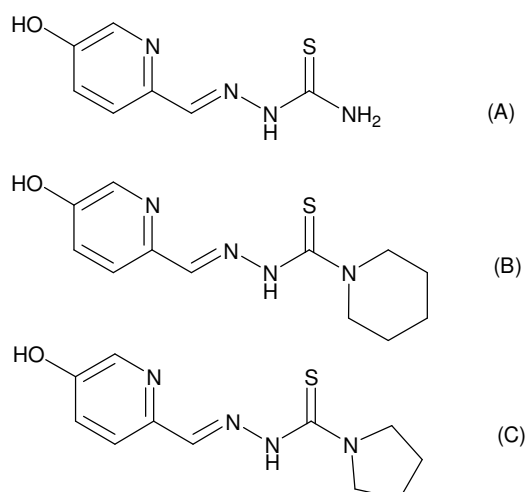

Figure 11. [4]N-disubstituted analogues of 5-HP (A)

Additionally the concentration required to inhibit 50% of the activity of alkaline phosphatase was 250 µM for 5-HP but 17 µM and 4 µM for the ^4N-disubstituted compounds B and C, respectively. Therefore it was suggested that ^{4}N-disubstituted α-N-heterocyclic thiosemicarbazones have additional modes of action.

(1)   Peyrone, M. *Anal. Chem. Pharm.* **1844** *LI,* 1–29.

(2)   Rosenberg, B.; VanCamp, L.; Trosko, J. E.; Mansour, V. N. *Nature* **1969**, *222*, 385–386.

(3)   Rosenberg, B. *Interdiscip. Sci. Rev.* **1978**, *3*, 134–147.

(4)   Rosenberg, B.; VanCamp, L.; Krigas, T. *Nature*, **1965**, *205*, 698–699.

(5)   Galanski, M.; Jakupec, M. J.; Keppler, B. K. *Current Med. Chem.* **2005**, *18*, 2075–2094.

(6)   O'Dwyer, P. J.; Stevenson, J. P.; Johnson, S. W. *Drugs* **2000**, *59*, 19–27.

(7)   Cvitkovic, E.; Bekradda, M. *Semin. Oncol.* **1999**, *26*, 647–662.

(8)   Graham, J.; Muhsin, M.; Kirkpatrick, P. *Nat. Rev. Drug. Discov.* **2004**, *3*, 11–12.

(9)   Jamieson, E. R.; Lippard S. J. *Chem. Rev.* **1999**, *99*, 2467–2498.

(10)   Appleton, T. G.; Hall, J. R.; Ralph, S. F.; Thompson, C. S. M. *Inorg. Chem.* **1989**, *28*, 1989–1993.

(11)   Fichtinger-Schepman, A. J.; Van der Veer, J. L.; Den Hartog, J. H. J.;Lohman, P. H. M.; Reedijk, J. *Biochemistry* **1985**, *24*, 707–713.

(12)   Reedijk, J. *Chem. Rev.* **1999**, *99*, 2499–2510.

(13)   The global burden of disease. 2004 Update. WHO (World health Organization) http://www.who.int/healthinfo/global_burden_disease/GBD_report_2004update_full.pdf

(14)   Clarke, M. J.; Zhu, F.; Frasca, D. R. *Chem. Rev.* **1999**, *99*, 2511–2533.

(15)   Jakupec, M. A.; Galanski, M.; Arion, V. B.; Hartinger, C. G.; Keppler, B. K. *Dalton Trans.* **2008**, *2*, 183–194.

(16)   Hartinger, C. G.; Zorbas-Seifried, S.; Jakupec, M. A.; Kynast, B.; Zorbas, H.; Keppler, B. K. *J. Inorg. Biochem.* **2006**, *100*, 891–904.

(17)   Geremia, S.; Alessio, E.; Todone, F. *Inorg. Chim. Acta* **1996**, *253*, 87–90.

(18)   Alessio, E.; Mestroni, G.; Bergamo, A.; Sava, G. *Curr. Top. Med. Chem.* **2004**, *4*, 1525–1535.

(19)   Berger, M. R.; Garzon, F. T.; Keppler, B. K.; Schmähl, D. *Anticancer Res.* **1989**, *9*, 761–766.

(20)   Jakupec, M. A.; Keppler B. K. *Metal Ions in Biological Systems* **2004,** *42*, 425–462.

(21)   Chitambar, C. R. *Curr. Opin. Oncol.* **2004**, *16*, 547–552

(22)   Collery, P.; Millart, H.; Kleisbauer, J. P.; Paillotin, D.; Robinet, G.; Durand, A.; Claeyssens, S.; Legendre, J. M.; Leroy, A.; Rousseau, A. *Anticancer Res.* **1994**, *14*, 2299–2306.

(23)   Vallabhajosula, S. R.; Harwig, J. K.; Siemens, J. K.; Wolf, W. *J. Nucl. Med* **1980**, *21*, 650–656.

(24)   Jackson, G. E.; Byrne, M. J. *J. Nucl. Med.* **1996**, *37*, 379–386.

(25) Finnegan, M.M.; Lutz, T.G.; Nelson, W.O.; Smith, A.; Orvig, C. *Inorg. Chem.* **1987**, *26*, 2171–2176.

(26) Bernstein, L. R.; Tanner, T.; Godfrey, C.; Noll, B. *Met.-Based Drugs* **2000,** *7*, 33–47.

(27) Lum, B. L.; Srinivas, S.; Beck, J. T.; Vesole, D.; Largey, M.; Valone, F. H.; Sayre, P. H. *Proc. Am. Soc. Clin. Oncol.* **2003**, *22*, abstract 943.

(28) Collery, P.; Domingo, J. L.; Keppler, B. K. *Anticancer Res.* **1996**, *16*, 687–691.

(29) Collery, P.; Jakupec, M. A.; Kynast, B.; Keppler, B. K. *Metal Ions in Biology and Medicine* **2006**, *9*, 521–524.

(30) Bernstein, L. R. *Pharmacological Reviews* **1998**, *50*, 665–682.

(31) Harris, W. R.; Pecoraro, V. L. *Biochemistry* **1983**, 22, 292–299.

(32) Gerweck, L. E. *Seminars in Radiation Oncology* **1998**, 8, 176–182.

(33) Cerqueira, N. M.; Pereira, S.; Fernandes, P. A.; Ramos, M. J. *Curr. Med, Chem.* **2005**, *12*, 1283–1294.

(34) Kolberg, M.; Strand, K. R.; Graff, P.; Andersson, K. K. *Biochim. Biophys. Acta* **2004**, *1699*, 1–34.

(35) Shao, J.; Zhou, B.; Chu, B.; Yen, Y. C*urr. Cancer Drug Targets* **2006**, *6*, 409–431.

(36) Chitambar, C. R.; Matthaeus, W. G.; Antholine, W. E.; Graff, K.; O'Brien, W. J. *Blood* **1988**, *72*, 1930.

(37) Brockman, R. W.; Thomson, J. R.; Bell, M. J.; Skipper, H. E. *Cancer Res*. **1956**, *16*, 167–170.

(38) French, F. A.; Blanz, E. J., Jr. *J. Med. Chem*. **1966**, *9*, 585–589.

(39) Agrawal, K. C.; Sartorelli, A. C. *J. Med. Chem.* **1969**, *12*, 771–774.

(40) French, F. A.; Blanz, E. J., Jr.; DoAmaral, J. R.; French, D. A. *J. Med. Chem.* **1970**, *13*, 1124–1130.

(41) French, F. A.; Blanz, E. J., Jr.; DoAmaral, J. R.; French, D. A. *J. Med. Chem.* **1970**, *13*, 1117–1124.

(42) French, F. A.; Blanz, E. J., Jr.; Shaddix, S. C.; Brockman, R. W. *J. Med. Chem.* **1974**, *17*, 172–181.

(43) DeConti, R. C.; Toftness, B. R.; Agrawal, K. C.; Tomchick, R.; Mead, J. A. R.; Bertino, J. R.; Sartorelli, A. C.; Creasey, W. A. *Cancer Res*. **1972**, *32*, 1455–1462.

(44) Krakoff, I. H.; Etcubanas, E.; Tan, C.; Mayer, K.; Bethune, V.; Burchenal, J. H. *Cancer Chemother. Rep*. **1974**, *58*, 207–212.

(45) Wang, Y.; Liu, M. C.; Lin, T. S.; Sartorelli, A. C. *J. Med. Chem.* **1992**, *35*, 3667–3671.

(46) Liu, M. C.; Lin, T. C.; Sartorelli, A. C. *J. Med. Chem.* **1992**, *35*, 3672–3677.

(47)   Makower, D.; Sznol, M.; Fehn, K.; MacDonald, S.; Mao, J.; Wadler, S. *Proc. Am. Soc. Clin. Oncol.* **2001**, *20* (abstr**.** 376).

(48)   Yu, Y.; Wong, J.; Lovejoy, D. B.; Kalinowski, D. S.; Richardson, D. R. *Clin. Cancer Res.* **2006**, *12*, 6876–6883.

(49)   Murren, J. R.; Modiano, M.; Plezia, P.; Doyon, A.; Bagulho, T.; Johnson, B.; Sznol, M. *Proc. Am. Soc. Clin. Oncol.* **2003**, *22* (abstr. 643).

(50)   Schelman, W. R.; Holen, K.; Mulkerin, D.; Kolesar, J.; Thomas, J.; Kruse, M.; Oliver, K.; Marnocha, R.; Eickhoff, J.; Wilding, G. *J. Clin. Oncol.* **2006** (ASCO Annual Meeting Proceedings), *24*, 12011.

(51)   Chang, J. E.; Morgan Meadows, S.; Traynor, A.; Kolesar, J.; Marnocha, R.; Lee, F.; Eickoff, J.; Beth, E.; Binger, K.; Wilding, G. *J. Clin. Oncol.* **2006** (ASCO Annual Meeting Proceedings), *24*, 13168.

(52)   Gojo, I.; Tidwell, M. L.; Greer, J.; Takebe, N.; Seiter, K.; Pochron, M. F.; Johnson, B.; Sznol, M.; Karp, J. E. *Leuk. Res.* **2007**, *31*, 1165–1173.

(53)   Karp, J. E.; Giles, F. J.; Gojo, I.; Morris, L.; Greer, J.; Johnson, B.; Thein, M.; Sznol, M.; Low, J. *Leuk. Res.* **2008**, *32*, 71–77.

(54)   Odenike, O. M; Larson, R. A; Gajria, D.; Dolan, M. E.; Delaney, S. M.; Karrison, T. G.; Ratain, M. J.; Stock, W. *Invest. New Drugs* **2008**, *26*, 233–239.

(55)   www.clinicaltrials.gov

(56)   Atieh, D. M.; Modiano, M.; Shriberg, L.; Brafman, L.; Sznol, M.; Vahdat, L. *J. Clin. Oncol.* **2004** (ASCO Annual Meeting Proceedings), *22*, 864.

(57)   Greeno, E.; Kindler, H. L.; Peeters, M.; Trowbridge, R.; Chong, G.; Valle, J. W.; Johnson, E. L.; Allain, E. L.; Burris, H. A. *J. Clin. Oncol.* **2006** (ASCO Annual Meeting Proceedings), *24*, 4123.

(58)   Traynor, A. M.; Levy, D. E.; Bayer, G. K.; Tate, J. M.; Thomas, S. P.; Mazurczak, M. A.; Graham, D. L.; Kolesar, J. M.; Schiller, J. H. *J. Clin. Oncol.* **2006** (ASCO Annual Meeting Proceedings), *24*, 17151.

(59)   Knox, J. J.; Hotte, S. J.; Kollmannsberger, C.; Winquist, E.; Fisher, B.; Eisenhauer, E. A. *Invest. New Drugs* **2007**, *25*, 471–477.

(60)   Mackenzie, M. J.; Saltman, D.; Hirte, H.; Low, J.; Johnson, C.; Pond, G.; Moore, M. J. *Invest. New Drugs* **2007**, *25*, 553–558.

(61)   Ma, B.; Goh, B. C.; Tan, E. H.; Lam, K. C.; Soo, R.; Leong, S. S.; Wang, L. Z.; Mo, F.; Chan, A. T. C.; Zee, B.; Mok, T. *Invest. New Drugs* **2008**, *26*, 169–173.

(62)   Attia, S.; Kolesar, J.; Mahoney, M. R.; Pitot, H. C.; Laheru, D.; Heun, J.; Huang, W.; Eickhoff, J.; Erlichman, C.; Holen, K. D. *Invest. New Drugs* **2008**, *26*, 369–379.

(63)   Burris, H. A., III; Moore, M. J.; Andersen, J.; Green, M. R.; Rothenberg, M. L.; Modiano, M. R.; Cripps, M. C.; Portenoy, R. K.; Storniolo, A. M.; Tarassoff, P.; Nelson, R.; Dorr, F. A.; Stephens, C. D.; Von Hoff, D. D. *J. Clin. Oncol.* **1997**, *15*, 2403–2413.

(64)   Moore, E. C.; Zedeck, M. S.; Agrawal, K. C.; Sartorelli, A. C. *Biochemistry* **1970**, 9, 4492–4498.

(65) Sartorelli, A. C.; Agrawal, K. C.; Tsiftsoglou, A. S.; Moore, E. C. *Adv. Enzyme Regul.* **1977**, *15*, 117–139.

(66) Thelander, L.; Gräslund, A. *J. Biol. Chem.* **1983**, *258*, 4063–4066.

(67) Finch, R. A.; Liu, M. C.; Cory, A. H.; Cory, J. G.; Sartorelli, A. C. *Adv. Enzyme Regul.* **1999**, *39*, 3–12.

(68) Shao, J.; Zhou, B.; Di Bilio, A. J.; Zhu, L.; Wang, T.; Qi, C.; Shih, J.; Yen, Y. *Mol. Cancer Ther.* **2006**, *5*, 586–592.

(69) Karon, M.; Benedict, W. F. *Science* **1972**, *178*, 62.

(70) Tsiftsoglou, A. S.; Hwang, K. M.; Agrawal, K. C.; Sartorelli, A. C. *Biochem. Pharmacol.* **1975**, *24*, 1631–1633.

(71) Chaston, T. B.; Lovejoy, D. B.; Watts, R. N.; Richardson, D. R. *Clin. Cancer Res.* **2003**, *9*, 402–414

(72) Agrawal, K. C.; Lee, M. H.; Booth, B. A.; Moore, E. C.; Sartorelli, A. C. *J. Med. Chem.* **1974**, *17*, 934–938.

2 Results

This Ph.D. thesis is based on the following papers and manuscripts, which are presented in the original format or as the submitted manuscripts:

Gallium(III) and Iron(III) Complexes of α-N-Heterocyclic Thiosemicarbazones: Synthesis, Characterization, Cytotoxicity, and Interaction with Ribonucleotide Reductase

Kowol, C. R.; Berger, R.; Eichinger, R.; Roller, A.; Jakupec, M. A.; Schmidt, P. P.; Arion, V. B.; Keppler, B. K.

J. Med. Chem. **2007**, *50*, 1254–1265.

Effect of Metal Ion Complexation and Chalcogen Donor Identity on the Antiproliferative Activity of 2-Acetylpyridine N,N-Dimethyl(chalcogen)semicarbazones

Kowol, C. R.; Eichinger, R.; Jakupec, M. A.; Galanski, M.; Arion, V. B.; Keppler, B. K.

J. Inorg. Biochem. **2007**, *101*, 1946–1957.

An Electrochemical Study of Antineoplastic Gallium, Iron and Ruthenium Complexes with Redox Noninnocent α-N-Heterocyclic Chalcogensemicarbazones

Kowol, C. R.; Reisner, E.; Chiorescu, I.; Arion, V. B.; Galanski, M.; Deubel, D. V.; Keppler, B. K.

Inorg. Chem. **2008**, *47*, 11032–11047.

Impact of Metal Coordination on Cytotoxicity of 3-Aminopyridine-2-carboxaldehyde Thiosemicarbazone (Triapine) and Novel Insights on Terminal Dimethylation

Kowol, C. R.; Trondl, R.; Heffeter, P.; Arion, V. B.; Jakupec, M. A.; Roller, A.; Galanski, M.; Berger, W.; Keppler, B. K.

J. Med. Chem., submitted.

Fluorescence Properties and Cellular Distribution of the Investigational Anti-cancer drug Triapine (3-Aminopyridine-2-carboxaldehyde Thiosemicarbazone) and its Zinc(II) Complex

Kowol, C. R.; Trondl, R.; Arion, V. B.; Jakupec, M. A.; Lichtscheidl, I.; Keppler, B. K.

Angew. Chem. Int. Ed., submitted.

2.1 Novel Gallium(III) and Iron(III) Complexes of α-N-Heterocyclic Thiosemicarbazones: Synthesis, Characterization, Cytotoxcicity and Interaction with Ribonucleotide Reductase[*]

Kowol, C. R.; Berger, R.; Eichinger, R.; Roller, A.; Jakupec, M. A.; Schmidt, P. P.; Arion, V. B.; Keppler, B. K.

---

[*] Parts of this publication were already presented as a manuscript in my diploma thesis

Gallium(III) and Iron(III) Complexes of α-N-Heterocyclic Thiosemicarbazones: Synthesis, Characterization, Cytotoxicity, and Interaction with Ribonucleotide Reductase

Christian R. Kowol,[†] Roland Berger,[†] Rene Eichinger,[†] Alexander Roller,[†] Michael A. Jakupec,[†] Peter P. Schmidt,[#] Vladimir B. Arion,*,[†] and Bernhard K. Keppler*,[†]

Institute of Inorganic Chemistry, Faculty of Chemistry, University of Vienna, Waehringer Strasse 42, A-1090 Vienna, Austria, and Max-Planck Institute for Bioinorganic Chemistry, Stiftstrasse 34-38, Mülheim an der Ruhr, D-45470 Germany

A series of gallium(III) and iron(III) complexes with five different [4]N-substituted α-N-heterocyclic thiosemicarbazones, viz., 2-acetylpyridine *N,N*-dimethylthiosemicarbazone (**1**), 2-acetylpyridine *N*-pyrrolidinylthiosemicarbazone (**2**), acetylpyrazine *N,N*-dimethylthiosemicarbazone (**3**), acetylpyrazine *N*-pyrrolidinylthiosemicarbazone (**4**), and acetylpyrazine *N*-piperidinylthiosemicarbazone (**5**), with the general formula [GaLCl$_2$] (HL = **1** and **2**) and [ML$_2$][Y] (M = Ga, HL = **1**−**5**, Y = PF$_6$; M = Fe, HL = **1**−**5**, Y = FeCl$_4$ and PF$_6$) were synthesized and characterized by elemental analysis, a number of spectroscopic methods (NMR, IR, UV−vis), mass spectrometry, and X-ray crystallography. The *in vitro* antitumor potency was studied in two human cancer cell lines (41M and SK-BR-3). The central metal ions exert pronounced effects in a divergent manner: gallium(III) enhances, whereas iron(III) weakens the cytotoxicity of the ligands. The capacity of ligand **1** and its Ga(III) and Fe(III) complexes to destroy the tyrosyl radical of the presumed target ribonucleotide reductase is reported.

Introduction

α-N-Heterocyclic thiosemicarbazones have been explored for their applicability as antitumor agents for half a century.[1] Their pharmacological potential has been recognized to include also antiviral, antimycobacterial, antifungal, and antimalarial properties,[2] and the enzyme ribonucleotide reductase has been identified as the principal target.[3−6] In fact, they are the strongest known inhibitors of this enzyme, both in cell-free assays and in intact tumor cells, being several orders of magnitude more effective than hydroxyurea, the first clinically applied ribonucleotide reductase inhibitor.[7,8] The enzyme that catalyzes the conversion of ribonucleotides to deoxyribonucleotides is produced at the transition from the G$_1$ to the S phase of the cell cycle as a prerequisite for DNA replication and is highly expressed in tumor cells, making it a suitable and well-established target for cancer chemotherapy. Mammalian (class Ia) ribonucleotide reductase is composed of an α$_2$ homodimer (R1 subunit) that contains the catalytically active center consisting of redox-active cysteines that are regenerated by the action of thioredoxin and a β$_2$ homodimer (R2 subunit) containing a tyrosyl radical and a diiron center which are essential for initiation of the nucleotide reduction process at the active site in R1.[9] Inhibitors of this enzyme are classified by their mode of interference with the enzyme's functions: (i) radical scavengers (e.g., hydroxyurea) that destroy the tyrosyl radical directly; (ii) chelating molecules (e.g., desferrioxamine) that remove iron from or prevent incorporation of iron into the metal binding site thereby quenching the tyrosyl radical indirectly or inhibiting its formation, and (iii) nucleotide and nucleoside analogues (e.g., gemcitabine, cladribine, fludarabine, cytarabine) that interfere with substrate binding.

The ribonucleotide reductase-inhibiting activity of α-N-heterocyclic thiosemicarbazones has primarily been explained by their iron-chelating properties, either by coordination of iron from the R2 subunit or by preformation of an iron chelate which then inhibits the enzyme, implying that iron complexes might actually be the active species. The observation that the preformed iron chelates are more potent inhibitors of ribonucleotide reductase in the absence of additional iron than the uncomplexed thiosemicarbazones supports the latter hypothesis, but any interaction restricted to the iron site of the enzyme is unable to explain the partially protective effects observed with thioredoxin and small dithiol compounds.[6,10,11] It was then proposed that preformed iron(III) chelates are readily reduced in blood or in the presence of thiols to the ferrous form[11−13] which is able to destroy the tyrosyl radical of the enzyme by a one-electron reduction in an oxygen-requiring reaction.[14] The assumption that the activity of α-N-heterocyclic thiosemicarbazones is not solely based on their iron-chelating properties has recently found support in the observation that 3-aminopyridine-2-carboxaldehyde-thiosemicarbazone (3-AP, triapine) induces iron-dependent free radical damage, thereby behaving distinctly different from classic iron-chelating drugs such as desferrioxamine.[15]

Apart from the well-established inhibition of ribonucleotide reductase, additional targets and modes of action have also been discussed. In particular, radical reactions similar to those induced by bleomycin may explain the formation of DNA strand breaks observed with 5-hydroxy-2-formylpyridine-thiosemicarbazone (5-HP)[16] and 1-formylisoquinoline-thiosemicarbazone,[17] suggesting the induction of direct DNA damage that might be reinforced by the inhibitory effects on ribonucleotide reductase.[7] Besides, inhibition of topoisomerase II by a mechanism distinctly different from that of etoposide has been suggested for a variety of [4]N-substituted thiosemicarbazones and, in particular, their copper(II) complexes.[18−20]

The major problem encountered in the development of α-N-heterocyclic thiosemicarbazones is the high general toxicity and, consequently, the low therapeutic index of many representatives of this class of compounds. Apart from its rapid inactivation by glucoronidation, 5-hydroxy-2-formylpyridine-thiosemicar-

* To whom correspondence should be addressed. Phone: +431427752600. Fax: +431427752680. E-mail: vladimir.arion@univie.ac.at; bernhard.keppler@univie.ac.at.
† University of Vienna.
# Max-Planck Institute for Bioinorganic Chemistry.

bazone, the first clinically evaluated representative, had been withdrawn because of severe hematological and gastrointestinal side effects.[21,22] More recently, however, triapine has entered the clinical stage of development.[23–26] This compound shows therapeutic activity over a certain range of dosages in preclinical tumor models without imposing intolerable host toxicity[27] and has led to a renewed interest in this class of compounds.

The rationale for preparing gallium(III) complexes of α-N-heterocyclic thiosemicarbazones is based on the fact that gallium(III) also inhibits the activity of ribonucleotide reductase[28] and is endowed with clinically useful antiproliferative properties.[29–31] Due to similarity in ligand binding affinity with iron(III), gallium(III) affects intracellular iron availability, but also interacts directly with ribonucleotide reductase, by competing with iron for its binding site in the R2 subunit of the enzyme.[32,33] Combining a central metal and a ligand that are directed at the same molecular target in different ways is being pursued as a strategy to produce highly potent ribonucleotide reductase inhibitors expected to benefit from a synergistic action of the two components.

A prototypic, highly cytotoxic gallium complex with 2-acetylpyridine *N,N*-dimethylthiosemicarbazone has been reported recently.[34] The concentration–effect curves of this complex closely parallel those of the uncomplexed thiosemicarbazone, indicating that the cytotoxic properties of the complex are largely governed by the ligand. However, an increase in cytotoxic potency gained by complexation with gallium has been observed. This seemed to be explainable by the metal-to-ligand stoichiometry of 1:2, raising the question whether gallium(III) specifically contributes to the biological activity or whether similar effects might be achieved by complexation to iron. Furthermore, structural rearrangements in solution have been recognized in the case of this complex, resulting in a mixture of species with 1:2 and 1:1 metal-to-ligand stoichiometry, complicating the interpretation of the biological results obtained with this compound.

The aim of the present study was the synthesis of a series of related α-N-heterocyclic thiosemicarbazone complexes allowing the exploration of structure–activity relationships with regard to the role of the central metal (gallium vs iron), the metal-to-ligand stoichiometry, and the impact of structural modifications of the thiosemicarbazone ligand.

Results and Discussion

Syntheses. Complex **6** (Figure 1) with metal-to-ligand stoichiometry 1:1 ([GaLCl$_2$]) has been obtained from **1** and GaCl$_3$ in a 2:1 molar ratio in boiling dry ethanol in 68% yield, whereas the synthesis of **7** has been performed starting from **2** and GaCl$_3$ in 1:2 molar ratio with 82% yield. The formation of **6** and **7** has been corroborated by elemental analyses and electron impact (EI) mass spectra. The latter showed the presence of intense molecular ion peaks at *m/z* 360 with relative intensity (r.i.) 53.7% for **6** and 386 (r.i. 98.4%) for **7**. Other signals observed (see Supporting Information) could easily be related to structural fragments emerging from molecular ions M$^+$. It should also be noted that electrospray ionization (ESI) did not provide ions that could be related to the structures of **6** and **7**. Starting from Ga(NO$_3$)$_3$ and the corresponding ligands **1–5** in 1:2 molar ratio in ethanol by subsequent addition of NH$_4$PF$_6$, complexes [GaL$_2$]$^+$ (**8–12**) have been isolated as hexafluorophosphates in 56–91% yield. Complexes **13–15** have been produced by reacting FeCl$_3$ with the corresponding ligand in 1:1 molar ratio in boiling dry ethanol, and complexes **16** and **17** in 3:2 molar ratio, respectively. The reaction of Fe(NO$_3$)$_3$·
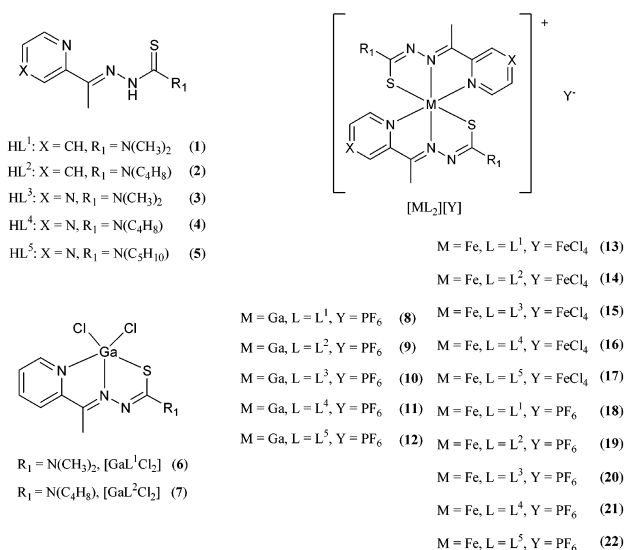

Figure 1. The library of thiosemicarbazones and their metal complexes.

9H$_2$O with the ligands **1–5** in 1:2 molar ratio, followed by addition of an excess of hexafluorophosphate, produced complexes **18–22** in 72–92% yield. The positive ion ESI mass spectra of **8–12** and **13–22** showed strong peaks (see Supporting Information) due to [GaL$_2$]$^+$ (L = L^1–L^5) and [FeL$_2$]$^+$ (L = L^1–L^5), correspondingly. The presence of counterions PF$_6^-$ or [FeCl$_4$]$^-$ has been proved by ESI mass spectra recorded in the negative ion mode. The electronic spectra of both gallium(III) and iron(III) complexes are dominated by intraligand transitions associated with pyridine or pyrazine ring, azomethine, and thione portions of the thiosemicarbazone moiety (see Supporting Information). Of note is the large increase in the magnitude of the band at ~400 nm, which is assumed to originate from the thioamide portion of the thiosemicarbazone HL, upon complexation (Figure S1). The high intensity of this band of the ligand in the complexed form is expected on the basis of reduced symmetry and in addition due to the increased lengths of the chromophore along the axis of the molecule in the complex (trans-configuration) when compared to the metal-free ligand, which usually adopts cis-configuration. The d–d band with the maximum at 894 nm (**18**) and 957 nm (**15**), respectively, in the case of iron complexes is presumably due to $^2T_{2g} \rightarrow {}^2T_{1g}$ transition of the d^5 low-spin system.[35] Selected complexes **6**, **8**, **14**, and **18** were shown to be stable for at least 15 h when dissolved in a mixture of DMSO/H$_2$O 1:100 (v/v) (see Figures S1–S4). We also observed that more concentrated solution of **8** in DMSO/H$_2$O 1:1 (v/v) produced X-ray diffraction quality single crystals of the same composition as the starting material after 48 h (in line with UV/vis data).

All gallium and iron complexes were found to crystallize very well from chloroform or chloroform–ethanol mixtures saturated with hexane or diethyl ether. This enabled their characterization in the solid state by X-ray crystallography.

Crystal Structures. ORTEP drawings of [Ga(L^1)Cl$_2$] (HL^1 = 2-acetylpyridine *N,N*-dimethylthiosemicarbazone) (**6**), the complex cation [Ga(L^3)$_2$]$^+$ (**10**), and [Fe(L^3)$_2$]$^+$ (**15**) (HL^3 = acetylpyrazine *N,N*-dimethylthiosemicarbazone) with the atom labeling schemes are shown in Figures 2 and 3, whereas those of complexes **11**, **13**, **16–18**, and **21** are quoted as Supporting Information (Figures S5–S10).

The geometry of the gallium ion in **6** is distorted square-pyramidal. The calculated τ value for the degree of trigonality is 0.28.[36] All compounds with metal-to-ligand stoichiometry
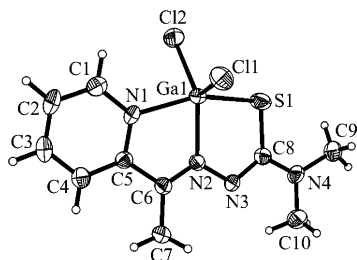
Figure 2. ORTEP drawing of [GaL^{1}Cl$_2$] (HL^1 = 2-acetylpyridine *N,N*-dimethylthiosemicarbazone) (**6**) with thermal ellipsoids depicted at 50% probability level.
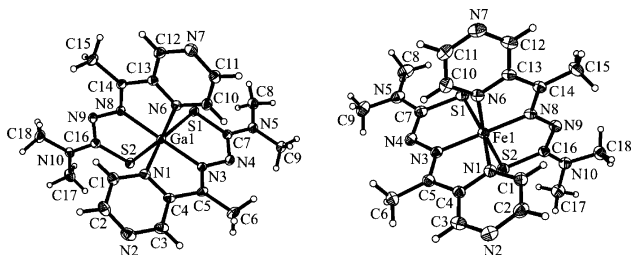

Figure 3. ORTEP drawing of the complex cations [Ga(L^3)$_2$]$^+$ (**10**) (left) and [Fe(L^3)$_2$]$^+$ (**15**) (right) (HL^3 = acetylpyrazine *N,N*-dimethylthiosemicarbazone) with thermal ellipsoids depicted at 50% probability level.

1:2 crystallize in centrosymmetric space groups as racemic mixtures of the two enantiomers of chiral octahedral gallium(III) or iron(III) complexes.

Cytotoxicity. The cytotoxic potencies of five [4]N-substituted α-N-heterocyclic thiosemicarbazones, seven gallium complexes, and ten iron complexes were investigated in the human tumor cell lines 41M (ovarian carcinoma) and SK-BR-3 (mammary carcinoma) by means of the colorimetric MTT assay. Generally, SK-BR-3 cells are less sensitive to the compounds investigated in this study, giving up to 38 times higher IC$_{50}$ values than 41M cells. All the complexes and the ligands have very high cytotoxic potencies, with IC$_{50}$ values ranging from picomolar to nanomolar concentrations (Table 1), and their concentration−effect curves are rather flat, gently declining over a range of 3 orders of magnitude (Figures 4−6), which contrasts with the steep concentration-effect curves usually observed with tumor-inhibiting metal compounds. This suggests that the cytotoxicity is mainly governed by the thiosemicarbazone ligands, which are highly cytotoxic themselves, while complexation to metal ions rather serves to modulate their mode of action and activity.

In order to give direction to the future development of this class of compounds, structure−activity relationships have been explored in following respects: (i) impact of complexation to gallium(III) or iron(III) as compared to the uncomplexed thiosemicarbazone; (ii) influence of the ligand-to-metal stoichiometry; (iii) structural modifications of the thiosemicarbazone and (iv) influence of the counterion in the iron(III) complex salts.

The effects of the central metal on the activity of ligands **1**−**5** are very pronounced, and notably they are divergent (Figure 4). Complexation to iron(III) weakens the cytotoxic properties to a remarkable extent. The IC$_{50}$ values of the iron complexes range from 13 to 172 nM in the cell line 41M and from 29 to 930 nM in SK-BR-3 cells, indicating roughly 12- to 2400-fold (41M) and 9- to 660-fold (SK-BR-3) lower cytotoxicities than those of the corresponding metal-free ligands, respectively. In contrast, 1:2 gallium(III) complexes (**8**−**12**) show an increase in cytotoxicity compared to the corresponding metal-free ligands

Table 1. Cytotoxicity of α-N-Heterocyclic Thiosemicarbazones (**1**−**5**), Their Gallium(III) Complexes (**6**−**12**), Iron(III) Complexes (**13**−**22**), Cisplatin, Ga(NO$_3$)$_3$, Fe(NO$_3$)$_3$, and NH$_4$PF$_6$ in Two Human Cancer Cell Lines[a]

	IC$_{50}$ (nM)	
compd	41M	SK-BR-3
	Ligands	
1	0.22 ± 0.14	2.7 ± 1.4
2	0.36 ± 0.07	3.1 ± 1.1
3	0.073 ± 0.005	1.4 ± 0.1
4	1.1 ± 0.4	5.0 ± 2.3
5	0.41 ± 0.03	2.2 ± 0.3
	Ga(III) Complexes	
6	0.19 ± 0.15	0.59 ± 0.27[b]
7	0.16 ± 0.07[b]	1.8 ± 0.2
8	0.053 ± 0.018[b]	0.56 ± 0.47[b]
9	0.18 ± 0.03[b]	0.52 ± 0.05[b]
10	0.0045 ± 0.0006[b]	0.17 ± 0.01[b]
11	0.065 ± 0.042[b]	0.47 ± 0.22[b]
12	0.27 ± 0.08[b]	0.79 ± 0.05[b]
	Fe(III) Complexes	
13	154 ± 10[b]	447 ± 63[b]
14	26 ± 7[b]	29 ± 12[b]
15	172 ± 24[b]	930 ± 206[b]
16	13 ± 9[b]	104 ± 37[b]
17	27 ± 6[b]	64 ± 24[b]
18	126 ± 32[b]	452 ± 36[b]
19	54 ± 25[b]	87 ± 11[b]
20	149 ± 20[b]	682 ± 267[b]
21	17 ± 8[b]	76 ± 11[b]
22	57 ± 22[b]	120 ± 22[b]
cisplatin	0.39 ± 0.07 μM	
Ga(NO$_3$)$_3$	70 ± 4 μM	>100 μM
Fe(NO$_3$)$_3$	>100 μM	>100 μM
NH$_4$PF$_6$	>100 μM	>100 μM

[a] 50% inhibitory concentrations in 41M and SK-BR-3 cells after exposure for 96 h in the MTT assay. Values are means ± standard deviations obtained from at least three independent experiments. [b] Different from corresponding uncomplexed thiosemicarbazone (compounds **1**−**5**) ($p \leq 0.1$; Wilcoxon rank sum test).

by a factor of 1.5 to 17 for 41M cells and 3 to 11 for SK-BR-3 cells, respectively. This results in IC$_{50}$ values in the low nanomolar or even in the picomolar range (0.0045−0.27 nM for 41M and 0.17−1.8 nM for SK-BR-3 cells). A pairwise comparison of the direct analogues [Ga(L$^{1-5}$)$_2$][PF$_6$] and [Fe(L$^{1-5}$)$_2$][PF$_6$] reveals that the gallium complexes are by a factor of 210 to 33000 (41M) and 150 to 4000 (SK-BR-3) more cytotoxic than the iron compounds, respectively.

Since structural rearrangements in solution, resulting in a mixture of species with 1:2 and 1:1 metal-to-ligand stoichiometry (eq 1), had been recognized in the case of [bis(2-acetylpyridine *N,N*-dimethylthiosemicarbazone)gallium(III)] tetrachlorogallate(III) and analogous compounds with tetrachlorogallate(III) as counteranion,[37] the complex salts with hexafluorophosphate have been prepared.

$$[GaL_2][GaCl_4] \leftrightarrow 2[GaLCl_2] \qquad (1)$$

In order to examine the influence of the ligand-to-metal stoichiometry, the gallium(III) complexes of the general formula [GaLCl$_2$], i.e., **6** and **7**, were hence compared with their [GaL$_2$][PF$_6$] congeners **8** and **9**, respectively (Figure 5). The cytotoxicity of complexes with metal-to-ligand stoichiometry 1:1 is either similar (**6** in 41M cells and **7** in both cell lines) or up to 4.6 times higher (**6** in SK-BR-3 cells) than those of the corresponding uncomplexed thiosemicarbazones. Although the former compounds contain two more easily replaceable chloro ligands, when compared to tridentate thiosemicarbazones, which

Figure 4. Concentration-effect curves of thiosemicarbazones HL (white symbols), their gallium(III) complexes [GaL$_2$][PF$_6$] (black symbols), and iron(III) complexes [FeL$_2$][PF$_6$] (gray symbols), obtained by the MTT assay in 41M cells (left panels: A, C, E, G, J) and SK-BR-3 cells (right panels: B, D, F, H, K). In each case, the thiosemicarbazone is less cytotoxic than the gallium complex, but more cytotoxic than the iron complex. A, B. Compounds **1** (white), **8** (black), and **18** (gray). C, D. Compounds **2** (white), **9** (black), and **19** (gray). E, F. Compounds **3** (white), **10** (black), and **20** (gray). G, H. Compounds **4** (white), **11** (black), and **21** (gray). J, K. Compounds **5** (white), **12** (black), and **22** (gray). Values are means ± standard deviations from at least three independent experiments.

30

Figure 5. Concentration-effect curves of thiosemicarbazones HL (white symbols) and their gallium(III) complexes [GaLCl$_2$] (black symbols, dashed line) and [GaL$_2$][PF$_6$] (black symbols, solid line), obtained by the MTT assay in 41M cells (left panels: A, C) and SK-BR-3 cells (right panels: B, D). The complexes with metal-to-ligand stoichiometry 1:1 are at least as cytotoxic as the uncomplexed thiosemicarbazones but do not exceed their congeners with stoichiometry 1:2. A, B. Compounds **1** (white), **6** (black; dashed lines), and **8** (black; solid lines). C, D. Compounds **2** (white), **7** (black; dashed lines), and **9** (black; solid lines). Values are means ± standard deviations from at least three independent experiments.

should allow covalent binding to biomolecules more readily, neither the shapes of their concentration-effect curves nor their cytotoxic potencies suggest any substantial differences in their pharmacological behavior as compared to the congeners with stoichiometry 1:2.

Structural modifications of two moieties of the thiosemicarbazone ligands (aromatic N-heterocycle: pyridine vs pyrazine; terminal amine group: dimethylamine vs pyrrolidine vs piperidine) have been explored for their effect on the cytotoxicity of the complexes with 1:2 metal-to-ligand stoichiometry. For comparison, the concentration-effect curves of the uncomplexed thiosemicarbazones HL, i.e., **1**−**5**, the gallium(III) complexes [GaL$_2$][PF$_6$] **8**−**12**, and the iron(III) complexes [FeL$_2$][PF$_6$] **18**−**22** are depicted in Figure 6. In general, cytotoxic potencies mostly range within 1 order of magnitude for each class of compounds, and the effects exerted by the structural modifications of the thiosemicarbazone moieties are quite small in comparison to the impact of the central metal described above. Within the uncomplexed thiosemicarbazones, cytotoxicity decreases in the following rank order in both cell lines based on IC$_{50}$ values: **3** > **1** ≈ **5** ≈ **2** > **4**.

Strikingly, the cytotoxicity-weakening effects of complexation with iron(III) become more pronounced with increasing cytotoxic potency of the thiosemicarbazone, resulting in an inverse rank order of the corresponding iron(III) complexes in 41M cells: **21** (ligand **4**) > **19** (ligand **2**) ≈ **22** (ligand **5**) > **18** (ligand **1**) ≥ **20** (ligand **3**). A similar tendency, though with a slightly deviating rank order, is discernible in SK-BR-3 cells. However, no structure−activity relationships with validity for both cell lines can be deduced from the concentration-effect curves of the gallium(III) complexes, and the rank orders with regard to cytoxic potency neither correspond to that of the uncomplexed thiosemicarbazones nor to that of the iron(III) analogues. Accordingly, there is no correlation between the cytotoxicity-

enhancing effects of complexation with gallium(III) and the cytotoxic potency of the uncomplexed thiosemicarbazones.

The counterions of the cationic iron(III) complexes seem to have a marginal, if any, impact on cytotoxicity, as the differences between the IC$_{50}$ values obtained with the complex salts containing either tetrachloroferrate(III) or hexafluorophosphate are mostly within the same range of variation.

Clarifying the question left open by a previous publication on the gallium(III) complex of 2-acetylpyridine *N,N*-dimethylthiosemicarbazone,[34] the work presented here clearly indicates that gallium(III) is able to enhance the cytotoxicity of α-N-heterocyclic thiosemicarbazones to an extent largely exceeding that of mere stoichiometric effects, whereas complexation to iron(III) is not only disadvantageous in comparison to gallium(III) but even results in a marked attenuation of the activity by 1 to 3 orders of magnitude. The latter observation deviates from findings reported in the literature for other α-N-heterocyclic thiosemicarbazones. On the one hand, it sharply contrasts with the enhancing effects of complexation with iron(III) on the cytotoxicity and the ribonucleotide reductase-inhibitory potency of 2-formylpyridine- and 1-formylisoquinoline-thiosemicarbazone[10] but also with the *in vivo* antileukemic behavior of a 2-acetylpyridine thiosemicarbazone analogue carrying a terminal hexahydroazepine group, which has been reported to be inactive unless complexed with iron(III).[38] On the other hand, the attenuating effects are much more pronounced than those reported for the complexation of ^4N-azabicyclononane-substituted thiosemicarbazones derived from 3-acetylpyridazine, 4-acetylpyrimidine, and acetylpyrazine with iron(II).[39] In consideration of the converse effects of iron(III) observed with the thiosemicarbazones studied here, the favorable properties obtained by complexation to gallium(III) can unequivocally and specifically be ascribed to this particular metal ion and are not the result of complexation in general or the
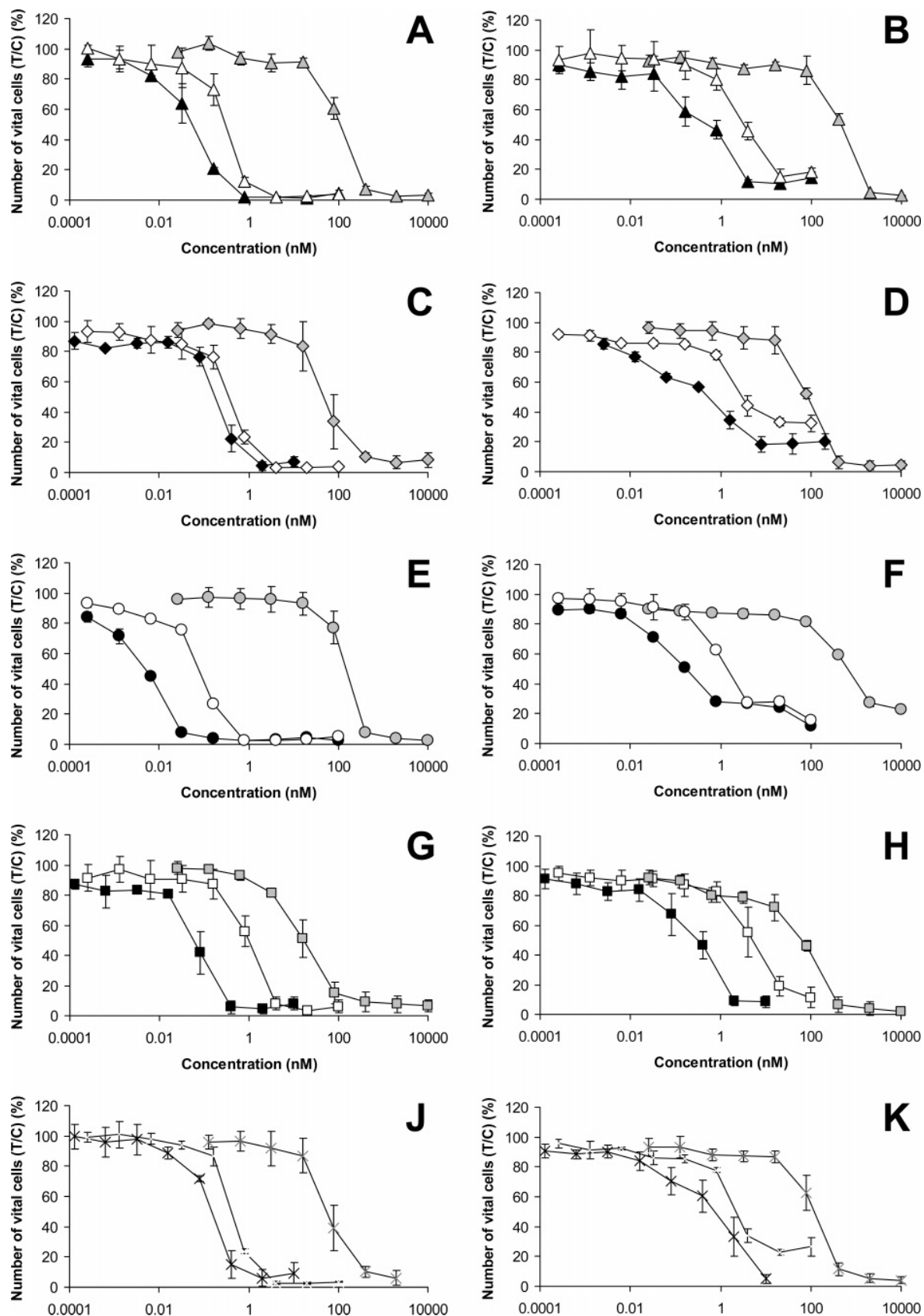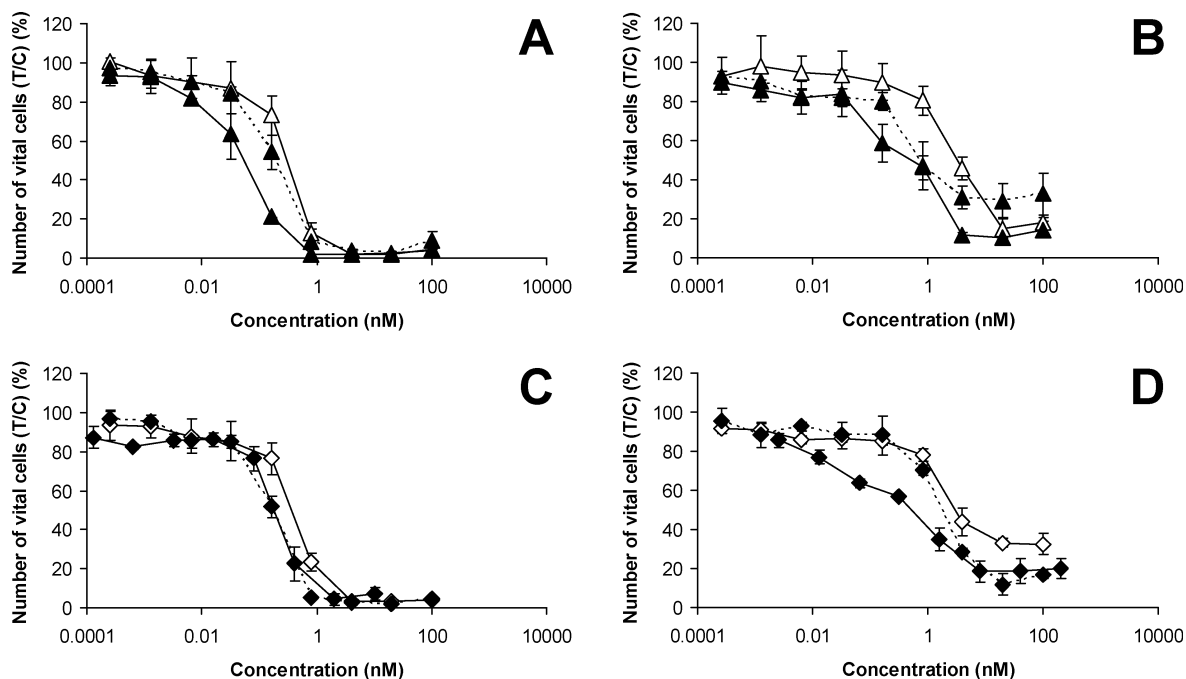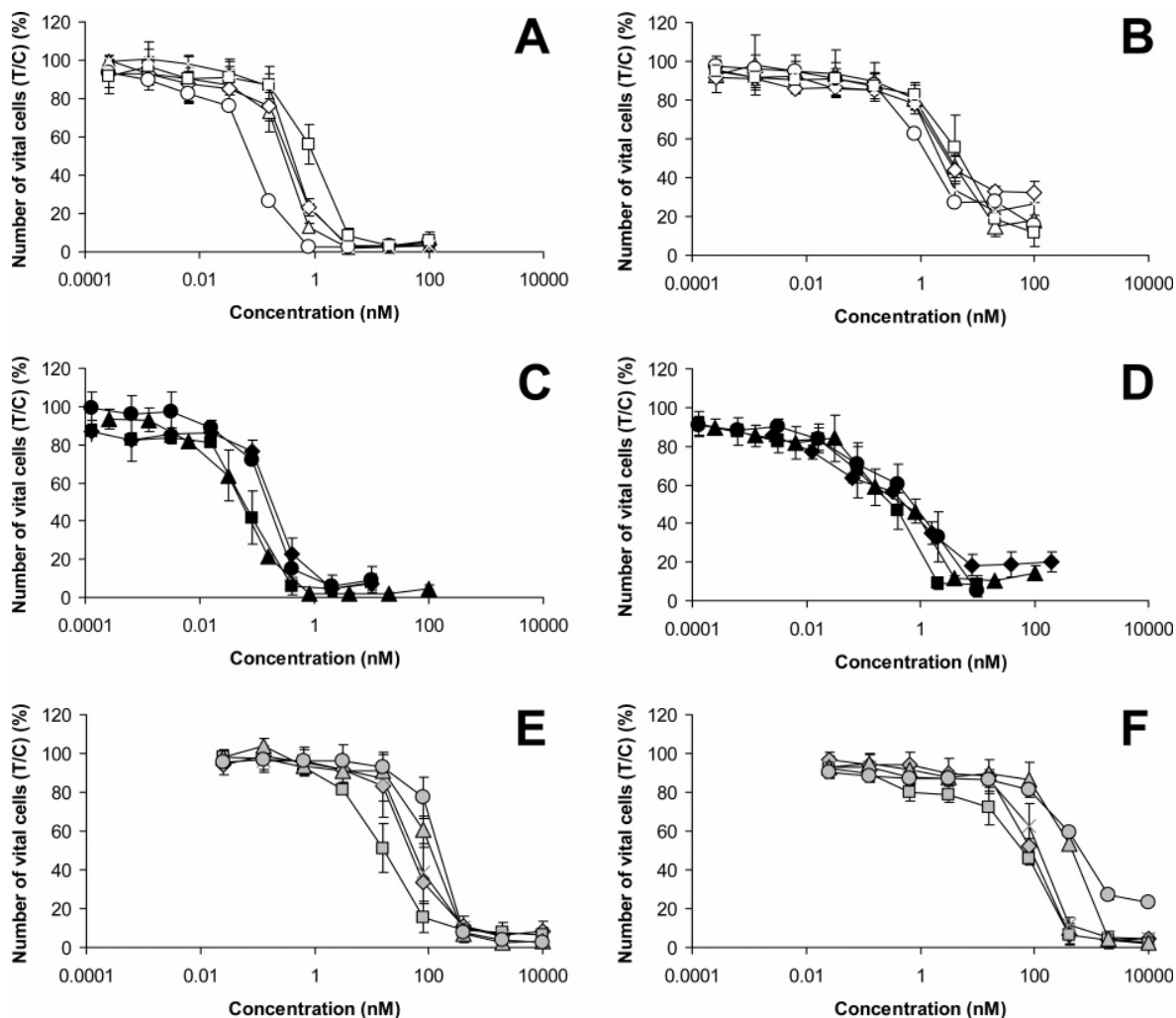
Figure 6. Concentration-effect curves of thiosemicarbazones HL (white symbols), their gallium(III) complexes [GaL$_2$][PF$_6$] (black symbols) and iron(III) complexes [FeL$_2$][PF$_6$] (gray symbols), obtained by the MTT assay in 41M cells (left panels: A, C, E) and SK−BR-3 cells (right panels: B, D, F). Within each class of compounds, cytotoxic potencies mostly range within 1 order of magnitude, and the structural modifications of the thiosemicarbazone moieties exert rather small effects in comparison to the impact of the central metal. A, B. Compounds **1** (−△−), **2** (−◇−), **3** (−○−), **4** (−□−) and **5** (−×−). C, D. Compounds **8** (−▲−), **9** (−◆−), **10** (−●−), **11** (−■−) and **12** (−×−). E, F. Compounds **18** (−▲−), **19** (−◆−), **20** (−●−), **21** (−■−) and **22** (−×−). Values are means ± standard deviations from at least three independent experiments.

geometry of the complex, which is essentially the same for both central metals (Figure 3).

These findings do not necessarily exclude the possibility that preformed iron chelates are the species actually exerting the biological effects *in vivo*, given the high affinity of the thiosemicarbazones for iron and the low concentrations of iron in cell culture media as compared to those encountered *in vivo*, but they clearly indicate that all thiosemicarbazones under investigation display their full antiproliferative potency when the metal-binding site is not occupied by iron. Whether the beneficial effects of coordination to gallium result from the pharmacological properties of this metal or from the fact that it prevents premature coordination to iron remains to be elucidated by further studies.

All five ligands used for synthesis of the complexes presented here are derived from a basic structure. As compared to the impact of complexation, the structural modifications of the thiosemicarbazones have comparatively little impact on their biological activity *in vitro*, suggesting that all thiosemicarbazone structures under investigation are capable of interacting with their common biological target in a comparable manner. The generally high cytotoxic potencies of compounds **1**−**5** are in

accordance with literature data that report inhibition of lymphoma cell growth by compounds **1**, **3**, **4** and related [4]N-disubstituted α-N-heterocyclic thiosemicarbazones with IC$_{50}$ values in the low nanomolar range.[40] When starting from the 2-acetylpyridine- or acetylpyrazine thiosemicarbazone structure, the dimethylation of the terminal nitrogen atom ([4]N) of the thiosemicarbazone chain has been recognized as the crucial modification in order to obtain this exceptionally high cytotoxicity.[40] This tremendous cytotoxicity has been found to be preserved when the dimethylamino group is replaced by cycloamine functions (pyrrolidine or piperidine), which is also confirmed by the results presented here.

Whether the conclusions drawn from our *in vitro* findings, in particular the favorable effects of complexation with gallium(III), can be transferred to the *in vivo* setting is subject to ongoing studies in animal tumor models. As to the antitumor activity of the uncomplexed thiosemicarbazones, results reported in the literature are fragmentary and rather conflicting: In contrast to 2-formylpyridine-thiosemicarbazone,[1,5,41] 3-aminopyridine-2-carboxaldehyde thiosemicarbazone (3-AP, triapine)[42] and other representatives lacking substituents at the terminal amine nitrogen, 2-acetylpyridine *N,N*-dimethylthiosemicarba-

Table 2. Mouse R2 Tyrosyl Radical Concentration [Y*] in μM Measured under Aerobic and Anaerobic Conditions for Samples Containing 30 μM Reconstituted R2 Monomer and 30−33 μM Tested Compound after 1, 15, and 1005 min Total Incubation Time at 298 K

	tyrosyl radical concentration [Y*] in μM							
time[min]	blank	blank + DMSO	blank + DMSO + DTT	**Ga(NO$_3$)$_3$**	**Fe(NO$_3$)$_3$**	**1**	**8**	**18**
			Aerobic					
1		17.7	16.5	16.6	17.2	17.4	16.8
15		17.4	16.9	18.2	7.0	9.3	5.1
1005		5.9	5.4	0.9	0.5	0.3	0.6
			Anaerobic					
1	19.8	19.1	20.9	17.3	18.3	8.5	15.9	3.2
15	18	18.4	22.4	18.2	19.8	0	0	0
1005	2.6	3.2	0	0	0	0	0	0
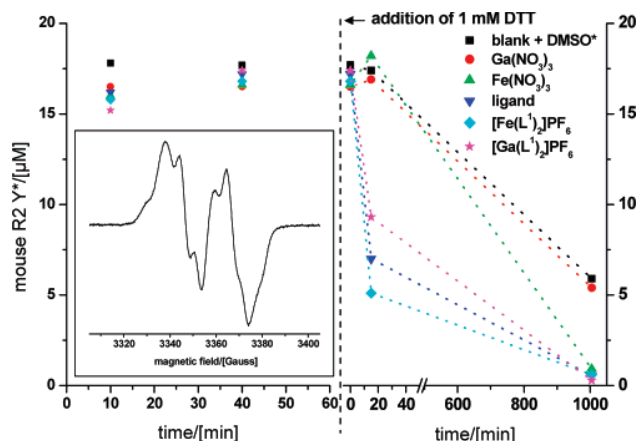
Figure 7. Mouse R2 tyrosyl radical concentration [Y*] in μM for samples containing 30 μM reconstituted R2 monomer and 33 μM tested compound after 10 and 40 min total incubation time at 298 K (left). Radical concentration [Y*] after addition of 1 mM DTT, measured after 1, 15, and 1005 min (right). Inset: X-band EPR spectrum of [Y*] of the blank at 40 K. Further EPR measuring conditions: 9.64 GHz, 100 kHz modulation frequency, 3 G modulation amplitude, 41 ms time constant, and 82 s recording time. *blank + DMSO (left) and blank + DMSO + DTT (right).
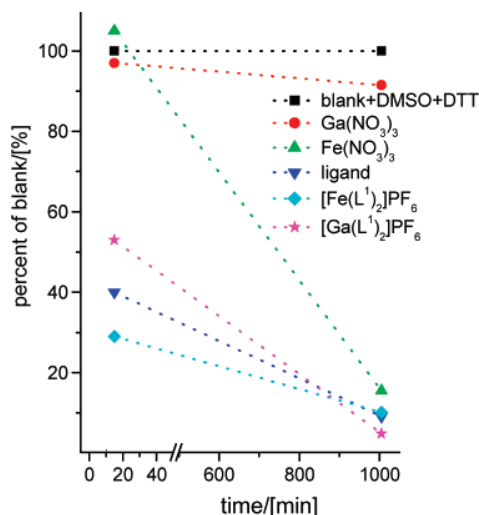
Figure 8. Percentage of the [Y*] concentrations in the samples from Figure 7 relating their Y* concentration to that of the blank, therefore accounting for the natural decay of the [Y*] concentration in mouse R2. Sample composition, incubation time, and conditions as in Figure 7.

zone is completely devoid of antileukemic activity in nontoxic doses in mice, whereas replacement of dimethylamine either by longer alkylamines or by bulky cycloamines results in restored activity, though at higher optimal doses,[43] suggesting that the introduction of a sterically more demanding substituent might be beneficial from a therapeutic point of view.

Interaction with Ribonucleotide Reductase. The sensitivity of the R2 specific tyrosine free radical in mouse ribonucleotide reductase R2 protein to 2-acetylpyridine N,N-dimethylthiosemicarbazone (**1**), its gallium(III) and iron(III) complexes [Ga(L^1)$_2$]-[PF$_6$] (**8**) and [Fe(L^1)$_2$][PF$_6$] (**18**), Ga(NO$_3$)$_3$, and Fe(NO$_3$)$_3$ was tested. A highly purified ribonucleotide reductase R2 protein (30 μM R2 monomer) in buffer containing 1% DMSO was incubated with 30−33 μM of the above-mentioned compounds along with the control sample (blank) for 10 min at 298 K. The frozen samples were analyzed by EPR spectroscopy, and the EPR spectra of the tyrosyl radical (Y*) were measured at 40 K. As the reaction time was short and the results after 10 min incubation time were not conclusive, the samples were thawed, and the compounds were allowed to react with ribonucleotide reductase R2 protein for further 30 min at 298 K. Measurement of the EPR spectra of the samples refrozen in liquid nitrogen showed no change of the EPR signal (Figure 7). The results obtained prompted us to investigate the same reaction in the presence of dithiothreitol (DTT) as a reductant. All six samples were thawed, and to each of them 1 mM (final concentration) of DTT was added. After incubation for 15 min, the samples were refrozen in liquid nitrogen and EPR spectra measured. As

seen in Table 2 and Figure 7, the R2 specific EPR signal decreased significantly for HL^1, [Ga(L^1)$_2$][PF$_6$], and [Fe(L^1)$_2$]-[PF$_6$] but remained almost unchanged for Ga(NO$_3$)$_3$, Fe(NO$_3$)$_3$, and control experiment. The samples were thawed again, allowed to react for further 16 h at 298 K, and refrozen and the EPR spectra remeasured. All thiosemicarbazone-containing samples (**1**, **8**, and **18**) showed relatively fast kinetics for the destruction of the tyrosyl radical Y* (Figure 7). In comparison, Y* is slowly destroyed in the blank on the long time scale (>16 h), which is known from stability measurements. This decay is accounted for in Figure 8 by relating the Y* concentration of the samples to that of the blank in %, whereas in Figure 9 it is shown that 1% DMSO has no effect on the natural decay. Figure 8 shows clearly that Ga(NO$_3$)$_3$ does not enhance the decay of Y* in DTT-containing buffer under the experimental conditions and that Fe(NO$_3$)$_3$ displays a lag time in the destruction kinetics of Y* compared to the ligand-containing samples. These samples already exhibited after 15 min incubation time a quenching of Y* by more than 50%, whereas the Fe(NO$_3$)$_3$ sample still contained the same amount of Y* as the blank but shows a similar quenching of more than 80% after 16.5 h.

Under anaerobic conditions, the quenching of Y* by **1**, **8**, and **18** is much faster than in the presence of oxygen (Table 2 and Figure 9). In addition, the three species show very different reactivity with [Fe(L^1)$_2$][PF$_6$] ≫ ligand ≫ [Ga(L^1)$_2$][PF$_6$] under anaerobic conditions, whereas their aerobic reactivity displays only moderate differences, nevertheless, in the same order. However, quenching of Y* seems to be an insufficient explanation for antitumor potency because of the reversed order of the
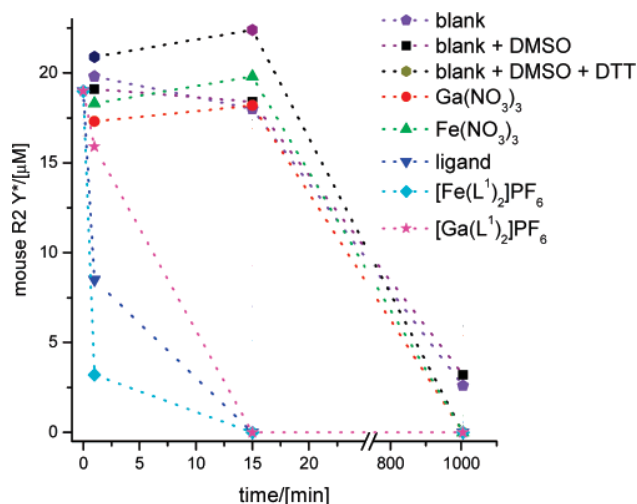
Figure 9. Mouse R2 tyrosyl radical concentration [Y*] in μM under anaerobic conditions for samples containing 30 μM reconstituted R2 monomer and 30 μM tested compound after 1, 15, and 1005 min total incubation time at 298 K. To underline that all samples had a similar starting concentration of [Y*] a virtual (not measured) starting data point at time 0 was included at the average [Y*] concentration of the other samples for the three ligand-containing samples displaying a fast Y* decay. EPR measuring conditions: 9.42 GHz and 77 K, all other settings as in Figure 7.

latter. This might suggest the existence of additional molecular targets less considered so far.

As for aerobic conditions, under anaerobic conditions the presence of DTT alone or with one of the metal nitrates shows no significant effect after 15 min incubation. However, the lack of oxygen in presence of DTT increases the instability of Y* also in the blank, so that it is decayed completely after 16.6 h incubation, preventing any conclusion on an additional reactivity of the two metal nitrates. This accelerated decay indicates that DTT acts as a slow radical quencher in the absence of oxygen. Surprisingly, Y* decays faster in the absence of DTT under anaerobic conditions than in presence of both oxygen and DTT, as can be seen from the Y* concentration of these blanks after 16.6 h in Figures 7 and 9. This together with the unexpected results from the anaerobic DTT containing blank and the aerobic Fe(NO$_3$)$_3$/DTT containing sample might be explained by reduction of Fe(III) to Fe(II) in the presence of DTT. Here, Fe(III) is available in mouse R2 solutions as R2 is isolated as Y*- and iron-free apoprotein and reconstituted with four Fe(II)/monomer[44] resulting in an optimal Y* yield of 0.7 $\pm$ 0.1 Y*/monomer. Although only two Fe(III) are bound tightly at the diiron binding site of each monomer, not more than 15% of the excess iron can be removed from the mouse R2 protein by, e.g., size exclusion chromatography.[45] Nevertheless, this excess Fe(III) most likely bound to the protein surface and the iron bound at the diiron binding site of R2 monomers, where no Y* has been formed, are available in solution[46] and might react with the DTT. During reconstitution, an Fe(II) is delivering an electron to the diiron-center-radical site from the surface of the R2 protein,[9,44] and in a similar way the delivery of an electron from bound Fe(II) to Y* in reconstituted R2 might quench the radical. This directly explains the faster radical decay in the anaerobic DTT containing blank. In the aerobic samples, formation of Fe(II) by DTT would initiate two counter-working reactions as the combination of Fe(II) and oxygen reconstitutes the tyrosyl radical again. The slower Y* decay in the DTT and oxygen containing blank (Figure 7) compared to the blank containing neither oxygen nor DTT (Figure 9) indicates that

the reconstitution is more efficient. This in turn explains the result from the aerobic Fe(NO$_3$)$_3$/DTT-containing sample (Figure 7), in which the oxygen compensates the tyrosyl radical destruction in the first 15 min but is used up on the long time scale, where the quenching by Fe(II) prevails.

Conclusions

The combination of [4]N-substituted α-N-heterocyclic thiosemicarbazone moieties with a central gallium(III) ion, both well-known inhibitors of the enzyme ribonucleotide reductase, yielded a series of highly potent antiproliferative coordination compounds that are being explored for their applicability as anticancer agents. Although the pharmacological properties of these complexes must be primarily attributed to the thiosemicarbazone ligands, gallium(III) unequivocally and specifically modulates their cytotoxic potency in a beneficial way. In contrast, coordination to iron(III), which is most likely the principal biotransformation process undergone by α-N-heterocyclic thiosemicarbazones *in vivo*, actually impairs the biological activity of all representatives of this class of compounds investigated in this study. Although slow Y* quenching on the hour time scale has been found in DTT-containing mouse R2 solution without the thiosemicarbazone ligand, the much faster reaction on the minute time scale in presence of the ligand clearly shows that the Y* in mammalian R2 protein is a direct and preferred target of α-N-heterocyclic thiosemicarbazones under slightly reducing conditions, which also prevail in cancer cells. The reversed order of cytotoxic activity [Ga(L^1)$_2$][PF$_6$] > HL^1 > [Fe(L^1)$_2$][PF$_6$] and Y* quenching kinetics [Fe(L^1)$_2$]-[PF$_6$] > HL^1 > [Ga(L^1)$_2$][PF$_6$] nicely displays the difference between a complex whole cell and a purified protein solution. A number of explanations, starting from the uptake kinetics to additional reactions with target(s) other than ribonucleotide reductase, are imaginable for this solely quantitative difference.

Experimental Section

All solvents and reagents were obtained from commercial suppliers and used without further purification. 2-Acetylpyridine *N,N*-dimethylthiosemicarbazone (**1**), 2-acetylpyridine *N*-pyrrolidinylthiosemicarbazone (**2**), acetylpyrazine *N,N*-dimethylthiosemicarbazone (**3**), acetylpyrazine *N*-pyrrolidinylthiosemicarbazone (**4**), and acetylpyrazine *N*-piperidinylthiosemicarbazone (**5**) have been prepared as described in the literature.[40,47] Elemental analyses were carried out on a Carlo Erba microanalyzer at the Microanalytical Laboratory of the University of Vienna and were within $\pm$0.4% of the theoretical values. Electrospray ionization mass spectrometry was carried out with a Bruker Esquire 3000 instrument (Bruker Daltonic, Bremen, Germany). Electron impact mass spectrometry was carried out at 70 eV with a Finnigan MAT 8230 (Bremen, Germany). Expected and experimental isotope distributions were compared. Infrared spectra were obtained from KBr or CsI pellets with a Perkin-Elmer FT-IR 2000 instrument (4000$-$200 cm^{-1}). UV$-$vis spectra were recorded on a Perkin-Elmer Lambda 650 UV$-$vis-spectrophotometer using samples dissolved in methanol (900$-$200 nm). **15** and **18** were also measured on a Hewlett-Packard 8453 UV$-$vis spectrophotometer (1100$-$200 nm). [1]H NMR spectra were recorded on a Bruker DPX400 spectrometer at 298 K. The residual [1]H present in DMSO-d_6 was used as internal reference. The assignment was proven by 2D NMR ([13]C,[1]H; [1]H,[1]H, and [13]C,[1]H via long-range couplings) spectra. Abbreviations for NMR data are: py = pyridine, pz = pyrazine, C$_{q,py}$ = quaternary carbon of pyridine, C$_{q,pz}$ = quaternary carbon of pyrazine. EPR measurements were performed on a Bruker ElexSys E500 EPR-spectrometer equipped with an EPR-910 Oxford Instruments helium-flow cryostat or on a Bruker ESP300E spectrometer in a quartz-Dewar filled with liquid nitrogen. An average spin concentration was calculated by comparison with a mouse R2 standard with a well-known radical content calibrated earlier against the copper standard.

Syntheses of Complexes. 2-Acetylpyridine *N,N*-Dimethylthiosemicarbazonato-*N,N,S*-dichlorogallium(III), Ga(L¹)Cl₂ (6). To 2-acetylpyridine *N,N*-dimethylthiosemicarbazone (**1**) (0.60 g, 2.70 mmol) in boiling dry ethanol (22 mL) was added an ethanolic gallium(III) chloride solution (2.29 mmol/mL) (0.59 mL, 1.35 mmol). After a few minutes, a yellow precipitate was formed. The reaction mixture was heated at 90 °C for 1 h. The product was separated from the hot solution by filtration, washed with dry ethanol, and dried *in vacuo*. Yield: 0.33 g (68%). Anal. (C₁₀H₁₃-Cl₂GaN₄S): C, H, N. ¹H and ¹³C NMR, mass spectrometry, IR and UV−vis spectroscopy data for **6** and all following complexes can be found in Supporting Information. Crystals suitable for X-ray data collection were obtained from chloroform saturated with *n*-hexane.

2-Acetylpyridine *N*-Pyrrolidinylthiosemicarbazonato-*N,N,S*-dichlorogallium(III), Ga(L²)Cl₂ (7). To 2-acetylpyridine *N*-pyrrolidinylthiosemicarbazone (**2**) (0.30 g, 1.21 mmol) in dry ethanol (24 mL) at 75 °C was added an ethanolic gallium(III) chloride solution (3.13 mmol/mL) (0.77 mL, 2.42 mmol) dropwise within 3 min. The reaction mixture was cooled down to room temperature and stirred overnight. The reaction mixture was allowed to stand at 4 °C for 1 h, and the yellow precipitate was filtered off, washed with dry ethanol, and dried *in vacuo*. Yield: 0.38 g (82%). Anal. (C₁₂H₁₅Cl₂GaN₄S): C, H, N, S. Crystals suitable for X-ray data collection were obtained from ethanol/chloroform 1:2 solution saturated with diethyl ether.

[Bis(2-acetylpyridine *N,N*-dimethylthiosemicarbazonato)-*N,N,S*-gallium(III)] Hexafluorophosphate, [Ga(L¹)₂]PF₆ (8). To 2-acetylpyridine *N,N*-dimethylthiosemicarbazone (**1**) (0.20 g, 0.90 mmol) in dry ethanol (20 mL) was added gallium(III) nitrate nonahydrate (0.19 g, 0.45 mmol) in ethanol (5 mL), and the mixture was stirred for 15 min at room temperature until all ligand had dissolved. Addition of ammonium hexafluorophosphate (0.29 g, 1.80 mmol) produced a yellow precipitate. The reaction mixture was stirred further for 30 min at room temperature. The precipitate was filtered off, washed with ethanol, and dried *in vacuo*. Yield: 0.27 g (91%). Anal. (C₂₀H₂₆F₆GaN₈PS₂): C, H, N.

[Bis(2-acetylpyridine *N*-pyrrolidinylthiosemicarbazonato)-*N,N,S*-gallium(III)] Hexafluorophosphate, [Ga(L²)₂]PF₆ (9). To 2-acetylpyridine *N*-pyrrolidinylthiosemicarbazone (**2**) (0.70 g, 2.82 mmol) in dry ethanol (70 mL) was added gallium(III) nitrate nonahydrate (0.59 g, 1.41 mmol) in dry ethanol (14 mL) at 50 °C. The reaction mixture was stirred for 1 h and then cooled down to room temperature with an ice bath. To the clear yellow solution was added ammonium hexafluorophosphate (0.23 g, 1.40 mmol) in dry ethanol (14 mL) in one portion. The reaction mixture was stirred for 30 min at room temperature and then cooled below 5 °C with an ice bath. The yellow precipitate formed was filtered off and washed with dry ethanol. The crude product was recrystallized from methanol (100 mL) and dried *in vacuo* at 50 °C. Yield: 0.77 g (77%). Anal. (C₂₄H₃₀F₆GaN₈PS₂): C, H, N, S.

[Bis(acetylpyrazine *N,N*-dimethylthiosemicarbazonato)-*N,N,S*-gallium(III)] Hexafluorophosphate, [Ga(L³)₂]PF₆ (10). To acetylpyrazine *N,N*-dimethylthiosemicarbazone (**3**) (0.30 g, 1.34 mmol) in ethanol (30 mL) at room-temperature was added gallium(III) nitrate nonahydrate (0.28 g, 0.67 mmol) in ethanol (9 mL) and stirred for 15 min until all ligand had dissolved. After the addition of ammonium hexafluorophosphate (0.44 g, 2.68 mmol), an orange solid formed. The precipitate was filtered off, washed with ethanol, and dried *in vacuo*. Yield: 0.40 g (90%). Anal. (C₁₈H₂₄F₆GaN₁₀PS₂): C, H, N. Crystals suitable for X-ray data collection were obtained from chloroform saturated with *n*-hexane.

[Bis(acetylpyrazine *N*-pyrrolidinylthiosemicarbazonato)-*N,N,S*-gallium(III)] Hexafluorophosphate, [Ga(L⁴)₂]PF₆ (11). To acetylpyrazine *N*-pyrrolidinylthiosemicarbazone (**4**) (0.50 g, 2.00 mmol) in dry ethanol (50 mL) at 50 °C was added gallium(III) nitrate nonahydrate (0.42 g, 1.00 mmol) in ethanol (10 mL). The reaction mixture was stirred for 30 min and then cooled down to room temperature with an ice bath. To the clear yellow solution was added ammonium hexafluorophosphate (0.16 g, 1.00 mmol) in dry ethanol (10 mL). The reaction mixture was stirred for 2 h at

room temperature and then allowed to stand at 4 °C overnight. The orange precipitate formed was filtered off, washed with dry ethanol, and dried *in vacuo*. Yield: 0.40 g (56%). Anal. (C₂₂H₂₈F₆GaN₁₀-PS₂): C, H, N, S. Crystals suitable for X-ray data collection were obtained from chloroform saturated with *n*-hexane.

[Bis(acetylpyrazine *N*-piperidinylthiosemicarbazonato)-*N,N,S*-gallium(III)] Hexafluorophosphate, [Ga(L⁵)₂]PF₆ (12). To acetylpyrazine *N*-piperidinylthiosemicarbazone (**5**) (0.32 g, 1.16 mmol) in dry ethanol (30 mL) at 50 °C was added gallium(III) nitrate nonahydrate (0.24 g, 0.58 mmol) in ethanol (6 mL). The reaction mixture was stirred for 40 min and then cooled down to room temperature with an ice bath. To the clear orange solution was added ammonium hexafluorophosphate (0.10 g, 0.61 mmol) in dry ethanol (6 mL). The reaction mixture was allowed to stand at 4 °C for 1.5 h. The orange precipitate was filtered off, washed with dry ethanol, and dried *in vacuo*. Yield: 0.25 g (57%). Anal. (C₂₄H₃₂F₆GaN₁₀PS₂): C, H, N, S.

[Bis(2-acetylpyridine *N,N*-dimethylthiosemicarbazonato)-*N,N,S*-iron(III)] Tetrachloroferrate(III), [Fe(L¹)₂][FeCl₄] (13). The complex has been prepared following the literature protocol.[35] Crystals suitable for X-ray data collection were obtained from chloroform saturated with *n*-hexane.

[Bis(2-acetylpyridine *N*-pyrrolidinylthiosemicarbazonato)-*N,N,S*-iron(III)] Tetrachloroferrate(III), [Fe(L²)₂][FeCl₄] (14). To 2-acetylpyridine *N*-pyrrolidinylthiosemicarbazone (**2**) (0.20 g, 0.80 mmol) in dry ethanol (24 mL) at 70 °C was added an ethanolic iron(III) chloride solution (0.26 mmol/mL) (3.1 mL, 0.80 mmol). The reaction mixture was stirred for 30 min, cooled down to room temperature, and then allowed to stand at 4 °C overnight. The black precipitate was filtered off, washed with dry ethanol, and dried *in vacuo*. Yield: 0.13 g (43%). Anal. (C₂₄H₃₀Cl₄Fe₂N₈S₂): C, H, N, S.

[Bis(acetylpyrazine *N,N*-dimethylthiosemicarbazonato)-*N,N,S*-iron(III)] Tetrachloroferrate(III), [Fe(L³)₂][FeCl₄] (15). To acetylpyrazine *N,N*-dimethylthiosemicarbazone (**3**) (0.23 g, 1.03 mmol) in boiling dry ethanol (15 mL) was added an ethanolic iron(III) chloride solution (0.17 mmol/mL) (6 mL, 1.03 mmol). The reaction mixture was refluxed for 30 min and cooled down to room temperature. The black precipitate was filtered off, washed with absolute ethanol, and dried *in vacuo*. Yield: 0.21 g (57%). Anal. (C₁₈H₂₄Cl₄Fe₂N₁₀S₂): C, H, N. Crystals suitable for X-ray data collection were obtained from chloroform saturated with *n*-hexane.

[Bis(acetylpyrazine *N*-pyrrolidinylthiosemicarbazonato)-*N,N,S*-iron(III)] Tetrachloroferrate(III), [Fe(L⁴)₂][FeCl₄] (16). To acetylpyrazine *N*-pyrrolidinylthiosemicarbazone (**4**) (0.30 g, 1.20 mmol) in dry ethanol (30 mL) at 70 °C was added an ethanolic iron(III) chloride solution (0.12 mmol/mL) (10 mL, 1.20 mmol). The reaction mixture was stirred for 30 min and cooled down to room temperature, and a second portion of an ethanolic iron(III) chloride solution (0.12 mmol/mL) (5 mL, 0.60 mmol) was added. The reaction mixture was allowed to stand at 4 °C for 45 min. The black precipitate formed was filtered off, washed with dry ethanol, and dried *in vacuo*. Yield: 0.41 g (90%). Anal. (C₂₂H₂₈Cl₄-Fe₂N₁₀S₂): C, H, N, S. Crystals suitable for X-ray data collection were obtained from chloroform saturated with *n*-hexane.

[Bis(acetylpyrazine *N*-piperidinylthiosemicarbazonato)-*N,N,S*-iron(III)] Tetrachloroferrate(III), [Fe(L⁵)₂][FeCl₄] (17). To acetylpyrazine *N*-piperidinylthiosemicarbazone (**5**) (0.32 g, 1.16 mmol) in dry ethanol (30 mL) at 70 °C was added an ethanolic iron(III) chloride solution (0.12 mmol/mL) (5 mL, 0.60 mmol). The reaction mixture was stirred for 40 min and then cooled down to room temperature. An ethanolic iron(III) chloride solution (0.12 mmol/mL) (10 mL, 1.20 mmol) was added again in one portion, leading to the precipitation of the product. The reaction mixture was allowed to stand at 4 °C for 1 h. The black precipitate was filtered off, washed with dry ethanol, and dried *in vacuo*. Yield: 0.41 g (88%). Anal. (C₂₄H₃₂Cl₄Fe₂N₁₀S₂): C, H, N, S. Crystals suitable for X-ray data collection were obtained from chloroform saturated with *n*-hexane.

[Bis(2-acetylpyridine *N,N*-dimethylthiosemicarbazonato)-*N,N,S*-iron(III)] Hexafluorophosphate, [Fe(L¹)₂]PF₆ (18). To

2-acetylpyridine *N,N*-dimethylthiosemicarbazone (**1**) (0.30 g, 1.35 mmol) in ethanol (15 mL), iron(III) nitrate nonahydrate (0.27 g, 0.67 mmol) in ethanol (5 mL) was added at room temperature. To the black solution formed was added ammonium hexafluorophosphate (0.44 g, 2.70 mmol) in ethanol (5 mL), and the mixture was stirred at room temperature for 1.5 h and subsequently refluxed for 1 h. After the reaction mixture cooled down to room temperature, the black precipitate was filtered off, washed with ethanol, and dried *in vacuo*. Yield: 0.32 g (72%). Anal. ($C_{20}H_{26}F_6FeN_8$-PS_2): C, H, N. Crystals suitable for X-ray data collection were obtained from chloroform saturated with *n*-hexane.

[Bis(2-acetylpyridine *N*-pyrrolidinylthiosemicarbazonato)-*N,N,S*-iron(III)] Hexafluorophosphate, [Fe(L²)₂]PF₆ (19). To 2-acetylpyridine *N*-pyrrolidinylthiosemicarbazone (**2**) (0.70 g, 2.82 mmol) in dry ethanol (70 mL) at 70 °C was added iron(III) nitrate nonahydrate (0.57 g, 1.41 mmol) in dry ethanol (15 mL). The reaction mixture was stirred for 30 min and cooled down to room temperature with an ice bath. To the clear dark solution was added ammonium hexafluorophosphate (0.23 g, 1.41 mmol) in dry ethanol (14 mL). The reaction mixture was stirred for 30 min at room temperature and then allowed to stand at 4 °C overnight. The black precipitate was filtered off, recrystallized from methanol (100 mL), and dried *in vacuo* at 50 °C. Yield: 0.88 g (91%). Anal. ($C_{24}H_{30}F_6$-FeN_8PS_2): C, H, N, S.

[Bis(acetylpyrazine *N,N*-dimethylthiosemicarbazonato)-*N,N,S*-iron(III)] Hexafluorophosphate, [Fe(L³)₂]PF₆ (20). To acetylpyrazine *N,N*-dimethylthiosemicarbazone (**3**) (0.30 g, 1.34 mmol) in ethanol (40 mL) was added iron(III) nitrate nonahydrate (0.27 g, 0.67 mmol) in ethanol (5 mL). The reaction mixture was stirred at room temperature for 30 min and filtered. The black precipitate formed after the addition of ammonium hexafluorophosphate (0.44 g, 2.70 mmol) was stirred at room temperature for 1 h, filtered off, washed with ethanol, and dried *in vacuo*. Yield: 0.40 g (92%). Anal. ($C_{18}H_{24}F_6FeN_{10}PS_2$): C, H, N.

[Bis(acetylpyrazine *N*-pyrrolidinylthiosemicarbazonato)-*N,N,S*-iron(III)] Hexafluorophosphate, [Fe(L⁴)₂]PF₆ (21). To acetylpyrazine *N*-pyrrolidinylthiosemicarbazone (**4**) (0.30 g, 1.20 mmol) in dry ethanol (30 mL) at 70 °C was added iron(III) nitrate nonahydrate (0.24 g, 0.60 mmol) in ethanol (6 mL). The reaction mixture was stirred for 30 min and then cooled down to room temperature with an ice bath. To the clear dark solution was added ammonium hexafluorophosphate (0.10 g, 0.61 mmol) in dry ethanol (6 mL). The reaction mixture was stirred for 1.5 h at room temperature and then allowed to stand at 4 °C overnight. The black precipitate was filtered off, washed with dry ethanol, and dried *in vacuo*. Yield: 0.37 g (89%). Anal. ($C_{22}H_{28}F_6FeN_{10}PS_2$): C, H, N, S. Crystals suitable for X-ray data collection were obtained from chloroform saturated with *n*-hexane.

[Bis(acetylpyrazine *N*-piperidinylthiosemicarbazonato)-*N,N,S*-iron(III)] Hexafluorophosphate, [Fe(L⁵)₂]PF₆ (22). To acetylpyrazine *N*-piperidinylthiosemicarbazone (**5**) (0.32 g, 1.16 mmol) in dry ethanol (30 mL) at 70 °C was added iron(III) nitrate nonahydrate (0.24 g, 0.60 mmol) in ethanol (6 mL). The reaction mixture was stirred for 30 min and then cooled down to room temperature with an ice bath. To the clear dark solution was added ammonium hexafluorophosphate (0.10 g, 0.61 mmol) in dry ethanol (6 mL). The reaction mixture was stirred at room temperature for 3 h. The black precipitate was filtered off, washed with dry ethanol, and dried *in vacuo*. Yield: 0.39 g (90%). Anal. ($C_{24}H_{32}F_6FeN_{10}PS_2$): C, H, N, S.

Crystallographic Structure Determination. X-ray diffraction measurements were performed on a Nonius Kappa CCD and a Bruker X8APEX II CCD-diffractometer. Details of the structure determination are given in Table S2.

Crystal data, data collection parameters, and structure refinement details for **6**, **10**, **11**, **13**, **15**−**18**, and **21** are given in Tables S2−S4. The structures were solved by direct methods and refined by full-matrix least-squares techniques. Non-hydrogen atoms were refined with anisotropic displacement parameters. H atoms were placed at calculated positions and refined as riding atoms in the subsequent least-squares model refinements. The isotropic thermal

parameters were estimated to be 1.2 times the values of the equivalent isotropic thermal parameters of the atoms to which hydrogens were bonded. The following computer programs were used: structure solution, SHELXS-97;[48] refinement, SHELXL-97;[49] molecular diagrams, ORTEP;[50] computer: Pentium IV; scattering factors.[51] Crystallographic data have been deposited with the Cambridge Crystallographic Data Center with numbers CCDC603767-603775. Copies of data can be obtained, free of charge, on application to CCDC, 12 Union Road, Cambridge CB2 1EZ, U.K. (deposit@ccdc.com.ac.uk).

Cell Lines and Culture Conditions. Human 41M (ovarian carcinoma) and SK-BR-3 (mammary carcinoma) cells were kindly provided by Lloyd R. Kelland (CRC Centre for Cancer Therapeutics, Institute of Cancer Research, Sutton, UK) and Evelyn Dittrich (General Hospital, Medical University of Vienna, Austria), respectively. Cells were grown in 75 cm² culture flasks (Iwaki) as adherent monolayer cultures in complete culture medium, i.e., Minimal Essential Medium (MEM) supplemented with 10% heat-inactivated fetal bovine serum, 1 mM sodium pyruvate, 4 mM L-glutamine, and 1% nonessential amino acids (100×) (all purchased from Gibco/Invitrogen). Cultures were maintained at 37 °C in a humidified atmosphere containing 5% CO₂.

Cytotoxicity Tests in Cancer Cell Lines. Cytotoxicity was determined by means of a colorimetric microculture assay (MTT assay, MTT = 3-(4,5-dimethyl-2-thiazolyl)-2,5-diphenyl-2*H*-tetrazolium bromide). 41M and SK-BR-3 cells were harvested from culture flasks by trypsinization and seeded into 96-well microculture plates (Iwaki). A cell density of 4×10^3 cells/well was chosen in order to ensure exponential growth throughout drug exposure. After a 24 h preincubation, cells were exposed to solutions of the test compounds in 200 μL/well complete culture medium for 96 h. For this purpose, the compounds were dissolved in DMSO and then serially diluted in complete culture medium such that the effective DMSO content did not exceed 0.5%. At the end of exposure, drug solutions were replaced by 100 μL/well RPMI1640 culture medium (supplemented with 10% heat-inactivated fetal bovine serum) plus 20 μL/well MTT solution in phosphate-buffered saline (5 mg/mL PBS). After incubation for 4 h, the medium/MTT mixtures were removed, and the formazan crystals formed by the mitochondrial dehydrogenase activity of vital cells were dissolved in 150 μL DMSO per well. Optical densities at 550 nm were measured with a microplate reader (Tecan Spectra Classic), using a reference wavelength of 690 nm in order to correct for unspecific absorption. The quantity of vital cells was expressed in terms of T/C values by comparison to untreated control microcultures, and IC₅₀ values were calculated from concentration-effect curves by interpolation. Evaluation is based on means from at least three independent experiments, each comprising six microcultures per concentration level. Differences between cytotoxic potencies of the uncomplexed ligands and their gallium(III) and iron(III) complexes were analyzed using the Wilcoxon rank sum test.[52]

Quenching of the Tyrosyl Radical of Mouse Ribonucleotide Reductase R2 Protein. Highly purified mouse ribonucleotide reductase R2 protein[44] was used for incubation with ligand **1** and its gallium(III) and iron(III) complexes **8** and **18**, correspondingly, as well as Ga(NO₃)₃ and Fe(NO₃)₃.

Ligand **1** and complexes **8** and **18** are well soluble in DMSO but only sparingly soluble in water. The final DMSO concentration in the protein solution was kept at 1.1%. The solubility of Ga(NO₃)₃ and Fe(NO₃)₃ in DMSO was tested and found to be below the mM range. Thus, Ga(NO₃)₃ and Fe(NO₃)₃ were dissolved in water. A concentrated solution of reconstituted mouse ribonucleotide reductase R2 protein was diluted to 30 μM R2 monomer in buffer (50 mM Tris/HCl, pH 7.6, and 100 mM KCl in H₂O). This solution should contain 12−21 μM tyrosyl radical (Y*) depending on the yield of the reconstitution. Solutions each containing 3 mM 2-acetylpyridine *N,N*-dimethylthiosemicarbazone (**1**), [Ga(L¹)₂][PF₆] (**8**), or [Fe(L¹)₂][PF₆] (**18**) in DMSO and Ga(NO₃)₃ or Fe(NO₃)₃ in water were prepared. Six samples were prepared by mixing 180 μL of 30 μM R2 monomer (15 μM R2) solution with each of the following: 2 μL of DMSO, 2 μL of 3 mM **1** in DMSO, 2 μL of 3

mM **8** in DMSO, 2 μL of 3 mM **18** in DMSO, 2 μL of 3 mM Ga(NO$_3$)$_3$ in water and 2 μL of DMSO, and 2 μL of 3 mM Fe(NO$_3$)$_3$ in water and 2 μL of DMSO in Eppendorf reaction vials and transferring them into 4 mm outer diameter quartz-glass EPR tubes. After a total incubation time of 10 and 40 min at 298 K, they were frozen slowly in liquid nitrogen, and EPR spectra were measured at 40 K. As dilution was negligible here, this yielded a 1:1 molar ratio of R2 monomer and the tested compound (30−33 μM each). The same operations were repeated twice in the presence of 1 mM dithiothreitol with 15 min and >16 h incubation time at 298 K.

A second series of samples were prepared in an anaerobic tent. The buffer solution as well as the other stable solutions (3 mM each of **1**, **8**, and **18** in DMSO and Ga(NO$_3$)$_3$ and Fe(NO$_3$)$_3$ in H$_2$O) were bubbled with argon for 30 min. They were degassed by the vacuum applied in the lock of the anaerobic tent and left standing open for equilibration inside the tent for more then 16 h. The concentrated protein solution was degassed with great care in the lock and diluted 40-fold with the anaerobic buffer. The 20 mM DTT solution was prepared freshly inside the tent from preweighed powder and anaerobic buffer. Solutions were mixed in Eppendorf reaction vials and transferred to the bottom of an EPR tube by a Hamilton syringe with a long needle. EPR tubes were sealed with stoppers made from butyl-rubber and frozen immediately in liquid nitrogen. As indicated by the aerobic results, DTT is starting the reaction, so all other compounds were mixed with the 30 μM R2 monomer solution in advance. The time for addition of DTT, transfer to the EPR tube, and freezing it was estimated to take about 1 min; thus, the first time point is set to 1 min. The EPR spectra were measured at 77 K. Three types of blanks were prepared: (i) 30 μM R2 monomer; (ii) 30 μM R2 monomer in 1% DMSO; (iii) 30 μM R2 monomer in 1% DMSO and 1 mM DTT. For the other five samples, final concentrations were 30 μM R2 monomer, 1% DMSO, 30 μM reactive species, and 1 mM DTT.

Supporting Information Available: Spectroscopic data [^{1}H and ^{13}C NMR spectra, mass spectra, IR, and UV−vis spectra (Figures S1−S4)], microanalytical data, results of kinetic measurements, crystallographic data, details of X-ray data collection and refinement, and the results of X-ray diffraction studies of **6**, **10**, **11**·CHCl$_3$, **13**, **15**, **16**·CHCl$_3$, **17**·CHCl$_3$, **18**, and **21** (Figures S5−S10). This material is available free of charge via the Internet at http://pubs.acs.org.

References

(1) Brockman, R. W.; Thomson, J. R.; Bell, M. J.; Skipper, H. E. Observations on the antileukemic activity of pyridine-2-carboxaldehyde thiosemicarbazone and thiocarbohydrazone. *Cancer Res.* **1956**, *16*, 167−170.

(2) West, D. X.; Padhye, S. B.; Sonawane, P. B. Structural and physical correlations in the biological properties of transition metal heterocyclic thiosemicarbazone and *S*-alkyldithiocarbazate complexes. *Struct. Bond.* **1991**, *76*, 1−50.

(3) Moore, E. C.; Zedeck, M. S.; Agrawal, K. C.; Sartorelli, A. C. Inhibition of ribonucleoside diphosphate reductase by 1-formylisoquinoline thiosemicarbazone and related compounds. *Biochemistry* **1970**, *9*, 4492−4498.

(4) Brockman, R. W.; Sidwell, R. W.; Arnett, G.; Shaddix, S. Heterocyclic thiosemicarbazones: correlation between structure, inhibition of ribonucleotide reductase, and inhibition of DNA viruses. *Proc. Soc. Exp. Biol. Med.* **1970**, *133*, 609−614.

(5) French, F. A.; Blanz, E. J., Jr.; Shaddix, S. C.; Brockman, R. W. α-(*N*)-Formylheteroaromatic thiosemicarbazones. Inhibition of tumor-derived ribunucleoside diphosphate reductase and correlation with in vivo antitumor activity. *J. Med. Chem.* **1974**, *17*, 172−181.

(6) Moore, E. C.; Sartorelli, A. C. Inhibition of ribonucleotide reductase by α-(*N*)-heterocyclic carboxaldehyde thiosemicarbazones. *Pharm. Ther.* **1984**, *24*, 439−447.

(7) Agrawal, K. C.; Sartorelli, A. C. The chemistry and biological activity of α-(*N*)-heterocyclic carboxaldehyde thiosemicarbazones. *Prog. Med. Chem.* **1978**, *15*, 321−356.

(8) Liu, M.-C.; Lin, T.-S.; Sartorelli, A. C. Chemical and biological properties of cytotoxic α-(*N*)-heterocyclic carboxaldehyde thiosemicarbazones. *Prog. Med. Chem.* **1995**, *32*, 1−35.

(9) Eklund, H.; Uhlin, U.; Farnegardh, M.; Logan, D. T.; Nordlund, P. Structure and function of the radical enzyme ribonucleotide reductase. *Prog. Biophys. Mol. Biol.* **2001**, *77*, 177−268.

(10) Saryan, L. A.; Ankel, E.; Krishnamurti, C.; Petering, D. H. Comparative cytotoxic and biochemical effects of ligands and metal complexes of α-*N*-heterocyclic carboxaldehyde thiosemicarbazones. *J. Med. Chem.* **1979**, *22*, 1218−1221.

(11) Preidecker, P. J.; Agrawal, K. C.; Sartorelli, A. C.; Moore, E. C. Effects of the ferrous chelate of 4-methyl-5-amino-1-formylisoquinoline thiosemicarbazone (MAIQ-1) on the kinetics of reduction of CDP by ribonucleotide reductase of the Novikoff tumor. *Mol. Pharmacol.* **1980**, *18*, 507−512.

(12) Antholine, W.; Knight, J.; Whelan, H.; Petering, D. H. Studies of 2-formylpyridine thiosemicarbazone and its iron and copper complexes with biological systems. *Mol. Pharmacol.* **1977**, *13*, 89−98.

(13) Borges, R. H. U.; Paniago, E.; Beraldo, H. Equilibrium and kinetic studies of iron(II) and iron(III) complexes of some α(N)-heterocyclic thiosemicarbazones. Reduction of the iron(III) complexes of 2-formylpyridine thiosemicarbazone and 2-acetylpyridine thiosemicarbazone by cellular thiol-like reducing agents. *J. Inorg. Biochem.* **1997**, *65*, 267−275.

(14) Thelander, L.; Gräslund, A. Mechanism of inhibition of mammalian ribonucleotide reductase by the iron chelate of 1-formylisoquinoline thiosemicarbazone. Destruction of the tyrosine free radical of the enzyme in an oxygen-requiring reaction. *J. Biol. Chem.* **1983**, *258*, 4063−4066.

(15) Chaston, T. B.; Lovejoy, D. B.; Watts, R. N.; Richardson, D. R. Examination of the antiproliferative activity of iron chelators: multiple cellular targets and different mechanism of action of triapine compared with desferrioxamine and the potent pyridoxal isonicotinoyl hydrazone analogue 311. *Clin. Cancer Res.* **2003**, *9*, 402−414.

(16) Karon, M.; Benedict, W. F. Chromatid breakage: differential effect of inhibitors of DNA synthesis during G$_2$ phase. *Science* **1972**, *178*, 62.

(17) Tsiftsoglou, A. S.; Hwang, K. M.; Agrawal, K. C.; Sartorelli, A. C. Strand scission of sarcoma 180 tumor cell DNA induced by 1-formylisoquinoline thiosemicarbazone. *Biochem. Pharmacol.* **1975**, *24*, 1631−1633.

(18) Miller, M. C., III; Bastow, K. F.; Stineman, C. N.; Vance, J. R.; Song, S. C.; West, D. X.; Hall, I. H. The cytotoxicity of 2-formyl and 2-acetyl-(6-picolyl)-^4N-substituted thiosemicarbazones and their copper(II) complexes. *Arch. Pharm. Pharm. Med. Chem.* **1998**, *331*, 121−127.

(19) Miller, M. C., III; Stineman, C. N.; Vance, J. R.; West, D. X.; Hall, I. H. The cytotoxicity of copper(II) complexes of 2-acetyl-pyridyl-^{4}N-substituted thiosemicarbazones. *Anticancer Res.* **1998**, *18*, 4131−4140.

(20) Miller, M. C., III; Stineman, C. N.; Vance, J. R.; West, D. X.; Hall, I. H. Multiple mechanisms for cytotoxicity induced by copper(II) complexes of 2-acetylpyrazine-*N*-substituted thiosemicarbazones. *Appl. Organomet. Chem.* **1999**, *13*, 9−19.

(21) DeConti, R. C.; Toftness, B. R.; Agrawal, K. C.; Tomchick, R.; Mead, J. A. R.; Bertino, J. R.; Sartorelli, A. C.; Creasey, W. A. Clinical and pharmacological studies with 5-hydroxy-2-formylpyridine thiosemicarbazone. *Cancer Res.* **1972**, *32*, 1455−1462.

(22) Krakoff, I. H.; Etcubanas, E.; Tan, C.; Mayer, K.; Bethune, V.; Burchenal, J. H. Clinical trial of 5-hydroxypicolinaldehyde thiosemicarbazone (5-HP; NSC-107392), with special reference to its iron-chelating properties. *Cancer Chemother. Rep.* **1974**, *58*, 207−212.

(23) Feun, L.; Modiano, M.; Lee, K.; Mao, J.; Marini, A.; Savaraj, N.; Plezia, P.; Almassian, B.; Colacino, E.; Fischer, J.; Mac Donald, S. Phase I and pharmacokinetic study of 3-aminopyridine-2-carboxaldehyde thiosemicarbazone (3-AP) using a single intravenous dose schedule. *Cancer Chemother. Pharmacol.* **2002**, *50*, 223−229.

(24) Giles, F. J.; Fracasso, P. M.; Kantarjian, H. M.; Cortes, J. E.; Brown, R. A.; Verstovsek, S.; Alvarado, Y.; Thomas, D. A.; Faderl, S.; Garcia-Manero, G.; Wright, L. P.; Samson, T.; Cahill, A.; Lambert, P.; Plunkett, W.; Sznol, M.; DiPersio, J. F.; Gandhi, V. Phase I and pharmacodynamic study of triapine, a novel ribonucleotide reductase inhibitor, in patients with advanced leukemia. *Leuk. Res.* **2003**, *27*, 1077−1083.

(25) Murren, J.; Modiano, M.; Clairmont, C.; Lambert, P.; Savaraj, N.; Doyle, T.; Sznol, M. Phase I and pharmacokinetic study of triapine, a potent ribonucleotide reductase inhibitor, administered daily for five days in patients with advanced solid tumors. *Clin. Cancer Res.* **2003**, *9*, 4092−4100.

(26) Wadler, S.; Makower, D.; Clairmont, C.; Lambert, P.; Fehn, K.; Sznol, M. Phase I and pharmacokinetic study of the ribonucleotide reductase inhibitor, 3-aminopyridine-2-carboxaldehyde thiosemicarbazone, administered by 96-hour intravenous continuous infusion. *J. Clin. Oncol.* **2004**, *22*, 1553−1563.

(27) Finch, R. A.; Liu, M.-C.; Grill, S. P.; Rose, W. C.; Loomis, R.; Vasquez, K. M.; Cheng, Y.-C.; Sartorelli, A. C. Triapine (3-aminopyridine-2-carboxaldehyde-thiosemicarbazone): a potent inhibitor of ribonucleotide reductase activity with broad spectrum of antitumor activity. *Biochem. Pharmacol.* **2000**, *59*, 983−991.

(28) Hedley, D. W.; Tripp, E. H.; Slowiaczek, P.; Mann, G. J. Effect of gallium on DNA synthesis by human T-cell lymphoblasts. *Cancer Res.* **1988**, *48*, 3014−3018.

(29) Bernstein, L. R. Mechanisms of therapeutic activity for gallium. *Pharmacol. Rev.* **1998**, *50*, 665−682.

(30) Collery, P.; Keppler, B.; Madoulet, C.; Desoize, B. Gallium in cancer treatment. *Crit. Rev. Oncol. Hematol.* **2002**, *42*, 283−296.

(31) Jakupec, M. A.; Keppler, B. K. Gallium in cancer treatment. *Curr. Top. Med. Chem.* **2004**, *4*, 1575−1583.

(32) Chitambar, C. R.; Narasimhan, J.; Guy, J.; Sem, D. S.; O'Brien, W. J. Inhibition of ribonucleotide reductase by gallium in murine leukemic L1210 cells. *Cancer Res.* **1991**, *51*, 6199−6201.

(33) Narasimhan, J.; Antholine, W. E.; Chitambar, C. R. Effect of gallium on the tyrosyl radical of the iron-dependent M2 subunit of ribonucleotide reductase. *Biochem. Pharmacol.* **1992**, *44*, 2403−2408.

(34) Arion, V. B.; Jakupec, M. A.; Galanski, M.; Unfried, P.; Keppler, B. K. Synthesis, structure, spectroscopic and in vitro antitumour studies of a novel gallium(III) complex with 2-acetylpyridine [4]*N*-dimethylthiosemicarbazone. *J. Inorg. Biochem.* **2002**, *91*, 298−305.

(35) West, D. X.; Lewis, N. C. Transition metal ion complexes of thiosemicarbazones derived from 2-acetylpyridine. Part 2. The [4]N-dimethyl derivative. *Transition Metal. Chem.* **1988**, *13*, 277−290.

(36) Addison, A. W.; Rao, T. N.; Reedijk, J.; Van Rijn, J.; Verschoor, G. C. Synthesis, structure, and spectroscopic properties of copper(II) compounds containing nitrogen-sulfur donor ligands: the crystal and molecular structure of aqua[1,7-bis(N-methylbenzimidazol-2′-yl)-2,6-dithiaheptane]copper(II) perchlorate. *J. Chem. Soc., Dalton Trans.* **1984**, *7*, 1349−1356.

(37) Kowol, C. R.; Arion, V. B.; Keppler, B. K. Unpublished results.

(38) Scovill, J. P.; Klayman, D. L.; Franchino, C. F. 2-Acetylpyridine thiosemicarbazones. 4. Complexes with transition metals as antimalarial and antileukemic agents. *J. Med. Chem.* **1982**, *25*, 1261−1264.

(39) Easmon, J.; Pürstinger, G.; Heinisch, G.; Roth, T.; Fiebig, H. H.; Holzer, W.; Jäger, W.; Jenny, M.; Hofmann, J. Synthesis, cytotoxicity, and antitumor activity of copper(II) and iron(II) complexes of [4]*N*-azabicyclo[3.2.2]nonane thiosemicarbazones derived from acyl diazines. *J. Med. Chem.* **2001**, *44*, 2164−2171.

(40) Easmon, J.; Heinisch, G.; Holzer, W.; Rosenwirth, B. Novel thiosemicarbazones derived from formyl- and acyldiazines: synthesis, effects on cell proliferation, and synergism with antiviral agents. *J. Med. Chem.* **1992**, *35*, 3288−3296.

(41) French, F. A.; Blanz, E. J., Jr. The carcinostatic activity of thiosemicarbazones of formyl heteroaromatic compounds. III. Primary correlation. *J. Med. Chem.* **1966**, *9*, 585−589.

(42) Cory, J. G.; Cory, A. H.; Rappa, G.; Lorico, A.; Liu, M.-C.; Lin, T.-S.; Sartorelli, A. C. Structure-function relationships for a new series of pyridine-2-carboxaldehyde thiosemicarbazones on ribonucleotide reductase activity and tumor cell growth in culture and in vivo. *Adv. Enzyme Regul.* **1995**, *35*, 55−68.

(43) Klayman, D. L.; Scovill, J. P.; Mason, C. J.; Bartosevich, J. F.; Bruce, J.; Lin, A. J. 2-Acetylpyridine thiosemicarbazones. 6. 2-Acetylpyridine and 2-butyrylpyridine thiosemicarbazones as antileukemic agents. *Arzneim.-Forsch./Drug Res.* **1983**, *33*, 909−912.

(44) Schmidt, P. P.; Rova, U.; Katterle, B.; Thelander, L.; Graslund, A. Kinetic evidence that a radical transfer pathway in protein R2 of mouse ribonucleotide reductase is involved in generation of the tyrosyl free radical. *J. Biol. Chem.* **1998**, *273*, 21463−21472.

(45) Schmidt, P. P. Unpublished results.

(46) Nyholm, S.; Thelander, L.; Gräslund, A. Reduction and loss of the iron center in the reaction of the small subunit of mouse ribonucleotide reductase with hydroxyurea. *Biochemistry* **1993**, *32*, 11569−11574.

(47) Klayman, D. L.; Scovill, J. P.; Bartosevich, J. F.; Mason, C. J. 2-Acetylpyridine thiosemicarbazones. 2. N^4,N^4-disubstituted derivates as potential antimalarial agents. *J. Med. Chem.* **1979**, *22*, 1367−1373.

(48) Sheldrick, G. M. *SHELXS-97, Program for Crystal Structure Solution*; University Göttingen: Göttingen, Germany, 1997.

(49) Sheldrick, G. M. *SHELXL-97, Program for Crystal Structure Refinement*; University Göttingen: Göttingen, Germany, 1997.

(50) Johnson, G. K. *Report ORNL-5138*; Oak Ridge National Laboratory: Oak Ridge, TN, 1976.

(51) *International Tables for X-ray Crystallography*; Kluwer Academic Press: Dodrecht, The Netherlands, 1992; Vol. C, Tables 4.2.6.8 and 6.1.1.4.

(52) Hollander, M.; Wolfe, D. A. *Nonparametric statistical inference*, 1st ed.; John Wiley & Sons: New York, 1973; pp 68−75.

JM0612618

Supporting Information

Gallium(III) and Iron(III) Complexes of α-N-heterocyclic Thiosemicarbazones: Synthesis, Characterization, Cytotoxicity and Interaction with Ribonucleotide Reductase

Christian R. Kowol, Roland Berger, Rene Eichinger, Alexander Roller, Michael A. Jakupec, Peter P. Schmidt,[#] Vladimir B. Arion,* Bernhard K. Keppler*

Institute of Inorganic Chemistry, Faculty of Chemistry, University of Vienna,

Waehringer Str. 42, A-1090 Vienna, Austria

[#] Max-Planck Institute for Bioinorganic Chemistry, Stiftstr. 34-38, Mülheim an der

Ruhr, D-45470 Germany

Supporting Information:

Spectroscopic data

2-Acetylpyridine ***N,N*-dimethylthiosemicarbazonato-*N,N,S*-dichlorogallium(III), Ga(L^1)Cl$_2$ (6).** EI-MS, *m/z* (r. i.): 360 (53.7), [M]$^{+\cdot}$; 345 (100), [M-CH$_3$]$^+$; 325 (32.6), [M-Cl]$^+$. IR spectrum in KBr (CsI), cm^{-1}: 1524 s, 1392 s, 1376 s, 1297 s, 1247 s, 356 s and 341 s (Ga-Cl). UV/vis (MeOH), λ_{max}, nm (ε, M^{-1} cm^{-1}): 255 (5540), 303 (8980), 405 (23410). ^{1}H NMR (400.13 MHz, dmso-*d$_6$*): δ = 8.91 (d, 1H, py), 8.33 (t, 1H, py), 8.11 (d, 1H, py), 7.83 (t, 1H, py), 3.28 (br. s, 6H, N(CH$_3$)$_2$), 2.59 (s, 3H, CCH$_3$). ^{13}C NMR (100.63 MHz, dmso-*d$_6$*): δ = 176.1 (C-S), 146.7 (C$_{py}$), 146.3 (C$_{q, py}$), 143.5 (C$_{py}$), 143.1 (C=N), 127.0 (C$_{py}$), 123.9 (C$_{py}$), 41.0 and 38.7 (N(CH$_3$)$_2$), 14.1 (CH$_3$).

2-Acetylpyridine ***N*-pyrrolidinylthiosemicarbazonato-*N,N,S*-dichlorogallium(III), Ga(L^2)Cl$_2$ (7).** EI-MS, *m/z* (r. i.): 386 (98.4), [M]$^{+\cdot}$; 371 (76.0), [M-CH$_3$]$^+$; 351 (72.5), [M-Cl]$^+$. IR spectrum in KBr, cm^{-1}: 1500 s, 1452 s, 1372 s, 1282 s. UV/vis (MeOH), λ_{max}, nm (ε, M^{-1} cm^{-1}): 256 (4950), 306 (8750), 407 (24310). ^{1}H NMR (400.13 MHz, dmso-*d$_6$*): δ = 8.92 (d, 1H, py), 8.33 (t, 1H, py), 8.10 (d, 1H, py), 7.83 (t, 1H, py), 3.68-3.66 (br. m, 4H, N(C$_4$H$_8$)), 2.58 (s, 3H, CCH$_3$), 1.96-1.92 (br. m, 4H, N(C$_4$H$_8$)). ^{13}C NMR (100.63 MHz, dmso-*d$_6$*): δ = 173.1 (C-S), 146.7 (C$_{py}$), 146.5 (C$_{q, py}$), 143.6 (C$_{py}$), 142.5 (C=N), 126.9 (C$_{py}$), 123.9 (C$_{py}$), 50.4, 49.0 and 25.1 (N(C$_4$H$_8$)), 14.0 (CH$_3$).

[Bis-(2-acetylpyridine ***N,N*-dimethylthiosemicarbazonato)-*N,N,S*-gallium(III)] hexafluorophosphate, [Ga(L^1)$_2$]PF$_6$ (8).** ESI-MS in EtOH (positive): *m/z* 511, [GaL$_2$]$^+$. IR spectrum in KBr, cm^{-1}: 1519 s, 1389 s, 1302 s, 1252 s, 843 s and 559 m (P-F). UV/vis (MeOH), λ_{max}, nm (ε, M^{-1} cm^{-1}): 252 (11730), 303 (18770), 406 (44000). ^{1}H NMR (400.13 MHz, dmso-*d$_6$*): δ = 8.25-8.20 (m, 4H, py), 7.92 (d, 2H, py), 7.60-7.54 (m, 2H, py), 3.25 (br. s, 12H, N(CH$_3$)$_2$), 2.83 (s, 6H, CCH$_3$). ^{13}C NMR (100.63 MHz, dmso-*d$_6$*): δ = 176.1 (C-S), 147.4 (C=N), 146.3 (C$_{q, py}$), 145.3 (C$_{py}$), 143.2 (C$_{py}$), 127.8 (C$_{py}$), 124.7 (C$_{py}$), 41.3 and 38.9 (N(CH$_3$)$_2$), 14.9 (CH$_3$).

[Bis-(2-acetylpyridine ***N*-pyrrolidinylthiosemicarbazonato)-*N,N,S*-gallium(III)]hexafluorophosphate, [Ga(L^2)$_2$]PF$_6$ (9).** ESI-MS in MeOH (positive), *m/z* 563, [GaL$_2$]$^+$; ESI-MS in MeOH (negative): *m/z* 145, [PF$_6$]$^-$. IR spectrum in KBr,

cm^{-1}: 1496 s, 1449 s, 1375 s, 1283 s, 841 s and 558 m (P-F). UV/vis (MeOH), λ_{max}, nm (ε, M^{-1} cm^{-1}): 254 (10220) 305 (17110), 409 (43160). ^{1}H NMR (400.13 MHz, dmso-d_6): δ = 8.25-8.19 (m, 4H, py), 7.92 (d, 2H, py), 7.60-7.54 (m, 2H, py), 3.74-3.71 (br. m, 4H, N(C$_4$H$_8$)), 3.62-3.58 (br. m, 2H, N(C$_4$H$_8$)), 3.50-3.44 (br. m, 2H, N(C$_4$H$_8$)), 2.82 (s, 6H, CCH$_3$), 1.94-1.88 (br. m, 8H, N(C$_4$H$_8$)). ^{13}C NMR (100.63 MHz, dmso-d_6): δ = 172.9 (C-S), 147.0 (C=N), 146.0 (C$_{q, py}$), 145.1 (C$_{py}$), 143.1 (C$_{py}$), 127.7 (C$_{py}$), 124.6 (C$_{py}$), 50.8, 49.2 and 25.2 (N(C$_4$H$_8$)), 15.0 (CH$_3$).

[Bis-(acetylpyrazine *N,N*-**dimethylthiosemicarbazonato)-*N,N,S*-gallium(III)] hexafluorophosphate, [Ga(L^3)$_2$]PF$_6$ (10).** ESI-MS in H$_2$O (positive): *m/z* 513, [GaL$_2$]$^+$. IR spectrum in KBr, cm^{-1}: 1537 s, 1509 s, 1397 s, 1298 s, 1257 s, 836 s and 558 m (P-F). UV/vis (MeOH), λ_{max}, nm (ε, M^{-1} cm^{-1}): 242sh (12150), 266 (13350), 323 (27730), 434 (37210). ^{1}H NMR (400.13 MHz, dmso-d_6): δ = 9.53 (d, 2H, pz), 8.86 (d, 2H, pz) 7.91 (dd, 2H, pz), 3.33 and 3.22 (br. s, 12H, N(CH$_3$)$_2$), 2.88 (s, 6H, CCH$_3$). ^{13}C NMR (100.63 MHz, dmso-d_6): δ = 175.7 (C-S), 149.0 (C$_{pz}$), 146.5 (C$_{pz}$), 145.9 (C=N), 140.4 (C$_{q, pz}$), 138,4 (C$_{pz}$), 41.4 and 39.3 (N(CH$_3$)$_2$), 15.0 (CH$_3$).

[Bis-(acetylpyrazine *N*-**pyrrolidinylthiosemicarbazonato)-*N,N,S*-gallium(III)] hexafluorophosphate, [Ga(L^4)$_2$]PF$_6$ (11).** ESI-MS in MeOH (positive): *m/z* 565, [GaL$_2$]$^+$; ESI-MS in MeOH (negative), *m/z* 145, [PF$_6$]$^-$. IR spectrum in KBr, cm^{-1}: 1497 s, 1448 s, 1374 s, 1280 s, 834 s and 557 m (P-F). UV/vis (MeOH), λ_{max}, nm (ε, M^{-1} cm^{-1}): 245sh (10860), 268 (12370), 324 (26980), 437 (37300). ^{1}H NMR (400.13 MHz, dmso-d_6): δ = 9.52 (s, 2H, pz), 8.86 (d, 2H, pz), 7.91 (dd, 2H, pz), 3.77-3.74 (br. m, 4H, N(C$_4$H$_8$)), 3.64-3.58 (br. m, 2H, N(C$_4$H$_8$)), 3.52-3.45 (br. m, 2H, N(C$_4$H$_8$)), 2.86 (s, 6H, CCH$_3$), 1.96-1.91 (br. m, 8H, N(C$_4$H$_8$)). ^{13}C NMR (100.63 MHz, dmso-d_6): δ = 172.3 (C-S), 149.0 (C$_{pz}$), 146.6 (C$_{pz}$), 145.5 (C=N), 140.5 (C$_{q, pz}$), 138,4 (C$_{pz}$), 51.0, 49.6 and 25.2 (N(C$_4$H$_8$)) 15.0 (CH$_3$).

[Bis-(acetylpyrazine *N*-**piperidinylthiosemicarbazonato)-*N,N,S*-gallium(III)] hexafluorophosphate, [Ga(L^5)$_2$]PF$_6$ (12).** ESI-MS in MeOH (positive): *m/z* 593, [GaL$_2$]$^+$; ESI-MS in MeOH (negative): *m/z* 145, [PF$_6$]$^-$. IR spectrum in KBr, cm^{-1}: 1440 s; 1294 s; 1252 s; 841 s and 558 m (P-F). UV/vis (MeOH), λ_{max}, nm (ε, M^{-1} cm^{-1}): 268

(12440), 324 (26530), 437 (37080). ^{1}H NMR (400.13 MHz, dmso-d_6): δ = 9.53 (d, 2H, pz), 8.88 (d, 2H, pz), 7.91 (dd, 2H, pz), 3.88 (br. s, 8H, N(C$_5$H$_{10}$)), 2.87 (s, 6H, CCH$_3$), 1.66-1.57 (br. m, 12H, N(C$_5$H$_{10}$)). ^{13}C NMR (100.63 MHz, dmso-d_6): δ = 174.7 (C-S), 149.2 (C$_{pz}$), 146.7 (C$_{pz}$), 146.2 (C=N), 140.3 (C$_{q, pz}$), 138,4 (C$_{pz}$), 51.0, 47.8, 26.3 and 24.8 (N(C$_5$H$_{10}$)), 15.2 (CH$_3$).

[Bis-(2-acetylpyridine *N*-**pyrrolidinylthiosemicarbazonato)-*N,N,S*-iron(III)] tetrachloroferrate(III), [Fe(L^2)$_2$][FeCl$_4$] (14).** ESI-MS in MeOH (positive): *m/z* 550, [FeL$_2$]$^+$. IR spectrum in KBr, cm^{-1}: 1540 s, 1503 s, 1450 s, 1285 s, 1195 s. UV/vis (MeOH), λ$_{max}$, nm (ε, M^{-1} cm^{-1}): 216sh (48640), 248 (33550), 300 (22370), 331 (23380), 381 (29720), 466sh (9170), 617 (800).

[Bis-(acetylpyrazine *N,N*-**dimethylthiosemicarbazonato)-*N,N,S*-iron(III)] tetrachloroferrate(III), [Fe(L^3)$_2$][FeCl$_4$] (15).** ESI-MS (positive): *m/z* 500, [FeL$_2$]$^+$; ESI-MS (negative): *m/z* 196, [FeCl$_4$]$^-$. IR spectrum in KBr (CsI), cm^{-1}: 1554 s, 1524 s, 1400 s, 1307 s, 1258 s, 384 s (Fe-Cl). UV/vis (MeOH), λ$_{max}$, nm (ε, M^{-1} cm^{-1}): 222sh (39810), 255sh (31310), 303sh (23600), 325 (24790), 402 (23470), 503sh (7910), 636 (690), 957 (500).

[Bis-(acetylpyrazine *N*-**pyrrolidinylthiosemicarbazonato)-*N,N,S*-iron(III)] tetrachloroferrate(III), [Fe(L^4)$_2$][FeCl$_4$] (16).** ESI-MS in MeOH (positive): *m/z* 552, [FeL$_2$]$^+$. IR spectrum in KBr, cm^{-1}: 1546 s, 1519 s, 1449 s, 1282 s. UV/vis (MeOH), λ$_{max}$, nm (ε, M^{-1} cm^{-1}): 221sh (46410), 257sh (35740), 301sh (26760), 330 (28410), 407 (27740), 502sh (9810), 654 (870).

[Bis-(acetylpyrazine *N*-**piperidinylthiosemicarbazonato)-*N,N,S*-iron(III)] tetrachloroferrate(III), [Fe(L^5)$_2$][FeCl$_4$] (17).** ESI-MS in MeOH (positive): *m/z* 580, [FeL$_2$]$^+$; ESI-MS in MeOH (negative): *m/z* 196, [FeCl$_4$]$^-$. IR spectrum in KBr, cm^{-1}: 1517 s, 1440 s, 1302 s, 1249 s, 1150 s. UV/vis (MeOH), λ$_{max}$, nm (ε, M^{-1} cm^{-1}): 227 (43060), 257sh (34460), 302sh (26160), 324 (27280), 408 (27510), 503sh (8820), 660 (860).

[Bis-(2-acetylpyridine *N,N*-dimethylthiosemicarbazonato)-*N,N,S*-iron(III)] **hexafluorophosphate, [Fe(L^1)$_2$]PF$_6$ (18).** ESI-MS in H$_2$O (positive): *m/z* 498, [FeL$_2$]$^+$. IR spectrum in KBr, cm^{-1}: 1554 s, 1400 s, 1315 s, 1250 s, 840 s and 558 m (P-F). UV/vis (MeOH), λ_{max}, nm (ε, M^{-1} cm^{-1}): 217sh (46680), 248 (30710), 300 (20570), 330 (20910), 378 (26770), 464sh (9410), 612 (850), 894 (540).

[Bis-(2-acetylpyridine *N*-pyrrolidinylthiosemicarbazonato)-*N,N,S*-iron(III)] **hexafluorophosphate, [Fe(L^2)$_2$]PF$_6$ (19).** ESI-MS in MeOH (positive): *m/z* 550, [FeL$_2$]$^+$; ESI-MS in MeOH (negative): *m/z* 145, [PF$_6$]$^-$. IR spectrum in KBr, cm^{-1}: 1503 s, 1452 s, 1291 s, 839 s and 558 m (P-F). UV/vis (MeOH), λ_{max}, nm (ε, M^{-1} cm^{-1}): 217sh (43770), 249 (28800), 299 (18820), 330 (19230), 383 (26280), 465sh (9000), 617 (800).

[Bis-(acetylpyrazine *N,N*-dimethylthiosemicarbazonato)-*N,N,S*-iron(III)] **hexafluorophosphate), [Fe(L^3)$_2$]PF$_6$ (20).** ESI-MS (positive): *m/z* 500, [FeL$_2$]$^+$. IR spectrum in KBr, cm^{-1}: 1558 s, 1527 s, 1403 s, 1309 s, 1259 s, 843 s and 558 m (P-F). UV/vis (MeOH), λ_{max}, nm (ε, M^{-1} cm^{-1}): 222sh (32780), 255sh (25090), 303sh (19040), 324 (19660), 404 (20280), 501sh (7210), 636 (770).

[Bis-(acetylpyrazine *N*-pyrrolidinylthiosemicarbazonato)-*N,N,S*-iron(III)] **hexafluorophosphate, [Fe(L^4)$_2$]PF$_6$ (21).** ESI-MS in MeOH (positive): *m/z* 552, [FeL$_2$]$^+$. IR spectrum in KBr, cm^{-1}: 1552 s, 1449 s, 1285 s, 848 s and 557 m (P-F). UV/vis (MeOH), λ_{max}, nm (ε, M^{-1} cm^{-1}): 223sh (36240), 256sh (26950), 301sh (20280), 328 (21240), 411 (22540), 502sh (8400), 659 (790).

[Bis-(acetylpyrazine *N*-piperidinylthiosemicarbazonato)-*N,N,S*-iron(III)] **hexafluorophosphate, [Fe(L^5)$_2$]PF$_6$ (22).** . ESI-MS (positive): *m/z* 580, [FeL$_2$]$^+$; ESI-MS in MeOH (negative): *m/z* 145, [PF$_6$]$^-$. IR spectrum in KBr, cm^{-1}: 1520 s, 1437 s, 1307 s, 1249 s, 845 s and 558 m (P-F). UV/vis (MeOH), λ_{max}, nm (ε, M^{-1} cm^{-1}): 227 (38630), 257sh (30120), 301sh (22750), 324 (23690), 410 (25980), 503sh (8690), 642 (870).

Table S1. Microanalytical data.

| Substance number	Theory	Found
6	C: 33.19, H: 3.62, N: 15.48.	C: 33.33, H: 3.38, N: 15.24
7	C: 37.15, H: 3.90, N: 14.44, S: 8.26.	C: 36.88, H: 3.80, N: 14.44, S: 8.17.
8	C: 36.55, H: 3.99, N: 17.05.	C: 36.28, H: 3.86, N: 16.80.
9	C: 40.64, H: 4.26, N: 15.80, S: 9.04.	C: 40.62, H: 4.13, N: 15.82, S: 8.91.
10	C: 32.79, H: 3.67, N: 21.25.	C: 32.77, H: 3.45, N: 20.98.
11	C: 37.15, H: 3.97, N: 19.69, S: 9.02.	C: 37.26, H: 3.86, N: 19.48, S: 8.90.
12	C: 38.99, H: 4.36, N: 18.94, S: 8.67.	C: 39.31, H: 4.40, N: 18.60, S: 8.48.
14	C: 38.53, H: 4.04, N: 14.98, S: 8.57.	C: 38.59, H: 4.04, N: 14.95, S: 8.45.
15	C: 30.97, H: 3.47, N: 20.06	C: 31.25, H: 3.43, N: 19.99.
16	C: 35.22, H: 3.76, N: 18.67, S: 8.55.	C: 35.41, H: 3.76, N: 18.40, S: 8.51.
17	C: 37.04, H: 4.14, N: 18.00, S: 8.24.	C: 36.86, H: 3.96, N: 17.69, S: 8.44.
18	C: 37.33, H: 4.07, N: 17.42.	C: 37.03, H: 3.86, N: 17.20.
19	C: 41.45, H: 4.35, N: 16.11, S: 9.22.	C: 41.22, H: 4.50, N: 15.68, S: 8.96.
20	C: 33.50, H: 3.75, N: 21.70	C: 33.43, H: 3.48, N: 21.42.
21	C: 37.88, H: 4.05, N: 20.08, S: 9.19.	C: 38.18, H: 4.02, N: 19.83, S: 9.13.
22	C: 39.73, H: 4.45, N: 19.31, S: 8.84.	C: 39.70, H: 4.55, N: 19.10, S: 8.93.

UV/vis spectra.
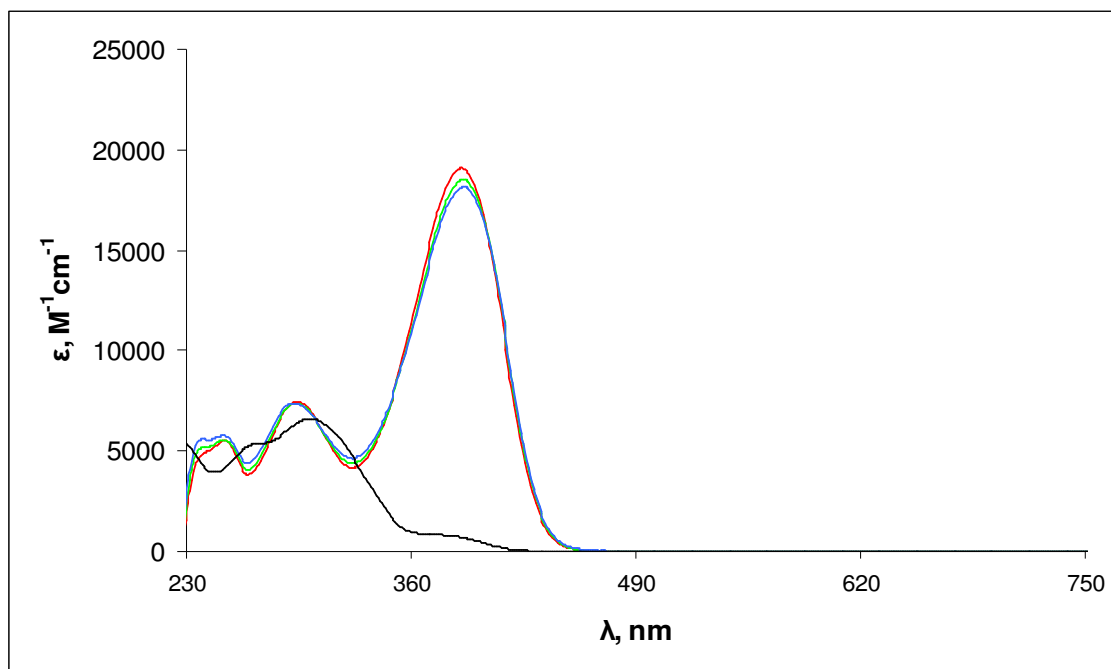
Figure S1. UV/vis spectroscopy data of **1** (black) and **6** in DMSO/H$_2$O 1 : 100.
First measurement of **6** (red), after 30 minutes (green), after 15 hours (blue).
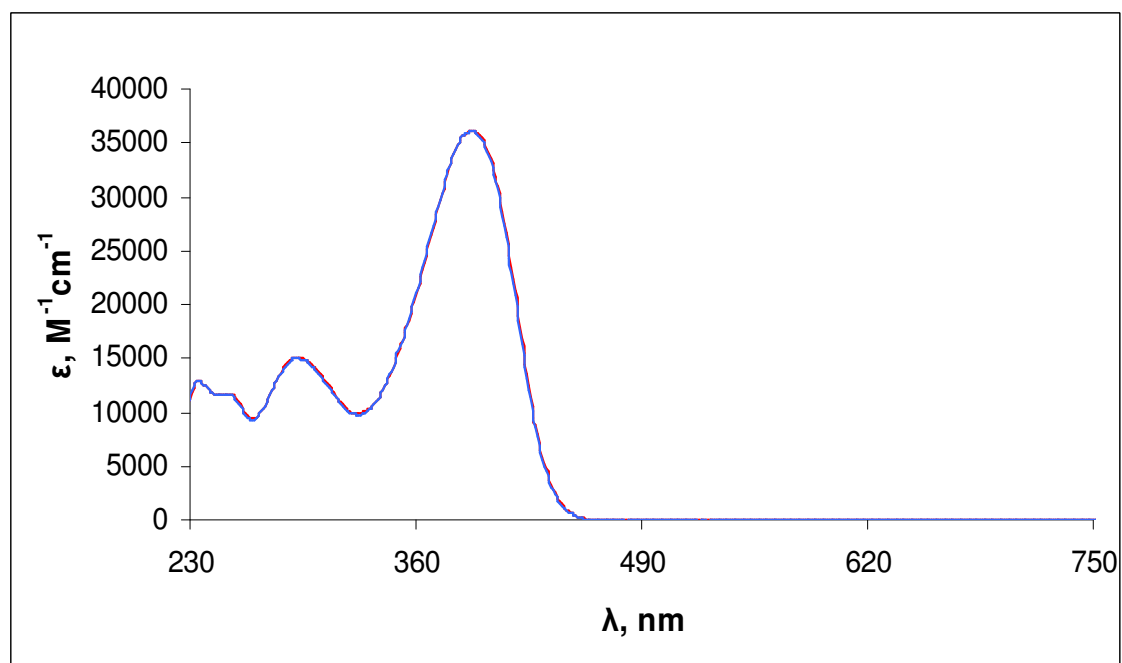

Figure S2. UV/vis spectroscopy data of **8** in DMSO/H$_2$O 1 : 100.
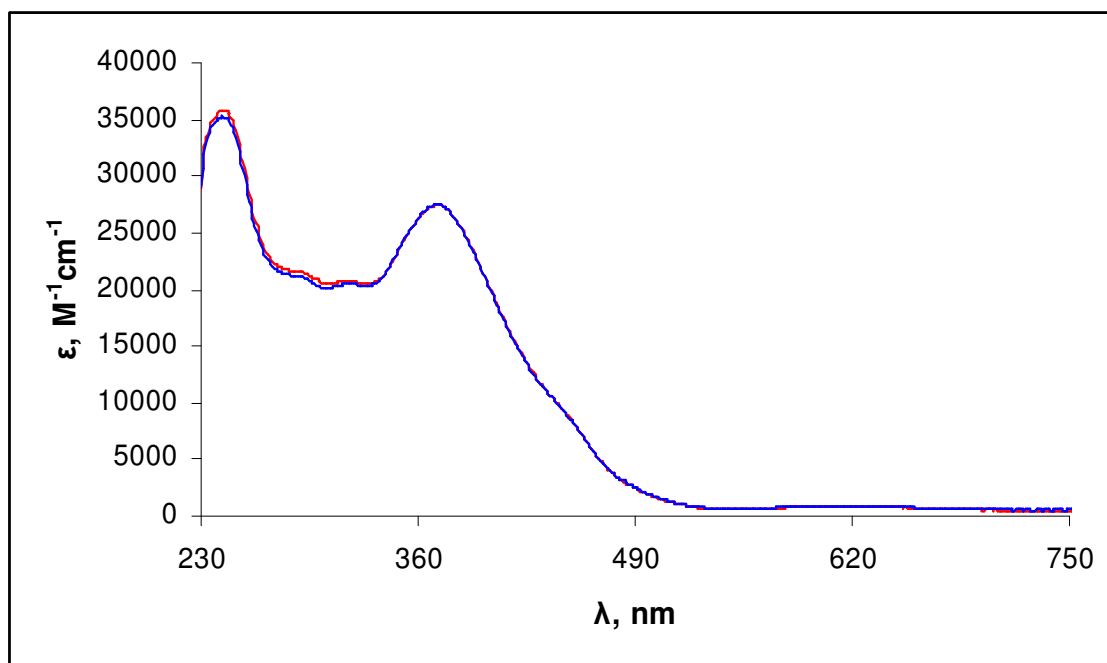First measurement (red), after 15 hours (blue).

Figure S3. UV/vis spectroscopy data of **14** in DMSO/H₂O 1 : 100.
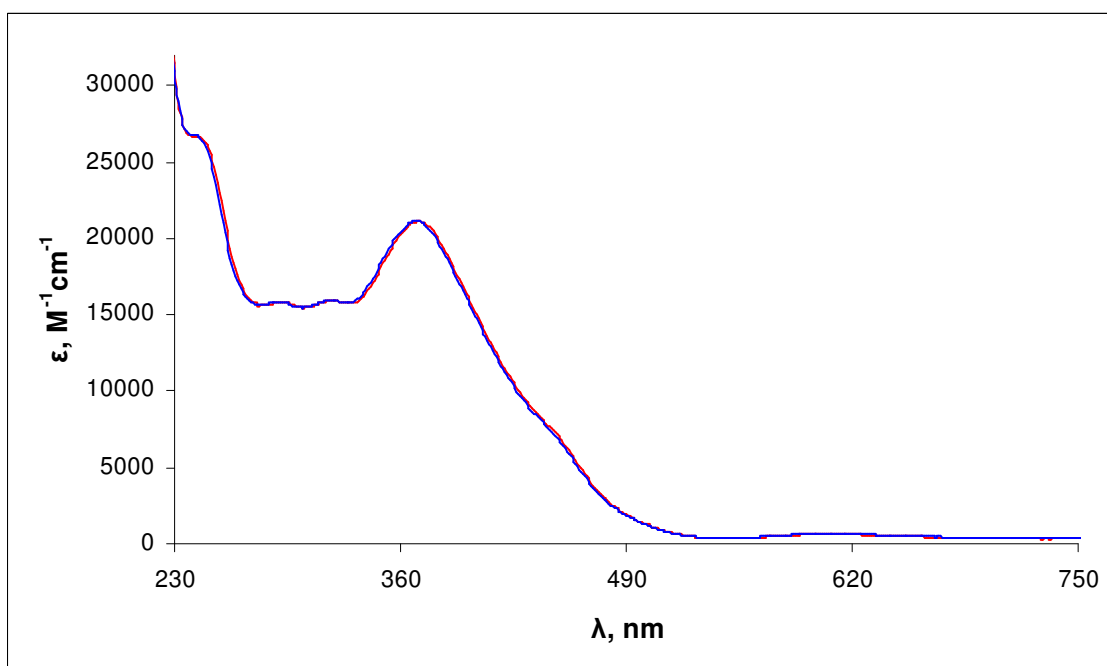First measurement (red), after 15 hours (blue).

Figure S4. UV/vis spectroscopy data of **18** in DMSO/H₂O 1 : 100.
First measurement (red), after 15 hours (blue).

X-Ray crystallographic data

Table S2. Details of data collection for **6, 10, 11, 13, 15-18, 21**.

Complex	6	10	11	13	15	16	17	18	21
Number of frames	265	389	502	344	216	379	379	1213	379
Seconds/frame	250	65	60	70	200	15	95	40	50
Scan width	2	2	1.5	2	2	2	2	1	2
Distance from the detector	30	30	30	30	30	30	30	37.5	30

Table S3. Crystal Data for **6, 10, 11, 13, 15**.

Complex	6	10	11·CHCl$_3$	13	15
empirical formula	C$_{10}$H$_{13}$Cl$_2$GaN$_4$S	C$_{18}$H$_{24}$F$_6$GaN$_{10}$PS$_2$	C$_{23}$H$_{29}$Cl$_3$F$_6$GaN$_{10}$PS$_2$	C$_{20}$H$_{26}$Cl$_4$Fe$_2$N$_8$S$_2$	C$_{18}$H$_{24}$Cl$_4$Fe$_2$N$_{10}$S$_2$
Fw	361.93	659.27	830.72	696.11	698.08
space group	$Pna2_1$	$P\bar{1}$	$P2_1/n$	$P2_1/n$	$P2_1/n$
a, Å	12.922(3)	8.699(2)	19.105(4)	14.831(3)	14.824(3)
b, Å	14.760(3)	11.906(2)	8.833(2)	13.259(3)	13.113(3)
c, Å	7.4060(10)	12.967(3)	19.865(4)	15.009(3)	15.004(3)
α, deg		79.31(3)			
β, deg		78.05(3)	102.00(3)	107.82(3)	109.27(3)
γ, deg		82.03(3)			
V, Å^3	1412.5(5)	1284.1(5)	3279.1(12)	2809.8(10)	2753.2(10)
Z	4	2	4	4	4
λ, Å	0.71073	0.71073	0.71073	0.71073	0.71073
ρ_{calcd}, g cm^{-3}	1.702	1.705	1.683	1.646	1.684
crystal size, mm^3	0.08 × 0.08 × 0.01	0.37 × 0.17 × 0.06	0.29 × 0.20 × 0.06	0.10 × 0.10 × 0.04	0.20 × 0.20 × 0.04
T, K	200	120	120	120	120
μ, mm^{-1}	2.461	1.371	1.329	1.589	1.623
R1^a	0.0313	0.0315	0.0347	0.0256	0.0362
wR2^b	0.0648	0.0790	0.0891	0.0706	0.0890
GOF^c	1.031	1.041	1.043	1.057	1.040

Table S4. Crystal Data and Details of Data Collection for **16, 17, 18, 21.**

Complex	**16·CHCl₃**	**17·CHCl₃**	**18**	**21**
empirical formula	$C_{23}H_{29}Cl_7Fe_2N_{10}S_2$	$C_{25}H_{33}Cl_7Fe_2N_{10}S_2$	$C_{20}H_{26}F_6FeN_8PS_2$	$C_{22}H_{28}F_6FeN_{10}PS_2$
Fw	869.53	897.59	643.42	697.47
space group	$P\bar{1}$	$P\bar{1}$	$P2_1/c$	$P2_1/n$
a, Å	8.880(2)	10.956(2)	8.4265(2)	12.609(3)
b, Å	13.369(3)	11.464(2)	17.9472(5)	12.979(3)
c, Å	15.996(3)	16.644(3)	18.4968(5)	18.280(4)
α, deg	79.39(3)	101.45(3)		
β, deg	76.45(3)	102.72(3)	100.4230(10)	106.05(3)
γ, deg	73.03(39)	110.98(3)		
V, Å³	1752.0(6)	1813.6(6)	2751.15(13)	2875.0(11)
Z	2	2	4	4
λ, Å	0.71073	0.71073	0.71073	0.71073
ρ_{calcd}, g cm⁻³	1.648	1.644	1.553	1.611
crystal size, mm³	$0.20 \times 0.17 \times 0.14$	$0.20 \times 0.09 \times 0.06$	$0.22 \times 0.14 \times 0.04$	$0.26 \times 0.17 \times 0.11$
T, K	120	120	100	120
μ, mm⁻¹	1.515	1.466	0.825	0.799
R1^a	0.0416	0.0373	0.0358	0.0375
wR2^b	0.1068	0.0915	0.0860	0.0986
GOF^c	1.041	1.031	1.006	1.068

^{a} R1 = $\Sigma||F_o| - |F_c||/\Sigma|F_o|$, ^{b} wR2 = $\{\Sigma[w (F_o^2 - F_c^2)^2] /\Sigma[w(F_o^2)^2]\}^{1/2}$. ^{c} GOF = $\{\Sigma[w(F_o^2 - F_c^2)^2] /(n - p)\}^{1/2}$, where n is the number of reflections and p is the total number of parameters refined.

Details of crystal structures of 6, 10, 11·CHCl$_3$, 13, 15, 16·CHCl$_3$, 17·CHCl$_3$, 18 and 21

The structure of **15** consists of the complex cations [Fe(L^3)$_2$]$^+$ and anions [FeCl$_4$]$^-$. An ORTEP drawing of [Fe(L^3)$_2$]$^+$ is shown in Figure 3. The iron atom is coordinated by the two approximately planar tridentate ligands. The coordination polyhedron approaches an octahedron, where the two ligands are bound to Fe(1) atom through a nitrogen atom of the pyrazine ring, and a nitrogen and sulphur atom of the thiosemicarbazide group in a meridional arrangement. The pattern of coordination is similar to that observed in [FeL$_2$][FeCl$_4$] (LH = 2-acetylpyridine *N*-pyrrolidinylthiosemicarbazone)[1]. The two sulphur atoms are located in *cis*-positions because of the planarity of the tridentate ligand. On coordination of two L$^-$ to iron(III) four five-membered chelate rings are formed: two C$_2$N$_2$Fe and two N$_2$CSFe (Fe1-N1-C4-C5-N3, Fe1-N3-N4-C7-S1, Fe1-N6-C13-C14-N8 and Fe1-N78-N9-C16-S2). The formation of four five membered chelate rings is presumably the reason for some distortion of the coordination geometry from an ideal octahedron[2]. Note that the angles ∠N1-Fe-S1 at 164.46(9)° and ∠N6-Fe-S2 at 165.74(10)° deviate markedly from the ideal value of 180°. The reason might be some repulsion between S1 and S2. The angle ∠N3-Fe-N8 is at 178.79(13)°.

There is a slight shortening of the bond distance between iron and the nitrogen of the pyridine ring (1.910(3) and 1.918(3) Å) compared to the distance between iron and the nitrogen in the thiosemicarbazide chain (1.979(3) and 1.988(3) Å).

The C-S bond distances C7-S1 at 1.760(4) Å and C16-S2 at 1.761(4) Å are longer compared to those reported in metal-free thiosemicarbazones (1.678(2) Å in 4-formylpyridine thiosemicarbazone, 1.692(4) in 2-acetylpyridine-*N*-pyrrolidinyl thiosemicarbazone or 1.707 Å in thiosemicarbazide)[1,3] indicating an increase of single-bond character for C-S bond in [Fe(L^3)$_2$][FeCl$_4$].

The geometric parameters of the cations of **13, 16 – 18** and **21** are very similar to those of **15**.

The structure of **10** consists of the complex cations [Ga(L^3)$_2$]$^+$ and the complex anions [PF$_6$]$^-$. The structure of the cation is shown in Figure 3. Like iron in complexes **13-22** the gallium atom is coordinated by two tridentate ligands in octahedral manner.

The angles ∠N1-Ga1-S1 and ∠N6-Ga1-S2 at 160.02(5)° and 159.77(5)° deviate markedly from the ideal value of 180° (the deviation is about 5° larger in comparison to the iron complexes). The angle ∠N3-Ga1-N8 is at 162.37(6)°, which differs by ca. 20° from the corresponding angles in the iron complexes.

There is also a slight shortening of the bond distance between gallium and the nitrogen of the pyridine ring (2.0361(17) and 2.0372(17) Å) compared to the distance between gallium and the nitrogen in the thiosemicarbazide fragment (2.1407(17) and 2.1639(16) Å). The Ga-N lengths are longer than the corresponding Fe-N distances.

The C-S bonds distances C7-S1 at 1.754(2) and C16-S2 at 1.745(2) Å are slightly shorter than in the analogous iron complexes, but there is also an increase of single-bond character for C-S bond in $[Ga(L^3)_2]^+$ in comparison to metal free thiosemicarbazones.

In conclusion the coordination polyhedron of this gallium(III) complex is different from that for the corresponding iron(III) complexes. The deviation from the ideal octahedron is more evident.

Complex **11** shows very similar geometric parameters to those of complex **10**.

The structure of the 1 : 1-complex **6** is shown in Figure 2. The gallium atom is coordinated by one approximately planar tridentate thiosemicarbazone and two chloro ligands. The thiosemicarbazone ligand is bound to the gallium atom in the same manner as in the 1 : 2-complexes (N,N,S - coordination).

The angle ∠N1-Ga1-S1 at 155.27(11)° shows the strongest deviation from the ideal value of 180° of all complexes. There is also a marked difference between Ga1-N1 at 2.049(3) Å and Ga1-N2 at 2.100(3) Å. The same picture as observed for complexes of 1 : 2 stoichiometry.

The C8-S1 at 1.740(4) Å is in the range of the bond length in the gallium 1 : 2-complexes. The angles ∠N2-Ga1-Cl1 and ∠N2-Ga1-Cl2 are different at 110.44(14)° and 138.14(14)°, respectively. The Ga1-Cl1 is at 2.1958(13) Å and Ga1-Cl2 at 2.2244(13) Å.

References:

(1) Sreekanth, A.; Fun, H-K.; Kurup, M.R.P. *Journal of Molecular Structure* **2005**, *737*, 61.

(2) Mathew, M.; Palenik, G. J. *J. Am. Chem. Soc.* **1969**, *91*, 6310

(3) Ryabova, N.A; Ponomarev, V.I.; Atovmyan, L.O.; Zelentsov, V.V.; Shipilov. V.I. *Zh. Koord. Khim.* **1978**, *4,* 119.
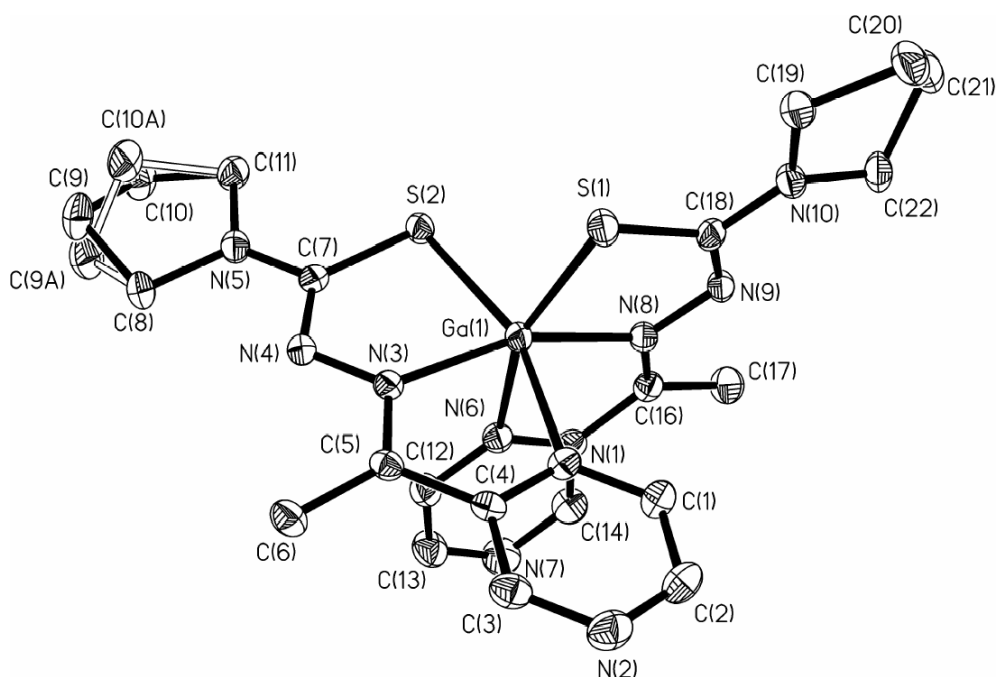
Figure S5. ORTEP drawing of [GaL$_2$]$^+$ (HL = acetylpyrazine *N*-pyrrolidinyl thiosemicarbazone) (**11**) with thermal ellipsoids depicted at 50% probability.

Figure S6. ORTEP drawing of [FeL$_2$]$^+$ (HL = 2-acetylpyridine *N,N*-dimethyl thiosemicarbazone) (**13**) with thermal ellipsoids depicted at 50% probability.

Figure S7. ORTEP drawing of [FeL$_2$]$^+$ (HL = acetylpyrazine *N*-pyrrolidinyl thiosemicarbazone) (**16**) with thermal ellipsoids depicted at 50% probability.

Figure S8. ORTEP drawing of [FeL$_2$]$^+$ (HL = acetylpyrazine *N*-piperidinyl thiosemicarbazone) (**17**) with thermal ellipsoids depicted at 50% probability.
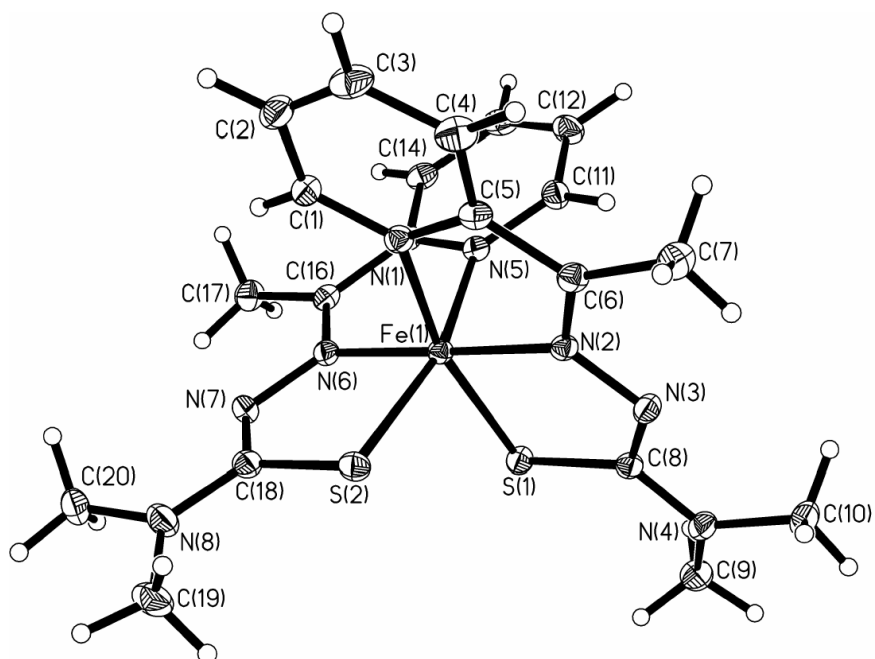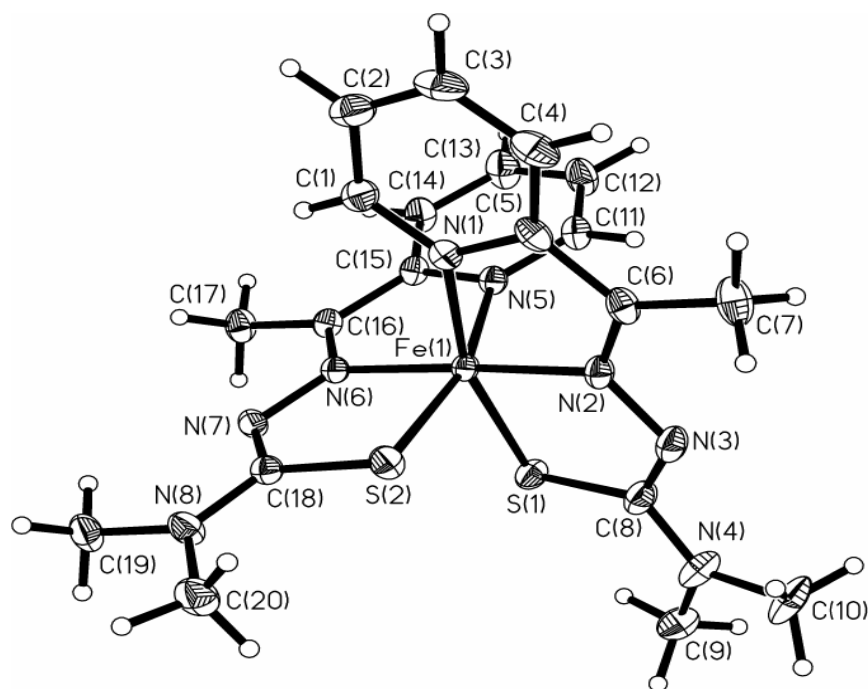
Figure S9. ORTEP drawing of $[FeL_2]^+$ (HL = 2-acetylpyridine *N,N*-dimethyl thiosemicarbazone) (**18**) with thermal ellipsoids depicted at 50% probability.
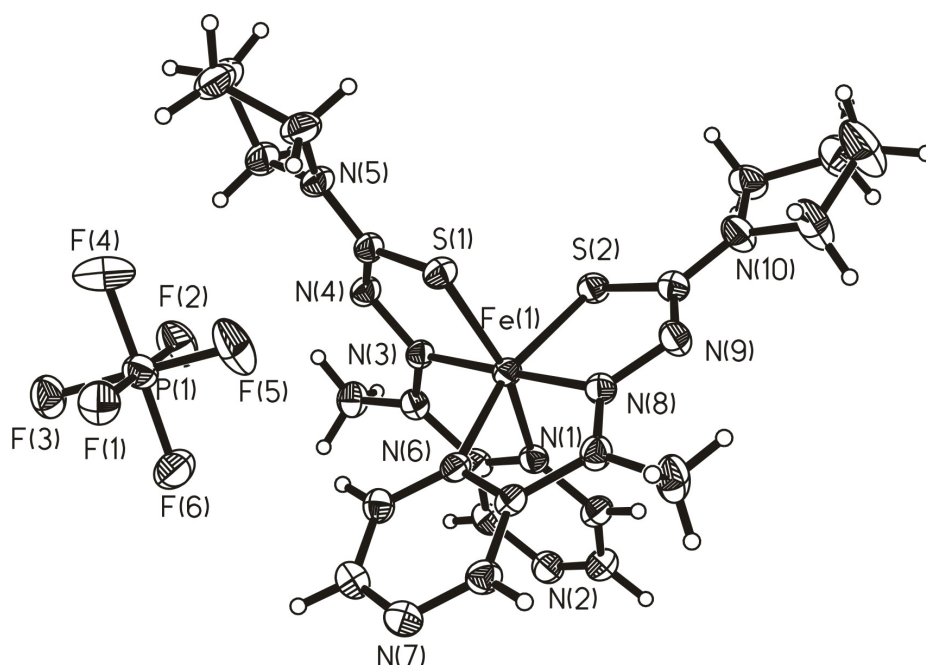
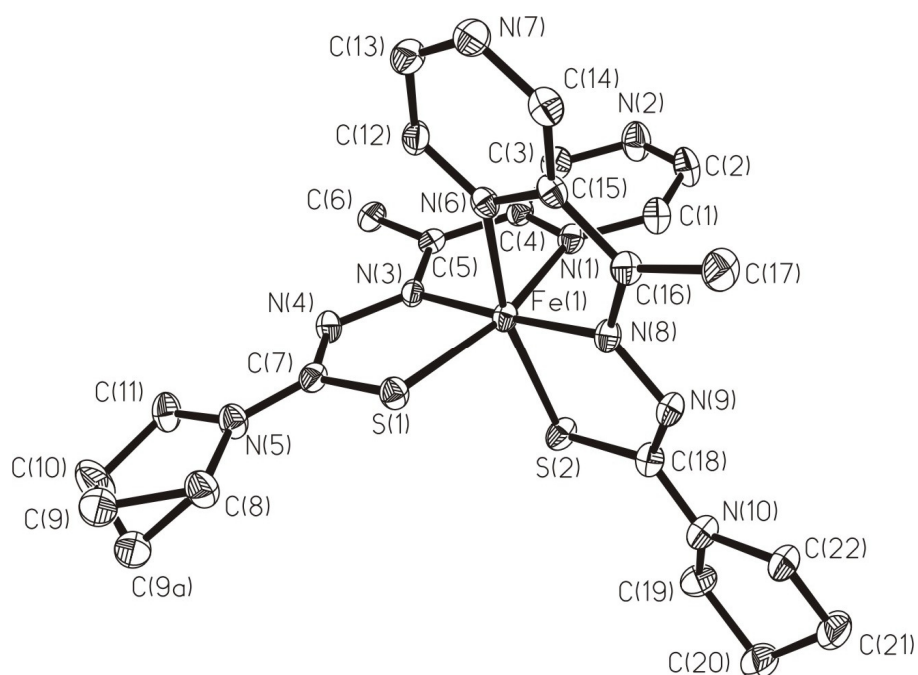**Figure S10.** ORTEP drawing of $[FeL_2][PF_6]$ (HL = acetylpyrazine *N*-pyrrolidinyl thiosemicarbazone) (**21**) with thermal ellipsoids depicted at 50% probability.
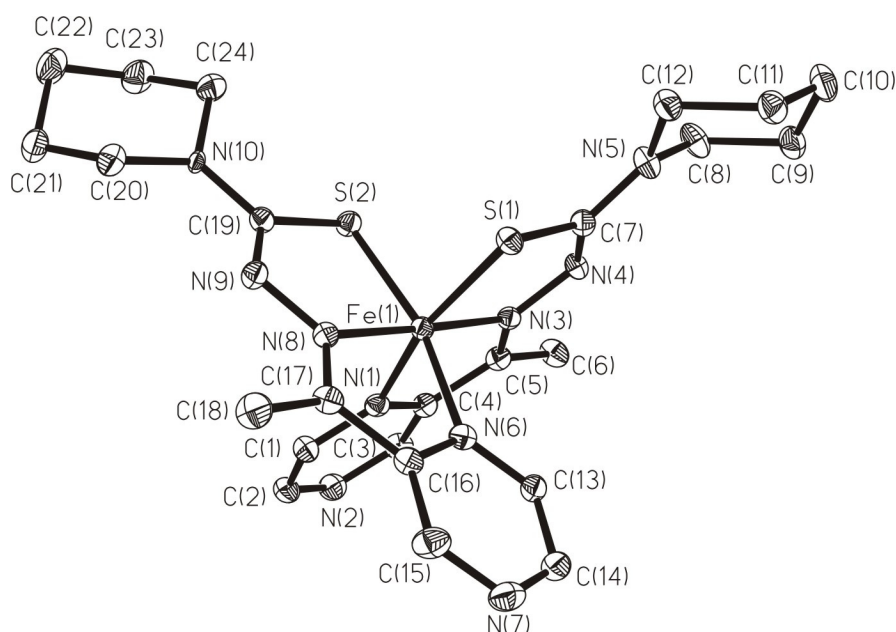
2.2 Effect of Metal Ion Complexation and Chalcogen Donor Identity on the Antiproliferative Activity of 2-Acetylpyridine N,N-Dimethyl-(chalcogen)semicarbazones

Kowol, C. R.; Eichinger, R.; Jakupec, M. A.; Galanski, M.; Arion, V. B.; Keppler, B. K. *J. Inorg. Biochem.* **2007**, *101*, 1946–1957.

Effect of metal ion complexation and chalcogen donor identity on the antiproliferative activity of 2-acetylpyridine N,N-dimethyl(chalcogen)semicarbazones

Christian R. Kowol, Rene Eichinger, Michael A. Jakupec, Markus Galanski, Vladimir B. Arion *, Bernhard K. Keppler *

Institute of Inorganic Chemistry, Faculty of Chemistry, University of Vienna, Waehringer Str. 42, A-1090 Vienna, Austria

This paper is dedicated to the memory of Edward I. Stiefel.

Abstract

Three chalcogensemicarbazones, viz., 2-acetylpyridine N,N-dimethylsemicarbazone (HL[1]), 2-acetylpyridine N,N-dimethylthiosemicarbazone (HL[2]) and 2-acetylpyridine N,N-dimethylselenosemicarbazone (HL[3]), their corresponding gallium(III) complexes [Ga(L[1–3])$_2$]PF$_6$ and the ruthenium(III) compound [Ru(L[2])$_2$]PF$_6$ have been prepared and characterised by X-ray crystallography and spectroscopic techniques (IR, UV/vis, ^{1}H, ^{13}C, ^{15}N, ^{77}Se NMR) in order to elucidate the effect of metal ion complexation and chalcogen donor identity on the cytotoxicity of chalcogensemicarbazones in two human tumour cell lines 41M (ovarian carcinoma) and SK-BR-3 (mammary carcinoma).
© 2007 Elsevier Inc. All rights reserved.

Keywords: Antitumour agents; Gallium; Ruthenium; Thiosemicarbazone; X-ray diffraction
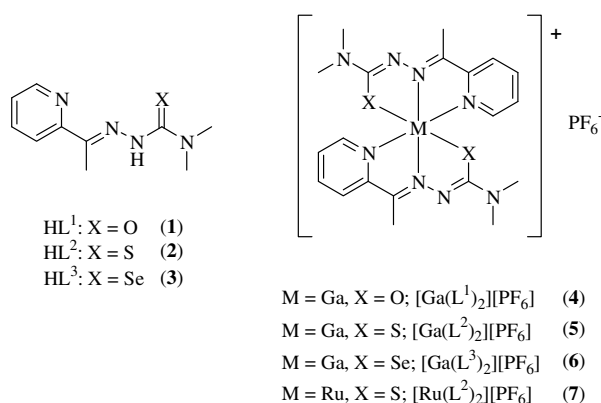
1. Introduction

α-N-Heterocyclic thiosemicarbazones possess a wide range of pharmacological properties, including antitumour, antimalarial, antibacterial, antifungal and antiviral activity [1]. Pyridine-2-carbaldehyde thiosemicarbazone, the first α-N-heterocyclic thiosemicarbazone with antitumour properties, has been reported half a century ago [2]. The enzyme ribonucleotide reductase (RR) has been identified as the principal target for this class of compounds [3,4]. The paramount role of the ribonucleotide reductase in DNA synthesis and the high expression in tumour cells, has made it a suitable and well established target in cancer chemotherapy [5]. The ribonucleotide reductase-inhibiting activity of α-N-heterocyclic thiosemicarbazones was supposed to be due to their pronounced iron-chelating properties, which enable sequestering of iron from the R2 subunit of the enzyme or prior formation of an iron complex, which then inhibits the enzyme [6]. In addition, iron-dependent free radical damage of RR in the case of 3-amino-pyridine-2-carboxaldehyde-thiosemicarbazone (3-AP, triapine) has also been suggested to be responsible for the observed inhibiting activity [7].

Thiosemicarbazones and their derivatives are versatile ligands as they exhibit various binding modes with transition and some main group metals. They can act as mono- or bidentate ligands binding to metal ions via different donor atoms. The coordination capacity of thiosemicarbazones can be further increased, if aldehydes or ketones, which contain additional functional group(s) in position(s) suitable for chelation, are used for their preparation [8].

---

* Corresponding authors.

E-mail addresses: vladimir.arion@univie.ac.at (V.B. Arion), bernhard.keppler@univie.ac.at (B.K. Keppler).

HL^1: X = O **(1)**
HL^2: X = S **(2)**
HL^3: X = Se **(3)**

M = Ga, X = O; [Ga(L^1)$_2$][PF$_6$] **(4)**
M = Ga, X = S; [Ga(L^2)$_2$][PF$_6$] **(5)**
M = Ga, X = Se; [Ga(L^3)$_2$][PF$_6$] **(6)**
M = Ru, X = S; [Ru(L^2)$_2$][PF$_6$] **(7)**

Scheme 1.

We recently synthesised a series of gallium(III) and iron(III) complexes of the general formula [ML$_2$][PF$_6$] with five different α-N-heterocyclic N,N-disubstituted thiosemicarbazones (HL), which use for coordination the NNS donor atom set, and found that the central metal ion has a pronounced but different effect on the cytotoxicity of the ligands [9]. Gallium(III) acts in a synergistic way with the thiosemicarbazones and enhances the cytotoxicity, whereas complexation to iron(III) results in a marked attenuation of the antiproliferative activity. Remarkably, we observed a reversed order of mouse R2 tyrosyl radical (Y*) quenching kinetics by gallium(III) and iron(III) thiosemicarbazonates in the presence of dithiothreitol. Structural modifications of the thiosemicarbazone (replacement of pyridine ring by pyrazine, and variation of substituents at the terminal N4-atom of the thiosemicarbazide moiety) have little impact on their antiproliferative activity *in vitro*, indicating a comparable manner of their interaction with a biological target. Extending this work on structure–activity relationships, we decided to study the effect of the chalcogen donor on the antiproliferative activity of both metal-free 2-acetylpyridine (chalcogen)semicarbazones and their gallium(III) complexes of 2:1 stoichiometry. In addition, the focus has been set on the elucidation of the effect of thiosemicarbazone coordination to metal ions other than gallium(III) and iron(III), and specifically to ruthenium(III), on cytotoxicity.

In order to carry out these investigations, we prepared the required 2-acetylpyridine (chalcogen)semicarbazones and their gallium(III) and ruthenium(III) complexes (Scheme 1), providing a detailed spectroscopic (IR, UV/vis, ^{1}H, ^{13}C, ^{15}N and ^{77}Se NMR) and structural characterisation (X-ray diffraction) of the novel compounds, and evaluated their antiproliferative activity in two human cancer cell lines (41M and SK-BR-3).

2. Experimental section

2.1. Materials and methods

All solvents and reagents were obtained from commercial suppliers and used without further purification. Ga(NO$_3$)$_3$ ·

8.15H$_2$O was purchased from Sigma–Aldrich. The amount of water was determined by thermogravimetric analysis. *N,N*-dimethylsemicarbazide, [10] [(DMSO)$_2$H][*trans*-RuCl$_4$(DMSO)$_2$], [11] and [Ga(L^2)$_2$][PF$_6$] [9] (**5**) have been prepared as described in the literature. CHN elemental analyses were carried out on a Perkin–Elmer 2400 CHN elemental analyser and CHNS on a Carlo Erba EA 1108 CHNS-O microanalyser at the Microanalytical Laboratory of the University of Vienna. Electrospray ionisation mass spectrometry was carried out with a Bruker Esquire 3000 instrument (Bruker Daltonic, Bremen, Germany). Electron impact mass spectra were measured on a Finnigan MAT 8230 mass spectrometer (Bremen, Germany), with an ionisation energy of 70 eV. Expected and experimental isotope distributions were compared. Infrared spectra were obtained from KBr pellets with a Perkin–Elmer FT-IR 2000 instrument (4000–400 cm^{-1}). Abbreviations used for IR spectra: s, strong; m, medium. UV/visible (UV/vis) spectra were recorded on a Perkin–Elmer Lambda 650 UV/vis spectrophotometer, using samples dissolved in methanol (900–200 nm). For stability measurements the samples were dissolved in DMSO and diluted with water such that the final DMSO content was 1%. Thermogravimetric analysis (TGA) and differential thermal analysis (DTA) measurements were carried out simultaneously with a Mettler Toledo TGA/SDTA851e apparatus, with a 3 °C/min heating rate under an air or nitrogen atmosphere. ^{1}H, ^{13}C, ^{15}N and ^{77}Se one- and two-dimensional NMR spectra were recorded in DMSO-d_6 with a 500 MHz Bruker FT-NMR spectrometer Avance III. The residual ^{1}H and ^{13}C present in DMSO-d_6 were used as internal references. ^{15}N and ^{77}Se chemical shifts were referenced relative to external ammonium chloride and diphenyl diselenide, respectively. Abbreviations used for NMR spectra: py = pyridine and C$_{q,py}$ = quaternary pyridine carbon, s, singlet, m, multiplet, d, doublet, br, broad.

2.2. Synthesis of the ligands

2.2.1. 2-Acetylpyridine N,N-dimethylsemicarbazone (1)

To *N,N*-dimethylsemicarbazide (1.00 g, 9.70 mmol) in 2-propanol (10 mL) was added 2-acetylpyridine (1.10 mL, 9.82 mmol), and the mixture was stirred at 0 °C for 20 h. Then the solution was evaporated to dryness under reduced pressure. To the remaining oily residue was added hexane (60 mL), and the mixture was stirred at 0 °C until a precipitate appeared. After 30 min the white solid was filtered off, washed with hexane and dried *in vacuo*. The bulk product was found to be a mixture of *E*- and *Z*-isomers. Yield: 1.79 g (90%). Anal. Calc. for C$_{10}$H$_{14}$N$_4$O (206.25): C, 58.24; H, 6.84; N, 27.17. Found: C, 57.82; H, 6.53; N, 26.80%. Re-crystallisation from 2-propanol afforded the pure *E*-isomer. Yield: 0.22 g (22%). Anal. Calc. for C$_{10}$H$_{14}$N$_4$O (206.25): C, 58.24; H, 6.84; N, 27.17. Found: C, 58.52; H, 6.79; N, 27.42%. ESI MS (electrospray ionisation mass spectra) in MeOH (positive): *m/z* 229 [M+Na]$^+$; (negative): *m/z* 205 [M–H]$^-$. IR spectrum in KBr of the *E*-isomer, cm^{-1}: 1653 (C=O) s, 1533 s, 1465 s, 1433 s, 1372 s,

1184 s, 786 m. *E-isomer:* UV/vis (MeOH), λ_{max}, nm (ε, M^{-1} cm^{-1}): 213 (8060), 289 (14450), 388 (1380). *E-isomer:* ^{1}H NMR (500.10 MHz, DMSO-d_6): δ = 8.94 (s, 1H, NH), 8.57 (m, 1H, py), 8.00 (m, 1H, py), 7.81 (m, 1H, py), 7.36 (m, 1H, py), 2.97 (s, 6H, N(CH$_3$)$_2$), 2.32 (s, 3H, CCH$_3$). ^{13}C NMR (125.81 MHz, DMSO-d_6): δ = 156.3 (C=O), 156.1 (C$_{q,py}$), 148.9 (C$_{py}$), 148.6 (C=N), 136.8 (C$_{py}$), 123.8 (C$_{py}$), 120.2 (C$_{py}$), 37.1 (N(CH$_3$)$_2$), 12.0 (CH$_3$). *Z-isomer:* ^{1}H NMR (500.10 MHz, DMSO-d_6): δ = 14.57 (s, 1H, NH), 8.75 (m, 1H, py), 8.07 (m, 1H, py), 7.71 (m, 1H, py), 7.52 (m, 1H, py), 2.96 (s, 6H, N(CH$_3$)$_2$), 2.34 (s, 3H, CCH$_3$). ^{13}C NMR (125.81 MHz, DMSO-d_6): δ = 155.1 (C=O), 153.3 (C$_{q,py}$), 147.8 (C$_{py}$), 138.8 (C$_{py}$), 137.9 (C=N), 124.4 (C$_{py}$), 124.3 (C$_{py}$), 36.2 (N(CH$_3$)$_2$), 22.3 (CH$_3$). Single crystals suitable for X-ray diffraction study were selected directly from the reaction vessel.

2.2.2. 2-Acetylpyridine N,N-dimethylthiosemicarbazone (2)

The ligand has been prepared following the literature protocol [12]. EI MS, m/z (relative intensity): 222 (28.6), $[M]^{+\bullet}$; 207 (26.5), $[M–CH_3]^+$. *E-isomer:* ^{1}H NMR (500.10 MHz, DMSO-d_6): δ = 9.62 (s, 1H, NH), 8.59 (m, 1H, py), 8.06 (d, $^3J_{H,H}$ = 8.5 Hz, 1H, py), 7.82 (m, 1H, py), 7.39 (m, 1H, py), 3.31 (s, 6H, N(CH$_3$)$_2$), 2.38 (s, 3H, CCH$_3$). *Z-isomer:* ^{1}H NMR (500.10 MHz, DMSO-d_6): δ = 15.42 (s, 1H, NH), 8.79 (m, 1H, py), 8.11 (m, 1H, py), 7.80 (m, 1H, py), 7.58 (m, 1H, py), 3.34 or 3.30 (s, 6H, N(CH$_3$)$_2$), 2.39 (s, 3H, CCH$_3$). *E′-isomer:* ^{1}H NMR (500.10 MHz, DMSO-d_6): δ = 14.70 (s, 1H, NH), 8.74 (m, 1H, py), 8.00 (m, 1H, py), 7.87 (d, $^3J_{H,H}$ = 7.9 Hz, 1H, py), 7.53 (m, 1H, py), 3.34 or 3.30 (s, 6H, N(CH$_3$)$_2$), 2.64 (s, 3H, CCH$_3$). Single crystals suitable for X-ray diffraction study were selected directly from the reaction vessel.

2.2.3. 2-Acetylpyridine N,N-dimethylselenosemicarbazone (3)

The ligand has been prepared following the literature protocol [13], but re-crystallised twice from dry ethanol. Anal. Calc. for C$_{10}$H$_{14}$N$_4$Se (269.21): C, 44.61; H, 5.24; N, 20.81. Found: C, 44.38; H, 5.20; N, 20.57%. EI MS, m/z (relative intensity): 270 (26.7), $[M]^{+\bullet}$; 255 (5.9), $[M–CH_3]^+$. IR spectrum in KBr, cm^{-1}: 1581 m, 1497 s, 1385 s, 1363 s, 1298 s, 1254 s, 1237 s, 781 s. UV/vis (MeOH), λ_{max}, nm (ε, M^{-1} cm^{-1}): 250sh (6360), 305sh (6120), 394 (11280). *E-isomer:* ^{1}H NMR (500.10 MHz, DMSO-d_6): δ = 9.82 (s, 1H, NH), 8.60 (m, 1H, py), 8.10 (m, 1H, py), 7.84 (m, 1H, py), 7.41 (m, 1H, py), 3.44 or 3.26 (br. s, 6H, N(CH$_3$)$_2$), 2.40 (s, 3H, CCH$_3$). ^{13}C NMR (125.75 MHz, DMSO-d_6): δ = 181.6 (C=Se), 155.5 (C$_{q,py}$), 152.2 (C=N), 149.1 (C$_{py}$), 137.1 (C$_{py}$), 124.5 (C$_{py}$), 120.7 (C$_{py}$), 12.7 (CH$_3$). ^{15}N NMR (50.70 MHz, DMSO-d_6): δ = 309.1 (C=N), 288.4 (N$_{py}$), 148.6 ($^1J_{N,H}$ = 92 Hz, NH). ^{77}Se NMR (95.39 MHz, DMSO-d_6): δ = −127.3 ppm. *Z-isomer:* ^{1}H NMR (500.10 MHz, DMSO-d_6): δ = 15.61 (s, 1H, NH), 8.81 (m, 1H, py), 8.13 (m, 1H, py), 7.83 (m, 1H, py), 7.60 (m, 1H, py), 3.44 or

3.26 (br. s, 6H, N(CH$_3$)$_2$), 2.41 (s, 3H, CCH$_3$). ^{13}C NMR (125.75 MHz, DMSO-d_6): δ = 180.3 (C=Se), 152.5 (C$_{q,py}$), 148.0 (C$_{py}$), 141.7 (C=N), 139.3 (C$_{py}$), 125.1 (C$_{py}$), 124.9 (C$_{py}$), 22.4 (CH$_3$). ^{15}N NMR (50.70 MHz, DMSO-d_6): δ = 311.4 (C=N), 157.3 (NH). ^{77}Se NMR (95.39 MHz, DMSO-d_6): δ = −127.3 ppm. *E′-isomer:* ^{1}H NMR (500.10 MHz, DMSO-d_6): δ = 14.60 (s, 1H, NH), 8.76 (m, 1H, py), 8.03 (m, 1H, py), 7.93 (d, $^3J_{H,H}$ = 7.9 Hz, 1H, py), 7.57 (m, 1H, py), 3.40 (s, 6H, N(CH$_3$)$_2$), 2.68 (d, $^4J_{H,H}$ = 1.1 Hz, 3H, CCH$_3$). ^{13}C NMR (125.75 MHz, DMSO-d_6): δ = 183.5 ($J_{C,Se}$ = 202 Hz, C–Se), 150.4 (C$_{py}$), 148.4 (C$_{q,py}$), 143.9 (C=N), 138.8 (C$_{py}$), 126.1 (C$_{py}$), 123.2 (C$_{py}$), 44.5 (N(CH$_3$)$_2$), 14.8 (CH$_3$). ^{15}N NMR (50.70 MHz, DMSO-d_6): δ = 276.4 (N$_{py}$), 229.4 ($^1J_{N,H}$ = 88 Hz, C=NH). ^{77}Se NMR (95.39 MHz, DMSO-d_6): δ = −366.9 ($J_{Se,H}$ = 7.0 Hz) ppm. Crystals suitable for X-ray data collection were obtained from chloroform saturated with *n*-hexane.

2.3. Synthesis of the complexes

2.2.4. [Bis-(2-acetylpyridine N,N-dimethylsemicarbazonato)-N,N,O-gallium(III)] hexafluorophosphate, [Ga(L^1)$_2$]PF$_6$ (4)

To 2-acetylpyridine *N,N*-dimethylsemicarbazone (1) (150 mg, 0.728 mmol) in ethanol (15 mL) at 0 °C was added solid Ga(NO$_3$)$_3$ · 8.15H$_2$O (147 mg, 0.365 mmol). The reaction mixture was stirred at 0 °C for 1 h. To the clear solution ammonium hexafluorophosphate (120 mg, 0.736 mmol) in ethanol (2 mL) was added dropwise. After 15 min the yellow precipitate was filtered off, washed with cold ethanol and dried *in vacuo*. Yield: 0.12 g (53%). Anal. Calc. for C$_{20}$H$_{26}$F$_6$GaN$_8$O$_2$P (625.16): C, 38.42; H, 4.19; N, 17.92. Found: C, 38.17; H, 4.12; N, 17.68%. ESI MS in MeOH (positive): m/z 479, $[GaL_2]^+$. IR spectrum in KBr, cm^{-1}: 1603 m, 1575 s, 1550 s, 1404 s, 1230 s, 840 s and 558 m (P–F). UV/vis (MeOH), λ_{max}, nm (ε, M^{-1} cm^{-1}): 220 (14990), 249 (7300), 304 (15810), 391 (41570). ^{1}H NMR (500.10 MHz, DMSO-d_6): δ = 8.25 (m, 2H, py), 8.11 (d, $^3J_{H,H}$ = 7.9 Hz, 2H, py), 7.86 (m, 2H, py), 7.57 (m, 2H, py), 3.13 and 2.86 (s, 12H, N(CH$_3$)$_2$), 2.70 (s, 6H, CCH$_3$). ^{13}C NMR (125.81 MHz, DMSO-d_6): δ = 167.1 (C–O), 147.4 (C$_{q,py}$), 145.4 (C$_{py}$), 143.7 (C$_{py}$), 139.3 (C=N), 126.6 (C$_{py}$), 123.2 (C$_{py}$), 36.4 and 35.6 (N(CH$_3$)$_2$), 12.6 (CH$_3$). Crystals suitable for X-ray data collection were obtained from acetonitrile saturated with diethyl ether.

2.2.5. [Bis-(2-acetylpyridine N,N-dimethylselenosemicarbazonato)-N,N,Se-gallium(III)] hexafluorophosphate, [Ga(L^3)$_2$]PF$_6$ (6)

To 2-acetylpyridine *N,N*-dimethylselenosemicarbazone (3) (50 mg, 0.185 mmol) in ethanol (8 mL) at 50 °C Ga(NO$_3$)$_3$ · 8.15H$_2$O (38 mg, 0.094 mmol) in ethanol (2 mL) was added. The yellow-green solution was stirred for 15 min and cooled to room temperature. After addition of ammonium hexafluorophosphate (60 mg, 0.368 mmol)

in ethanol (1 mL) the reaction mixture was stirred for 15 min, and the yellow precipitate was filtered off, washed with ethanol (2×5 mL) and dried *in vacuo*. Yield: 52 mg (75%). Anal. Calc. for $C_{20}H_{26}N_4GaN_8PSe_2$ (751.08): C, 31.98; H, 3.49; N, 14.92. Found: C, 31.68, H, 3.51; N, 14.63%. ESI MS in MeOH (positive): *m/z* 607, $[GaL_2]^+$; ESI MS in MeOH (negative): *m/z* 145, $[PF_6]^-$. IR spectrum in KBr, cm^{-1}: 1603 m, 1516 s, 1393 s, 1300 s, 1256 s, 843 s and 558 m (P–F). UV/vis (MeOH), λ_{max}, nm (ε, $M^{-1} cm^{-1}$): 225sh (20150), 250sh (11950), 311 (14870), 398 (30810). ^{1}H NMR (500.10 MHz, DMSO-d_6): $\delta =$ 8.24–8.19 (m, 4H, py), 7.92 (d, $^3J_{H,H} = 5.0$ Hz, 2H, py), 7.57 (m, 2H, py), 3.30 (br. s, 12H, $N(CH_3)_2$ partially superimposed with the water signal), 2.88 (s, 6H, CCH_3). ^{13}C NMR (125.75 MHz, DMSO-d_6): $\delta = 173.8$ ($J_{C,Se} = 165$ Hz, C–Se), 149.0 (C=N), 145.4 ($C_{q,py}$), 144.4 (C_{py}), 142.6 (C_{py}), 127.7 (C_{py}), 124.7 (C_{py}), 42.9 and 39.3 ($N(CH_3)_2$), 15.6 (CH_3). ^{77}Se NMR (95.39 MHz, DMSO-d_6): $\delta = -371.7$ ppm. Crystals suitable for X-ray data collection were obtained from acetone saturated with *n*-hexane.

2.2.6. [Bis-(2-acetylpyridine N,N-dimethylthiosemicarbazonato)-N,N,S-ruthenium(III)] hexafluorophosphate, $[Ru(L^2)_2]PF_6$ (7)

To 2-acetylpyridine *N,N*-dimethylthiosemicarbazone (**2**) (93 mg, 0.418 mmol) in methanol (5 mL) at 70 °C [(DMSO)$_2$H][*trans*-RuCl$_4$(DMSO)$_2$] (100 mg, 0.180 mmol) in methanol (5 mL) was added dropwise. The mixture was stirred at 70 °C for 3 h, cooled down to room temperature and allowed to stand at 4 °C overnight. Then ammonium hexafluorophosphate (70 mg, 0.429 mmol) in methanol (2 mL) was added, and the reaction mixture was stirred for 2 h. The black-green precipitate was filtered

off, washed with cold methanol and dried *in vacuo*. Yield: 57 mg (47%). Anal. Calc. for $C_{20}H_{26}F_6N_8PRuS_2$ (688.64): C, 34.88; H, 3.81; N, 16.27; S, 9.31. Found: C, 34.84; H, 3.87; N, 16.06; S, 9.14%. ESI MS in MeOH (positive): *m/z* 544, $[RuL_2]^+$. IR spectrum in KBr, cm^{-1}: 1559 s, 1550 s, 1507 s, 1399 s, 1310 s, 1251 s, 839 s and 558 m (P–F). UV/vis (MeOH), λ_{max}, nm (ε, $M^{-1} cm^{-1}$): 245sh (17690), 299sh (16280), 343sh (24540), 382 (29570), 460sh (6340), 593 (1750), 771sh (600). Crystals suitable for zX-ray data collection were obtained from chloroform saturated with *n*-hexane.

2.4. Crystallographic structure determination

X-ray diffraction measurements were performed on an X8APEX II CCD diffractometer at 100 K. Single crystals were positioned at 40 mm from the detector and 1007, 1936, 4029, 1336, 1066 and 2203 frames were measured, each for 10, 5, 10, 50, 10 and 20 s over 1° scan width for **1–4**, **6** and **7**, correspondingly. The data were processed using SAINT software [14]. Crystal data, data collection parameters, and structure refinement details for **1–4**, **6** and **7** are given in Table 1. The structures were solved by direct methods and refined by full-matrix least-squares techniques. Non-hydrogen atoms were refined with anisotropic displacement parameters. H atoms were placed at calculated positions and refined as riding atoms in the subsequent least squares model refinements. The isotropic thermal parameters were estimated to be 1.2 times the values of the equivalent isotropic thermal parameters of the non-hydrogen atoms to which hydrogen atoms are bonded. In complex $\mathbf{6} \cdot 2(CH_3)_2CO$ one of the lattice acetone molecules is disordered over two positions with site occupation

Table 1
Crystal data and details of data collection for **1–4**, **6** and 7

Complex	1	2	3	$4 \cdot 0.5(C_2H_5)_2O$	$6 \cdot 2(CH_3)_2CO$	7
Empirical formula	$C_{10}H_{14}N_4O$	$C_{10}H_{14}N_4S$	$C_{10}H_{14}N_4Se$	$C_{22}H_{31}F_6GaN_8O_{2.5}P$	$C_{26}H_{38}F_6GaN_8O_2PSe_2$	$C_{20}H_{26}F_6N_8PRuS_2$
F_w	206.25	222.31	269.21	662.22	867.25	688.64
Space group	Pbca	$P\bar{1}$	$P\bar{1}$	$P\bar{1}$	$P\bar{1}$	$P2_1/c$
a (Å)	8.7233(6)	7.2207(2)	7.2858(2)	13.0897(7)	8.7651(8)	18.2142(4)
b (Å)	15.4944(10)	7.9483(2)	8.0019(2)	15.6031(8)	13.3241(12)	18.5378(9)
c (Å)	15.9332(12)	9.8302(3)	9.9160(3)	15.8977(7)	16.4686(15)	18.7028(11)
α (°)		86.676(2)	87.326(1)	64.375(3)	79.755(6)	
β (°)		79.757(3)	78.797(1)	83.561(3)	74.596(6)	102.298(3)
γ (°)		76.987(3)	76.898(2)	78.325(4)	71.971(6)	
V (Å³)	2153.6(3)	540.83(5)	552.33(3)	2865.9(2)	1753.6(3)	2782.6(3)
Z	8	2	2	2	2	4
λ (Å)	0.71073	0.71073	0.71073	0.71073	0.71073	0.71073
ρ_{calcd} (g cm⁻³)	1.272	1.365	1.619	1.535	1.642	1.644
Crystal size (mm³)	$0.75 \times 0.45 \times 0.30$	$0.36 \times 0.28 \times 0.28$	$0.40 \times 0.26 \times 0.24$	$0.20 \times 0.20 \times 0.05$	$0.40 \times 0.25 \times 0.15$	$0.57 \times 0.20 \times 0.20$
T (K)	100	100	100	100	100	100
μ (mm⁻¹)	0.087	1.365	3.372	1.535	2.975	0.837
R_1 [a]	0.0386	0.0474	0.0177	0.0496	0.0380	0.0429
wR_2 [b]	0.1117	0.1440	0.0479	0.1249	0.0891	0.1031
GOF [c]	1.024	1.116	1.005	1.010	1.002	1.192

[a] $R_1 = \sum ||F_o| - |F_c|| / \sum |F_o|$.

[b] $wR_2 = \{\sum [w(F_o^2 - F_c^2)^2] / \sum [w(F_o^2)^2]\}^{1/2}$.

[c] $GOF = \{\sum [w(F_o^2 - F_c^2)^2] / (n - p)\}^{1/2}$, where n is the number of reflections and p is the total number of parameters refined.

factors (SOF) 0.60 and 0.40, respectively. In the asymmetric unit of $4 \cdot 0.5(C_2H_5)_2O$ one of the two PF_6 anions and the lattice diethyl ether molecule are disordered over two positions with SOF 0.862 and 0.138, 0.561 and 0.439, respectively. The following computer programs were used: structure solution, SHELXS-97 [15] refinement, SHELXL-97 [16] molecular diagrams, ORTEP [17] computer: Pentium IV. Scattering factors were taken from the literature [18].

2.5. Cell lines and culture conditions

Human 41M (ovarian carcinoma) and SK-BR-3 (mammary carcinoma) cells were kindly provided by Lloyd R. Kelland (CRC Centre for Cancer Therapeutics, Institute of Cancer Research, Sutton, UK) and Evelyn Dittrich (General Hospital, Medical University of Vienna, Austria), respectively. Cells were grown in 75 cm^2 culture flasks (Iwaki/Asahi Technoglass, Gyouda, Japan) as adherent monolayer cultures in complete culture medium, i.e. minimal essential medium (MEM) supplemented with 10% heat-inactivated fetal bovine serum, 1 mM sodium pyruvate, 4 mM L-glutamine and 1% non-essential amino acids (100×) (all purchased from Sigma–Aldrich, Vienna, Austria). Cultures were maintained at 37 °C in a humidified atmosphere containing 5% CO$_2$.

2.6. Cytotoxicity tests in cancer cell lines

Antiproliferative effects were determined by means of a colorimetric microculture assay (MTT assay, MTT = 3-(4,5-dimethyl-2-thiazolyl)-2,5-diphenyl-2H-tetrazolium bromide). Cells were harvested from culture flasks by trypsinization and seeded into 96-well microculture plates (Iwaki/Asahi Technoglass, Gyouda, Japan) in densities of 4×10^3 cells/well, in order to ensure exponential growth throughout drug exposure. After a 24 h pre-incubation, 41M and SK-BR-3 cells were exposed to serial dilutions of the test compound in 200 μL/well complete culture medium for 96 h under an atmosphere containing 5% CO$_2$.

At the end of incubation, all media were replaced by 100 μL/well RPMI 1640 medium (supplemented with 10% heat-inactivated foetal bovine serum and 2 mM L-glutamine) plus 20 μL/well MTT solution in phosphate-buffered saline (5 mg/ml). After incubation for 4 h, the medium/MTT mixtures were removed, and the formazan crystals formed by the mitochondrial dehydrogenase activity of vital cells were dissolved in 150 μL DMSO per well. Optical densities at 550 nm were measured with a microplate reader (Tecan Spectra Classic), using a reference wavelength of 690 nm to correct for unspecific absorption. The quantity of vital cells was expressed in terms of T/C values by comparison to untreated control microcultures, and 50% inhibitory concentrations (IC$_{50}$) were calculated from concentration–effect curves by interpolation. Evaluation is based on means from at least three independent experiments, each comprising six microcultures per concentration level.

3. Results and discussion

3.1. Synthesis of ligands and metal complexes

The ligands used in this study for the preparation of gallium(III) and ruthenium(III) complexes were synthesised by three different methods. Condensation of N,N-dimethylsemicarbazide with 2-acetylpyridine in 2-propanol at 0 °C afforded HL^1 as a mixture of E- and Z-isomers (see discussion of the NMR data). Re-crystallisation from 2-propanol afforded the pure E-isomer, which was further used for complexation with gallium(III). HL^2 was synthesised by multistep reactions ended up by substitution of the S-methyl group of methyl-3-[1-(2-pyridyl)ethylidene]hydrazinecarbothioate (compound A in Scheme 2) by dimethylamine [12]. The third ligand HL^3 was prepared by methylation of HL^2 with methyl iodide in the presence of a base, followed by replacement of the thiomethyl group by selenium using sodium hydrogen selenide [13] (Scheme 3):

The gallium complexes [Ga(L$^{1-3}$)$_2$]PF$_6$ (4–6) were prepared as yellow microcrystalline materials in 53–91% yield by reaction of Ga(NO$_3$)$_3 \cdot 8.15H_2O$ with the corresponding 2-acetylpyridine N,N-dimethyl(chalcogen)semicarbazone
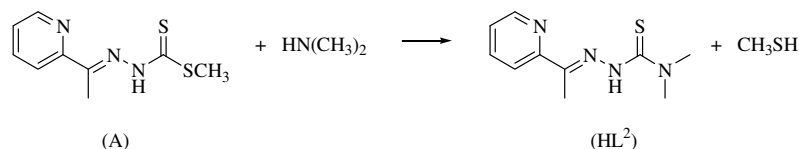
Scheme 2.
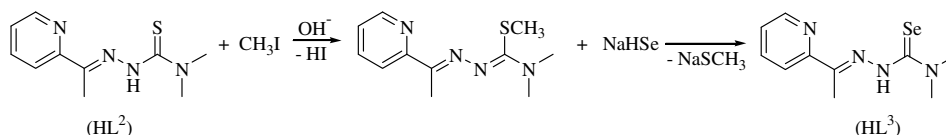
Scheme 3.

in 1:2 molar ratio in ethanol, followed by addition of an excess of NH_4PF_6. The ruthenium(III) compound $[Ru(L^2)_2]PF_6$ (**7**) was obtained as a green-black powder in 47% yield, starting from $(DMSO)_2H[RuCl_4(DMSO)_2]$ and an excess of HL^2 in methanol with subsequent addition of NH_4PF_6.

3.2. Electronic absorption spectroscopy

The UV/vis spectra of the metal-free ligands **1–3** and the gallium complexes **4–6** are dominated by intraligand transitions associated with the pyridine ring, azomethine and C=X (X = O, S, Se) portions of the ligands. The coordination of the ligands to the metal caused a very large increase of the magnitude of the lowest energy band. In the case of the semicarbazone ligand HL^1 this is especially pronounced, and an intensity increase by a factor of ~30 can be observed upon coordination to gallium (Fig. 1). This is presumably due to the increased length of the chromophore in the complex compared to the small extent of the electron density delocalisation in the metal-free ligand which was also corroborated by the non-planar conforma-
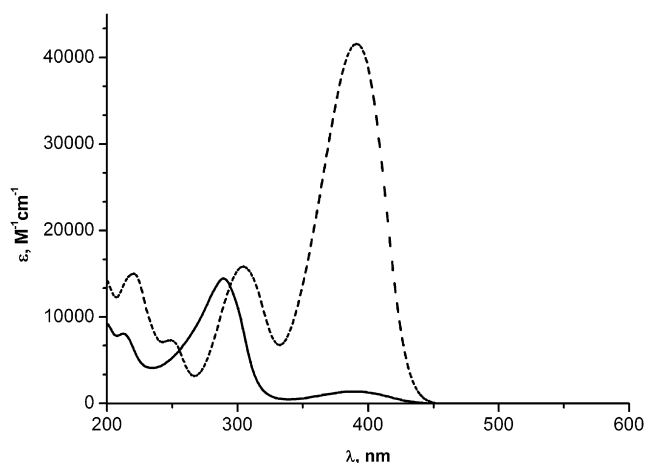

Fig. 1. The electronic absorption spectra of HL^1 (solid line) and $[Ga(L^1)_2][PF_6]$ (dashed line) in methanol.
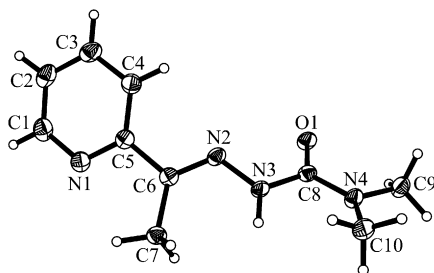

Fig. 2. ORTEP plot of HL^1 with atom numbering scheme. The thermal ellipsoids are drawn at 50% probability level. Selected bond lengths (Å) and bond angles (°): C6–N2 1.2901(19), N2–N3 1.3793(17), N3–C8 1.3872(19), C8–O1 1.2426(19), C8–N4 1.358(2); N1–C5–C6–N2 154.43(14), N2–N3–C8–O1 14.3(2)°.

tion of HL^1 found by X-ray diffraction (Fig. 2). The ruthenium(III) complex **7** displays a strong band at 382 nm with an extinction coefficient of about 30,000 and three weak absorptions at 460 (sh, shoulder), 593 and 771 (sh) nm, with extinction coefficients of 6340, 1750 and 600 $M^{-1} cm^{-1}$, respectively.

The aqueous solution behaviour with respect to hydrolysis of **4–7** was studied in $DMSO/H_2O$ 1:100 (v/v) at 298 K over 20 h by UV/vis spectroscopy. The complexes **5–7** were quite stable, as can be seen from their electronic absorption spectra (Figs. S2–S4). In contrast the semicarbazone complex **4** showed a 25% decrease of the intensity of the band with an absorption maximum at 391 nm (Fig. S1).

3.3. Thermal behaviour

The thermal properties of **4–7** have been studied by thermogravimetric analysis (TGA) measurements between 25 and 500 °C in air. The TG curves showed all complexes to be non-solvated. Complexes **4–6** are all stable up to 240 °C. Above this temperature begins the decomposition of the complexes, which is not accompanied by significant exothermic or endothermic effects. Complex **4** measured under a nitrogen atmosphere showed a similar decomposition profile with that obtained in air. The ruthenium complex **7** measured in air is slightly less stable (decomposition begins at 220 °C). A large endothermic peak attributed to the pyrolysis of the complex can be observed on the DTA curve at about 400 °C.

3.4. Mass spectrometry

The ESI mass spectrum of HL^1 recorded in the positive ion mode showed a peak at m/z 229 due to $[M+Na]^+$, while in the negative mode a peak at m/z 205 attributed to $[M-H]^-$ was observed. For the metal-free thio- and selenosemicarbazones (HL^2 and HL^3) the ESI mass spectra exhibited only small peaks due to $[M+Na]^+$ and a few peaks also at higher m/z, which have not been identified. However, both ligands studied by EI MS displayed molecular ion peaks $[M]^{+\cdot}$ at m/z 270 and 222 with relative intensities of 28.6% and 26.7%, respectively. The positive ion ESI mass spectra of the gallium(III) complexes **4** and **6** as well as the ruthenium complex **7** showed strong peaks attributable to $[ML_2]^+$ at m/z 479, 607 and 544, correspondingly. The counterion PF_6^- is easily detectable in the negative ion mode at m/z 145. The isotopic patterns of all identified signals fit well with the theoretical isotopic distributions.

3.5. ^1H, ^{13}C, ^{15}N and ^{77}Se NMR spectroscopy

The ^1H NMR spectra of the three ligands in DMSO-d_6 indicate that they are all isomeric mixtures. The metal-free thio- and selenosemicarbazones (HL^2 and HL^3) show each three sets of signals. The selenosemicarbazone ligand was

studied in detail by one- and two-dimensional NMR spectroscopy to get further information about the isomers present in solution. Besides measurements of ^{1}H, ^{13}C and ^{15}N nuclei, investigation of HL[3] offers the possibility of getting chemical shift information of the [77]Se nucleus (spin 1/2, 7.6% natural abundance).

The most remarkable differences caused by the presence of different isomeric forms were observed in the ^{1}H NMR spectrum of HL[3] for the N–H signals at 9.82, 14.60 and 15.61 ppm, respectively, with relative intensities 0.4:1:0.1; the strong downfield shifts to 14.60 and 15.61 ppm are accounted for by involvement of N–H in intramolecular hydrogen bonding. Assignment of the signals to the respective E- and Z-isomers of HL[3], was based on a ^{1}H, [1]H-NOESY (nuclear Overhauser and exchange spectroscopy) spectrum, the ^{1}H chemical shift of the NH moieties and additionally on the remarkable shift differences of the ^{13}C NMR resonances of the 2-acetylpyridine methyl group.

In the ^{1}H, ^{1}H NOESY spectrum, a correlation between the N–H signal at 9.82 ppm and the methyl group protons of the 2-acetylpyridine moiety at 2.40 ppm was detected, being an expected feature of the E-isomer (Scheme 4). This result is also in line with N–H chemical shifts for E-configured thiosemicarbazones reported by other authors [19]. The Z-isomer displaying the N–H resonance at 15.61 ppm shows a distinctive shift of the ^{13}C NMR signal of the 2-acetylpyridine methyl group (22.4 ppm) in comparison to the E-isomer (12.7 ppm). This difference can be explained by the γ-effect [20], which implies that the change of the chemical environment at the hydrazinic N–H has a marked influence on the carbon atom in γ-position, in our case the 2-acetylpyridine methyl group.

Both, the E- as well as the Z-isomer gave rise to comparable shift correlation signals in the two-dimensional ^{1}H, ^{15}N NMR spectra, which were available via one-bond HSQC (heteronuclear single quantum coherence) and long-range HMBC (heteronuclear multiple bond correlation) experiments. The azomethine nitrogens showed resonances at 311.4 and 309.1 ppm (E- and Z-isomer), respectively, whereas signals of NH nitrogen atoms were found at 157.3 and 148.6 ppm. For the E-species, a typical $^1J_{N,H}$ coupling of 92 Hz was detected. In the ^{77}Se NMR spectrum, a broad resonance of the E isomers was detected at −127.3 ppm, probably superimposing with the signal of the least abundant Z isomer. This chemical shift is in the range of the values documented in the literature for selenourea derivatives [21].

The most abundant in DMSO-d_6 is the third isomer of HL[3]. In the ^{1}H NMR spectrum, a doublet at 2.68 ppm ($J_{H,H}$ = 1.1 Hz) of the 2-acetylpyridine methyl group was detected, but the coupling partner could not easily be assigned. In a long-range ^{1}H, ^{1}H-COSY (correlation spectroscopy) experiment (optimised for very small $J_{H,H}$ values) coupling to the broad N–H proton signal at δ 14.60 was found and additionally verified via a homonuclear decoupling experiment. Irradiation of the N–H proton at 14.60 ppm led to disappearing of the splitting of the methyl group protons at 2.68 ppm in accordance with the chemical structure of isomer E′ (Scheme 4). Further evidence for the E′ structure was obtained from ^{1}H, ^{15}N correlated NMR spectra. The ^{15}N chemical shift of the quaternary NH resonance at 229.4 ppm (typical $^1J_{N,H}$ coupling of 88 Hz) was significantly different to those of the E- and Z-isomers (157.3 and 148.6 ppm). In addition, a strong cross-peak between the 2-acetylpyridine methyl group and the NH proton at δ 14.60 could be found in the long-range ^{1}H, ^{15}N HMBC spectrum.

The second signal at δ −366.9 ppm (besides the broad signal at −127.3 ppm for the E- and Z-isomer), observed for HL[3] in the directly measured ^{77}Se NMR spectrum without proton decoupling, was sharp (when compared to the first one) and splitted into a doublet with a coupling constant of J = 7.0 Hz (Fig. S5). Coupling to a neighbouring proton was proven via (i) measurement of a proton decoupled ^{77}Se NMR spectrum and (ii) a ^{1}H, ^{77}Se COSY experiment showing a correlation signal to the NH proton at 14.60 ppm and indicating that the splitting is due to a NH⋯Se interaction (Fig. S6). These findings are in good agreement with [77]Se–[1]H coupling constants for NH⋯Se hydrogen bonds (J = 5.4–13.1 Hz) reported by other authors [22,23], providing strong evidence that the set of signals with the N–H proton at 14.60 ppm can be attributed to the E′-isomer (Scheme 4).

It is known that the thiosemicarbazone ligand HL[2] exists in CDCl₃ solution in three isomeric forms [24]. We found three sets of signals with relative intensities 1:0.6:0.3 for E, E′ and Z isomers in DMSO-d_6. In contrast, the ^{1}H NMR spectrum of the prepared semicarbazone ligand HL[1] in DMSO-d_6 showed only two sets of signals, with varying ratios of relative intensities (0.5–1:1). The two N–H resonances were observed at 14.57 and 8.94 ppm, respectively. However, the sample re-crystallised from 2-propanol showed only one set of signals with N–H at 8.94 ppm. This set of signals was also found in the ^{1}H NMR spectrum of the single crystal characterised by X-ray crystallography (vide infra) and undoubtedly attributed to the E-isomer. The ^{13}C NMR spectrum of the E-isomer showed a signal of the 2-acetylpyridine methyl group at 12.0 ppm, compared to 22.3 ppm for the second set of signals. This result together with the downfield shift of the N–H signal provided evidence for Z-configuration of the second isomer. Evaporation of the mother liquor after separation of the E-isomer and addition of hexane resulted in enrichment of the mixture by the Z-isomer (observed ratio

E-isomer   Z-isomer   E′-isomer
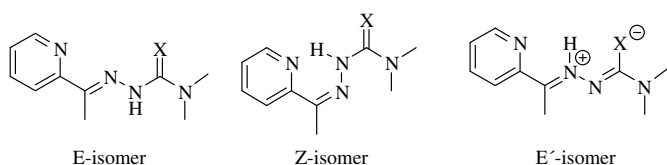
Scheme 4.

1.4:1). Measurements after 24 h showed the same ratio of the species present in solution, indicating that no isomerisation occurred with time. The existence of two isomers of the semicarbazone, not only in solution but also in the solid state, was confirmed by the two C=O stretching vibrations at 1658 and 1653 cm^{-1} in the IR spectra of the bulk product. The first one disappeared after re-crystallisation of the mixture from 2-propanol.

In contrast to the metal-free ligands, the ^{1}H NMR spectra of complexes **4–6** showed only one set of signals due to stabilisation of ligand configuration upon coordination to the metal and the equivalence of both ligands bound to gallium(III) in solution. The most remarkable difference between the ^{1}H NMR spectra of the gallium(III) complexes **4–6** and those of the metal-free ligands is the absence of any NH signal for **4–6**, indicating deprotonation of the ligands upon complexation. This is in good agreement with the ^{77}Se NMR spectrum of **6** with a resonance at δ -371.7 ppm, well comparable with the chemical shift for the E'-isomer of the metal-free ligand HL^3.

3.6. X-ray crystallography

The result of X-ray diffraction study of HL^1 is shown in Fig. 2. Selected bond distances (Å) and angles are quoted in the legend to Fig. 2. HL^1 crystallised in the orthorhombic space group *Pbca* and adopted an essentially non-planar conformation, so that the atoms N2, N3, O1 and N4 come out from the mean plane of the pyridine ring by 0.566, 0.604, 2.427 and 1.361 Å, correspondingly. The C8–O1 and N2–N3 bond lengths of 1.2426(19) and 1.3793(17) Å are equal within 3σ with those reported for acetone semicarbazone [25] at 1.242(2) and 1.385(2) Å, correspondingly. The crystal structure showed an intermolecular hydrogen bonding interaction between the atom N3 as proton donor and atom O1^i of the neighbouring molecule as proton acceptor with the following parameters: N3–H 0.863, H···O1^i 2.183, N3···O1 3.028 Å and ∠N3–H···O1 166.24° [symmetry code (i) *x*+0.5, *y*, −*z*+1]. An essentially planar conformation of HL^1 was found in HL^1 · CH$_3$OH, in which a hydrogen bonding interaction between the molecule of methanol as proton donor and the C=O group of

Fig. 4. ORTEP plot of HL^3 with atom numbering scheme. The thermal ellipsoids are drawn at 50% probability level. Selected bond lengths (Å) and bond angles (°): C6–N2 1.3004(15), N2–N3 1.3524(14), N3–C8 1.3431(15), C8–Se 1.8788(11), C8–N4 1.3471(15); N1–C5–C6–N2 5.57(15), N2–N3–C8–Se 2.35(14)°.

the semicarbazone ligand as proton acceptor was found (Fig. S1).

HL^2 and HL^3 crystallise in the triclinic space group *P*$\bar{1}$. The ligands adopt the E'-isomeric form in the nomenclature of the conformations of thiosemicarbazones derived from 2-acetylpyridine [26]. This conformation is different from that found in 2-acetylpyridine *N*(4)-alkylthiosemicarbazone (non-hydrogen bonding isomer *E*), where alkyl = methyl [27], ethyl [26]. The nitrogen atom N2 in both HL^2 and HL^3 acts as proton donor to both the pyridine nitrogen atom N1 and the chalcogen atom (S or Se) to give a bifurcated arrangement. The parameters of the bifurcated hydrogen bond in HL^2 and HL^3 are as follows: N2–H 0.88, H···N1 2.26, N2···N1 2.660(3) Å, ∠N2–H···N1 107.2°; H···S 2.37, N2···S 2.864(2) Å, ∠N2–H···S 115.7° and N2–H 0.88, H···N1 2.26, N2···N1 2.6578(14) Å, ∠N2–H···N1 107.3°; H···Se 2.44, N2···Se 2.9593(10) Å, ∠N2–H···Se 118.6°. It is also worth noting that a search in the CSD [28] revealed that HL^3 is the first metal-free selenosemicarbazone characterised by X-ray diffraction (see Fig. 4).
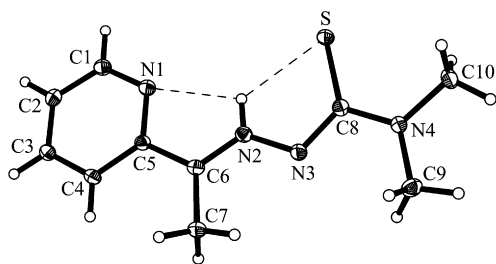

Fig. 3. ORTEP plot of HL^2 with atom numbering scheme. The thermal ellipsoids are drawn at 50% probability level. Selected bond lengths (Å) and bond angles (°): C6–N2 1.299(3), N2–N3 1.354(3), N3–C8 1.350(4), C8–S 1.723(3), C8–N4 1.351(4); N1–C5–C6–N2 6.42(36), N2–N3–C8–S 2.14(34)°.
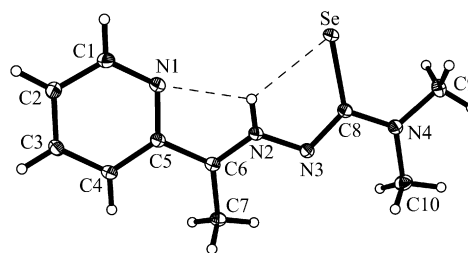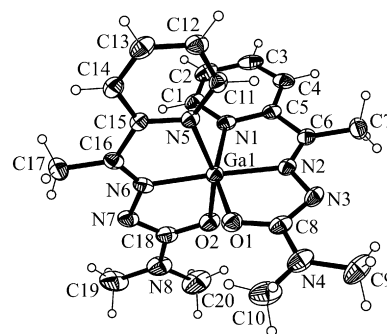

Fig. 5. ORTEP plot of the first independent cation [Ga^{III}(L^1)$_2$]$^+$ in **4** with atom numbering scheme. The thermal ellipsoids are drawn at 50% probability level. Selected bond lengths (Å) and bond angles (°): Ga1–N1 2.077(3), Ga1–N5 2.081(3), Ga1–N2 2.003(3), Ga1–N6 1.989(3), Ga1–O1 1.968(3), Ga1–O2 1.967(3), C6–N2 1.288(5), C16–N6 1.300(5), N2–N3 1.375(4), N6–N7 1.370(4), N3–C8 1.353(5), N7–C18 1.356(5), C8–O1 1.289(5), C18–O2 1.300(5), C8–N4 1.364(4), C18–N8 1.354(5) Å; ∠N1–Ga1–N2 78.27(13), ∠N5–Ga1–N6 78.92(13), ∠N2–Ga1–O1 78.74(13), N6–Ga1–O2 78.97(13)°.

The asymmetric unit of **4** · (C₂H₅)₂O comprises two crystallographically independent enantiomeric cations [Ga(L¹)₂]⁺ with the same chirality at the gallium center, two PF₆⁻ anions and one disordered diethyl ether molecule. The structure of the first independent cation is displayed in Fig. 5. The gallium atom is coordinated by the two approximately planar tridentate ligands, in contrast to the nonplanar conformation of the metal-free semicarbazone HL¹ (Fig. 2). The coordination polyhedron approaches an octahedron, where the two ligands are bound to Ga through a nitrogen atom of the pyridine ring and a nitrogen and an oxygen atom of the semicarbazide moiety. The bonds C8–O1 of 1.289(5) and C18–O2 of 1.300(5) Å are longer compared to the analogous bond in HL¹ [1.2426(19)], indicating the more pronounced single-bond character of these bonds in **4**. Note that the angles ∠N1–Ga1–O1 at 156.81(12)° and ∠N5–Ga1–O2 at 157.22(22)° deviate markedly from the ideal value of 180°, whereas ∠N6–Ga1–N2 at 176.86(14) is close to 180°.

Complex **6** · 2(CH₃)₂CO crystallises in the triclinic space group P1̄. The unit cell consists of a racemic mixture of the two enantiomers of chiral octahedral [Ga(L³)₂]⁺ complex cations, two counter anions PF₆⁻ and two lattice acetone molecules. The structure of the complex cation is shown in Fig. 6. Each ligand is monodeprotonated and coordinates to gallium via the pyridine nitrogen atom and nitrogen and selen donors of the selenosemicarbazide moiety, forming two five-membered metallocycles, correspondingly. Selected bond distances and bond angles are given in the legend to Fig. 6. The bond distances C8–Se1 of 1.914(3) and C18–Se2 of 1.907(4) Å are comparable to that reported for [FeL₂][FeCl₄] (HL = 2-acetylpyridine-3-azabicyclo[3.2.2]nonylselenosemicarbazone) [29] of 1.928(11) Å and are longer than that of the metal-free selenosemicarbazone HL³ at 1.8788(11) Å. As for the semicarbazone complex **4**, the angles ∠N1–Ga–Se1 at 159.98(8)° and ∠N5–Ga–Se2 at 159.64(8)° deviate markedly from the

ideal value of 180°, in contrast to ∠N2–Ga–N6 at 168.79(12)° which is about 8° smaller than the corresponding angle in complex **4**. Interestingly these values are quite similar to those found in the analogous thiosemicarbazone complex [Ga(L²)₂][GaCl₄] [30] [∠N1–Ga–S1 at 158.89(9)°, ∠N5–Ga–S2 at 160.12(7)° and ∠N2–Ga–N6 at 171.18(9)°]. Of note are the large differences between ∠Ga1–O1–C8 at 111.8(3)° and ∠Ga1–X–C8 (X = S, Se) at 94.16(11) and 90.65(11), respectively, which are due to large variations in C═X (X = O, S, Se) bond lengths. In contrast the ∠Ga–N1–C5 differs in all three structures only within 3°. The search of CSD [28] showed that this is the first gallium(III) selenosemicarbazonate characterised by X-ray diffraction.

Compound **7** crystallises in the monoclinic space group P2₁/c as a racemic mixture of the two enantiomers of the chiral octahedral ruthenium(III) complex. The ruthenium(III) ion is coordinated by the two almost planar tridentate ligands, which are monodeprotonated (vide infra) and adopt the same conformation as in the metal-free state (Fig. 7). Each ligand is bound to ruthenium through a nitrogen atom of the pyridine ring, a nitrogen atom and a sulfur atom of the thiosemicarbazide moiety. The bonding distances of ruthenium to the nitrogen atoms of the pyridine rings (Ru–N1 and Ru–N5) are equal within 3σ and significantly (⩾18σ) longer than those of ruthenium to nitrogen atoms in the thiosemicarbazide moieties (Ru–N2 and Ru–N6). The interatomic distances Ru–S1 and Ru–S2 (2.2852(10) and 2.2805(11) Å) are significantly longer than that found in [Ru^III Cl₂(L)(PPh₃)] at 2.2513(12) Å with HL = phenanthrenquinone thiosemicarbazone, but clearly shorter than those observed for ruthenium(II) complexes [Ru^II Cl(L)(PPh₃)₂] at 2.3608(14) Å (HL = phenanthrenquinone thiosemicarbazone) or [Ru^II Cl(L²)(PPh₃)₂] · 3CH₂Cl₂ at 2.3725(13) Å [31]. The bond distances C8–S1
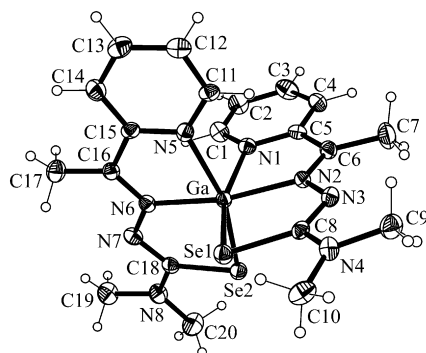

Fig. 6. ORTEP plot of [Ga^III(L³)₂]⁺ in **6** with atom numbering scheme. The thermal ellipsoids are drawn at 50% probability level. Selected bond lengths (Å) and bond angles (°): Ga–N1 2.134(3), Ga–N5 2.110(3), Ga–N2 2.080(3), Ga–N6 2.077(3), Ga–Se1 2.4908(6), Ga–Se2 2.4856(6), C6–N2 1.300(4), C16–N6 1.302(5), N2–N3 1.359(4), N6–N7 1.376(4), N3–C8 1.339(4), N7–C18 1.331(5), C8–Se1 1.914(4), C18–Se2 1.907(4), C8–N4 1.341(4), C18–N8 1.371(5) Å; ∠N1–Ga–N2 77.02(11), ∠N5–Ga–N6 76.65(12), ∠N2–Ga–Se1 83.58(8), ∠N6–Ga–Se2 83.74(9)°.

Fig. 7. ORTEP plot of [Ru^III(L²)₂]⁺ in **7** with atom numbering scheme. The thermal ellipsoids are drawn at 40% probability level. Selected bond lengths (Å) and bond angles (°): Ru–N1 2.077(3), Ru–N5 2.087(3), Ru–N2 2.005(3), Ru–N6 2.006(3), Ru–S1 2.2852(10), Ru–S2 2.2805(11), C6–N2 1.307(6), C16–N6 1.310(5), N2–N3 1.370(5), N6–N7 1.370(5), N3–C8 1.321(7), N7–C18 1.322(5), C8–S1 1.773(5), C18–S2 1.766(4), C8–N4 1.338(6), C18–N8 1.342(5) Å; ∠N1–Ru–N2 78.10(14), ∠N5–Ru–N6 78.18(13), ∠N2–Ru–S1 83.09(11), ∠N6–Ru–S2 83.29(10)°.

and C18–S2 (1.773(5) and 1.766(4) Å, respectively) are more than 8σ longer than that in metal-free thiosemicarbazone HL^2 (1.723(3) Å), indicating an increased single-bond character of the C–S bonds in $[Ru^{III}(L^2)_2]PF_6$. The distribution of electron density over thiosemicarbazide moieties (see legend to Fig. 3) along with the presence of the PF_6^- counter anion are in agreement with the monodeprotonated nature of the coordinated ligands and formal oxidation state 3+ of ruthenium in **7**. The hexafluorophosphate anion was found to be disordered over two positions with P–F bond lengths typical for this species [32].

Table 2
Antiproliferative activity of α-N-heterocyclic (*chalcogen*) semicarbazones, their gallium(III) and ruthenium(III) complexes in two human cancer cell lines

Compounds		IC_{50}^a (nM)			
		41M		SK-BR-3	
Ligands	**1**	5800	±1100	8500	±4300
	2[b]	0.22	±0.14	2.7	±1.4
	3	0.010	±0.001	0.21	±0.10
Ga complexes	**4**	4800	±900	5000	±2300
	5[b]	0.053	±0.018	0.56	±0.47
	6	0.0045	±0.00002	0.069	±0.038
Ru complex	**7**	910	±170	580	±30

[a] 50% inhibitory concentrations in 41M and SK-BR-3 cells after exposure for 96 h in the MTT assay. Values are means ± SD obtained from at least three independent experiments.
[b] Values taken from Ref. [9].

3.7. Antiproliferative activity in cancer cell lines

The cytotoxic potencies of the seleno- and semicarbazone ligands HL^1 and HL^3 and their gallium(III) complexes as well as the ruthenium(III) complex of the thiosemicarbazone HL^2 were compared with the previously characterised metal-free thiosemicarbazone HL^2 and the gallium(III) complex $[Ga(L^2)_2][PF_6]$ (**5**) [9] in the human tumour cell lines 41M (ovarian carcinoma) and SK-BR-3 (mammary carcinoma) by means of the colorimetric MTT assay. All complexes and the ligands show high cytotoxic potencies, with IC_{50} values ranging from picomolar to low micromolar concentrations (Table 2). As for the thiosemicarbazone compounds reported in a previous article [9], their concentration–effect curves are rather flat, with a slope extending over a range of two to three orders of magnitude (Fig. 8).

The main purpose of this work was to explore the effect of the chalcogen atom (O, S, Se) in (chalcogen)semicarbazones, and in the corresponding complexes, on their cytotoxicity. Among the several publications concerning the biological activity of selenosemicarbazones and semicarbazones [13,33–35], only a few focus on antineoplastic effects.

The effect of the chalcogen on the activity of ligands **1–3** and gallium(III) complexes **4–6** is very pronounced (Fig. 8). The cytotoxicity increases with the atomic number of the chalcogen. The highest cytotoxicity is observed with the selenosemicarbazones with IC_{50} values in low picomolar concentrations, followed by the thiosemicarbazones in the

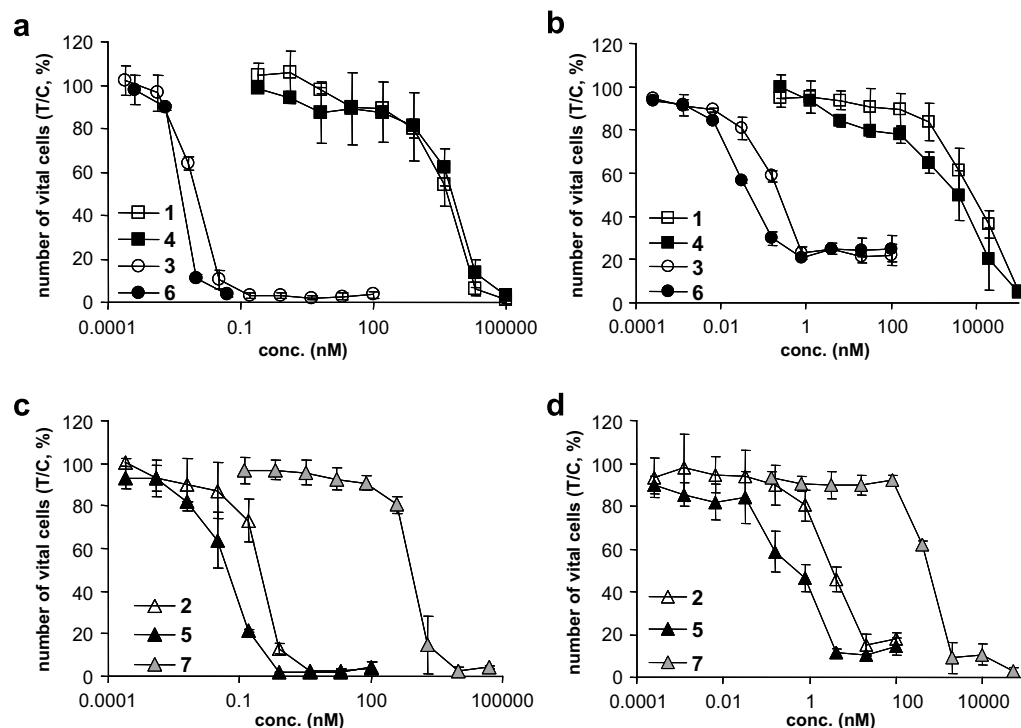Fig. 8. Concentration–effect curves of 2-acetylpyridine N,N-dimethyl(chalcogen)semicarbazones (**1–3**) (white symbols), their gallium(III) complexes [GaL₂][PF₆] (**4–6**) (black symbols) and ruthenium(III) complexes [RuL₂][PF₆] (**7**) (grey symbols), obtained by the MTT assay in 41M cells (left panels: a, c) and SK-BR-3 cells (right panels: b, d). Values are means ± standard deviations from at least three independent experiments.

pico- to nanomolar range and the semicarbazones in the low micromolar range. The difference between the potencies of the selenosemicarbazone HL^3 and the thiosemicarbazone HL^2 is about 13–22-fold depending on the cell line. The IC_{50} values of thiosemicarbazone HL^2 and semicarbazone HL^1 differ by at least three and up to five orders of magnitude (3100–65000) (Fig. 8).

We previously showed that the cytotoxic potency increases when α-N-heterocyclic thiosemicarbazones are bound to gallium(III) [9]. In the case of 2-acetylpyridine-N,N-dimethylsemicarbazone HL^1 and 2-acetylpyridine-N,N-dimethylselenosemicarbazone HL^3, this shift in cytotoxicity is less pronounced. The selenosemicarbazone HL^3 shows a 2–3 times lower activity than its corresponding gallium(III) complex (**6**), while the effect of complexation is small in the case of the semicarbazone HL^1 and its gallium complex (**4**). The lower stability of **4** in water could be a reasonable explanation, as the complex most probably dissociates to some extent within the time period of the experiment.

Although the effect of certain metal ions on the biological activity of thiosemicarbazones is well documented, there are only a few publications on complexes with ruthenium(III) [31,36,37]. The ruthenium(III) compound **7** that was tested in this work shows a large shift of IC_{50} to 0.9 and 0.58 μM in 41M and SK-BR-3 as compared to the ligand HL^2 (0.22 and 2.7 nM, respectively). This is a 4100 times lower cytotoxicity than that of the uncomplexed ligand and even 17000 times lower than that of the gallium(III) complex **5** in 41M cells. In SK-BR-3 cells, the effect on the cytotoxicity is somewhat less pronounced, with IC_{50} values differing by factors of 210 and 1000 in comparison to thiosemicarbazone **2** and gallium(III) compound **5**, respectively. Remarkably the ruthenium(III) complex shows IC_{50} values in the same order of magnitude as the iron(III) complex (0.126 μM in 41M cells and 0.45 μM in SK-BR-3 cells) studied previously [9]. This result confirms our assumption of the positive influence of gallium(III) on the cytotoxicity of N,N-disubstituted α-N-heterocyclic thiosemicarbazones in comparison to other metal ions. The effect of ruthenium(III) is comparable to that of iron(III), which might be due to their reasonable stability upon chelation by the thiosemicarbazones and the similar reactivity profiles.

4. Conclusions

The first gallium(III)-semicarbazone and gallium(III)-selenosemicarbazone complexes have been synthesised and characterised by X-ray crystallography. These preparations along with the synthesis of the ruthenium(III) complex with a thiosemicarbazone ligand with the same stoichiometry as for gallium(III) made it possible to study the effect of metal ion complexation and chalcogen donor identity on the antiproliferative activity of 2-acetylpyridine-N,N-dimethyl(chalcogen)semicarbazones. The antiproliferative activity of chalcogensemicarbazones was found to be strongly dependent on the identity of the chalcogen atom (O, S, Se) changing in the order $HL^1 \ll HL^2 < HL^3$ in both cancer cell lines (41M and SK-BR-3). A similar trend was found for the corresponding gallium(III) complexes: $[Ga(L^1)_2]^+ \ll [Ga(L^2)_2]^+ < [Ga(L^3)_2]^+$. Although the antiproliferative activity of the gallium complexes prepared is primarily determined by that of the corresponding chalcogensemicarbazones, the effect of complexation to gallium is obvious. In all cases enhancement of cytotoxicity is observed when going from metal-free ligands HL^{1-3} to the corresponding gallium complexes $[Ga(L^{1-3})_2]^+$. The rather small enhancement of the cytotoxicity of $[Ga(L^1)_2]^+$ as compared to HL^1 is probably caused by dissociation (to certain extent) of the complex in the cell culture medium, as evidenced by UV/vis measurement of aqueous solution of this complex. The effect of complexation of HL^2 to ruthenium(III) is opposite to that of binding to gallium(III). Taking into account our previous results on the cytotoxicity of HL^2, $[Ga(L^2)_2]^+$, and $[Fe(L_2)_2]^+$, the effect of ruthenium(III) appears to be comparable with or even somewhat more attenuating than that of iron(III), resulting in the following rank order: $[Ru(L^2)_2]^+ \leqslant [Fe(L^2)_2] \ll HL^2 < [Ga(L^2)_2]^+$.

Appendix A. Supplementary material

Crystal data and details of data collection for **1** · CH_3OH, UV/vis spectra of **4–7** measured at 298 K over 20 h in 1% $DMSO/H_2O$, directly measured ^{77}Se NMR and the ^1H, ^{77}Se COSY NMR spectra. Crystallographic data for the structures reported in this paper have been deposited with the Cambridge Crystallographic Data Center as supplementary publication nos. CCDC 647093–647099. Copies of the data can be obtained free of charge on application to The Director, CCDC, 12 Union Road, Cambridge CB2 1EZ, UK (fax: +44 1223 336 033; e-mail: deposit@ccdc.cam.ac.uk). Supplementary data associated with this article can be found, in the online version, at doi:10.1016/j.jinorgbio.2007.07.026.

References

[1] D.X. West, S.B. Padhye, P.B. Sonawane, Struct. Bond. 76 (1991) 1–50.

[2] R.W. Brockman, J.R. Thomson, M.J. Bell, H.E. Skipper, Cancer Res. 16 (1956) 167–170.

[3] E.C. Moore, M.S. Zedeck, K.C. Agrawal, A.C. Sartorelli, Biochemistry 9 (1970) 4492–4498.

[4] F.A. French, E.J. Blanz Jr., S.C. Shaddix, R.W. Brockman, J. Med. Chem. 17 (1974) 172–181.

[5] J. Shao, B. Zhou, B. Chu, Y. Yen, Curr. Cancer Drug Targets 6 (2006) 409–431.

[6] E.C. Moore, A.C. Sartorelli, Pharm. Ther. 24 (1984) 439–447.

[7] T.B. Chaston, D.B. Lovejoy, R.N. Watts, D.R. Richardson, Clin. Cancer Res. 9 (2003) 402–414.

[8] J.S. Casas, M.S. Garcia-Tasende, J. Sordo, Coord. Chem. Rev. 209 (2000) 197–261.

[9] C.R. Kowol, R. Berger, R. Eichinger, A. Roller, M.A. Jakupec, P.P. Schmidt, V.B. Arion, B.K. Keppler, J. Med. Chem. 50 (2007) 1254–1265.

[10] C. Vogelesang, Recl. Trav. Chim. Pays-Bas 62 (1943) 5–11.

[11] E. Alessio, G. Balducci, M. Calligaris, G. Costa, W.M. Attia, G. Mestroni, Inorg. Chem. 30 (1991) 609–618.

[12] D.L. Klayman, J.P. Scovill, J.F. Bartosevich, C.J. Mason, J. Med. Chem. 22 (1979) 1367–1373.

[13] D.L. Klayman, J.P. Scovill, J.F. Bartosevich, C.J. Mason, Eur. J. Med. Chem. 16 (1981) 317–320.

[14] SAINT-PLUS (Version 7.06a) and APEX2, Bruker-Nonius AXS Inc., Madison, WI, USA, 2004.

[15] G.M. Sheldrick, SHELXS-97, Program for Crystal Structure Solution, University of Göttingen, Germany, 1997.

[16] G.M. Sheldrick, SHELXL-97, Program for Crystal Structure Refinement, University of Göttingen, Germany, 1997.

[17] C.K. Johnson, Report ORNL-5138, Oak Ridge National Laboratory, 840 Oak Ridge, TN, 1976.

[18] International Tables for X-ray Crystallography, vol. C, Tables 4.2.6.8 and 6.1.1.4, Kluwer Academic Press, Dordrecht, The Netherlands, 1992.

[19] J. Easmon, G. Heinisch, W. Holzer, Heterocycles 29 (1989) 1399–1408.

[20] J. Easmon, G. Heinisch, W. Holzer, Sci. Pharm. 61 (1993) 3–10.

[21] A.A. Isab, M.I.M. Wazeer, M. Fettouhi, S. Ahmad, W. Ashraf, Polyhedron 25 (2006) 2629–2636.

[22] R. Wu, G. Hernandez, J.D. Odom, R.B. Dunlap, L.A. Silks, Chem. Commun. 10 (1996) 1125–1126.

[23] T. Okamura, K. Taniuchi, K. Lee, H. Yamamoto, N. Ueyama, A. Nakamura, Inorg. Chem. 45 (2006) 9374–9380.

[24] D. Kovala-Demertzi, A. Domopoulou, M. Demertzis, J. Valdes-Martinez, S. Hernandez-Ortega, G. Espinosa-Perez, D.X. West, M.M. Salberg, G.A. Bain, P.D. Bloom, Polyhedron 15 (1996) 2587–2596.

[25] D.V. Naik, G.J. Palenik, Acta Cryst.B. 30 (1974) 2396–2401.

[26] D.X. West, G.A. Bain, R.J. Butcher, J.P. Jasinski, Y. Li, R.Y. Pozdniakiv, Polyhedron 15 (1996) 665–674.

[27] E. Bermejo, R. Carballo, A. Castiñeiras, R. Dominquez, A.E. Liberta, C. Maichle-Mössmer, M.M. Salberg, D.X. West, Eur. J. Inorg. Chem. (1999) 965–973.

[28] Cambridge Structure Database, Version 5.28, November 2006.

[29] D.X. West, B.L. Mokijewski, H. Gebremedhin, T.J. Romack, Transition Met. Chem. 17 (1992) 384–386.

[30] V.B. Arion, M.A. Jakupec, M. Galanski, P. Unfried, B.K. Keppler, J. Inorg. Biochem. 91 (2002) 298–305.

[31] S. Grguric-Sipka, C.R. Kowol, S-M. Valiahdi, R. Eichinger, M.A. Jakupec, A. Roller, S. Shova, V.B. Arion, B.K. Keppler, Eur. J. Inorg. Chem. 18 (2007) 2870–2878.

[32] P.D. Beer, H. Sikanyika, C. Blackburn, J.F. McAleer, M.G.B. Drew, J. Chem. Soc. Dalton Trans. (1990) 3295–3300.

[33] D.L. Klayman, J.P. Scovill, C.J. Mason, J.F. Bartosevich, J. Bruce, A.J. Lin, Arzneim.-Forsch. 33 (1983) 909–912.

[34] T.R. Todorović, A. Bacchi, N.O. Juranić, D.M. Sladić, G. Pelizzi, T.T. Božić, N.R. Filipović, K.K. Anđelković, Polyhedron 26 (2007) 3428–3436.

[35] K.C. Agrawal, B.A. Booth, R.L. Michaud, E.C. Moore, A.C. Sartorelli, Biochem. Pharmacol. 23 (1974) 2421–2429.

[36] F. Bregant, S. Pacor, S. Ghosh, S.K. Chattopadhyah, G. Sava, Anticancer Res. 13 (1993) 1011–1017.

[37] U.K. Mazumder, M. Gupta, S.S. Karki, S. Bhattacharya, S. Rathinasamy, S. Thangavel, Chem. Pharm. Bull. 52 (2004) 178–185.

SUPPLEMENTARY MATERIAL

Effect of Metal Ion Complexation and Chalcogen Donor Identity on the Antiproliferative Activity of 2-Acetylpyridine N,N-Dimethyl(chalcogen)semicarbazones

Christian R. Kowol, Rene Eichinger, Michael A. Jakupec, Markus Galanski, Vladimir B. Arion, Bernhard K. Keppler

Supplementary Material:

UV/vis stability measurements

Figure S1. UV/vis spectroscopy data of **4** in DMSO/H_2O 1 : 100. First measurement

(black), after 5 h (red), after 10 h (green), after 15 h (blue) and after 20 h (cyan).
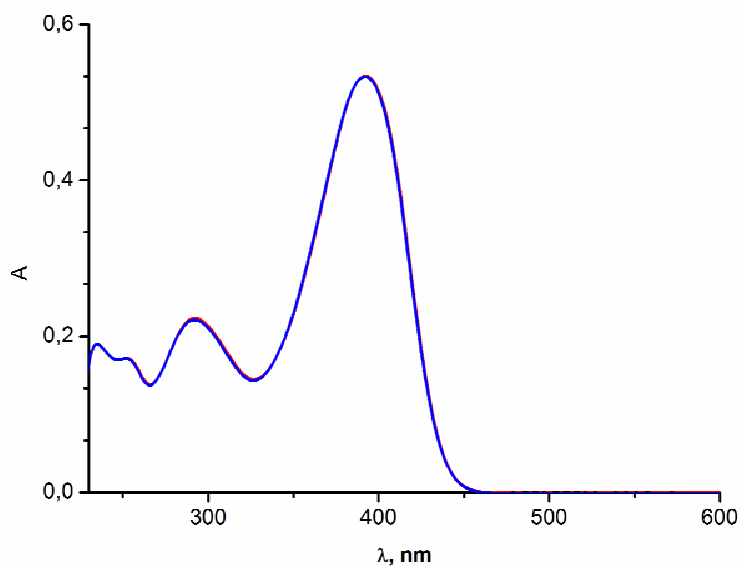
Figure S2. UV/vis spectroscopy data of **5** in DMSO/H_2O 1 : 100. First measurement

(red), after 15 h (blue).
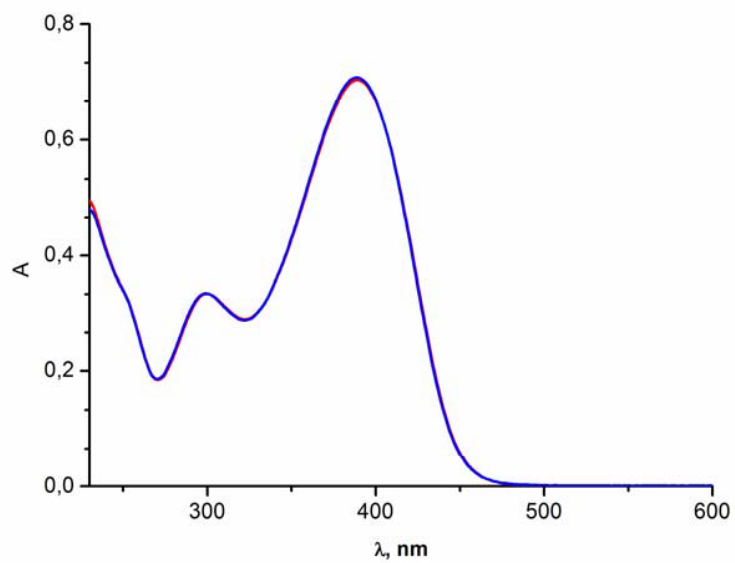
Figure S3. UV/vis spectroscopy data of **6** in DMSO/H_2O 1 : 100. First measurement (red), after 20 h (blue).
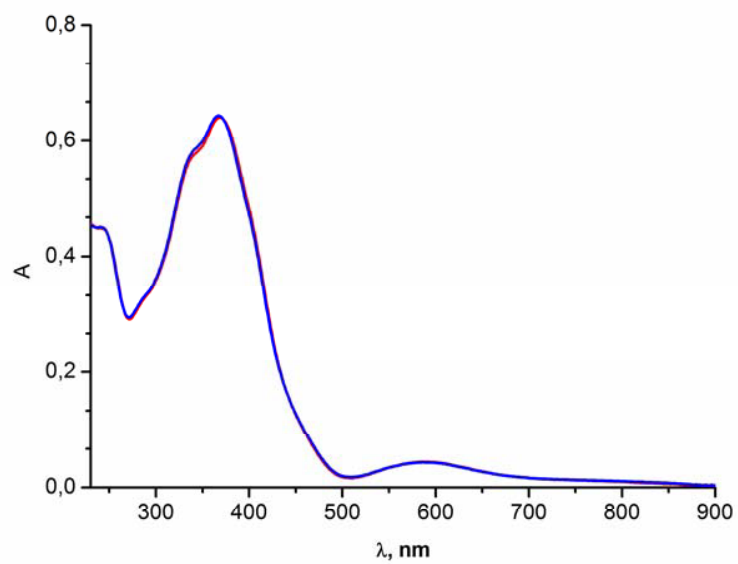
Figure S4. UV/vis spectroscopy data of **7** in DMSO/H_2O 1 : 100. First measurement (red), after 20 h (blue).

^{1}H-^{77}Se COSY and ^{77}Se NMR spectrum
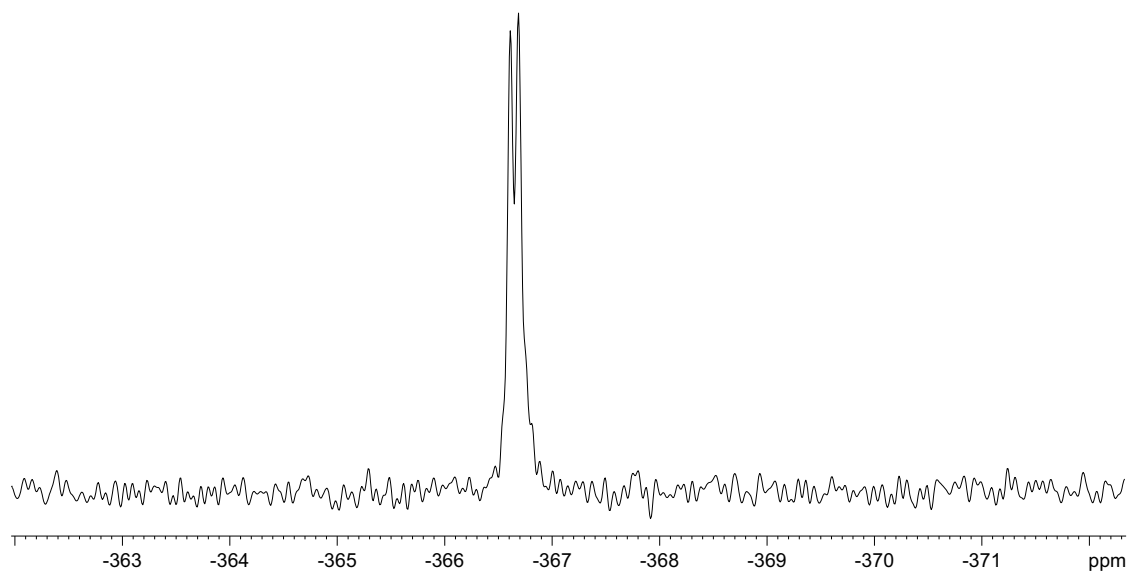
Figure S5. ^{77}Se NMR spectrum of the E′-isomer of HL^3 displaying a doublet at −366.9 ppm (*J*= 7 Hz)
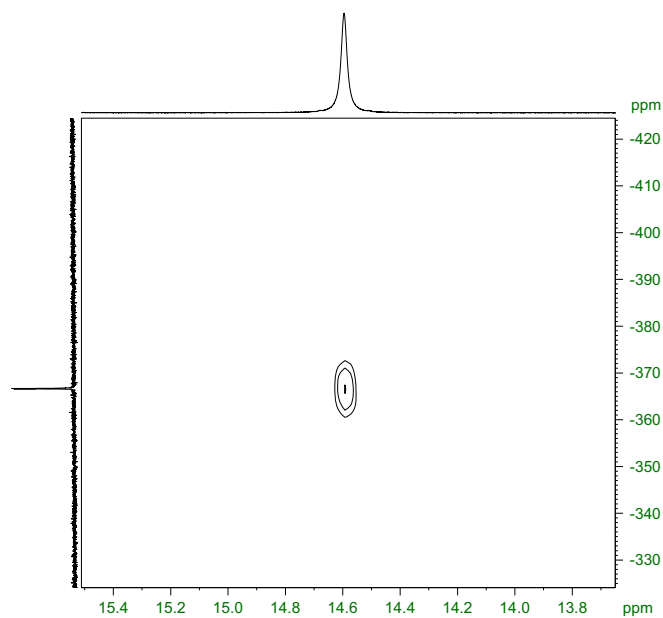
Figure S6. ^{1}H,^{77}Se COSY NMR spectrum of the E′-isomer of HL^3.

S4

Crystal data and discussion of the structure of 1·CH₃OH

The ligand adopts a conformation with the C5–N1 bond of the pyridine ring trans to the azomethine bond C6–N2. The N2–N3 distance of 1.378(2) Å is comparable to those found in 2HL·[Zn(H₂O)₆]ClO₄[i] of 1.355(4) and 1.354(4) Å, where HL = 2-formylpyridine-*N*-oxide semicarbazone and it is shorter than the accepted length of single N–N bond (1.45 Å),[ii] indicating some extent of electron density delocalisation over the semicarbazide moiety. The double bond nature of the C8–O1 bond is also evident [1.228(2) Å]. The ligand crystallizes with a methanol molecule involved in two intermolecular hydrogen bonding interactions. As a proton donor O2 forms the hydrogen bond O2–H···O1 [O2–H 0.84, H···O1 1.92, O2···O1 2.726(3) Å, ∠O2–H···O1 160.0°] and as proton acceptor the H bond O2···H–N3 (−x + 2, −y, −z + 1) [O2···H 2.56, O2···N3 3.149(3), H–N3 0.88 Å, ∠O2···H–N3 125.3°].
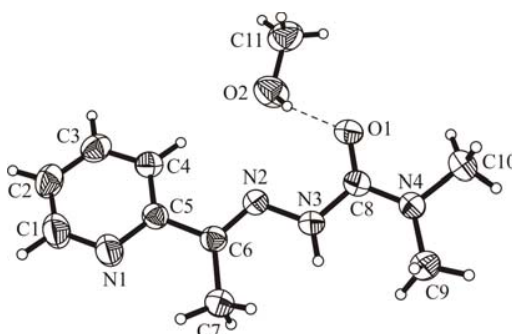
Figure S7. ORTEP plot of HL¹·CH₃OH with atom numbering scheme. The thermal ellipsoids are drawn at 40% probability level. Selected bond lengths (Å) and bond angles (deg): C6–N2 1.282(3), N2–N3 1.378(2), N3–C8 1.376(3), C8–O1 1.228(2), C8–N4 1.349(3); N1–C5–C6–N2 −167.1(2), N2–N3–C8–O1 −2.7(3)°.

X-ray diffraction measurements were performed on an X8APEX II CCD diffractometer at 293 K. The single crystal of **1**·CH_3OH was positioned at 40 mm from the detector and 1014 frames were measured, each for 10 s over 1° scan width.

Table S1. Crystal data and details of data collection for **1**·CH_3OH.

Complex	**1**·CH_3OH
empirical formula	$C_{11}H_{18}N_4O_2$
Fw	238.29
Space group	$P2_1/n$
a, Å	10.7324(7)
b, Å	8.5870(5)
c, Å	14.5715(9)
α, deg	
β, deg	104.488(4)
γ, deg	
V, Å^3	1300.19(14)
Z	4
λ, Å	0.71073
ρ_{calcd}, g cm^{-3}	1.217
crystal size, mm^3	0.30 × 0.16 × 0.16
T, K	293
μ, mm^{-1}	0.086
$R1^a$	0.0510
$wR2^b$	0.1682
GOF^c	1.030

^{a} R1 = $\Sigma||F_o| - |F_c||/\Sigma|F_o|$, ^{b} $wR2 = \{\Sigma[w\,(F_o^2 - F_c^2)^2]\,/\Sigma[w(F_o^2)^2\,]\}^{1/2}$. ^{c} GOF = $\{\Sigma[w(F_o^2 - F_c^2)^2]\,/(n - p)\}^{1/2}$, where n is the number of reflections and p is the total number of parameters refined.

[i] Q. Yu, L-G. Zhu, H-D. Bian, J-H. Deng, X-E. Yang, G-Q. Guo, H. Liang, Jiegou Huaxue 24 (2005) 1271−1275.

[ii] P. Müller, R. Herbst-Irmer, A. L. Spek, T. R. Schneider, M. R. Sawaya, Crystal Structure Refinement. A Crystallographer's Guide to SHELXL, Oxford University Press, 2006

2.3 An Electrochemical Study of Antineoplastic Gallium, Iron and Ruthenium Complexes with Redox Noninnocent α-N-Heterocyclic Chalcogensemicarbazones

Kowol, C. R.; Reisner, E.; Chiorescu, I.; Arion, V. B.; Galanski, M.; Deubel, D. V.; Keppler, B. K.

Inorganic Chemistry

Article

An Electrochemical Study of Antineoplastic Gallium, Iron and Ruthenium Complexes with Redox Noninnocent α-N-Heterocyclic Chalcogensemicarbazones

Christian R. Kowol,[†] Erwin Reisner,*[,†,‡] Ion Chiorescu,[†] Vladimir B. Arion,*[,†] Markus Galanski,[†] Dirk V. Deubel,[†] and Bernhard K. Keppler[†]

Institute of Inorganic Chemistry, University of Vienna, Währingerstrasse 42, A-1090 Vienna, Austria, and Inorganic Chemistry Laboratory, University of Oxford, South Parks Road, Oxford OX1 3QR, U.K.

The electrochemical properties of a series of α-N-heterocyclic chalcogensemicarbazones (HL), namely, thiosemi-carbazones, selenosemicarbazones, and semicarbazones, and their gallium(III), iron(III), and ruthenium(III) complexes with the general formula $[ML_2][Y]$ (M = Ga, Fe or Ru; Y = PF_6^-, NO_3^-, or $FeCl_4^-$) were studied by cyclic voltammetry. The novel compounds were characterized by elemental analysis, a number of spectroscopic methods (NMR, UV−vis, IR), mass spectrometry and by X-ray crystallography. All complexes show several, mostly reversible, redox waves attributable to the reduction of the noninnocent chalcogensemicarbazone ligands at lower potentials (< −0.4 V vs NHE) than the metal-centered iron or ruthenium redox waves (>0 V vs NHE) in organic electrolyte solutions. The cyclic voltammograms of the gallium complexes display at least two consecutive reversible one-electron reduction waves. These reductions are shifted by ~0.6 V to lower potentials in the corresponding iron and ruthenium complexes. The electrochemical, chemical, and spectroscopic data indicate that the ligand-centered reduction takes place at the $CH_3C{=}N$ double bond. Quantum chemical calculations on the geometric and electronic structures of 2-acetylpyridine $^4N,^4N$-dimethylthiosemicarbazone (HL^B), the corresponding metal complexes $[Ga(L^B)_2]^+$ and $[Fe^{II}(L^B)_2]$, and the one-electron reduction product for each of these species support the assignment of the reduction site and elucidate the observed order of the ligand-centered redox potentials, $E_{1/2}([Fe^{II}(L)_2]) < E_{1/2}(HL) < E_{1/2}([Ga(L)_2]^+)$. The influence of water on the redox potentials of the complexes is reported and the physiological relevance of the electrochemical data for cytotoxicity as well as for ribonucleotide reductase inhibitory capacity are discussed.

Introduction

Metal-based anticancer prodrugs may be activated selectively in the hypoxic tumor tissue upon reduction by biological reducing agents.[1,2] Electron-transfer can occur either to the metal-center, or, if in the biologically accessible range, to noninnocent ligands, resulting in reactive species capable of attacking biologically relevant target molecules either by ligand displacement at the low valent metal center or by radicals formed at the ligand entity, respectively. An *activation-by-reduction* step is thought to be important for platinum(IV) complexes that have been evaluated in clinical development, for example, tetraplatin ($[PtCl_4(1,2\text{-}(NH_2)_2\text{-}C_6H_{10})]$, abandoned), satraplatin ($[PtCl_2(OAc)_2(NH_3)(NH_2\text{-}C_6H_{11})]$, phase III), and iproplatin ($[PtCl_2(OH)_2(NH_2{}^iPr)_2]$, abandoned),[3] as well as for the activation of investigational ruthenium(III) prodrugs such as *trans*-$[RuCl_4(indazole)_2]^-$ (KP1019) and *trans*-$[RuCl_4(imidazole)(S\text{-}DMSO)]^-$ (NAMI-A), both of which have already finished phase I clinical trials.[4−6] Indeed, an increasing metal-centered redox potential was shown to correlate with higher cytotoxicity for a series of platinum(IV)[7] and azole-based ruthenium(III) compounds.[8] Metal-centered redox potentials can be tuned and

---

* To whom correspondence should be addressed. Phone: +431427752615. Fax: +431427752680. E-mail: erwin.reisner@chem.ox.ac.uk (E.R.); vladimir.arion@univie.ac.at (V.B.A.).
† University of Vienna.
‡ University of Oxford.

(1) Reisner, E.; Arion, V. B.; Keppler, B. K.; Pombeiro, A. J. L. *Inorg. Chim. Acta* **2008**, *361*, 1569–1583.
(2) Clarke, M. J.; Zhu, F.; Frasca, D. R. *Chem. Rev.* **1999**, *99*, 2511–2533.
(3) Hall, M. D.; Hambley, T. W. *Coord. Chem. Rev.* **2002**, *232*, 49–67.

predicted by application of Lever's parametrization method, facilitating markedly the design of bioreductive drugs.[1,9,10] Although hypoxia-selective organic drugs are under intensive investigation, for example, nitroimidazoles,[11] little is known about reductively activated metal-based compounds containing electronically noninnocent ligands with physiologically accessible redox potentials. One such example is ferrocenyl hydroxytamoxifen, containing a ferrocene-moiety attached to a hydroxylated form of the estrogen receptor modulator tamoxifen, which shows high activity on estrogen receptor positive and negative cell lines.[12,13]

Thiosemicarbazones are versatile redox noninnocent ligands with a wide range of coordination modes in metal complexes, in particular, when their binding capacity is further increased by condensation of the thiosemicarbazide with an aldehyde or ketone containing an additional donor atom in a suitable position for chelation.[14] In addition to their exciting coordination chemistry, thiosemicarbazones have evoked considerable interest because of their broad spectrum of pharmacological activity. In particular, α-N-heterocyclic thiosemicarbazones were found to possess antitumor, antimalarial, antibacterial, antifungal, and antiviral activity,[15] and ^{64}Cu-bis(thiosemicarbazonate) complexes are under investigation as hypoxia-selective positron emission tomography tracers.[16] The enzyme ribonucleotide reductase (RR) has been identified as the principal molecular target.[17] Ribonucleotide reductase converts ribonucleotides to deoxyribonucleotides necessary for DNA synthesis and is highly expressed in tumor cells making it a suitable and well established target in cancer chemotherapy.[18] Initially, the inhibition of RR was attributed to the ability of thiosemicarbazones as strong chelators to remove iron from the enzyme active site, but later, it was found that preformed iron chelates of some thiosemicarbazones with a terminal NH_2 group ($^4NH_2$) show higher RR inhibitory activity than the uncomplexed thio-

semicarbazones.[19−21] This is in agreement with data on 3-aminopyridine-2-carboxaldeyde thiosemicarbazone (Triapine), an investigational drug currently in phase II clinical trials, where an increase in cytotoxicity upon coordination to iron was found.[22]

We reported previously that in the presence of the reductant dithiothreitol (DTT) iron(III) complexes with ^4N-disubstituted α-N-heterocyclic thiosemicarbazone ligands show the fastest destruction of the R2 specific tyrosine free radical in mouse RR followed by the metal-free ligands and the corresponding gallium(III) complexes.[23] In the absence of DTT, no tyrosyl radical quenching was observed. The cytotoxicity data for the same compounds tested in the cancer cell lines 41 M (ovarian carcinoma) and SK-BR-3 (mammary carcinoma) are in reversed order: the gallium complexes exhibited slightly higher cytotoxicity in the low nanomolar range in comparison to the metal-free ligand, whereas the iron(III) complexes displayed a much lower cytotoxicity in the micromolar range. Thus, iron is essential for the fast quenching of the tyrosyl radical in RR, but it is not solely responsible for the antitumor potency of the ^4N-disubstituted thiosemicarbazone derivatives suggesting the existence of additional molecular targets. The requirement of an adequate reductant (e.g., DTT) for successful radical quenching indicates that the iron(III) complex is reduced to its iron(II) form prior radical quenching.

These findings prompted us to prepare a series of gallium(III), iron(III), and ruthenium(III) complexes of the general formula $[ML_2][Y]$ (M = Ga, Fe and Ru; Y = PF_6^-, NO_3^- or $FeCl_4^-$), where HL is a chalcogensemicarbazone ligand (Charts 1 and 2), and to investigate the effect of coordination to the metal on their metal- and ligand-centered redox properties by carrying out detailed electrochemical investigations and quantum chemical calculations. We were particularly interested to clarify if the redox properties/potentials of the prepared compounds are of physiological relevance, that is, to elucidate whether a relation between their electrochemical properties and antiproliferative activity or R2 specific tyrosine free radical quenching ability can be found.

Experimental Section

All solvents and reagents were obtained from commercial suppliers and used without further purification. The ligands HL^A, HL^B, $HL^E−HL^G$ and complexes **1A**, **1B**, **1E−1G**, **2A**, **2B**, **2E−2G**, **2′A−2′G**,[23] as well as HL^J, HL^K, **1J**, **1K**, **3B**,[24] and HL^{D25} were prepared as described previously. HL^C was synthesized

(4) Alessio, E.; Mestroni, G.; Bergamo, A.; Sava, G. *Curr. Top. Med. Chem.* **2004**, *4*, 1525–1535.

(5) Clarke, M. J. *Coord. Chem. Rev.* **2003**, *236*, 209–233.

(6) Hartinger, C. G.; Zorbas-Seifried, S.; Jakupec, M. A.; Kynast, B.; Zorbas, H.; Keppler, B. K. *J. Inorg. Biochem.* **2006**, *100*, 891–904.

(7) Hall, M. D.; Amjadi, S.; Zhang, M.; Beale, P. J.; Hambley, T. W. *J. Inorg. Biochem.* **2004**, *98*, 1614–1624.

(8) Jakupec, M. A.; Reisner, E.; Eichinger, A.; Pongratz, M.; Arion, V. B.; Galanski, M.; Hartinger, C. G.; Keppler, B. K. *J. Med. Chem.* **2005**, *48*, 2831–2837.

(9) Lever, A. B. P. *Inorg. Chem.* **1990**, *29*, 1271–1285.

(10) Reisner, E.; Arion, V. B.; Eichinger, A.; Kandler, N.; Giester, G.; Pombeiro, A. J. L.; Keppler, B. K. *Inorg. Chem.* **2005**, *44*, 6704–6716.

(11) Brown, J. M. *Cancer Res.* **1999**, *59*, 5863–5870.

(12) Top, S.; Tang, J.; Vessieres, A.; Carrez, D.; Provot, C.; Jaouen, G. *Chem. Commun.* **1996**, 955–956.

(13) Hillard, E.; Vessieres, A.; Thouin, L.; Jaouen, G.; Amatore, C. *Angew. Chem., Int. Ed.* **2006**, *45*, 285–290.

(14) (a) Gerbeleu, N. V.; Arion, V. B.; Burgess, J. *Template Synthesis of Macrocyclic Compunds*, Wiley-VCH: Weinheim, Germany, 1999; Chapter 2. (b) Casas, J. S.; Garcia-Tasende, M. S.; Sordo, J. *Coord. Chem. Rev.* **2000**, *209*, 197–261.

(15) West, D. X.; Padhye, S. B.; Sonawane, P. B. *Struct. Bonding (Berlin)* **1991**, *76*, 1–50.

(16) Bonnitcha, P. D.; Vavere, A. L.; Lewis, J. S.; Dilworth, J. R. *J. Med. Chem.* **2008**, *51*, 2985–2991.

(17) Moore, E. C.; Zedeck, M. S.; Agrawal, K. C.; Sartorelli, A. C. *Biochemistry* **1970**, *9*, 4492–4498.

(18) Shao, J.; Zhou, B.; Chu, B.; Yen, Y. *Curr. Cancer Drug Targets* **2006**, *6*, 409–431.

(19) Saryan, L. A.; Ankel, E.; Krishnamurti, C.; Petering, D. H. *J. Med. Chem.* **1979**, *22*, 1218–1221.

(20) Preidecker, P. J.; Agrawal, K. C.; Sartorelli, A. C.; Moore, E. C. *Mol. Pharmacol.* **1980**, *18*, 507–512.

(21) Thelander, L.; Gräslund, A. *J. Biol. Chem.* **1983**, *258*, 4063–4066.

(22) Finch, R. A.; Liu, M.-C.; Cory, A. H.; Cory, J. G.; Sartorelli, A. C. *Adv. Enzyme Regul.* **1999**, *39*, 3–12.

(23) Kowol, C. R.; Berger, R.; Eichinger, R.; Roller, A.; Jakupec, M. A.; Schmidt, P. P.; Arion, V. B.; Keppler, B. K. *J. Med. Chem.* **2007**, *50*, 1254–1265.

(24) Kowol, C. R.; Eichinger, R.; Jakupec, M. A.; Galanski, M.; Arion, V. B.; Keppler, B. K. *J. Inorg. Biochem.* **2007**, *101*, 1946–1957.

(25) West, D. X.; Ingram, J. J., III.; Kozub, N. M.; Bain, G. A.; Liberta, A. E. *Transition Met. Chem.* **1996**, *21*, 213–218.

80

Chart 1. Chalcogensemicarbazone Ligands Used in This Study
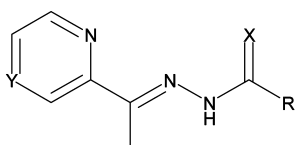
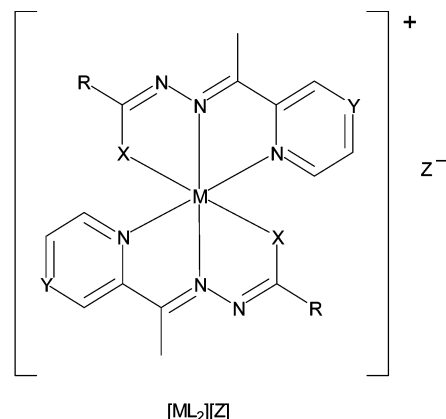|	
X = S, Y = CH, R = N(C$_4$H$_8$)	(**HL^A**)
X = S, Y = CH, R = N(CH$_3$)$_2$	(**HL^B**)
X = S, Y = CH, R = NH(C$_6$H$_5$)	(**HL^C**)
X = S, Y = CH, R = NH(p-C$_6$H$_4$NO$_2$)	(**HL^D**)
X = S, Y = N, R = N(C$_4$H$_8$)	(**HL^E**)
X = S, Y = N, R = N(C$_5$H$_{10}$)	(**HL^F**)
X = S, Y = N, R = N(CH$_3$)$_2$	(**HL^G**)
X = S, Y = N, R = NH(C$_6$H$_5$)	(**HL^H**)
X = S, Y = N, R = NH(p-C$_6$H$_4$NO$_2$)	(**HL^I**)
X = O, Y = CH, R = N(CH$_3$)$_2$	(**HL^J**)
X = Se, Y = CH, R = N(CH$_3$)$_2$	(**HL^K**)

(**HL^M**)

Chart 2. Library of Metal Chalcogensemicarbazonate Complexes

[ML$_2$][Z]

M = Ga, L = L^A, Z = PF$_6$	(**1A**)	M = Fe, L = L^A, Z = PF$_6$	(**2A**)
M = Ga, L = L^B, Z = PF$_6$	(**1B**)	M = Fe, L = L^B, Z = PF$_6$	(**2B**)
M = Ga, L = L^C, Z = PF$_6$	(**1C**)	M = Fe, L = L^C, Z = PF$_6$	(**2C**)
M = Ga, L = L^D, Z = NO$_3$	(**1D**)	M = Fe, L = L^D, Z = NO$_3$	(**2D**)
M = Ga, L = L^E, Z = PF$_6$	(**1E**)	M = Fe, L = L^E, Z = PF$_6$	(**2E**)
M = Ga, L = L^F, Z = PF$_6$	(**1F**)	M = Fe, L = L^F, Z = PF$_6$	(**2F**)
M = Ga, L = L^G, Z = PF$_6$	(**1G**)	M = Fe, L = L^G, Z = PF$_6$	(**2G**)
M = Ga, L = L^H, Z = NO$_3$	(**1H**)	M = Fe, L = L^H, Z = NO$_3$	(**2H**)
M = Ga, L = L^I, Z = NO$_3$	(**1I**)	M = Fe, L = L^I, Z = NO$_3$	(**2I**)
M = Ga, L = L^J, Z = PF$_6$	(**1J**)	M = Fe, L = L^A, Z = FeCl$_4$	(**2'A**)
M = Ga, L = L^K, Z = PF$_6$	(**1K**)	M = Fe, L = L^B, Z = FeCl$_4$	(**2'B**)
		M = Fe, L = L^E, Z = FeCl$_4$	(**2'E**)
		M = Fe, L = L^F, Z = FeCl$_4$	(**2'F**)
		M = Fe, L = L^G, Z = FeCl$_4$	(**2'G**)
		M = Ru, L = L^B, Z = PF$_6$	(**3B**)

by condensation of equimolar amounts of ^{4}N-phenylthiosemicarbazide and 2-acetylpyridine in boiling ethanol in 60% yield. Acetylpyrazine hydrazone was obtained by reacting acetylpyrazine with an excess of hydrazine hydrate as the reagent and solvent at room temperature for 24 h.

Elemental analyses were carried out on a Carlo Erba microanalyzer at the Microanalytical Laboratory of the University of Vienna. Electrospray ionization mass spectrometry was carried out with a Bruker Esquire 3000 instrument (Bruker Daltonic, Bremen, Germany). Expected and experimental isotope distributions were compared. Infrared spectra were obtained from KBr pellets with a Perkin-Elmer FT-IR 2000 instrument (4000−400 cm^{-1}). UV−vis spectra were recorded on a Perkin-Elmer Lambda 650 spectrophotometer using samples dissolved in methanol (900−210 nm). The iron complexes were measured on a Hewlett-Packard 8453 UV−vis spectrophotometer (1100−210 nm). Thermogravimetric analysis (TGA) and differential thermal analysis (DTA) measurements were carried out simultaneously with a Mettler Toledo TGA/SDTA851e apparatus, with a 3 °C/min heating rate under an air atmosphere. ^{1}H, ^{13}C, and ^{15}N one- and two-dimensional NMR spectra were recorded by using DMSO-d_6 as the solvent with a Bruker DPX 400 or a 500 MHz Bruker FT-NMR spectrometer Avance III. The residual ^{1}H and ^{13}C present in DMSO-d_6 were used as internal references. ^{15}N NMR chemical shifts were referenced relative to ammonium chloride as the external standard. Abbreviations for NMR data: py = pyridine, pz = pyrazine, ph = phenyl or p-nitrophenyl, C$_{q,py}$ = quaternary carbon of pyridine, C$_{q,pz}$ =

quaternary carbon of pyrazine, C$_{q,ph}$ = quaternary carbon of phenyl or p-nitrophenyl.

Electrochemistry. Cyclic voltammograms were measured in a three-electrode cell using a 2.0 mm-diameter glassy carbon or platinum disk working electrode, a platinum auxiliary electrode, and a Ag|Ag$^+$ reference electrode containing 0.10 M AgNO$_3$, the potential of which was corrected using an internal standard of ferrocenium/ferrocene. Measurements were performed at room temperature using an EG&G PARC 273A potentiostat/galvanostat. Deaeration of solutions was accomplished by passing a stream of argon through the solution for 5 min prior to the measurement and then maintaining a blanket atmosphere of argon over the solution during the measurement. Square wave voltammograms (SWVs) were recorded at 2 mV step height, 25 mV pulse, and a frequency of 100 Hz (scan rate 100 mV/s). The potentials were measured in 0.20 M [n-Bu$_4$N][BF$_4$]/CH$_3$CN, using [Fe(η^5-C$_5$H$_5$)$_2$] ($E_{1/2}$ = +0.69 V vs. NHE)^{26} as internal standard, and are quoted relative to the normal hydrogen electrode (NHE). **HL^C**, **HL^G**, and the nitro group containing compounds **HL^D**, **HL^I**, **1D**, **1I**, **2D**, and **2I** were

(26) Barette, W. C., Jr.; Johnson, H. W., Jr.; Sawyer, D. T. *Anal. Chem.* **1984**, *56*, 1890–1898.

measured in 0.20 M [*n*-Bu$_4$N][BF$_4$]/DMF ($E_{1/2}$ = +0.72 V vs NHE)[26] because of their low solubility in CH$_3$CN. For the cyclic voltammetry measurement in 0.15 M [*n*-Bu$_4$N][BF$_4$] in CH$_3$CN/H$_2$O or DMF/H$_2$O (7:3 v/v), a 2.0 mm-diameter glassy carbon working electrode, a platinum auxiliary electrode, and a Ag|Ag$^+$ reference electrode containing 3 M NaCl were used.

Synthesis of Ligands and Metal Complexes. Acetylpyrazine 4*N*-Phenylthiosemicarbazone (HL^H). To 4*N*-phenylthiosemicarbazide[27] (500 mg, 3.0 mmol) in boiling ethanol (15 mL) acetylpyrazine (365 mg, 3.0 mmol) was added, and the mixture was stirred under reflux for 5 h. After the reaction mixture was cooled to room temperature, the white solid was filtered off, washed with ethanol, and dried in vacuo. Yield: 590 mg (73%). Anal. Calcd for C$_{13}$H$_{13}$N$_5$S (M_r = 271.34 g/mol): C, 57.54; H, 4.83; N, 25.81. Found: C, 57.45; H, 4.86; N, 25.56. ESI-MS in MeOH (positive): *m/z* 294, [HL^H + Na]$^+$. ESI-MS in MeOH (negative): *m/z* 270, [HL^H − H]$^-$. IR spectrum in KBr, cm^{-1} (selected bands): 3305 s, 3217 s, 1588 m, 1528 s, 1517 s, 1469 s, 1445 s, 1362 m, 1304 m, 1259 m, 1190 s, 1169 s, 1014 m, 854 s, 806 m, 749 s, 690 s, 590 m, 555 m. UV−vis (MeOH), λ_{max}, nm (ε, M^{-1} cm^{-1}): 251 (10020), 326 (27950), 420sh (1930). ^{1}H NMR (400.13 MHz, DMSO-d_6): δ 10.84 (s, 1H, N−NH) 10.33 (s, 1H, NH), 9.79 (d, $^4J_{H,H}$ = 1.0 Hz, 1H, pz), 8.65−8.63 (m, 2H, pz), 7.53 (d, $^3J_{H,H}$ = 7.6 Hz, 2H, ph), 7.40 (t, $^3J_{H,H}$ = 7.6 Hz, 2H, ph), 7.25 (t, $^3J_{H,H}$ = 7.6 Hz, 1H, ph), 2.45 (s, 3H, CH$_3$) ppm. ^{13}C NMR (125.81 MHz, DMSO-d_6): δ 178.0 (C=S), 150.4 (C$_{q,pz}$), 147.6 (*C*=N), 144.6 (C$_{pz}$), 144.0 (C$_{pz}$), 143.6 (C$_{pz}$), 139.6 (C$_{q,ph}$), 128.6 (C$_{ph}$), 127.0 (C$_{ph}$), 126.2 (C$_{ph}$), 12.7 (CH$_3$) ppm. Single crystals suitable for X-ray data collection were obtained from a methanolic solution of HL^H saturated with dichloromethane.

Acetylpyrazine 4*N*-*p*-Nitrophenylthiosemicarbazone (HL^I). To acetylpyrazine hydrazone (300 mg, 2.20 mmol) in acetonitrile (7 mL) *p*-nitrophenyl isothiocyanate (397 mg, 2.20 mmol) in acetonitrile (6 mL) was added, and the reaction mixture was allowed to stir for 2 h at room temperature. The pale-yellow solid formed was filtered off, washed with acetonitrile, and dried in vacuo. Yield: 520 mg (75%). Anal. Calcd for C$_{13}$H$_{12}$N$_6$O$_2$S (M_r = 316.34 g/mol): C, 49.36; H, 3.82; N, 26.57. Found: C, 49.51; H, 3.85; N, 26.44. ESI-MS in MeOH (negative): *m/z* 315, [HL^I − H]$^-$. IR spectrum in KBr, cm^{-1} (selected bands): 3274 m, 3209 m, 3063 m, 1598 m, 1558 s, 1492 s, 1466 m, 1330 s, 1289 m, 1013 m, 850 s, 806 s, 751 m, 698 m, 625 m. UV−vis (MeOH), λ_{max}, nm (ε, M^{-1} cm^{-1}): 333 (34500), 424sh (3430). ^{1}H NMR (500.32 MHz, DMSO-d_6): δ 11.25 (s, 1H, N−NH), 10.58 (s, 1H, NH), 9.75 (d, $^4J_{H,H}$ = 1.0 Hz, 1H, pz), 8.68−8.66 (m, 2H, pz), 8.27 (m, 2H, ph), 8.00 (m, 2H, ph), 2.48 (s, 3H, CH$_3$) ppm. ^{13}C NMR (125.81 MHz, DMSO-d_6): δ 177.4 (C=S), 150.2 (C$_{q,pz}$), 148.9 (*C*=N), 145.8 (C$_{q,ph}$), 144.8 (C$_{pz}$), 144.3 (C$_{q, ph}$), 144.0 (C$_{pz}$), 143.7 (C$_{pz}$), 125.8 (C$_{ph}$), 124.1 (C$_{ph}$), 13.0 (CH$_3$) ppm.

N,N-Dimethyl-2-(1-pyridin-2-ylethyl)hydrazinecarbothioamide (HL^M). The ligand was prepared following the literature protocol.[28] Anal. Calcd for C$_{10}$H$_{16}$N$_4$S (M_r = 224.33 g/mol): C, 53.54; H, 7.19; N, 24.98; S, 14.29. Found: C, 53.49; H, 7.35; N, 25.11; S, 14.19. ESI-MS in MeOH (negative): *m/z* 223, [HL^M − H]$^-$. IR spectrum in KBr, cm^{-1} (selected bands): 3225 m, 3167 m, 2960 m, 1597 m, 1514 s, 1437 m, 1378 s, 1320 m, 1146 m, 1115 m, 1002 m, 963 m, 915 m, 828 m, 789 s, 662 m, 547 m. UV−vis (MeOH), λ_{max}, nm (ε, M^{-1} cm^{-1}): 246 (15030). ^{1}H NMR (500.10 MHz, DMSO-d_6): δ 8.88 (d, $^3J_{NH,NH}$ = 5.7 Hz, 1H, S=CN*H*), 8.50 (m, 1H, py), 7.77 (dt, $^3J_{H,H}$ = 7.6 Hz, $^4J_{H,H}$ = 1.9 Hz, 1H, py),

7.53 (d, $^3J_{H,H}$ = 7.9 Hz, 1H, py), 7.26 (m, 1H, py), 5.69 (dd, $^3J_{NH,NH}$ = 5.7 Hz, $^3J_{NH,CH}$ = 3.2 Hz, 1H, CHN*H*), 4.11 (dq, $^3J_{H,H}$ = 6.6 Hz, $^3J_{NH,CH}$ = 3.2 Hz, 1H, CH), 3.08 (s, 6H, N(CH$_3$)$_2$), 1.30 (d, $^3J_{H,H}$ = 6.6 Hz, 3H, CCH$_3$) ppm. ^{13}C NMR (125.81 MHz, DMSO-d_6): δ 182.8 (C=S), 163.0 (C$_{q,py}$), 149.2 (C$_{py}$), 137.0 (C$_{py}$), 122.7 (C$_{py}$), 121.7 (C$_{py}$), 61.0 (CH), 40.6 (N(CH$_3$)$_2$), 20.0 (CCH$_3$) ppm. ^{15}N NMR (50.70 MHz, DMSO-d_6): δ 291.2 (N$_{py}$), 116.7 ($^1J_{N,H}$ = 98 Hz, CHNH), 76.8 ($^1J_{N,H}$ = 78 Hz, NH), 72.5 (N(CH$_3$)$_2$) ppm. Single crystals suitable for X-ray data collection were obtained by slow evaporation of a methanolic solution of HL^M.

[Bis(2-acetylpyridine 4*N*-Phenylthiosemicarbazonato)-N,N,S-gallium(III)]hexafluorophosphate Monohydrate, [Ga(L^C)$_2$]PF$_6$·H$_2$O (1C). To 2-acetylpyridine 4*N*-phenylthiosemicarbazone (HL^C) (50 mg, 0.185 mmol) in dry ethanol (5 mL) at room temperature gallium(III) nitrate nonahydrate (40 mg, 0.096 mmol) in ethanol (2 mL) was added, and the reaction mixture was allowed to stir for 2 h. The solution was filtered to remove undissolved material, and ammonium hexafluorophosphate (60 mg, 0.37 mmol) was added to the filtrate. The yellow solid formed was filtered off after 30 min, washed with ethanol, and dried in vacuo. Yield: 50 mg (70%). Anal. Calcd for C$_{28}$H$_{26}$F$_6$GaN$_8$PS$_2$·H$_2$O (M_r = 771.39 g/mol): C, 43.60; H, 3.66; N, 14.53. Found: C, 43.28; H, 3.53; N, 14.44. ESI-MS in MeOH (positive): *m/z* 607, [Ga(L^C)$_2$]$^+$; ESI-MS in MeOH (negative): *m/z* 145, [PF$_6$]$^-$. IR spectrum in KBr, cm^{-1} (selected bands): 3389 m, 1598 m, 1498 m, 1457 s, 1429 s, 848 vs, 558 m. UV−vis (MeOH), λ_{max}, nm (ε, M^{-1} cm^{-1}): 230sh (32670), 254 (31090), 263sh (29710), 300 (15850), 405 (43350). ^{1}H NMR (400.13 MHz, DMSO-d_6): δ 10.26 (s, 2H, NH), 8.36 (d, $^3J_{H,H}$ = 7.8 Hz, 2H, py), 8.30 (m, 2H, py), 8.10 (d, $^3J_{H,H}$ = 5.1 Hz, 2H, py), 7.79 (d, $^3J_{H,H}$ = 8.1 Hz, 4H, ph), 7.67 (m, 2H, py), 7.38 (t, $^3J_{H,H}$ = 8.1 Hz, 4H, ph), 7.10 (t, $^3J_{H,H}$ = 7.3 Hz, 2H, ph), 2.95 (s, 6H, CH$_3$) ppm. ^{13}C NMR (100.63 MHz, DMSO-d_6): δ 172.5 (C−S), 152.1 (*C*=N), 145.6 (C$_{q,py}$), 145.6 (C$_{py}$), 143.4 (C$_{py}$), 140.5 (C$_{q,ph}$), 129.6 (C$_{ph}$), 128.8 (C$_{ph}$), 125.7 (C$_{py}$), 124.4 (C$_{ph}$), 122.2 (C$_{ph}$), 16.1 (CH$_3$) ppm.

[Bis(2-acetylpyridine 4*N*-*p*-Nitrophenylthiosemicarbazonato)-N,N,S-gallium(III)]nitrate Monohydrate, [Ga(L^D)$_2$]NO$_3$·H$_2$O (1D). To 2-acetylpyridine 4*N*-*p*-nitrophenylthiosemicarbazone (HL^D) (100 mg, 0.32 mmol) in boiling methanol (25 mL) gallium(III) nitrate nonahydrate (67 mg, 0.16 mmol) in methanol (2 mL) was added, and the reaction mixture was stirred under reflux for 1 h. The yellow solid was separated from the hot solution by filtration, washed with methanol, and dried in vacuo. Yield: 50 mg (41%). Anal. Calcd for C$_{28}$H$_{24}$GaN$_{11}$O$_7$S$_2$·H$_2$O (M_r = 778.43 g/mol): C, 43.20; H, 3.37; N, 19.79. Found: C, 43.04; H, 3.40; N, 19.56. ESI-MS in MeOH (positive): *m/z* 697, [Ga(L^D)$_2$]$^+$. ESI-MS in MeOH (negative): *m/z* 695, [Ga(L^D)$_2$ − 2H]$^-$. IR spectrum in KBr, cm^{-1} (selected bands): 3078 w, 1574 s, 1495 s, 1437 s, 1404 m, 1324 s, 1302 s, 1260 s, 1108 s, 848 m, 750 m. UV−vis (MeOH), λ_{max}, nm (ε, M^{-1} cm^{-1}): 251sh (24650), 296sh (19880), 330sh (26520), 396 (66330), 409sh (62220). ^{1}H NMR (400.13 MHz, DMSO-d_6): δ 10.77 (s, 2H, NH), 8.48 (d, $^3J_{H,H}$ = 8.1 Hz, 2H, py), 8.35 (m, 2H, py), 8.31 (m, 4H, ph), 8.18 (d, $^3J_{H,H}$ = 4.8 Hz, 2H, py), 8.08 (m, 4H, ph), 7.73 (m, 2H, py), 3.03 (s, 6H, CH$_3$) ppm. ^{13}C NMR (100.63 MHz, DMSO-d_6): δ 172.4 (C−S), 155.7 (*C*=N), 146.5 (C$_{q,ph}$), 145.9 (C$_{py}$), 145.3 (C$_{q,py}$), 143.7 (C$_{py}$), 142.6 (C$_{q,ph}$), 129.5 (C$_{py}$), 126.4 (C$_{py}$), 125.8 (C$_{ph}$), 121.3 (C$_{ph}$), 16.7 (CH$_3$) ppm.

[Bis(acetylpyrazine 4*N*-Phenylthiosemicarbazonato)-N,N,S-gallium(III)]nitrate Monohydrate, [Ga(L^H)$_2$]NO$_3$·H$_2$O (1H). To acetylpyrazine 4*N*-phenylthiosemicarbazone (HL^H) (100 mg, 0.37 mmol) in boiling methanol (5 mL) gallium(III) nitrate nonahydrate (80 mg, 0.19 mmol) in methanol (3 mL) was added, and the mixture was stirred under reflux for 4 h. The yellow solid was

(27) Pulvermacher, G. *Chem. Ber.* **1893**, *26*, 613–630.
(28) Klayman, D. L.; Scovill, J. P.; Bartosevich, J. F.; Bruce, J. *J. Med. Chem.* **1983**, *26*, 35–39.

separated from the hot solution by filtration, washed with methanol, and dried in vacuo. Yield: 50 mg (39%). Anal. Calcd for $C_{26}H_{24}GaN_{11}O_3S_2 \cdot H_2O$ ($M_r = 690.42$ g/mol): C, 45.23; H, 3.80; N, 22.32. Found: C, 45.22; H, 3.51; N, 22.20. ESI-MS in MeOH (positive): m/z 609, $[Ga(L^H)_2]^+$. IR spectrum in KBr, cm^{-1} (selected bands): 3276 m, 1599 s, 1541 s, 1489 s, 1420 s, 1328 m, 1150 s, 1096 s, 762 s, 698 m, 592 m. UV−vis (MeOH), λ_{max}, nm (ε, M^{-1} cm^{-1}): 230sh (32850), 257 (24810), 270sh (23860), 322 (24570), 430 (31950). ^{1}H NMR (500.32 MHz, DMSO-d_6): δ 10.46 (s, 2H, NH), 9.66 (s, 2H, pz), 8.96 (d, $^3J_{H,H} = 2.8$ Hz, 2H, pz), 8.09 (m, 2H, pz), 7.79 (d, $^3J_{H,H} = 7.6$ Hz, 4H, ph), 7.40 (t, $^3J_{H,H} = 7.8$ Hz, 4H, ph), 7.13 (t, $^3J_{H,H} = 7.6$ Hz, 2H, ph), 2.99 (s, 6H, CH$_3$) ppm. ^{13}C NMR (125.81 MHz, DMSO-d_6): δ 172.3 (C−S), 150.8 (C=N), 150.2 (C$_{pz}$), 147.2 (C$_{pz}$), 140.3 (C$_{q,ph}$), 139.8 (C$_{q,py}$), 138.9 (C$_{pz}$), 129.6 (C$_{ph}$), 124.8 (C$_{ph}$), 122.5 (C$_{ph}$), 16.1 (CH$_3$) ppm. ^{15}N NMR (50.70 MHz, DMSO-d_6): δ 244.7 (N$_{pz,uncoordinated}$) ppm. Crystals suitable for X-ray data collection were obtained from an acetone solution of **1H** saturated with diethyl ether.

[Bis(acetylpyrazine ^4N-p-Nitrophenylthiosemicarbazonato)-N,N,S-gallium(III)]nitrate Monohydrate Methanol Solvate, [Ga-(L^I)$_2$]NO$_3 \cdot$H$_2$O$\cdot$0.5CH$_3$OH (1I). To acetylpyrazine ^4N-p-nitrophenylthiosemicarbazone (**HL^I**) (50 mg, 0.158 mmol) in boiling methanol (5 mL) triethylamine (24 μL, 0.173 mmol) and gallium(III) nitrate nonahydrate (33 mg, 0.079 mmol) in methanol (1 mL) were added, and the mixture was stirred under reflux for 3 h. The precipitate was separated from the hot solution by filtration, washed with methanol, and dried in vacuo. Yield: 49 mg (78%). Anal. Calcd for $C_{26}H_{22}GaN_{13}O_7S_2 \cdot H_2O \cdot 0.5CH_3OH$ ($M_r = 796.43$ g/mol): C, 39.96; H, 3.29; N, 22.86; S, 8.05. Found: C, 40.01; H, 3.12; N, 22.29; S, 7.78. ESI-MS in MeOH (positive): m/z 699, $[Ga(L^I)_2]^+$. ESI-MS in MeOH (negative): m/z 697, $[Ga(L^I)_2 - 2H]^-$. IR spectrum in KBr, cm^{-1} (selected bands): 3072 m, 1595 m, 1571 m, 1495 s, 1442 s, 1402 m, 1324 s, 1304 s, 1151 m, 1091 s, 853 m, 750 m. UV−vis (MeOH), λ_{max}, nm (ε, M^{-1} cm^{-1}): 219sh (34850), 266 (16800), 309sh (29000), 336 (35740), 415 (42820). ^{1}H NMR (500.32 MHz, DMSO-d_6): δ 10.92 (s, 2H, NH), 9.76 (d, $^4J_{H,H} = 1.3$ Hz, 2H, pz), 9.02 (d, $^3J_{H,H} = 2.8$ Hz, 2H, pz), 8.33 (m, 4H, ph), 8.16 (dd, $^3J_{H,H} = 2.8$ Hz, $^4J_{H,H} = 1.3$ Hz, 2H, pz), 8.09 (m, 4H, ph), 3.08 (s, 6H, CH$_3$) ppm. ^{13}C NMR (125.81 MHz, DMSO-d_6): δ 171.8 (C−S), 154.1 (C=N), 150.6 (C$_{pz}$), 147.3 (C$_{pz}$), 145.9 (C$_{q,ph}$), 142.5 (C$_{q,ph}$), 139.1 (C$_{q,pz}$), 138.8 (C$_{pz}$), 125.5 (C$_{ph}$), 121.2 (C$_{ph}$), 16.3 (CH$_3$) ppm.

[Bis(2-acetylpyridine ^4N-Phenylthiosemicarbazonato)-N,N,S-iron(III)]hexafluorophosphate, [Fe(L^C)$_2$]PF$_6$ (2C). To 2-acetylpyridine ^4N-phenylthiosemicarbazone (**HL^C**) (80 mg, 0.296 mmol) in ethanol (7 mL) iron(III) nitrate nonahydrate (67 mg, 0.166 mmol) in ethanol (1 mL) was added, and the reaction mixture was allowed to stir for 5 h at room temperature. Ammonium hexafluorophosphate (100 mg, 0.613 mmol) was added, and the mixture was stirred for further 45 min. The precipitate was filtered off, washed with ethanol, and dried for one week at 50 °C. Yield: 75 mg (68%). Anal. Calcd for $C_{28}H_{26}F_6FeN_8PS_2$ ($M_r = 739.50$ g/mol): C, 45.48; H, 3.54; N, 15.15. Found: C, 45.66; H, 3.69; N, 15.11. ESI-MS in MeOH (positive): m/z 594, $[Fe(L^C)_2]^+$; ESI-MS in MeOH (negative): m/z 145, $[PF_6]^-$. IR spectrum in KBr, cm^{-1} (selected bands): 3366 s, 1601 m, 1540 m, 1504 s, 1458 s, 1435 s, 1318 m, 1161 s, 842 vs, 556 m. UV−vis (MeOH), λ_{max}, nm (ε, M^{-1} cm^{-1}): 256 (48440), 388 (33880), 632 (890), 836 (1060).

[Bis(2-acetylpyridine ^4N-p-Nitrophenylthiosemicarbazonato)-N,N,S-iron(III)]nitrate Monohydrate, [Fe(L^D)$_2$]NO$_3 \cdot$H$_2$O (2D). To 2-acetylpyridine ^4N-p-nitrophenylthiosemicarbazone (**HL^D**) (150 mg, 0.476 mmol) in boiling methanol (37 mL) iron(III) nitrate nonahydrate (97 mg, 0.240 mmol) in methanol (2 mL) was added,

and the reaction mixture allowed to stir for 1 h. The black solid was separated from the hot solution by filtration, washed with methanol, and dried in vacuo. Yield: 115 mg (63%). Anal. Calcd for $C_{28}H_{24}FeN_{11}O_7S_2 \cdot H_2O$ ($M_r = 764.55$ g/mol): C, 43.99; H, 3.43; N, 20.15. Found: C, 44.34; H, 3.23; N, 19.83. ESI-MS in MeOH (positive): m/z 684, $[Fe(L^D)_2]^+$. ESI-MS in MeOH (negative): m/z 682, $[Fe(L^D)_2 - 2H]^-$. IR spectrum in KBr, cm^{-1} (selected bands): 3308 m, 3060 m, 1498 s, 1452 s, 1325 s, 1303 s, 1256 s, 1157 s, 1111 s, 854 m, 751 m. UV−vis (MeOH), λ_{max}, nm (ε, M^{-1} cm^{-1}): 237sh (42530), 321sh (27470), 385 (62820), 474sh (7990), 595 (1360), 837 (1220).

[Bis(acetylpyrazine ^4N-Phenylthiosemicarbazonato)-N,N,S-iron(III)]nitrate Monohydrate, [Fe(L^H)$_2$]NO$_3 \cdot$H$_2$O (2H). To acetylpyrazine ^4N-phenylthiosemicarbazone (**HL^H**) (80 mg, 0.295 mmol) in boiling ethanol (5 mL) iron(III) nitrate nonahydrate (60 mg, 0.149 mmol) in ethanol (2 mL) was added, and the mixture was stirred under reflux for 5 h. The black solid was filtered off from the hot solution, washed with ethanol, and dried in vacuo. Yield: 70 mg (70%). Anal. Calcd for $C_{26}H_{24}FeN_{11}O_3S_2 \cdot H_2O$ ($M_r = 676.53$ g/mol): C, 46.16; H, 3.87; N, 22.77. Found: C, 46.35; H, 3.74; N, 22.48. ESI-MS in MeOH (positive): m/z 596, $[Fe(L^H)_2]^+$. IR spectrum in KBr, cm^{-1} (selected bands): 3245 m, 1597 s, 1547 m, 1428 s, 1342 m, 1148 s, 1094 s, 763 s, 695 m, 585 m. UV−vis (MeOH), λ_{max}, nm (ε, M^{-1} cm^{-1}): 258 (45730), 311sh (22780), 417 (29810), 515sh (6790), 675 (1140), 875 (1010).

[Bis(acetylpyrazine ^4N-p-Nitrophenylthiosemicarbazonato)-N,N,S-iron(III)]nitrate Monohydrate, [Fe(L^I)$_2$]NO$_3 \cdot$H$_2$O (2I). To acetylpyrazine ^4N-p-nitrophenylthiosemicarbazone (**HL^I**) (50 mg, 0.158 mmol) in boiling methanol (10 mL), iron(III) nitrate nonahydrate (32 mg, 0.079 mmol) in methanol (2 mL) was added, and the reaction mixture was allowed to stir under reflux for 2 h. The black solid was separated from the hot solution by filtration, washed with methanol, and dried in vacuo. Yield: 37 mg (61%). Anal. Calcd for $C_{26}H_{22}FeN_{13}O_7S_2 \cdot H_2O$ ($M_r = 766.53$ g/mol): C, 40.74; H, 3.16; N, 23.75. Found: C, 40.77; H, 3.13; N, 23.63. ESI-MS in MeOH (positive): m/z 686, $[Fe(L^I)_2]^+$. IR spectrum in KBr, cm^{-1} (selected bands): 3054 m, 1596 m, 1564 m, 1497 s, 1439 s, 1329 s, 1302 s, 1259 m, 1147 s, 1087 s, 850 m, 750 m. UV−vis (MeOH), λ_{max}, nm (ε, M^{-1} cm^{-1}): 226sh (42630), 330 (32320), 399 (47700), 502sh (7440), 662 (1440), 884 (1120).

Crystallographic Structure Determination. X-ray diffraction measurements were performed on a Bruker X8 APEX II CCD-diffractometer. A single crystal of suitable size was protected by Parathone-N oil, attached to a glass fiber, and mounted on a goniometer head at 40 mm from the detector, and 1375, 1594, and 1144 frames were measured, each for 90, 5, and 90 s over 1° scan width. The data were processed using SAINT software.[29] The structures were solved by direct methods and refined by full-matrix least-squares techniques. Non-hydrogen atoms were refined with anisotropic displacement parameters. Hydrogen atoms were placed at calculated positions and refined as riding atoms in the subsequent least-squares model refinements. The isotropic thermal parameters were estimated to be 1.2 times the values of the equivalent isotropic thermal parameters of the atoms to which hydrogens were bound. The following computer programs were used: structure solution, SHELXS-97;[30] refinement, SHELXL-97;[31] molecular diagrams,

(29) *SAINT-Plus*, version 7.06a; *APEX2*; Bruker-Nonius AXS Inc.: Madison, WI, 2004.
(30) Sheldrick, G. M. *SHELXS-97, Program for Crystal Structure Solution*; University Göttingen: Göttingen, Germany, 1997.
(31) Sheldrick, G. M. *SHELXL-97, Program for Crystal Structure Refinement*; University Göttingen: Göttingen, Germany, 1997.

83

Table 1. Crystal Data and Details of Data Collection for **HL^H**, **HL^M**, and **1H**

	HL^H	**HL^M**	**1H·H₂O**
empirical formula	C₁₃H₁₃N₅S	C₁₀H₁₆N₄S	C₂₆H₂₆GaN₁₁O₄S₂
fw	271.34	224.33	690.42
space group	P1̄	P2₁/c	Pna2₁
a [Å]	5.7844(14)	5.4716(2)	14.9818(5)
b [Å]	10.036(3)	18.9799(7)	22.0746(7)
c [Å]	11.314(4)	11.8689(4)	8.6006(3)
α [deg]	76.005(12)		
β [deg]	87.021(9)	97.289(2)	
γ [deg]	89.220(9)		
V [Å³]	636.5(3)	1222.63(8)	2844.37(16)
Z	2	4	4
λ [Å]	0.71073	0.71073	0.71073
ρ_calcd [g cm⁻³]	1.416	1.219	1.612
cryst size [mm³]	0.16 × 0.01 × 0.01	0.30 × 0.20 × 0.20	0.26 × 0.10 × 0.10
T [K]	100	296	100
μ [mm⁻¹]	0.247	0.241	1.171
R1^a	0.0440	0.0436	0.0267
wR2^b	0.0920	0.1362	0.0721
GOF^c	1.031	1.015	1.055

^{a} $R1 = \Sigma||F_o| - |F_c||/\Sigma|F_o|$. ^{b} $wR2 = (\Sigma[w(F_o^2 - F_c^2)^2]/\Sigma[w(F_o^2)^2])^{1/2}$. ^{c} $GOF = (\Sigma[w(F_o^2 - F_c^2)^2]/(n - p))^{1/2}$, where n is the number of reflections and p is the total number of parameters refined.

ORTEP;[32] computer, Pentium IV; scattering factors.[33] Crystal data, data collection parameters and structure refinement details for **HL^H**, **HL^M**, and **1H** are given in Table 1.

Computational Details. The geometries of the 2-acetylpyridine $^4N,^4N$-dimethylthiosemicarbazone ligand **HL^B**, its deprotonated form **(L^B)⁻**, the metal complexes [Ga(L^B)₂]⁺, [Fe^II(L^B)₂], and the reduced form of each of these species were optimized using a combination of the exchange functional of Becke[34a] and the correlation functional of Perdew[34b] (BP86), as implemented in Gaussian 03.[35] The LANL2DZ effective core potentials (ECPs)[36] and the corresponding valence-basis sets were used for the metals, and the 6−31G(d,p) basis sets were used for the other atoms. Vibrational frequencies calculated at this level confirm that all structures are minima on the potential energy surfaces. Improved energies were calculated at the BP86 level together with the same ECPs and valence-basis set on the metal atoms but totally uncontracted and augmented with one set of f functions on Fe,[37] together with the 6−311+G(3d) basis set on the S atoms, and the 6−311+G(d,p) basis sets on the other atoms. Free energies in vacuo were calculated by addition of corrections from unscaled zero-point energy (ZPE), thermal energy, work, and entropy evaluated at the BP86 level at 298.15 K, 1 atm to the improved energies. Standard reduction potentials (SRPs) were calculated according to our previous approach,[38] which was carefully validated for the reduction of 61 ruthenium(III/II) complexes (bearing formal charges from 3+/2+ to 1−/2−) in four solvents and shall be readily transferable to other metal complexes because the metal ion is not solvent-exposed in any of those Ru complexes. The SRP prediction is based on a thermodynamic cycle and involves the calculation of solvation free energies using the Poisson−Boltzmann finite element method,[39] as implemented in Jaguar 7,[40] with dielectric constant of 37.5 representing acetonitrile as the solvent. In the present work, the only difference to our previous SRP calculation approach[38] is the use of the BP86 functional, which leads to excellent agreement with experimental SRPs (see below) and was employed for similar purposes as well.[41a] The overestimation of the contribution of exchange energy by the B3LYP functional[42] is well documented[41b] and may result in the overestimation of the stability of high-multiplicity spin states in iron complexes. A comparison of the relative energies of the electronic states of [Fe^II(L^B)₂] and [Fe^II(L^B)₂]⁻ and of the SRPs calculated using the BP86 and B3LYP improved energies is given in the Supporting Information (Tables S1 and S2) and indicates that multireference approaches would be worth considering if permitted by the available computational resources. Other promising methods for this particular purpose include the spectroscopy oriented configuration interaction (SORCI) method and a ligand field theory (LFT)-based approach.[41c] Atomic partial charges at BP86 were calculated using the Mulliken[43a] scheme based on basis functions as implemented in Gaussian, the Hirshfeld[43b] scheme based on electron density as implemented in ADF,[44] and the ESP[43c] scheme of fitting atomic charges to reproduce the electrostatic potential in Jaguar.[40]

Results and Discussion

Synthesis and Characterization. The ligand 2-acetylpyrazine ^4N-phenylthiosemicarbazone (**HL^H**) (Chart 1) was

(32) Johnson, G. K. *Report ORNL-5138*; Oak Ridge National Laboratory: Oak Ridge, TN, 1976.

(33) *International Tables for X-ray Crystallography*; Kluwer Academic Press: Dodrecht, The Netherlands, 1992; Vol. *C*, Tables 4.2.6.8 and 6.1.1.4.

(34) (a) Becke, A. D. *Phys. Rev. A* **1988**, *38*, 3098–3100. (b) Perdew, J. P. *Phys. Rev. B* **1986**, *33*, 8822–8824.

(35) Frisch, M. J.; Trucks, G. W.; Schlegel, H. B.; Scuseria, G. E.; Robb, M. A.; Cheeseman, J. R.; Montgomery, J. A., Jr.; Vreven, T.; Kudin, K. N.; Burant, J. C.; Millam, J. M.; Iyengar, S. S.; Tomasi, J.; Barone, V.; Mennucci, B.; Cossi, M.; Scalmani, G.; Rega, N.; Petersson, G. A.; Nakatsuji, H.; Hada, M.; Ehara, M.; Toyota, K.; Fukuda, R.; Hasegawa, J.; Ishida, M.; Nakajima, T.; Honda, Y.; Kitao, O.; Nakai, H.; Klene, M.; Li, X.; Knox, J. E.; Hratchian, H. P.; Cross, J. B.; Bakken, V.; Adamo, C.; Jaramillo, J.; Gomperts, R.; Stratmann, R. E.; Yazyev, O.; Austin, A. J.; Cammi, R.; Pomelli, C.; Ochterski, J. W.; Ayala, P. Y.; Morokuma, K.; Voth, G. A.; Salvador, P.; Dannenberg, J. J.; Zakrzewski, V. G.; Dapprich, S.; Daniels, A. D.; Strain, M. C.; Farkas, O.; Malick, D. K.; Rabuck, A. D.; Raghavachari, K.; Foresman, J. B.; Ortiz, J. V.; Cui, Q.; Baboul, A. G.; Clifford, S.; Cioslowski, J.; Stefanov, B. B.; Liu, G.; Liashenko, A.; Piskorz, P.; Komaromi, I.; Martin, R. L.; Fox, D. J.; Keith, T.; Al-Laham, M. A.; Peng, C. Y.; Nanayakkara, A.; Challacombe, M.; Gill, P. M. W.; Johnson, B.; Chen, W.; Wong, M. W.; Gonzalez, C.; Pople, J. A. *Gaussian 03*, revision D.01; Gaussian, Inc.: Wallingford, CT, 2004; www.gaussian.com.

(36) (a) Wadt, W. R.; Hay, P. J. *J. Chem. Phys.* **1985**, *82*, 284–298. (b) Hay, P. J.; Wadt, W. R. *J. Chem. Phys.* **1985**, *82*, 299–310.

(37) Ehlers, A. W.; Böhme, M.; Dapprich, S.; Gobbi, A.; Höllwarth, A.; Jonas, V.; Köhler, K. F.; Stegmann, R.; Veldkamp, A.; Frenking, G. *Chem. Phys. Lett.* **1993**, *208*, 111–114.

(38) Chiorescu, I.; Deubel, D. V.; Arion, V. B.; Keppler, B. K. *J. Chem. Theory Comput.* **2008**, *4*, 499–506.

(39) (a) Tannor, D. J.; Marten, B.; Murphy, R. B.; Friesner, R. A.; Sitkoff, D.; Nicholls, A.; Ringnalda, M. N.; Goddard, W. A., III; Honig, B. *J. Am. Chem. Soc.* **1994**, *116*, 11875–11882. (b) Marten, B.; Kim, K.; Cortis, C.; Friesner, R. A.; Murphy, R. B.; Ringnalda, M. N.; Sitkoff, D.; Honig, B. *J. Phys. Chem.* **1996**, *100*, 11775–11788.

(40) *Jaguar*, version 7.0; Schrödinger, LCC: New York, 2007; www.schrodinger.com.

(41) (a) Ketterer, N. A.; Fan, H.; Blackmore, K. J.; Yang, X.; Ziller, J. W.; Baik, M.-H.; Heyduk, A. F. *J. Am. Chem. Soc.* **2008**, *130*, 4364–4374. (b) Reiher, M.; Salomon, O.; Hess, B. A. *Theor. Chem. Acc.* **2001**, *107*, 48–55. (c) Fouqueau, A.; Casida, M. E.; Daku, L. M. L.; Hauser, A.; Neese, F. *J. Chem. Phys.* **2005**, *122*, 44110/1–44110/13.

(42) (a) Becke, A. D. *J. Chem. Phys.* **1993**, *98*, 5648–5652. (b) Lee, C.; Yang, W.; Parr, R. G. *Phys. Rev. B* **1988**, *37*, 785–789.

(43) (a) Mulliken, R. S. *J. Chem. Phys.* **1955**, *23*, 1833–1840. (b) Hirshfeld, F. L. *Theor. Chim. Acta* **1977**, *44*, 129–138. (c) Chirlian, L. E.; Miller, M. *J. Comput. Chem.* **1987**, *8*, 894–905.

(44) (a) Te Velde, G.; Bickelhaupt, F. M.; van Gisbergen, S. J. A.; Fonseca Guerra, C.; Baerends, E. J.; Snijders, J. G.; Ziegler, T. *J. Comput. Chem.* **2001**, *22*, 931–967. (b) *ADF 2007.01*; SCM, Theoretical Chemistry, Vrije Universiteit: Amsterdam, The Netherlands, 2007; http://www.scm.com.

synthesized by condensation of ^4N-phenylthiosemicarbazide with acetylpyrazine in boiling ethanol in 73% yield. 2-Acetylpyrazine ^4N-p-nitrophenylthiosemicarbazone (**HL^I**) was prepared as a pale-yellow powder by reaction of p-nitrophenyl isothiocyanate with acetylpyrazine hydrazone in acetonitrile in 75% yield. Acetylpyrazine hydrazone was obtained by reacting acetylpyrazine with an excess hydrazine hydrate as the reagent and solvent. The gallium(III) complex **1C** (Chart 2) was synthesized by reaction of Ga(NO$_3$)$_3$·9H$_2$O with 2-acetylpyridine ^4N-phenylthiosemicarbazone in 1:2 molar ratio in ethanol at room temperature, followed by addition of excess NH$_4$PF$_6$. Complexes **1D**, **1H**, and **1I** were isolated as nitrates, which precipitated shortly after addition of Ga(NO$_3$)$_3$·9H$_2$O to the boiling solution of the corresponding ligand. These complexes show also lower aqueous solubility than the nitrate salts of complexes **1A**−**1C**, **1E**−**1G**, **1J**, and **1K** which because of their good solubility in (m)ethanolic solution were isolated as hexafluorophosphates. The difference in the solubility is also evident for the corresponding iron(III) complexes. Complexes **2D**, **2H**, and **2I** were obtained as nitrate salts by reaction of Fe(NO$_3$)$_3$·9H$_2$O with a boiling solution of the ligand, whereas **2C** was isolated as a hexafluorophosphate salt. In contrast to the nonsolvated complexes with secondary amine substituted ligands (**1A**, **1B**, **1E**−**1G**, and iron(III) analogs), microanalytical data for the novel complexes show that they all crystallize with one water molecule. X-ray diffraction studies showed that this water molecule is involved in hydrogen bonding with the NH group of the anilinyl and nitroanilinyl moiety (see below). The presence of crystal water was also confirmed by thermogravimetric analysis (TGA) of complex **1D**, where the loss of water between 40 and 110 °C was observed. A large endothermic peak in the differential thermal analysis (DTA) at 250 °C indicated the pyrolysis of the complex. Taking into account the observed thermal behavior, complex **2C** was dried at 50 °C over one week to give a nonsolvated product.

The UV−vis spectra of the metal-free ligands as well as the gallium(III) complexes are dominated by intraligand transitions associated with the pyridine or pyrazine ring, azomethine, and thione portions of the ligands. The extinction coefficient of the lowest energy band increases dramatically upon coordination of the thiosemicarbazone ligands **HL** to Ga(III) to give [Ga(L$_2$)]$^+$ concomitant with a small shift of the absorbance maximum (420 → 430 nm for **HL^H** → **1H** and 424 → 415 nm for **HL^I** → **1I**). The increased extinction coefficient is presumably because of the change in the ligand conjugation caused by the deprotonation of the ligands upon complexation.

The reduced analog of **HL^B**, namely **HL^M**, was prepared by reduction of an ethanolic solution of methyl 3-[1-(2-pyridyl)ethylidene]hydrazinecarbothioate[28] with NaBH$_4$ and subsequent nucleophilic substitution of the S-methyl group by dimethylamine (Chart 1) or by direct reduction of **HL^B** with NaBH$_4$ in ethanol. The reduction of the C=N double bond in **HL^B** is accompanied by the disappearence of two UV−vis absorption bands with the maxima at 314 and 396 nm as shown in Figure 1. The presence of these two bands
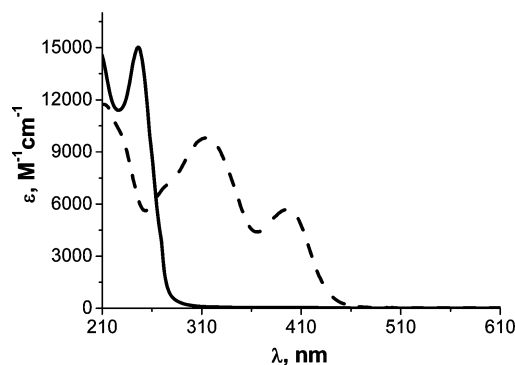

Figure 1. Electronic absorption spectra of ligand **HL^B** (dashed line) and its reduced form **HL^M** (solid line) in methanol. [**HL^B** λ_{max}, nm (ε, M^{-1} cm^{-1}), 231sh (9690), 272sh (6920), 314 (9800), 396 (5680); **HL^M** λ_{max}, nm (ε, M^{-1} cm^{-1}), 246 (15030)].

for the π-delocalized thiosemicarbazone chromophore in **HL^B** might be explained by the existence of at least two isomers with different electronic structures in solution, as confirmed by ^{1}H NMR measurements in methanol-d_4. In contrast, the ligands **HL^H** and **HL^I**, which adopt only one isomeric form in solution according to ^{1}H NMR spectra in methanol-d_4, display only one strong absorption band at 326 and 333 nm, respectively. Coordination of the thiosemicarbazone ligands **HL^H** and **HL^I** to the iron(III) leads to the following changes in their UV−vis spectra: a large increase of the band around 400 nm, appearance of two new bands between 502 and 675 nm (d → π^* transition), and around 880 nm the d → d band corresponding to the $^2T_{2g}$ → $^2T_{1g}$ transition of the d^5 low-spin system.[45]

The ^{1}H NMR spectra of the ligands **HL^H** and **HL^I** recorded in DMSO-d_6 indicate that, in contrast to **HL^B**, **HL^K**,[24] and other thiosemicarbazones,[46] they exist in solution only as E isomers. Interestingly, the analogous pyridinyl containing ligands **HL^C** and **HL^H** show small amounts (<10%) of a second isomer with strongly downfield shifted N−H signals at 14.58 and 14.92 ppm, respectively, resulting from intramolecular hydrogen bonding.[25] Like for other reduced thiosemicarbazone ligands,[47] the ^{1}H NMR spectrum of **HL^M** indicates the presence of only one isomeric form in solution. Two N−H signals at 8.88 ppm and 5.69 ppm could be observed, where the first one is split into a doublet with a coupling constant of $^3J_{H,H}$ = 5.7 Hz and the second one into a doublet of doublet with $^3J_{H,H}$ = 5.7 Hz and $^3J_{H,H}$ = 3.2 Hz. The coupling constant of 3.2 Hz is also observed for the doublet of quartet of the CH signal at 4.11 ppm, with the quartet splitting ($^3J_{H,H}$ = 6.6 Hz) originating from the coupling with the CH_3CH−N methyl group at 1.30 ppm (d, $^3J_{H,H}$ = 6.6 Hz). Consequently, the signal at 8.88 ppm can be attributed to the S=CNH proton and that at 5.69 ppm to the CHNH proton. A 2D ^{1}H−^{15}N HSQC NMR spectrum shows one resonance at 116.7 ppm associated to the proton signal at 8.88 ppm and a second resonance at 76.8 ppm coupled with the proton at 5.69 ppm. The long-range ^{1}H−^{15}N

(45) Sreekanth, A.; Fun, H.-K.; Kurup, M. R. P. *J. Mol. Struct.* **2005**, *737*, 61–67.

(46) Easmon, J.; Heinisch, G.; Holzer, W. *Heterocycles* **1989**, *29*, 1399–1408.

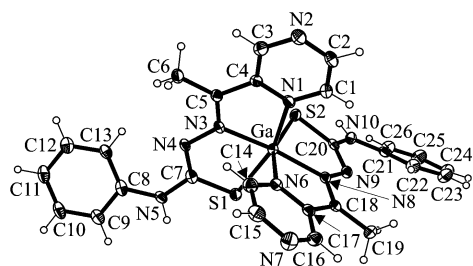(47) Easmon, J.; Heinisch, G.; Holzer, W. *Sci. Pharm.* **1993**, *61*, 3–10.

85

Figure 2. ORTEP plot with thermal ellipsoids at 50% probability level for complex cation [Ga(L^H)$_2$]$^+$ in **1H** with atom labeling scheme. Selected bond distances (Å) and angles (deg): C5−N3 = 1.292(3), C18−N8 = 1.297(4), N3−N4 = 1.367(3), N8−N9 = 1.364(3), N4−C7 = 1.320(4), N9−C20 = 1.325(4), C7−S1 = 1.734(3), C20−S2 = 1.743(3), C7−N5 = 1.356(4), C20−N10 = 1.346(3); N1−Ga−N3 = 76.98(9), N6−Ga−N8 = 76.16(9), N3−Ga−S1 = 83.34(6), N8−Ga−S2 = 83.72(7).

HMBC spectrum shows that the two N−H groups couple with each other and, in addition, that the signal at 116.7 ppm ($^1J_{N,H}$ = 98 Hz) couples with the tertiary CH signal δ = 4.11 ppm, whereas the nitrogen resonance at 76.8 ppm ($^1J_{N,H}$ = 78 Hz) exhibits a cross peak with the CH$_3$ group resonance at 1.30 ppm. All this confirms the above-mentioned assignments. In addition, three pyridine protons give a cross peak with the ^{15}N resonance at 291.2 ppm, which can be ascribed to the pyridine nitrogen.

In contrast to some of the metal-free ligands, the ^{1}H NMR spectra of the gallium complexes **1C**, **1D**, **1H**, and **1I** show only one set of signals because of the stabilization of the ligand configuration upon coordination to the metal and the equivalence of both ligands bound to gallium(III) in solution. The most remarkable difference between the ^{1}H NMR spectra of the gallium complexes and those of the metal-free ligands is the absence of one of the N−H signals, indicating deprotonation of the ligands upon complexation. Because it was difficult to distinguish between the two quaternary carbon atoms of the pyridine and pyrazine ring, respectively, and the carbon of the adjacent C=N double bond, complex **1H** was studied by multinuclear (^{1}H, ^{13}C, and ^{15}N) one- and two-dimensional NMR spectroscopy. Exact assignment of the quaternary carbon atoms was necessary for the correlation of the ^{13}C NMR chemical shifts with the redox potentials (see Figure 9). In general, the ^{13}C NMR chemical shifts of the C=N bond of the gallium complexes occur at lower field than the quaternary carbon atoms of the heterocycle (for detailed discussion see Supporting Information).

Crystal Structures. [Ga(L^H)$_2$]NO$_3$·H$_2$O (**1H**) crystallized in the orthorhombic space group *Pna*2$_1$, while **HL^H** crystallized in the triclinic centrosymmetric space group $P\bar{1}$. The structure of the complex cation is shown in Figure 2, and the molecular structure of the metal-free ligand **HL^H** is shown in Figure 3. Selected bond distances (Å) and angles (deg) are quoted in the legends to the Figures 2 and 3. The asymmetric unit of **1H** consists of a distorted octahedral [Ga(L^H)$_2$]$^+$ complex cation, a counteranion NO$_3^-$, and a cocrystallized water molecule. Each ligand is monodeprotonated and coordinates to gallium via the pyrazine nitrogen atom [Ga−N1 = 2.142(2) Å, Ga−N6 = 2.155(2) Å], an azomethine nitrogen [Ga−N3 = 2.033(2) Å, Ga−N8 = 2.044(2) Å], and a sulfur donor atom [Ga−S1 = 2.3266(8) Å, Ga−S2 = 2.3249(8) Å], forming two five-membered
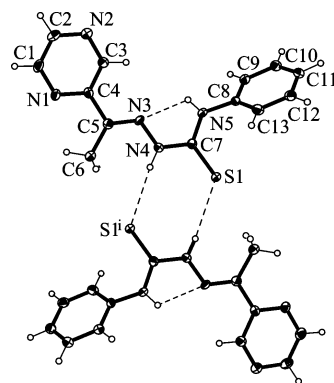

Figure 3. Centrosymmetric dimeric associate of **HL^H**, emphasizing the intra- and intermolecular hydrogen-bonding interactions; symmetry code i: −x + 3, −y + 1, −z + 1. Selected bond distances (Å) and angles (deg): C4−C5 = 1.481(4), C5−N3 = 1.284(3), N3−N4 = 1.367(3), N4−C7 = 1.366(3), C7−S1 = 1.677(3), C7−N5 = 1.335(3), N5−C8 = 1.425(3); $\Theta_{C3-C4-C5-N3}$ = 12.3(4), $\Theta_{N3-N4-C7-S1}$ = 174.06(18).

chelate rings, correspondingly. Both coordinated ligands are essentially planar, with exception of the phenyl group at the terminal nitrogen atom of the thiosemicarbazide moiety. The deviation from planarity of the phenyl ring in each coordinated ligand can be described by torsion angles $\Theta_{C13-C8-N5-C7}$ and $\Theta_{C20-N10-C21-C22}$ of 8.2(5)° and −21.5(4)°, respectively. The bond distances C7−S1 of 1.734(3) Å and C20−S2 of 1.743(3) Å are comparable to those reported for [Ga(L^G)$_2$][PF$_6$] (**HL^G** = acetylpyrazine $^4N,^4N$-dimethylthio-semicarbazone)^{23} at 1.754(2) and 1.745(2) Å and are significantly longer than that of the metal free ligand **HL^H** at 1.677(3) Å. Of note are the angles N1−Ga−S1 at 159.55(7)° and N6−Ga−S2 at 156.90(7)°, which deviate markedly from the ideal value of 180°. The reason might be some repulsion between S1 and S2 (S1···S2 = 3.572 Å). The molecules of **1H** are involved into a network of intermolecular hydrogen bonds, with the NH groups of both thiosemicarbazone ligands and the water molecule acting as proton donors and the oxygens of the water and the nitrate counterion acting as proton acceptor (N10−H···O3···H−O4···H−N5).

The crystal structure of the ligand **HL^H** has an essentially nonplanar conformation (Figure 3), which differs markedly from that imposed by coordination. The phenyl ring C8−C13 and the pyrazine ring form dihedral angles of 54.2 and 164.7° with the central mean plane through N3, N4, C7, and N5 atoms of the thiosemicarbazide residue. Two rotations, one about C4−C5 bond and another about N4−C7 bond by ∼180° in the metal-free ligand are necessary to achieve the conformation adopted by both ligands in [Ga(L^H)$_2$]$^+$. The molecules of **HL^H** are associated in centrosymmetric dimers via hydrogen bonding interactions of the type N4−H···S1 (−x + 3, −y + 1, −z + 1) [N4−H = 0.88 Å, H···S1 = 2.691 Å, N4···S1 = 3.568 Å, N4−H···S1 = 174.08°]. Although it is weak, the intramolecular H bond N5−H···N3 [N5−H = 0.794 Å, H···N3 = 2.159 Å, N5···N3 = 2.585 Å, N5−H···N3 = 113.90°] is also of note.

The result of X-ray diffraction study for **HL^M** is displayed in Figure 4. The reduction of the azomethine bond is evidenced by the sp^3-hybridized atoms C6 (tetrahedral configuration) and N2 and by the lengths of the bonds
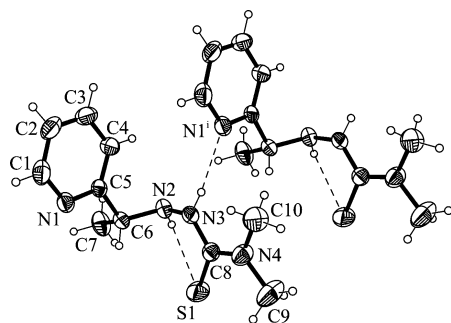
Figure 4. ORTEP plot of a fragment of the crystal structure of **HL^M** with thermal ellipsoids at 40% probability level, showing the intra- and intermolecular hydrogen-bonding interactions; symmetry code i: $x - 1$, y, z. Selected bond distances (Å) and angles (deg): C5−C6 = 1.503(3), C6−N2 = 1.471(2), N2−N3 = 1.418(2), N3−C8 = 1.359(3), C8−S1 = 1.685(2), C8−N4 = 1.340(3) Å; $\Theta_{N1-C5-C6-N2}$ = −151.70(16), $\Theta_{C5-C6-N2-N3}$ = −75.1(2), $\Theta_{N2-N3-C8-S1}$ = −10.6(3).

Table 2. Summary of the Electrochemical Data^a for the Metal Complexes

	gallium complexes		
	$E_{1/2}$/^{I}L^{red}	$E_{1/2}$/^{II}L^{red}	$E_{1/2}$/^{III}L^{red}
1A	−0.96	−1.25	−1.81^{c,e}
1B	−0.93	−1.22	−1.77^{c,e}
1C	−0.79	−1.05	−1.63^c
1D^b	−0.70^c	NA^f	NA^f
1E	−0.60	−0.88	−1.56
1F	−0.58	−0.84	−1.49
1G	−0.58	−0.85	−1.51
1H	−0.46	−0.72	−1.35
1I^b	−0.38^d	−0.62^d	NA^f
1J	−1.03	−1.34	−2.04^c
1K	−0.94	−1.22	−1.73^{c,e}

	iron complexes				
	$E_{1/2}$/^{C}Fe^{red}	$E_{1/2}$/^{A}Fe^{red}	$E_{1/2}$/^{I}L^{red}	$E_{1/2}$/^{II}L^{red}	E_p/^{III}L^{red}
2A	0.06		−1.62^d	−2.01^{c,g}	−2.01^{c,g}
2B	0.08		−1.61^d	−1.99^{c,g}	−1.99^{c,g}
2C	0.18		−1.44^d	−1.72^d	−2.15^{c,e}
2D^b	0.27		NA^f	NA^f	NA^f
2E	0.32		−1.23	−1.65	−2.12^{c,e}
2F	0.32		−1.21	−1.64	−2.09^{c,e}
2G	0.34		−1.22	−1.64	−2.13^{c,e}
2H	0.43		−1.08	−1.47	−1.97^{c,e}
2I^b	0.51		NA^f	NA^f	NA^f
2′A	0.06	0.30	−1.60^c		
2′B	0.08	0.30	−1.61^d		
2′E	0.31^g	0.31^g	−1.20^c		
2′F	0.31^g	0.31^g	−1.21^d		
2′G	0.32^g	0.32^g	−1.22^d		

	ruthenium complex				
	$E_{1/2}$/Ru$^{III/II}$	$E_{1/2}$/Ru$^{IV/III}$	$E_{1/2}$/^{I}L^{red}	E_p/^{II}L^{red}	E_p/^{III}L^{red}
3B	+0.21	+1.27	−1.56	−2.00^{c,g}	−2.00^{c,e,g}

^{a} Potentials in $V \pm 0.01$ vs NHE in 0.20 M [n-Bu$_4$N][BF$_4$]/CH$_3$CN. ^{b} Measured in 0.20 M [n-Bu$_4$N][BF$_4$]/DMF. ^{c} For the irreversible wave, the E_p values are given. ^{d} $^{ox}i_p$/$^{red}i_p$ between 0.6 and 0.8 at 0.2 V/s. ^{e} Two- or multielectron process (see text). ^{f} For complexes with nitro-containing ligands, the reduction of this group at approximately −1.0 V vs NHE prevented the detection of further ligand-centered redox waves (see text). ^{g} Could not be detected as separate waves.

involving these atoms. The overall conformation of the molecule is strongly distorted. The dihedral angle between the pyridine ring and the plane through the N3, C8, N4, and S1 atoms of the thiosemicarbazide moiety is 85.9°. The molecules of **HL^M** are involved in intramolecular hydrogen bonding interactions of the type N2−H···S1 [N2−H = 0.881 Å, H···S1 = 2.529 Å, N2···S1 = 2.950 Å, N2−H−S1 = 110.10°] and in a strong intermolecular H bond N3−H··· N1 ($x - 1$, y, z) [N3−H = 0.834 Å, H···N3 = 2.218 Å, N3···N1 = 3.041 Å, N3−H···N1 = 169.00°]. A search at CSD[48] did not show any deposited X-ray diffraction data for reduced thiosemicarbazones.

Electrochemical Studies. Ligand-Centered Reduction. The electrochemical data for the metal complexes and ligands under study are summarized in Tables 2 and S3 (Supporting Information), respectively, and their electrochemical behavior is shown in Scheme 1. In general, the complexes show several redox waves attributable to the reduction of the noninnocent thiosemicarbazone ligands at lower potentials (<−0.4 V vs NHE) than the metal-centered redox waves for the iron and ruthenium complexes (>0 V vs NHE; see below). The cyclic voltammograms of 0.20 M [n-Bu$_4$N][BF$_4$]/ CH$_3$CN solutions of the gallium thiosemicarbazonate complexes **1A−1I** display two consecutive reversible one-electron (as confirmed by controlled potential electrolysis of **1B**) redox waves with $^{ox}i_p$/$^{red}i_p$ = 1.0 at $v > 50$ mV/s with ΔE_p = 60−70 mV at 0.20 V/s (Scheme 1a, Figure 5). The redox potential of the first ligand reduction (wave ^{I}L^{red}) occurs between −0.38 and −0.96 V, and the second (wave ^{II}L^{red}) between −0.62 and −1.25 V vs NHE depending on the ligand identity (Table 2). As expected, complex **1A** with the 2-pyridinyl and 4-pyrrolidinyl substituents at the thiosemicarbazone ligands shows the most negative redox potentials, whereas complex **1I** with the more electron-withdrawing moieties nitroanilinyl and 2-pyrazinyl (the latter being weaker σ-donor and stronger π-acceptor than the 2-pyridinyl moiety) has the most positive redox potential for the ligand-centered reductions.

After these two consecutive reversible reduction processes a third irreversible redox wave ^{III}L^{red} is observed for the

pyridinyl complexes **1A−1C** between −1.63 and −1.81 V vs. NHE, whereas wave ^{III}L^{red} is a reversible one-electron reduction process at −1.35 and −1.56 V vs NHE for the pyrazinyl containing complexes **1E−1H** and is followed by a fourth partially quasi-reversible one-electron reduction wave, ^{IV}L^{red}, at approximately −1.80 V vs NHE (ΔE_p = 100−150 mV) (Figure 6a). For complex **1H**, this fourth reduction wave is irreversible because it overlaps with a further wave at approximately −1.95 V vs NHE. Waves ^{III}L^{red} and ^{IV}L^{red} were not detected for **1D** and **1I**, both containing a nitro-group attached to the thiosemicarbazone ligand, but instead a quasi-reversible (ΔE_p = 90−100 mV) reduction of the NO$_2$ group[49] at $E_{1/2}$ = −1.04 and −1.01 V vs NHE was observed, respectively. Complexes with nitro-derivatives are scarcely soluble in CH$_3$CN and were therefore measured in 0.20 M [n-Bu$_4$N][BF$_4$]/DMF. However, no variations in redox properties/potentials of the complexes

(48) *Cambridge Structure Database*, version 5.29; Cambridge Crystallographic Data Centre: Cambridge, U.K., 2007.

(49) Geske, D. H.; Ragle, J. L.; Bambenek, M. A.; Balch, A. L. *J. Am. Chem. Soc.* **1964**, *86*, 987–1002.

87

Scheme 1. Overview of the Electrochemical Behavior of the Studied Ga (a), Fe (b), and Ru (c) Complexes
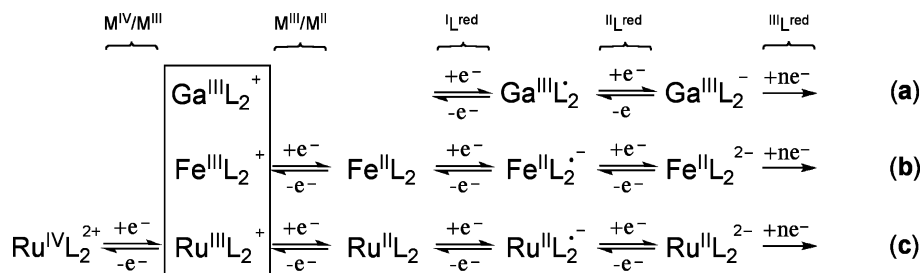
have been observed in DMF or CH$_3$CN electrolyte solutions as established for complex **2D**.

The influence of the chalcogen atom X of the chalcogensemicarbazone ligands (Chart 1) on the redox potential was studied with complexes **1B**, **1J**, and **1K**, which contain a sulfur, oxygen, or selenium atom, respectively. Complex **1J** (X = O) displays the lowest reduction potentials at −1.03 and −1.34 V vs NHE for ^{I}L^{red} and ^{II}L^{red}, respectively, whereas **1K** (X = Se) and **1B** (X = S) have similar redox potentials at −0.93 to −0.94 and −1.22 V vs NHE for the corresponding redox waves. Thio- and selenosemicarbazone

Figure 5. Cyclic voltammograms of (a) **1A** and (b) **1F** in CH$_3$CN containing 0.20 M [n-Bu$_4$N][BF$_4$] at a scan rate of 0.20 V s^{-1} using a platinum working electrode. Square wave voltammograms (SWVs); (c) of 1.0 mM **1A** (black line) and **1F** (gray line) electrolyte solutions were measured with 2 mV step height, 25 mV pulse, and 100 Hz frequency. The solid line on the bottom right refers to the current (10 μA) for a−c. For the assignment of waves, see text.

Figure 6. Cyclic voltammograms of **1G** (a), and **2E** (b), and **3B** (c) in CH$_3$CN containing 0.20 M [n-Bu$_4$N][BF$_4$] at a scan rate of 0.20 V s^{-1} using a glassy carbon working electrode, displaying the ligand (L^{red}), the Fe^{III}/Fe^{II} (^{C}Fe^{red}), and the Ru^{III}/Ru^{II} and Ru^{IV}/Ru^{III} redox couples.

ligands are known to have comparable NMR spectra,[50] and the gallium complexes **1B** and **1K** also possess similar ^{1}H and ^{13}C NMR chemical shifts with the largest deviation in the ^{13}C NMR spectra of the C−X resonance (detected at 176.1 and 173.8 ppm, respectively).[23,24] Complex **1J** shows a considerably different spectrum with the C−X resonance at 167.1 ppm and strong upfield shifts for both carbon resonances at the CH$_3$C=N moiety (**1B** 14.9, 149.0 ppm; **1K** 15.6, 147.4 ppm; **1J** 12.6, 139.3 ppm); in accordance with the lower redox potential of complex **1J** (see below).

The ligand-centered reduction of the iron complexes **2A−2I** (for Fe^{III} → Fe^{II} process see below) is similar to that for the gallium analogs, although the corresponding redox potentials ^{I}L^{red} and ^{II}L^{red} are considerably more negative between −1.08 and −1.62 V, and −1.47 and −2.01 V vs NHE, respectively (Scheme 1b, Figure 6b, Table 2). In the case of **2A** and **2B** the wave ^{II}L^{red} at −2.01 and −1.99 V vs NHE overlaps with ^{III}L^{red} resulting in two indistinguishable redox waves. Complexes **2C−2H** are reduced at ^{III}L^{red} between −1.97 and −2.15, close to the solvent cutoff potential. The lower redox potentials of the iron(II) compared to the gallium(III) complexes are in line with the calculated higher LUMO energy level (see below) and the neutral charge of the iron(II) complexes (compared to the positively charged gallium complexes). For the nitro group containing complexes **2D** and **2I** only one ligand-centered irreversible reduction wave at −0.97 and −0.93 V vs NHE was detected, which can be attributed to the reduction of the nitro group. This is only slightly shifted to more positive potential compared to that in the analogous gallium complexes. The presence of the tetrachloridoferrate counteranion in **2′A−2′G** prevented the accurate detection of the second reduction wave ^{II}L^{red} in these complexes, because the counteranion reacts readily with the ligand radical formed upon reduction at ^{I}L^{red}.

The ruthenium complex **3B** shows the first ligand reduction at $E_{1/2}$ = −1.56 V vs NHE (Scheme 1c, Figure 6c), whereas ^{II}L^{red}, like for the pyridine containing iron complexes **2A** and **2B**, overlaps with ^{III}L^{red} resulting in an irreversible reduction wave at −2.00 V (see Supporting Information, Figure S1).

Increasing electron donor properties of substituents are known to increase the effective negative net charge on the corresponding molecules and result usually in a decrease of
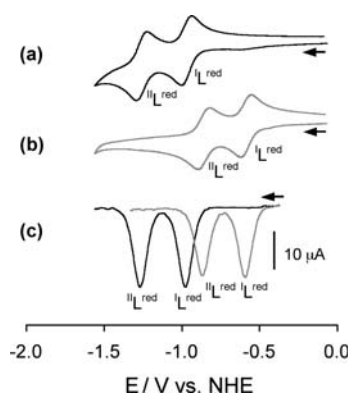
(50) Castle, T. C.; Maurer, R. I.; Sowrey, F. E.; Went, M. J.; Reynolds, C. A.; McInnes, E. J. L.; Blower, P. J. *J. Am. Chem. Soc.* **2003**, *125*, 10040–10049.

Figure 7. Plot of pK_a values of attached amine moieties on thiosemicarbazone ligands vs ligand- and metal-centered $E_{1/2}$ values for the gallium (**1A−1I**, top) and iron (**2A−2I**, bottom) complexes. For the complexes **1D**, **2D**, and **2I**, the reduction of the nitro group prevented the detection of ^{I}L^{red} and/or ^{II}L^{red}. ^{C}Fe^{red} = Fe^{III}/Fe^{II} redox couple of complex cation; L^{red} = ligand-centered reduction; thiosemicarbazone complexes with pyrazine (pz) or pyridine (py) moieties are shown separately. Linear equations for gallium complexes: ^{I}L^{red} (pz) $E_{1/2}$ (V) = $-0.359 - 0.0206 \cdot pK_a$ (r = 0.996); ^{II}L^{red} (pz) $E_{1/2}$ (V) = $-0.600 - 0.0233 \cdot pK_a$ (r = 0.985); ^{I}L^{red} (py) $E_{1/2}$ (V) = $-0.673 - 0.0247 \cdot pK_a$ (r = 0.997); ^{II}L^{red} (py) $E_{1/2}$ (V) = $-0.902 - 0.0302 \cdot pK_a$ (r = 0.997). Linear equations for iron complexes: Fe^{III}/Fe^{II} (pz) $E_{1/2}$ (V) = $0.524 - 0.018 \cdot pK_a$ (r = 0.995); Fe^{III}/Fe^{II} (py) $E_{1/2}$ (V) = $0.285 - 0.0197 \cdot pK_a$ (r = 0.995); ^{I}L^{red} (pz) $E_{1/2}$ (V) = $-0.969 - 0.0227 \cdot pK_a$ (r = 0.998); ^{I}L^{red} (py) $E_{1/2}$ (V) = $-1.302 - 0.0284 \cdot pK_a$ (r = 0.999); ^{II}L^{red} (pz) $E_{1/2}$ (V) = $-1.334 - 0.0279 \cdot pK_a$ (r = 0.997); ^{II}L^{red} (py) $E_{1/2}$ (V) = $-1.499 - 0.0455 \cdot pK_a$ (r = 0.999).

their redox potentials. Plotting the pK_a values of the attached amine moieties [pyrrolidine (11.31), piperidine (11.12), dimethylamine (10.73), aniline (4.87) and p-nitroaniline (1.02)][51] versus $E_{1/2}$ results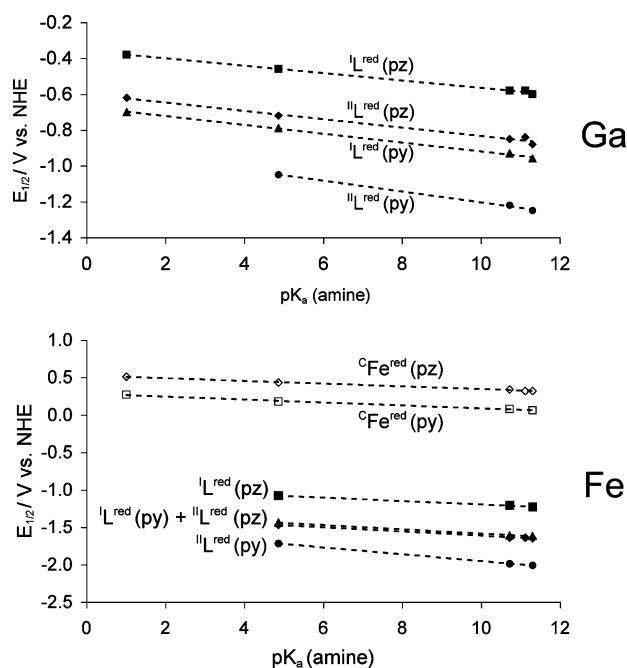 in a linear relationship (Figure 7). The resultant linear equations (see caption of Figure 7) and the pK_a values of the attached amine moieties can be used to predict the redox potentials of novel 2-acetylpyridine(pyrazine) thiosemicarbazone gallium(III) and iron(III) complexes in CH₃CN solution. The increased redox potential of complexes containing a pyrazine (**1E−1I**, **2E−2I**) instead of a pyridine (**1A−1D**, **2A−2D**) moiety can also be rationalized by the increased net donor properties of the latter [E_L(pyridine) = 0.25 V, E_L(pyrazine) = 0.33][9] and the different pK_a values [pK_a(pyrazine) = 0.65, pK_a(pyridine) = 5.23], respectively.[51]

The metal-free thiosemicarbazone ligands **HL^A**–**HL^I** exhibit an irreversible reduction response at −1.01 to −1.47 V vs NHE (Table S3, Supporting Information). The second reduction wave could only be observed occasionally and was hardly reproducible, indicating the instability of the radical formed after the first reduction process. For the p-nitrophenyl ligands **HL^D** and **HL^I**, a quasi-reversible nitro reduction wave

was detected at −1.04 and −1.03 V vs NHE, respectively.[49] In agreement with the peripheral position of the nitro group in the ligands, their reduction potentials are only slightly more negative than those of the corresponding ligands in the gallium and iron complexes. In addition, an irreversible prewave was observed at E_p = −0.82 and −0.80 V vs NHE, respectively, which was also reported for o-nitrotoluene and m-nitrotoluene in aprotic solvents.[52] In contrast to the ligand-centered reduction in the metal complexes where both ligands are forced to adopt the same configuration, the metal-free ligands are present as different isomers in solution, therefore showing no conclusive correlation between the E_p and pK_a values of the amine moieties of the ligand. In particular, for ligand **HL^B** three different isomers were found in DMSO solution,[24] two of them with strong intramolecular hydrogen bonds, whereas ligand **HL^H** in the same solvent is present as one isomer (see NMR data). The metal-ion stabilizes the reduced ligand radicals preventing their decomposition on the time-scale of cyclic voltammetry and allowing for the observation of two or three reversible ligand-centered redox waves upon coordination. The gallium-complexes are reduced at ∼0.3−0.8 V more positive redox potential than the uncoordinated ligands, whereas the same ligand-centered reductions in the iron(II) and ruthenium(II) complexes occur at ∼0.0−0.4 V more negative redox potentials than in the metal-free thiosemicarbazones. Therefore complexation to different metal ions strongly influences the ligand-centered redox potentials, offering the possibility to specifically shift them into the physiologically accessible range.

Metal-Centered Redox Processes. The cyclic voltammograms of the iron complexes **2A−2I** (Figure 8a, Table 2) display one reversible single-electron reduction wave, ^{C}Fe^{red}, at 0.06 to 0.51 V vs NHE, which is assigned to the Fe^{III} → Fe^{II} process of the cationic complex ($^{ox}i_p$ /$^{red}i_p$ = 1.0 for v > 0.05 V/s with ΔE_p = 0.60−0.70 at 0.2 V/s). As observed for the ligand-centered redox behavior, an increasing net electron-donor character of the ligands (expressed by their basicity; pK_a values of substituents) correlates with a decrease in redox potential of the iron-centered redox couples (Figure 7). Whereas complexes **2A−2I** showed only one reduction wave (Figure 8a), the analogous complexes **2′A−2′G** displayed a second wave at 0.31 ± 0.01 V vs NHE, which is attributed to the reduction of the tetrachloridoferrate anion, ^{A}Fe^{red} (Figure 8b). Wave ^{A}Fe^{red} overlaps in **2′E−2′G** with the reduction wave of the complex cation, ^{C}Fe^{red}, and could not be resolved by cyclic or square wave voltammetry, indicating that a set of two anionic tridentate ligands **HL^E−HL^G** acts as a net electron-donor as strong as four tetrahedrally coordinated chlorido ligands. The current height of the Fe^{III}/Fe^{II} redox couple in **2′E−2′G** (same concentration and experimental conditions) was approximately 2-fold compared to that of **2E−2G**, as confirmed by cyclic and square wave voltammetry (Figure 8). Therefore, the unresolved wave in **2′E−2′G** arises from an overlap of the Fe^{III}/Fe^{II} waves of the cationic iron complex and the tetrachlo-

(51) *CRC Handbook of Chemistry and Physics*; Lide, D. R., Ed.; CRC Press: Boca Raton, FL, 2004.

(52) Nunez-Vergara, L. J.; Bonta, M.; Navarrete-Encina, P. A.; Squella, J. A. *Electrochim. Acta* **2001**, *46*, 4289–4300.
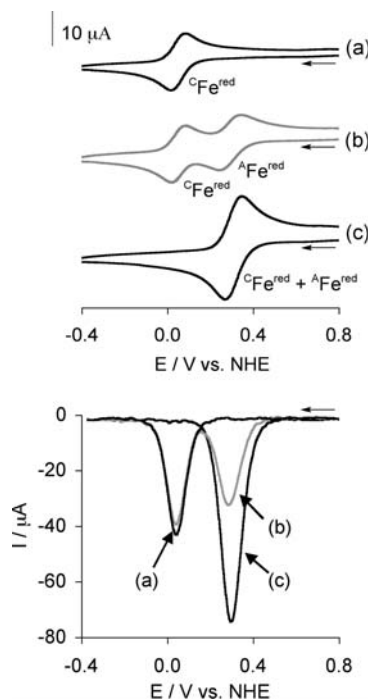
89

Figure 8. Cyclic voltammograms (top, 0.20 V s^{-1}) and square wave voltammograms (bottom, 2 mV step height, 25 mV pulse, 100 Hz frequency) of (a) **2A** (black), (b) **2′A** (gray), (c) **2′E** (black) in 0.20 M [n-Bu$_4$N][BF$_4$]/CH$_3$CN by using a platinum working electrode. ^{C}Fe^{red} indicates the metal-centered reduction of the cathodic complex, and ^{A}Fe^{red} the reduction of the [FeCl$_4$]$^-$ counteranion.
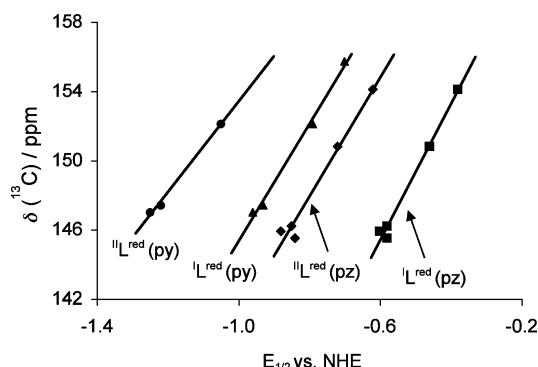

Figure 9. Plot of δ(^{13}C=N) of the CH$_3$C=N moiety vs $E_{1/2}$ of complexes **1A**−**1H** (pz = pyrazine; py = pyridine). Linear equations: ^{I}L^{red} (pz) $E_{1/2}$ (V) = (δ − 168.96)/39.35 (r = 0.987); ^{II}L^{red} (pz) $E_{1/2}$ (V) = (δ − 175.32)/34.29 (r = 0.972); ^{I}L^{red} (py) $E_{1/2}$ (V) = (δ − 179.19)/33.89 (r = 0.993); ^{II}L^{red} (py) $E_{1/2}$ (V) = (δ − 179.61)/26.23 (r = 0.995).

ridoferrate anion indicating the two-electron nature of this reduction wave (Figure 8). The presence of two overlapped one-electron processes in **2′E**−**2′G** was confirmed by controlled potential electrolysis of **2′F** at 0.14 V vs NHE.

The ruthenium(III) complex shows two reversible metal-centered redox waves with the first one at +0.21 V for the Ru^{III} → Ru^{II} redox couple and the second at +1.27 vs NHE attributable to the Ru^{III} → Ru^{IV} redox process (Figure 6c). The 1.06 V difference for the Ru^{III} → Ru^{II} and Ru^{III} → Ru^{IV} redox couples is small compared to the commonly observed separation of these two redox waves of ∼1.6 V for octahedral ruthenium complexes in nonaqueous solvents.[53] However,

this difference can be explained by the distortion of the octahedral geometry resulted from coordination of the tridentate thiosemicarbazonate ligands to ruthenium, which makes direct comparisons with other sterically noncon-strained complexes difficult.

Location of Ligand-Centered Reduction Site. Most of the literature dealing with electrochemical properties of α-*N*-heterocyclic thiosemicarbazone complexes is exclusively focused on the metal-centered redox reactions,[54−57] neglecting the ligand-centered redox processes. If reductions are described that are associated with the ligand, the position where reduction takes place in the thiosemicarbazone moiety is either undefined[58−60] or changes between the thione portion[61] and the azomethine part,[62] whereas no further studies are reported to support these assumptions. Detailed investigations on the reduction pathway were performed for the metal-free 2-formylpyridine thiosemicarbazone in metha-nol.[63] The data showed that the ligand is first protonated at the azomethine nitrogen then cleaved at the N−N bond, forming thiourea and the 2-pyridinemethaniminium ion, which is then further reduced to protonated 2-picolylamine. Two other reduction mechanisms were excluded in that study, namely, the reduction at the pyridine ring resulting in dihydropyridine and the formation of the thiol by reduction of the C=S double bond. The direct reduction of the azomethine bond was already reported for the same ligand in water 20 years ago.[64] There is only one publication dealing with the metal ion influence on the redox potentials of a thiosemicarbazone ligand.[65] Although the reference electrode was not specified, making a quantitative comparison impos-sible, the reported redox potentials of the perchlorate salt of the iron(III) complex **2B** and the ligand **HL^B** appeared at considerably different values for all reduction waves than observed in the present study. To the best of our knowledge,

(53) Reisner, E.; Arion, V. B.; Guedes da Silva, M. F. C.; Lichtenecker, R.; Eichinger, A.; Keppler, B. K.; Kukushkin, V. Yu.; Pombeiro, A. J. L. *Inorg. Chem.* **2004**, *43*, 7083–7093.
(54) Bindu, P.; Kurup, M. R. P.; Satyakeerty, T. R. *Polyhedron* **1998**, *18*, 321–331.
(55) Prabhakaran, R.; Renukadevi, S. V.; Karvembu, R.; Huang, R.; Mautz, J.; Huttner, G.; Subashkumar, R.; Natarajan, K. *Eur. J. Med. Chem.* **2008**, *43*, 268–273.
(56) Sengupta, P.; Dinda, R.; Ghosh, S.; Sheldrick, W. S. *Polyhedron* **2003**, *22*, 447–453.
(57) Ainscough, E. W.; Brodie, A. M.; Denny, W. A.; Finlay, G. J.; Ranford, J. D. *J. Inorg. Biochem.* **1998**, *70*, 175–185.
(58) Kovala-Demertzi, D.; Domopoulou, A.; Demertzis, M. A.; Papageor-giou, A.; West, D. X. *Polyhedron* **1997**, *16*, 3625–3633.
(59) Costa, R. F. F.; Rebolledo, A. P.; Matencio, T.; Calado, H. D. R.; Ardisson, J. D.; Cortes, M. E.; Rodrigues, B. L.; Beraldo, H. *J. Coord. Chem.* **2005**, *58*, 1307–1319.
(60) Graminha, A. E.; Vilhena, F. S.; Batista, A. A.; Louro, S. R. W.; Ziolli, R. L.; Teixeira, L. R.; Beraldo, H. *Polyhedron* **2008**, *27*, 547–551.
(61) Aguirre, M.; Borras, J.; Castineiras, A.; Garcia-Monteagudo, J. M.; Garcia-Santos, I.; Niclos, J.; West, D. X. *Eur. J. Inorg. Chem.* **2006**, 1231–1244.
(62) Chattopadhyay, S. K.; Chattopadhyay, D.; Banerjee, T.; Kuroda, R.; Ghosh, S. *Polyhedron* **1997**, *16*, 1925–1930.
(63) Pessôa, M. M. B.; Andrade, G. F. S.; dos Santos, M. R.; Temperini, M. L. A. *J. Electroanal. Chem.* **2003**, *545*, 117–122.
(64) Vire, J. C.; De Jager, R. L.; Dupont, D. G.; Patriarche, G. J.; Christian, G. D. *Fresenius J. Anal. Chem* **1981**, *307*, 277–282.
(65) Kovala-Demertzi, D.; Domopoulou, A.; Demertzis, M. A.; Valdes-Martinez, J.; Hernandez-Ortega, S.; Espinosa-Perez, G.; West, D. X.; Salberg, M. M.; Bain, G. A.; Bloom, P. D. *Polyhedron* **1996**, *15*, 2587–2596.

90

this is the first detailed electrochemical study of the influence of metal ions and the chalcogen donor identity on the redox properties of thiosemicarbazones.

There are two locations, where the ligand-centered reduction of the complexes can take place: either at the C=N double bond of the 2-acetylpyridine moiety (CH₃C=N) or at the C=N double bond in close proximity to the chalcogen atom. By comparison of the ^{13}C NMR data of the gallium complexes **1A−1I** with the $E_{1/2}$ redox potentials, a good correlation can be found for both carbon resonances of the CH₃C=N moiety (Figures 9 and S2, Supporting Information); an increasing redox potential at $^{I}L^{red}$ and $^{II}L^{red}$ correlates with enhanced electronic deshielding resulting in downfield chemical shifts for the corresponding ^{13}C nucleus. This allows for the prediction of the ligand-centered redox potentials of the gallium complexes by NMR shifts, and vice versa. In contrast, no correlation could be found for the C−S resonance (**1A** 172.9 ppm; **1B** 176.1 ppm; **1C** 172.5 ppm; **1D** 172.4 ppm).[23,24] Therefore, we suppose that the one-electron ligand-centered reduction takes place at the CH₃C=N bond. This is in agreement with quantum chemical calculations (see below) and the chemical reduction of this C=N bond for the metal-free and coordinated ligands. The addition of NaBH₄ to an ethanolic solution of ligand **HL^B** resulted in the reduction of the C=N bond and the formation of ligand **HL^M**, which displays its first reduction wave only at −2.10 V vs NHE. Similarly, reduction of the nitrate salt of **1B** (precipitated after addition of diethyl ether to the 1:2 mixture of Ga(NO₃)₃ and **HL^B**) with NaBH₄ yielded a product containing the uncoordinated reduced ligand **HL^M** in around 50% yield.

Quantum Chemical Studies. Density functional calculations were performed to elucidate (i) why the ligand-centered reductions of the iron(II) complexes [Fe^{II}(L)₂] (formed by reduction of the iron(III) complex [Fe^{III}(L)₂]$^+$) have a lower standard reduction potential (SRP) than the nonmetalated thiosemicarbazones (HL) and (ii) to locate the site of reduction at the thiosemicarbazone ligands. The reduction of a compound should be strongly facilitated by forming a complex with a cationic metal ion, which should have been reflected by a considerably higher redox potential. The one-electron-reduction events involving the species, (L^B)$^-$, HL^B, [Ga(L^B)₂]$^+$ (**1B**), and [Fe^{II}(L^B)₂] (**2B**), yielding their reduced forms, (L^B)$^{2-}$, (HL^B)$^-$, [Ga(L^B)₂], and [Fe^{II}(L^B)₂]$^-$, respectively, have been investigated and compared. Note that the deprotonated species (L^B)$^-$ shall serve as the intuitive reference compound in our calculations, because the reduction potential of (L^B)$^-$ may be controlled by either protonation (HL^B) or metalation ([Ga(L^B)₂]$^+$ and [Fe^{II}(L^B)₂]). Table 3 shows an excellent agreement of our calculated and experimental SRPs, validating the computational approach employed for this study (all energies and SRP values are calculated in acetonitrile solution).

Figure 10 displays the predicted structures of the most stable isomers of (L^B)$^-$, HL^B, and their reduced forms, while other plausible isomers of (L^B)$^-$ and HL^B are shown in Supporting Information, Figure S3. Figure 10 also displays

Table 3. Calculated and Experimental Standard Redox Potentials (SRP, in V vs NHE), Hirshfeld Partial Charges in the Oxidized and Reduced Forms, and LUMO Energy Level of the Oxidized Species (E_{LUMO}, in eV)

| | SRP ($E_{1/2}$); $^{I}L^{red}$ | | partial charges | | | | |
| | | | ox | | red | | |
compound	calcd	exptl	M^a	L	M^a	L	E_{LUMO}
(L^B)$^{-/2-}$	−1.69			−1.00		−2.00	1.12
[Fe(L^B)₂]$^{0/-}$	−1.56	−1.61	0.02	−0.01	0.02	−0.51	−2.45
(HL^B)$^{0/-}$	−1.12	−1.21	0.08	−0.08	0.07	−1.07	−3.03
[Ga(L^B)₂]$^{+/0}$	−0.86	−0.93	0.32	0.34	0.32	−0.16	−5.85

^{a} H, Ga, and Fe, respectively.

Table 4. Calculated Metal−Ligand Bond Lengths in Ångstrom

| | metal−S | | metal−N(N−N) | | metal−N(py) | |
compound	ox	red	ox	red	ox	red
[Ga(L^B)₂]$^{+/0}$	2.41	2.45	2.09	2.06	2.14	2.12
[Fe(L^B)₂]$^{0/-}$	2.32	2.34	1.90	1.90	1.94	1.94

the structure of the gallium complex [Ga(L^B)₂]$^+$, while the other metal complexes have the same overall shape but with noticeable differences in the bond distances (see Tables 4 and S4, Supporting Information). The predicted structures of **HL^B** and [Ga(L^B)₂]$^+$ are in good to excellent agreement with available X-ray crystallographic structures (Supporting Information, Table S4). The calculations reveal structural changes in the entire compounds upon reduction. In the free ligand (L^B)$^-$ (Figure 10, top), the C−S bond is elongated (+0.04 Å) upon reduction, the adjacent C=N bond is shortened (−0.03 Å), the N−N bond is elongated (+0.03 Å), the acetylpyridine C=N bond is elongated (+0.03 Å), the adjacent C−C bond is shortened (−0.02 Å), and the C=N bond in the pyridine is elongated (+0.04 Å). Similar structural changes occur when the protonated species **HL^B** is reduced (Figure 10). Upon reduction of the metal complexes [Ga(L^B)₂]$^+$ and [Fe^{II}(L^B)₂], the structures within the ligands change in a similar manner, but to a lesser extent as compared to the nonmetalated species (Supporting Information, Table S4). The reduction of the metal complexes is also accompanied by relatively minor changes in the metal−ligand distances (Table 4). The Ga−N bonds are slightly shortened (−0.02 and −0.03 Å), whereas the Ga−S bonds are elongated (+0.04 Å). In contrast, the Fe−N distances remain constant, while the Fe−S bonds are slightly elongated (+0.02 Å).

Table 3 lists the electron-density-based Hirshfeld partial charges on the ligands, the metals, and the proton in the four initial species and their reduced forms. The calculated charges at the H, Fe, and Ga atoms in **HL^B**, [Fe^{II}(L^B)₂], and [Ga(L^B)₂]$^+$ are +0.08, +0.02, and +0.32, respectively, while the charge on each ligand is −0.08, −0.01, and +0.34, adding up to a total charge of 0, 0, and +1 in these compounds. Upon reduction, the charges at H, Fe, and Ga remain constant, while the additional electronic charge is distributed over the ligands. Partial charges calculated using various other approaches are given in Supporting Information, Table S5. While the absolute values differ from the Hirshfeld charges, the overall trend of the charges increasing in the order Fe < H < Ga is supported by each approach. The intuitive assumption that the reduction of a compound

91

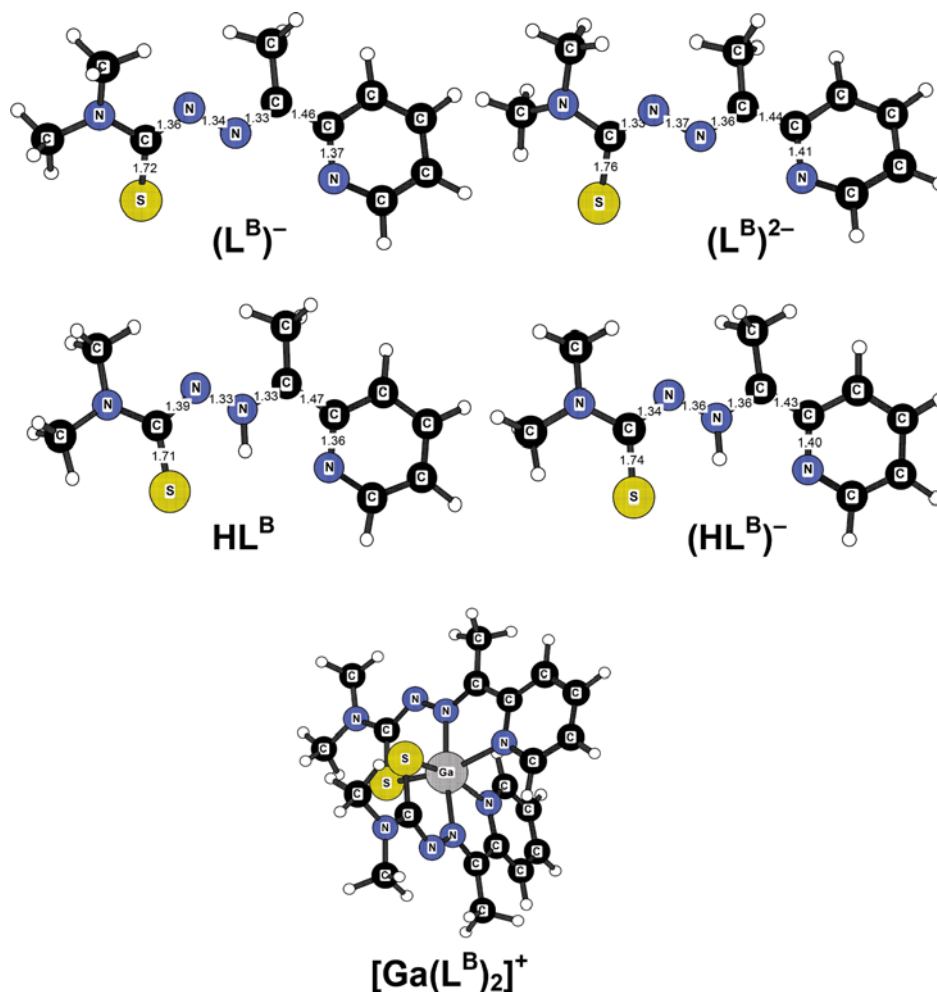**Figure 10.** Calculated structures of $(\mathbf{L^B})^-$, $(\mathbf{L^B})^{2-}$, $\mathbf{HL^B}$, $(\mathbf{HL^B})^-$, and $[Ga(\mathbf{L^B})_2]^+$. Bond lengths in Å.

is facilitated when it binds to a metal ion appears to be valid only if the deprotonated free ligand $(\mathbf{L^B})^-$ is considered as the reference compound, whereas a proton promotes the reduction of the thiosemicarbazone more strongly than does the iron(II) ion with its d^6 low-spin electron configuration.

Figure 11 displays the semioccupied molecular orbital (SOMO) of the four reduced species $(\mathbf{L^B})^{2-}$, $(\mathbf{HL^B})^-$, $[Fe^{II}(\mathbf{L^B})_2]^-$, and $[Ga(\mathbf{L^B})_2]$. This orbital corresponds in each case to the lowest unoccupied orbital (LUMO) of the oxidized form (Supporting Information, Figure S4). The LUMO energy levels of the oxidized species are also listed in Table 3 and correlate with the reduction potentials: the lower the LUMO energy, the easier the reduction. The SOMO of $(\mathbf{L^B})^{2-}$ and its conjugate acid $(\mathbf{HL^B})^-$ are very similar; they are distributed over the entire π system and have both bonding and antibonding character leading to the bond distance changes upon reduction (see above). For instance, as the SOMO of $(\mathbf{HL^B})^-$ has a bonding contribution to the C=N bond adjacent to the sulfur atom (marked with b in Figure 11), this bond is shortened when an electron occupies this orbital. The SOMO of $(\mathbf{HL^B})^-$ has an antibonding contribution to the C=N bond adjacent to the pyridyl group (marked with a in Figure 11), thus elongating this bond upon reduction. This result is consistent with the chemoselective hydrogenation of the latter C=N bond by $NaBH_4$ (see

above). The SOMO of the reduced metal complexes show the same bonding and antibonding patterns as those in the SOMO of the free ligand. In contrast to the SOMO of the gallium species, the SOMO of the reduced iron complex contains a small fraction of a metal d orbital. Note that none of the iron−ligand bond lengths shortens during reduction, indicating an enhanced Pauli repulsion between the ligand orbitals and the partially filled d shell in the reduced iron complex.

Biological Relevance and Comparison of Electrochemical Data with Cytotoxicity and R2 Specific Tyrosine Free Radical Quenching. The influence of water on the redox potentials of the gallium, iron, and ruthenium complexes was studied by measuring complexes **1B**, **1C**, **1G**, **1H**, **1I**, **2B**, **2C**, **2D**, **2G**, **2H**, **2I**, and **3B** in CH_3CN/H_2O (7:3 v/v) or DMF/H_2O (7:3 v/v) mixtures. The low solubility of the complexes prevented the measurement in pure aqueous electrolyte solutions. The metal-centered redox waves for the $M^{III} \rightarrow M^{II}$ process for the iron and ruthenium complexes remained reversible (involving net 1+/0 net charged complexes) in the aqueous organic electrolyte solutions and are slightly shifted to more negative values with a maximum

(66) Richardson, D. R.; Sharpe, P. C.; Lovejoy, D. B.; Senaratne, D.; Kalinowski, D. S.; Islam, M.; Bernhardt, P. V. *J. Med. Chem.* **2006**, *49*, 6510–6521.
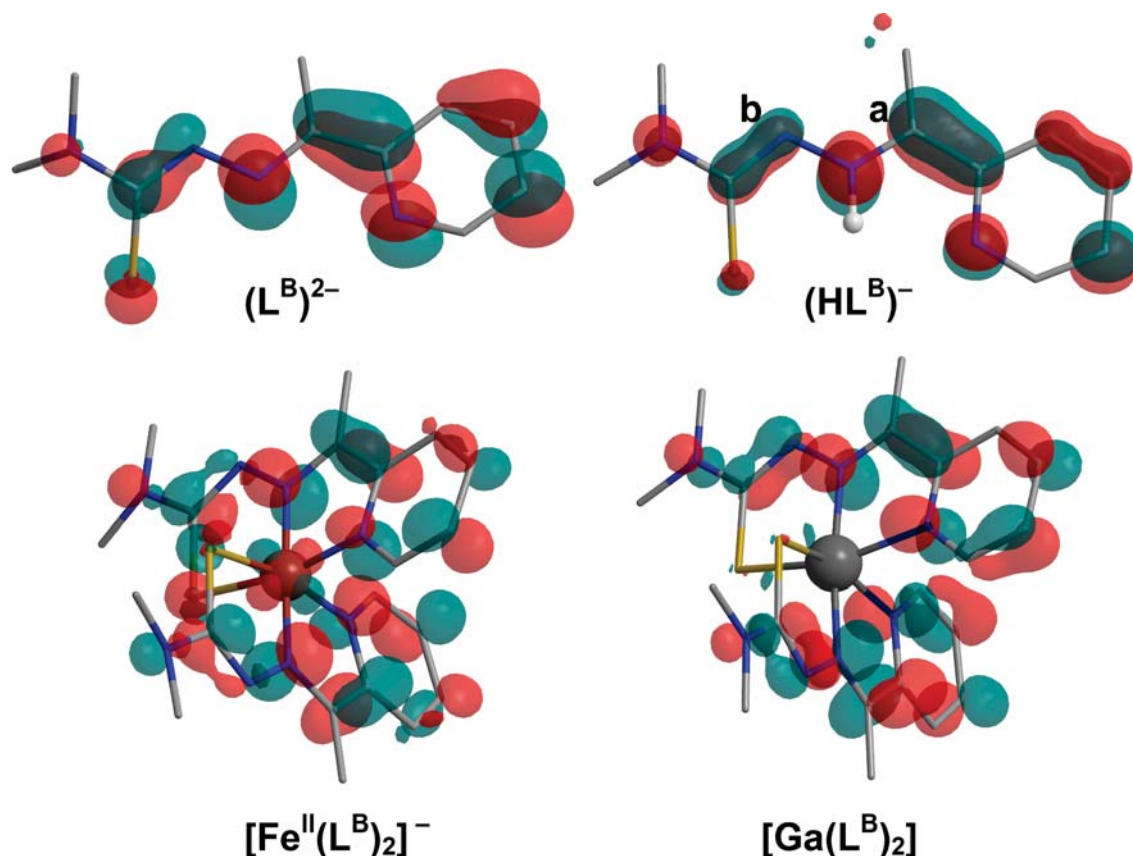
Figure 11. SOMO of the reduced species.

shift of -70 mV for **2D**. Iron dipyridinyl thiosemicarbazone complexes measured in CH_3CN/H_2O (7:3 v/v) were reported to give reversible Fe^{III}/Fe^{II} redox potentials of $+0.153$ to $+0.225$ V vs NHE.[66] The direct dipyridinyl analogs of complex **2B** and **2C** exhibit redox potentials of $+0.166$ and $+0.225$ V vs NHE, respectively, implying a more positive potential of the phenyl substituted complex in comparison to the ^4N-dimethyl-substituted one in line with our results. In general, higher potentials are observed for dipyridinyl complexes due to the electron withdrawing properties of the pyridinyl group. Furthermore, a series of 5-substituted 2-formylpyridine thiosemicarbazone complexes measured in water possess reversible iron redox potentials from $+0.024$ to $+0.386$ V vs NHE.[67]

Because water has a smaller potential window, the ligand-centered reductions for the iron complexes could be studied only in the case of **2G** and **2H**. These turned out to be completely irreversible indicating that the generated radicals upon reduction can no longer be stabilized by the metal center resulting in fast radical quenching by the water. We can therefore assume that the generated ligand-radicals are highly reactive under physiological conditions. In contrast to the iron-centered redox processes, the reduction potentials (E_p) for the first ligand reduction (wave $^IL^{red}$; involving net $0/1-$ charged complexes) is shifted by $+100$ mV and for the second ligand-centered reduction (wave $^{II}L^{red}$; involving net $1-/2-$ charged complexes) by approximately $+300$ mV for both complexes compared to the measurements in CH_3CN electrolyte solutions. The first ligand-centered reduction potential (wave $^IL^{red}$; involving net $1+/0$ net charged

complexes) of the gallium complexes **1B**, **1C**, **1G**, **1H**, and **1I** showed a slightly cathodically shifted redox potential (ca., -50 mV), whereas the second ligand-reduction at $^{II}L^{red}$ was anodically shifted up to $+150$ mV compared to the measurements in pure organic electrolyte solutions. In general, redox couples involving positive net charged species are shifted to more negative redox potentials in aqueous solutions (compared to organic medium) and vice versa. This behavior has been explained previously[1,10] on the basis of the Born model of solvation. In accordance with this model, stabilization of a more positively or more negatively charged species occurs through the higher solvation energy of water resulting in decreasing or increasing redox potentials, respectively. The Born equation shows that the solvation energy is proportional to the squared charge, what explains the larger shift for the $1-/2-$ charged species (wave $^{II}L^{red}$ in iron(II) complexes) compared to the $0/1-$ and $1+/0$ net charged complexes.

The physiological accessibility of the M^{III}/M^{II} redox couple between 0.06 and 0.51 V vs NHE by biological reducing agents was studied by UV−vis spectroscopy measurements of complexes **2B**, **2G**, and **3B** in 1% aqueous DMSO solution with a 5-fold excess of ascorbic acid ($E_{1/2} = +0.06$ vs NHE[68]). Complex **2G** is reduced immediately after addition of ascorbic acid accompanied by a color change from brown to green. For the ruthenium(III) complex, the UV−vis spectrum changes within minutes, whereas for **2B** only small

(67) Knight, J. M.; Whelan, H.; Petering, D. H. *J. Inorg. Biochem.* **1979**, *11*, 327–338.

(68) *CRC Handbook of Biochemistry and Molecular Biology*; Fasman, G. D., ED.; CRC Press: Cleveland, OH, 1976; p 122.

changes can be observed after hours. These results are in accordance with the M^{III}/M^{II} redox potentials of the metal complexes. One major goal of this study was to introduce electron-withdrawing substituents such as nitro-groups into the thiosemicarbazone ligands to shift the ligand-centered redox potentials in the direction of the physiologically accessible range. Indeed, several gallium complexes have redox potentials for $^{I}L^{red}$ around −0.4 vs NHE, which is given as a guiding value for the redox potential reachable in cells.[69] Unfortunately, the low solubility in DMSO/H$_2$O mixtures with a maximal content of 1% DMSO prevents the cytotoxicity measurements of the novel synthesized compounds. Therefore the comparison of the IC$_{50}$ values and the electrochemical data can only be done for the ^{4}N-disubstituted ligands and complexes. The cytotoxicity data of the 41 M cancer cell line show the overall trend that the iron(III) complexes exhibit the lowest cytotoxicity (13−172 nM) followed by the metal-free ligand (0.073−1.1 nM) and the gallium complexes (0.0045−0.27 nM).[23] The same trend, but less pronounced, can be found in the SK-BR-3 cancer cell line.[23] The direct comparison reveals that the gallium(III) complexes are by a factor of 210 to 33000 (41M) and 150 to 4000 (SK-BR-3) more cytotoxic than the corresponding iron complexes, respectively. Interestingly, the coordinated thiosemicarbazone ligands are most easily reduced in the case of the gallium complexes, followed by the metal-free ligands and shifted to very low redox values in the case of the iron complexes, what correlates with the previously obtained cytotoxic data. But as mentioned above, we should be aware that the physiologically accessible range of the redox potential of cells is given from −0.4 to +0.8 V vs NHE.[69] The order of the R2 specific tyrosine free radical destruction in mouse ribonucleotide reductase is in contrast to the cytotoxicity data and the electrochemical results of the ligand-centered reductions: fastest inhibition of the enzyme occurs in the case of the iron complexes suggesting that the redox properties of iron play an important role in the radical quenching process.

Final Remarks

The syntheses of a series of gallium-, iron-, and ruthenium-chalcogensemicarbazonate complexes are reported; the electrochemical properties of these compounds are investigated in detail, and their biological relevance is discussed. The electrochemical behavior of these complexes can be specified by (i) physiologically accessible metal-centered redox potentials for the iron(III) and ruthenium(III) complexes, (ii) formation of stable ligand radicals on the time-scale of cyclic voltammetry upon reduction of the noninnocent chalcogensemicarbazone ligands in aprotic solvents, (iii) quenching of these reductively induced ligand radicals by water, (iv) shift of the ligand-centered redox potential in the physiologically accessible range for some gallium complexes when electron-withdrawing moieties are incorporated into the ligand, and (v) ligand-reduction for the gallium complexes occurs at the CH$_3$C═N double bond. Quantum chemical calculations show that reduction of the coordinated and metal-free thiosemicarbazone ligands occurs at a π-orbital that spreads over the entire thiosemicarbazone moiety. The ligand-centered reductions $^{I}L^{red}$ and $^{II}L^{red}$ take place at 0.3−0.8 V more positive potentials for the gallium complexes than for the uncoordinated (protonated) ligands. The latter on the other hand are easier to reduce than the corresponding iron(II) complexes. The redox potentials increasing in the order $[Fe^{II}(L^{B})_2] < HL^{B} < [Ga(L^{B})_2]^{+}$ are consistent with the trend of the calculated partial charges, Fe < H < Ga, in these compounds and with the energy levels of their LUMO. The presented results on the electrochemical behavior of potential antitumor chalcogensemicarbazonate complexes allow for the future design of potential drugs with predictable and desired redox properties.

Supporting Information Available: Detailed discussion of the NMR data of **1H**, redox potentials of the metal-free ligands **HL^{A}**−**HL^{M}**, cyclic voltammogram of **3B** with ligand centered reductions and plot of $\delta(^{13}CH_3)$ of the CH$_3$C═N moiety versus $E_{1/2}$ of complexes **1A**−**1H**, calculated relative energies of plausible isomers of **HL^{B}** and its deprotonated form, calculated bond lengths and partial charges of $(L^{B})^{-}$, **HL^{B}**, $[Fe^{II}(L^{B})_2]$, $[Ga(L^{B})_2]^{+}$, and their one-electron reduction products, plots of the LUMO of the reduced species, comparison of the standard reduction potentials calculated at B3LYP and BP86, relative energies of plausible electronic states of $[Fe^{II}(L^{B})_2]$ and $[Fe^{II}(L^{B})_2]^{-}$, and X-ray crystallographic files in CIF format for **HL^{H}**, **HL^{M}**, and **1H·**H$_2$O. This material is available free of charge via the Internet at http://pubs.acs.org.

IC8013249

(69) Kirlin, W. G.; Cai, J.; Thompson, S. A.; Diaz, D.; Kavanagh, T. J.; Jones, D. P. *Free Radical Biol. Med.* **1999**, *27*, 1208–1218.

Supporting Information

An Electrochemical Study of Antineoplastic Gallium, Iron and Ruthenium Complexes with Redox Non-Innocent α-N-Heterocyclic Chalcogensemicarbazones

Christian R. Kowol,[†] Erwin Reisner,[†,‡,]* Ion Chiorescu,[†] Vladimir B. Arion,[†,]* Markus Galanski,[†] Dirk V. Deubel,[†] Bernhard K. Keppler[†]

[†] Institute of Inorganic Chemistry, University of Vienna, Währingerstr. 42, A-1090 Vienna, Austria

[‡] Inorganic Chemistry Laboratory, University of Oxford, South Parks Road, Oxford OX1 3QR, UK

Detailed discussion of the NMR data of 1H

The quaternary carbon atoms of the pyrazine moiety and the C=N double bond were detected via a long-range ^{1}H–^{13}C HMBC NMR experiment. Shift correlation signals of the methyl protons of C6 and carbon atoms C4 and C5 at 139.8 and 150.8 ppm, respectively, were found, but could not be assigned unequivocally on the basis of their chemical shifts. With the aim to find a long-range shift correlation between one of the pyrazine protons namely that of C2 and the quaternary atom C4, which would exclude a long-range coupling via five bonds to carbon atom C5, accurate assignment of pyrazine protons of C1, C2 and C3 was needed. In the ^{1}H NMR spectrum of **1H**, three multiplets at 9.66 (d, 1.1 Hz), 8.96 (d, 2.8 Hz) and 8.09 ppm (dd, 1.1 and 2.8 Hz) of the pyrazine moiety were detected. In a homonuclear decoupling experiment, the proton at 9.66 was irradiated resulting in two doublets (at 8.96 and 8.09 ppm) with vicinal coupling constants of 2.8 Hz. By using this technique, the proton of C3 at 9.66 was assigned. The resonance of proton at C2 was allocated via a long-range ^{1}H–^{15}N HMBC NMR measurement optimized for coupling constants of 10 Hz, since both protons of C2 and C3 should show a correlation signal to the same ^{15}N nucleus. ^{1}H–^{15}N cross peaks at 9.66/244.7 and 8.09/244.7 ppm, respectively, were detected providing evidence that proton of C2 resonates at 8.09 ppm. In addition, a long-range coupling of proton at C2 (8.09 ppm) with the quaternary carbon atom C4 at 139.8 ppm was found undoubtedly confirming the chemical shift of carbon atoms C4 and C5 (150.8 ppm).

S1
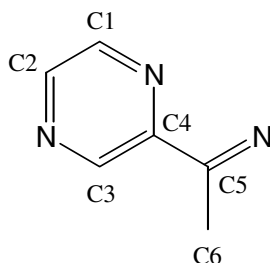
Table S1. Comparison of standard reduction potentials (SRPs, in V *vs*. NHE) calculated at B3LYP and BP86.

Compound	B3LYP	BP86	exp
$(\mathbf{L^B})^{-/2-}$	−1.81	−1.69	
$(\mathbf{HL^B})^{0/-}$	−1.18	−1.12	−1.21
$[\mathbf{Ga(L^B)_2}]^{+/0}$	−1.35	−0.86	−0.93
$[\mathbf{Fe(L^B)_2}]^{0/-}$	−2.00	−1.56	−1.61

Table S2. Relative energies (in kcal/mol) of plausible electronic states of $[\mathrm{Fe^{II}(L^B)_2}]$ and $[\mathrm{Fe^{II}(L^B)_2}]^-$.

	multiplicity	B3LYP	BP86
$[\mathrm{Fe^{II}(L^B)_2}]$	1	10.6	0
	3	5.9	15.0
	5	0	20.6
$[\mathrm{Fe^{II}(L^B)_2}]^-$	2	13.5	0
	4	0	6.3

Table S3. Redox potentials[a] of the metal-free ligands $\mathbf{HL^A}$–$\mathbf{HL^M}$.

Ligand	E_p / $^1\mathrm{L}^{red}$
A	−1.26
B	−1.21
C[b]	−1.47
D[b]	n/a[c]
E	−1.06
F	−1.02
G	−1.01
H[b]	−1.31
I[b]	n/a[c]
J	−1.83
K	−1.13
M	n/a[d]

a) Potentials in V ± 0.02 *vs*. NHE in 0.20 M [*n*-Bu₄N][BF₄]/CH₃CN; b) measured in 0.20 M [*n*-Bu₄N][BF₄] / DMF; c) for the nitro-containing ligands, only the reduction of this group at *ca*. −1.0 V *vs*. NHE and a pre-wave at *ca*. 0.80 V *vs*. NHE can be observed (see text); d) first reduction at −2.10 V *vs*. NHE.

Table S4. Calculated bond lengths (in Å).

Compound		C1–S ox	C1–S red	C1–N1 ox	C1–N1 red	N1–N2 ox	N1–N2 red	N2–C2 ox	N2–C2 red	C2–C3 ox	C2–C3 red	C3–N3 ox	C3–N3 red	Metal–S ox	Metal–S red	Metal–N2 ox	Metal–N2 red	Metal–N3 ox	Metal–N3 red
(L^B)$^{-/2-}$	Calc	1.719	1.757	1.364	1.327	1.340	1.373	1.331	1.356	1.464	1.442	1.373	1.414						
(HL^B)$^{0/-}$	Calc	1.713	1.739	1.389	1.343	1.327	1.360	1.328	1.364	1.466	1.428	1.362	1.395						
	X-ray^a	1.723		1.350		1.353		1.299		1.474		1.352							
[Ga(L^B)$_2$]$^{+/0}$	Calc	1.755	1.759	1.362	1.346	1.338	1.355	1.331	1.343	1.464	1.445	1.370	1.387	2.412	2.453	2.089	2.057	2.141	2.119
	X-ray^b	1.741		1.342		1.356		1.304		1.465		1.361		2.373		2.032		2.131	
[Fe(L^B)$_2$]$^{0/-}$	Calc	1.747	1.752	1.349	1.336	1.358	1.369	1.344	1.355	1.442	1.428	1.383	1.400	2.318	2.341	1.902	1.902	1.942	1.944

(L^B)$^-$

HL^B

[M(L^B)$_2$]
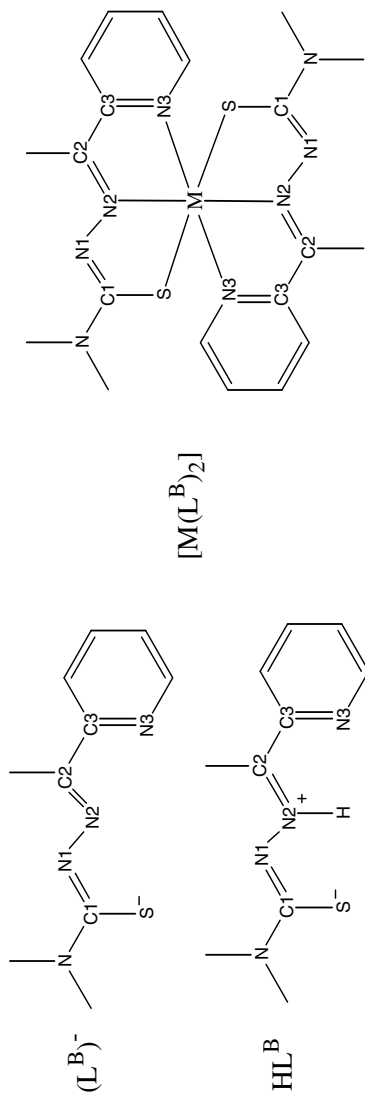
^{a} Kowol, C. R.; Eichinger, R.; Jakupec, M. A.; Galanski, M.; Arion, V. B.; Keppler, B. K. *J. Inorg. Biochem.* **2007**, *101*, 1946–1957.

^{b} Arion, V. B.; Jakupec, M. A.; Galanski, M.; Unfried, P.; Keppler, B.K. *J. Inorg. Biochem.* **2002**, *91*, 298–305.

Table S5. Calculated partial charges on the ligands and on the metal or hydrogen.

Compound	moiety	Mulliken (lb)[a]		Mulliken (sb)[b]		ESP (sb)[c]		Hirshfeld[d]	
		ox	red	ox	red	ox	red	ox	red
$(L^B)^{-/2-}$		−1.00	−2.00	−1.00	−2.00	−1.00	−2.00	−1.00	−2.00
$(HL^B)^{0/-}$	H	0.30	0.29	0.29	0.28	−0.04	−0.01	0.08	0.07
	L	−0.30	−1.29	−0.29	−1.28	0.04	−0.99	−0.08	−1.07
$[Ga(L^B)_2]^{+/0}$	Ga	1.90	1.92	0.94	1.00	0.42	0.48	0.32	0.32
	L	−0.45	−0.96	0.03	−0.50	0.29	−0.24	0.34	−0.16
$[Fe(L^B)_2]^{0/-}$	Fe	−0.82	−0.84	−0.02	−0.02	−0.16	−0.10	0.02	0.02
	L	0.41	−0.08	0.01	−0.49	0.08	−0.45	−0.01	−0.51

[a] Large basis set. Totally uncontracted LANL2DZ on Ga and augmented with one set of f functions on Fe, together with the 6-311+G(d,p) basis sets on the other atoms, and the 6-311+G(3d) on S.
[b] Small basis set. LANL2DZ on the metal, 6-31G(d,p) on the other atoms.
[c] Same small basis set, denoted LACVP** in Jaguar.
[d] Scalar relativistic ZORA, TZV2P basis on the metals and TZVP basis set on the other atoms.
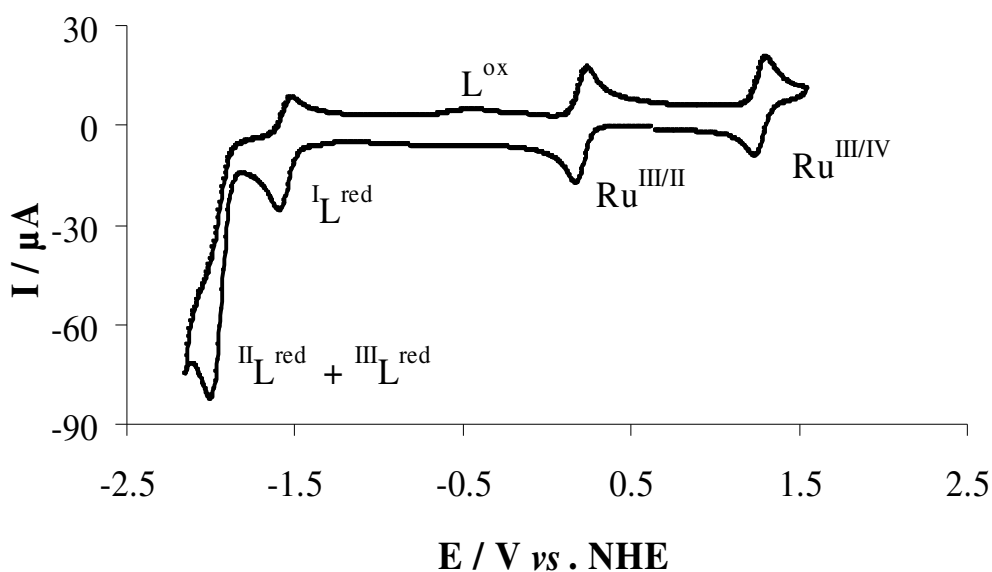
Figure S1. Cyclic voltammogram of **3B** in CH_3CN containing 0.20 M [n-Bu$_4$N][BF$_4$] at a scan rate of 0.20 V s^{-1} using a glassy carbon working electrode.
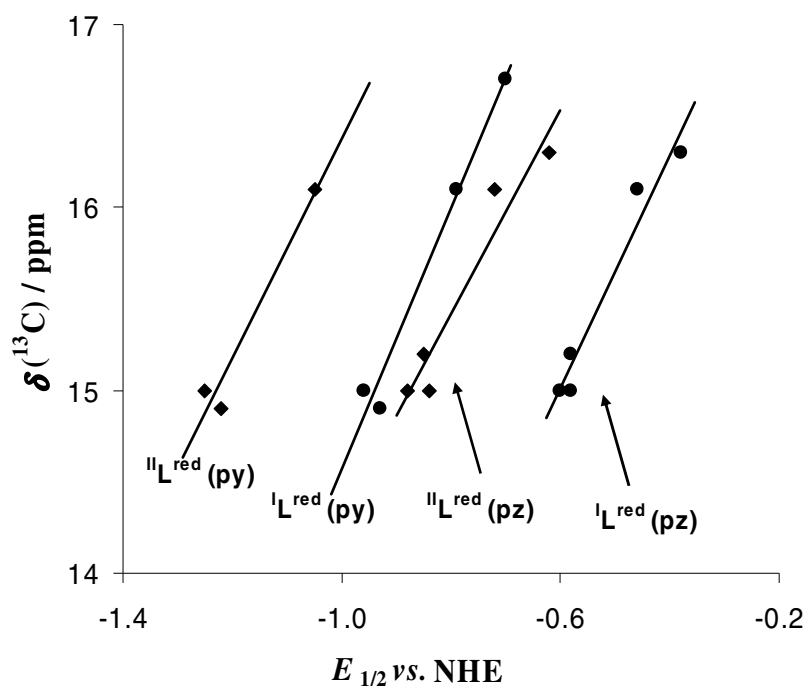
Figure S2. Plot of $\delta(^{13}CH_3)$ of the $CH_3C{=}N$ moiety *vs.* $E_{1/2}$ of complexes **1A–1H**. Linear equations:

$^IL^{red}$ (pz): $E_{1/2}$ (V) = $(\delta - 18.86)/6.41$ (r = 0.95); $^{II}L^{red}$ (pz): $E_{1/2}$ (V) = $(\delta - 19.87)/5.56$ (r = 0.93); $^IL^{red}$

(py): $E_{1/2}$ (V) = $(\delta - 21.67)/7.09$ (r = 0.98); $^{II}L^{red}$ (py): $E_{1/2}$ (V) = $(\delta - 22.41)/6.03$ (r = 0.95).

(a) 0

(b) 3.4

(c) 4.7

(d) 7.7

(e) 12.9

(f) 15.8

(g) 0

(h) 6.7

(i) 6.7

(j) 9.8

HL^B

(L^B)$^-$
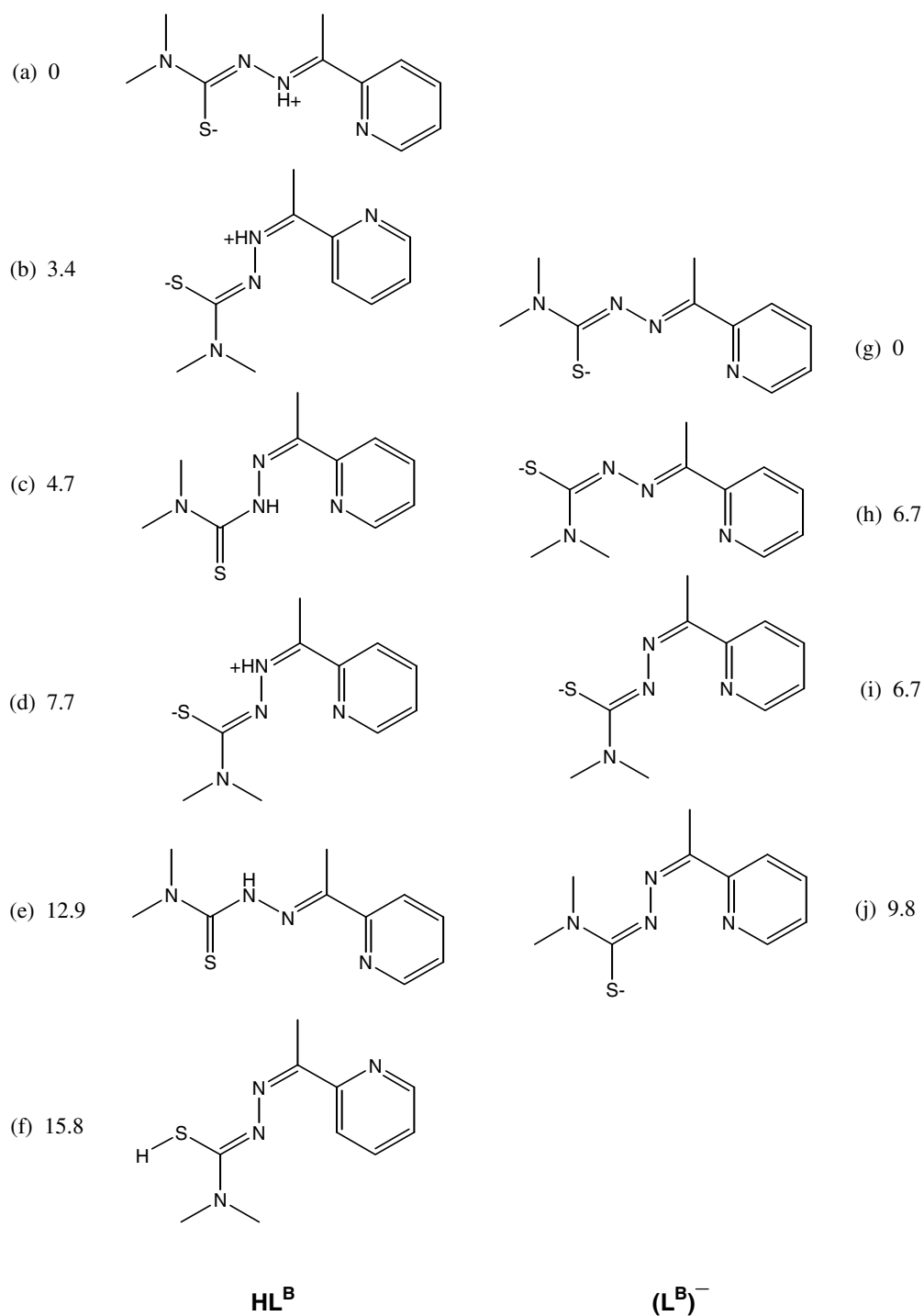
Figure S3. Calculated relative energies (in kcal/mol) of plausible isomers of 2-acetylpyridine *N,N*-dimethylthiosemicarbazone (HL^B) and its deprotonated form (L^B)$^-$ in acetonitrile.
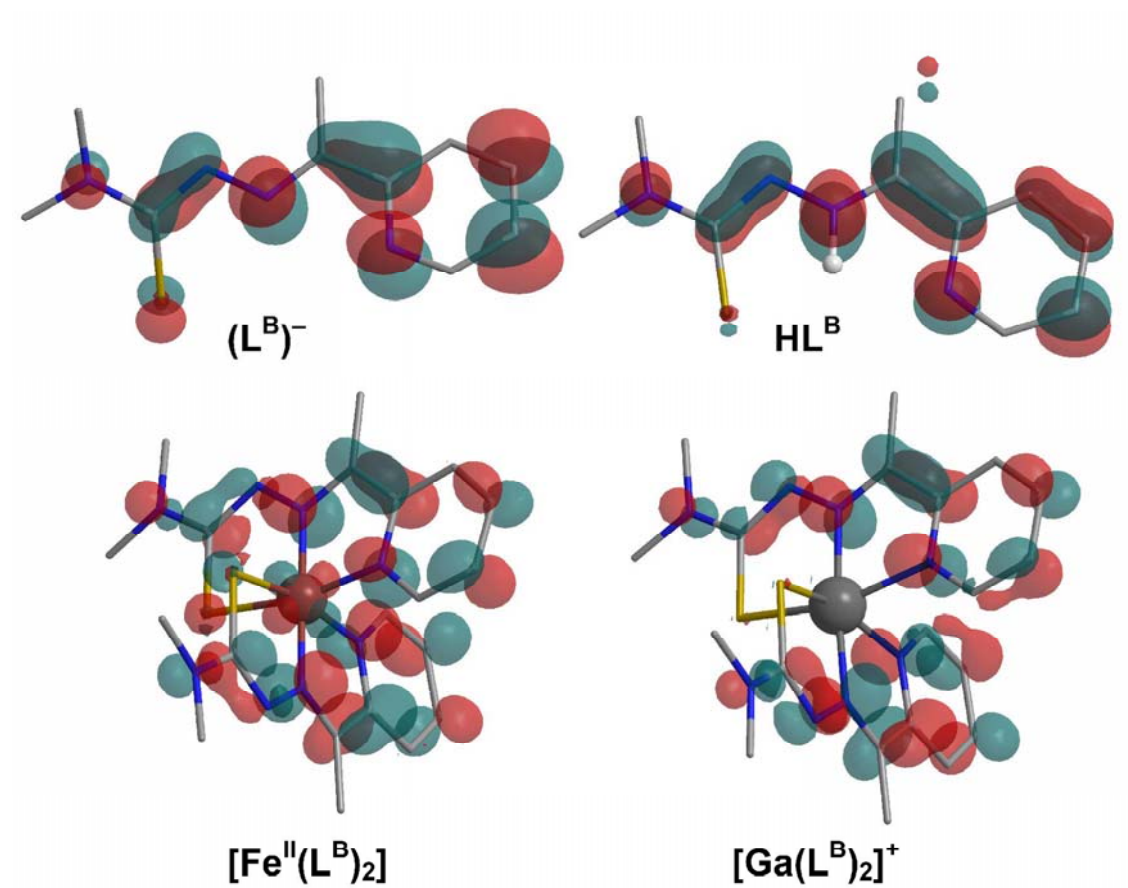
Figure S4. LUMO of the oxidized species $(L^B)^-$, HL^B, $[Fe^{II}(L^B)_2]$ and $[Ga(L^B)_2]^+$.

2.4 Impact of Metal Coordination on Cytotoxicity of 3-Aminopyridine-2-carboxaldehyde Thiosemicarbazone (Triapine) and Novel Insights on Terminal Dimethylation

Kowol, C. R.; Trondl, R.; Heffeter, P.; Arion, V. B.; Jakupec, M. A.; Roller, A.; Galanski, M.; Berger, W.; Keppler, B. K.

Impact of Metal Coordination on Cytotoxicity of 3-Aminopyridine-2-carboxaldehyde Thiosemicarbazone (Triapine) and Novel Insights into Terminal Dimethylation

Christian R. Kowol,[‡] Robert Trondl,[‡] Petra Heffeter,[#] Vladimir B. Arion,[‡,]* Michael A. Jakupec,[‡]

Alexander Roller,[‡] Markus Galanski,[‡] Walter Berger,[#] Bernhard K. Keppler[‡,]*

[‡] University of Vienna, Institute of Inorganic Chemistry, Währinger Str. 42, A-1090 Vienna, Austria

[#] Medical University of Vienna, Institute of Cancer Research, Borschkeg. 8a, A-1090 Vienna, Austria

_____

* To whom correspondence should be addressed. Address: Institute of Inorganic Chemistry, University of Vienna, Waehringer Str. 42, A-1090 Vienna, Austria. Phone: +431427752600. Fax: +431427752680. E-mail: vladimir.arion@univie.ac.at; bernhard.keppler@univie.ac.at

Abstract

The first metal complexes of 3-aminopyridine-2-carboxaldehyde thiosemicarbazone (Triapine) were synthesized. Triapine was prepared by a novel three-step procedure in 64% overall yield. In addition, a series of related ligands, namely, 2-formylpyridine thiosemicarbazone, 2-acetylpyridine thiosemicarbazone, 2-pyridineformamide thiosemicarbazone and their [4]N-dimethylated derivatives (including the [4]N-dimethylated analog of Triapine) were prepared, along with their corresponding gallium(III) and iron(III) complexes with the general formula $[M(L)_2]^+$, where HL is the respective thiosemicarbazone. The compounds were characterized by elemental analysis, ^{1}H and ^{13}C NMR, IR and UV-vis spectroscopies, mass spectrometry and cyclic voltammetry. In addition, Triapine and its iron(III) and gallium(III) complexes were studied by X-ray crystallography. All ligands and complexes were tested for their in vitro antiproliferative activity in two human cancer cell lines (41M and SK-BR-3), and structure-activity relationships were established. In general, the coordination to gallium(III) increased the cytotoxicity, while the iron(III) complexes show reduced cytotoxic activity as compared to the metal-free thiosemicarbazones. Selected compounds were investigated for the capacity of inhibiting ribonucleotide reductase by incorporation of ^{3}H-cytidine into DNA.

Introduction

Thiosemicarbazones are versatile ligands, as they adopt various binding modes with transition and main group metal ions.[1] These can act as mono- or bidentate ligands,[2] and their coordination capacity can be further increased, if aldehydes or ketones which contain additional functional group(s) in position(s) suitable for chelation are used for their preparation.[3,4] Beside their exciting coordination chemistry, thiosemicarbazones are known to possess a wide range of pharmaceutical properties such as antitumor, antiviral, antifungal, antibacterial and antimalarial activity.[5] In addition, ^{64}Cu-bis(thiosemicarbazonate) complexes are under investigation as hypoxia-selective positron emission

tomography tracers.[6] The first thiosemicarbazone with antitumor properties, namely 2-formylpyridine thiosemicarbazone, was reported about 50 years ago.[7] Further studies showed that a prerequisite for biological activity is a nitrogen heterocycle which contains a suitable functional group for condensation with thiosemicarbazide derivatives in α-position.[8] 5-Hydroxy-2-formylpyridine thiosemicarbazone (5-HP) was the first compound of this series which entered phase I clinical trials. However, 5-HP is rapidly transformed in the body and eliminated as an inactive glucuronide conjugate.[9,10] In addition, 5-HP showed severe hematological and gastrointestinal side effects which prevented its further clinical development. The currently most promising thiosemicarbazone as antitumor agent is 3-aminopyridine-2-carboxaldehyde thiosemicarbazone (Triapine, 3-AP), which entered several phase I and II clinical trials.[11,12,13,14,15]

As the principal molecular target of α-N-heterocyclic thiosemicarbazones the enzyme ribonucleotide reductase (RR) has been identified.[16,17,18] This enzyme catalyzes the conversion of ribonucleotides into deoxyribonucleotides, providing the precursors required for DNA synthesis and repair. α-N-Heterocyclic thiosemicarbazones are the most potent inhibitors of RR known so far. They are several orders of magnitude more effective than hydroxyurea, the first clinically applied RR inhibitor.[19] Faster proliferation of tumor cells as compared to normal cells and therefore higher expression of RR make this enzyme a suitable and well established target in cancer chemotherapy.[20] The human RR consists of two homodimeric subunits: R1 and R2. The first subunit harbors the nucleotide binding site and the second subunit a diiron center and a tyrosyl radical. Transfer of the radical electron from tyrosine (Y122) of R2 occurs by a proton-coupled mechanism via a chain of hydrogen-bonded amino acids over a distance of 35 Å to cysteine (C439) of R1 subunit, where it generates a thiyl radical essential for reduction of the substrates.[21] Recently, a second R2 subunit, called p53R2, has been identified in human cells with ~80% sequence homology with R2, but with p53-dependent expression.[22] The p53 protein actively suppresses tumor formation, and the majority of human tumors have been found to contain mutations in p53 or defects in the pathways responsible for its activation.[23] Thus the discovery of p53R2 revealed a link between the most important tumor suppressor and the synthesis of deoxyribonucleotides.

We reported previously that the gallium(III) complexes of [4]N-disubstituted α-N-heterocyclic thiosemicarbazones (HL), with the composition [Ga(L)$_2$]$^+$, exhibit enhanced cytotoxicity in the low nanomolar range, in human cancer cell lines. In contrast, the corresponding iron(III) complexes displayed a much lower cytotoxicity (in the micromolar range) than the metal-free ligands.[24] EPR measurements on isolated mouse R2 subunits of RR showed that the effects of the complexation to gallium(III) and iron(III) on the destruction of the R2 specific tyrosine free radical in the presence of the reductant dithiothreitol (DTT) are in the reverse order. The iron(III) complexes show the fastest destruction of the tyrosyl radical in RR, followed by the metal-free ligands and the corresponding gallium(III) complexes.[24] In the case of Triapine, iron also enhances radical quenching.[25] However, in contrast to [4]N-dimethylated α-N-heterocyclic thiosemicarbazones, addition of iron(III) to Triapine results only in small changes in cytotoxicity.[26,27]

In order to evaluate the effect of complexation on the cytotoxicity of Triapine, the gallium(III) and iron(III) complexes were synthesized for the first time. For elucidation of further structure-activity relationships, a series of related ligands and their corresponding gallium(III) and iron(III) complexes were prepared (Scheme 1). In particular, the effects of the amino group and its position as well as the influence of [4]N-disubstitution on cytotoxicity were investigated, including for the first time the Triapine analog 3-aminopyridine-2-carboxaldehyde [4]N-dimethylthiosemicarbazone. In addition, selected compounds were tested for their capacity of inhibiting ribonucleotide reductase by a ^{3}H-cytidine DNA incorporation assay.

HL^A

HL^B

HL^C

HL^D; Triapine

HL^E

HL^F

HL^G

HL^H

M = Ga, L = L^A, Y = NO$_3$; [Ga(L^A)$_2$][NO$_3$]   (**1A**)

M = Ga, L = L^B, Y = NO$_3$; [Ga(L^B)$_2$][NO$_3$]   (**1B**)

M = Ga, L = L^C, Y = NO$_3$; [Ga(L^C)$_2$][NO$_3$]   (**1C**)

M = Ga, L = L^D, Y = NO$_3$; [Ga(L^D)$_2$][NO$_3$]   (**1D**)

M = Ga, L = L^E, Y = PF$_6$; [Ga(L^E)$_2$][PF$_6$]   (**1E**)

M = Ga, L = L^F, Y = PF$_6$; [Ga(L^F)$_2$][PF$_6$]   (**1F**)

M = Ga, L = L^G, Y = NO$_3$; [Ga(L^G)$_2$][NO$_3$]   (**1G**)

M = Ga, L = L^H, Y = PF$_6$; [Ga(L^H)$_2$][PF$_6$]   (**1H**)

M = Fe, L = L^A, Y = NO$_3$; [Fe(L^A)$_2$][NO$_3$]   (**2A**)

M = Fe, L = L^B, Y = NO$_3$; [Fe(L^B)$_2$][NO$_3$]   (**2B**)

M = Fe, L = L^C, Y = NO$_3$; [Fe(L^C)$_2$][NO$_3$]   (**2C**)

M = Fe, L = L^D, Y = NO$_3$; [Fe(L^D)$_2$][NO$_3$]   (**2D**)

M = Fe, L = L^E, Y = PF$_6$; [Fe(L^E)$_2$][PF$_6$]   (**2E**)

M = Fe, L = L^F, Y = PF$_6$; [Fe(L^F)$_2$][PF$_6$]   (**2F**)

M = Fe, L = L^G, Y = NO$_3$; [Fe(L^G)$_2$][NO$_3$]   (**2G**)

M = Fe, L = L^H, Y = NO$_3$; [Fe(L^H)$_2$][NO$_3$]   (**2H**)

Scheme 1. Library of the synthesized compounds; underlined species were studied by X-ray crystallography.

Results and Discussion

Syntheses. The first reported synthesis of Triapine (**HL^D**) with an overall yield of 9% started from 2-chloro-3-nitropyridine, which was treated with sodium diethylmalonate, and then by 50% sulfuric acid to give 2-methyl-3-nitropyridine.[28] This was further oxidized with selenium dioxide to 3-nitropyridine-

2-carboxaldehyde. Protection of the aldehyde group of the latter by conversion into the cyclic ethylene

acetal and reduction of the nitro group by catalytic hydrogenation using Pd/C yielded 3-aminopyridine-

2-carboxaldehyde, which was finally subjected to condensation with thiosemicarbazide and deprotected

by concentrated HCl (Scheme S1, see Supporting Information). An improved five-step synthesis starting

from the same material, 2-chloro-3-nitropyridine, via a palladium-mediated Suzuki coupling in the first

step, afforded 2-methyl-3-nitropyridine, which was further converted into an enamine intermediate.

Oxidation of the latter with $NaIO_4$ led to 3-nitropyridine-2-carboxaldehyde, which was then reacted with

thiosemicarbazide. In the final step the nitro derivative was reduced with either $SnCl_2$ or Na_2S to yield

Triapine in an overall yield of 55% (Scheme S2).[29] The best overall yield of 64% was achieved in a

four-step synthesis. 3-Amino-2-chloropyridine was converted via a Heck reaction using styrene,

followed by protection of the NH_2 group and then ozonolysis to the desired carboxaldehyde. The latter

was transformed into Triapine by condensation with thiosemicarbazide and deprotection (Scheme S3).[30]

In this study, we developed a novel straightforward three-step synthesis of Triapine in 64% overall yield,

starting from the commercially available 3-amino-2-bromopyridine as shown in Scheme 2.
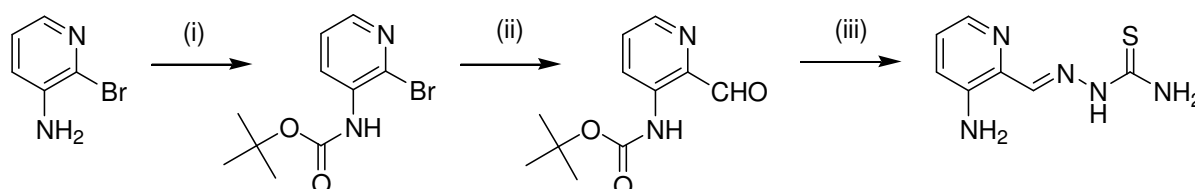
Scheme 2. Novel synthetic pathway to Triapine (**HL^D**). Reagents and conditions: (i) sodium bis(trimethylsilyl)amide (~1M/THF), (Boc)$_2$O, 82%; (ii) *n*-BuLi, *N*-formylpiperidine, 86%; (iii) thiosemicarbazide, conc. HCl, NaHCO$_3$, 91%; overall yield 64%.

In the first step the amino group was protected with di-*tert*-butyl dicarbonate in dry THF, using

sodium bis(trimethylsilyl)amide[31] as a base. Treatment of the *tert*-Boc protected 3-amino-2-

bromopyridine with *n*-BuLi in dry THF resulted in the lithiated species, which was further reacted with

N-formylpiperidine to give the carboxaldehyde.[32] Finally, the condensation reaction with

thiosemicarbazide in ethanol in the presence of concentrated HCl afforded Triapine hydrochloride,

which was converted into the free base (**HL^D**) by treatment with sodium bicarbonate.[29] The Triapine

analog 3-aminopyridine-2-carboxaldehyde ^{4}N-dimethylthiosemicarbazone (**HL^H**) was prepared in 84% yield by using the same protocol. However, the conversion into the free base was performed by treatment of the hydrochloride with excess *N*-methylmorpholine.

The gallium(III) complexes [Ga(L^A)$_2$]$^+$ (**1A**) and [Ga(L^D)$_2$]$^+$ (**1D**) were prepared by reaction of Ga(NO$_3$)$_3$·9H$_2$O with the corresponding ligand (**HL^A** or **HL^D**) in methanol in the presence of NaOCH$_3$ or triethylamine as a base in 27 and 72% yield, respectively (Scheme 1). The ^{1}H NMR spectra of these two complexes showed the presence of 0.5 and 0.15 equiv of methanol, correspondingly, in accord with the microanalytical data. Reaction of 2-acetylpyridine thiosemicarbazone (**HL^B**) and 2-pyridineformamide thiosemicarbazone (**HL^C**) with Ga(NO$_3$)$_3$·9H$_2$O in 2:1 molar ratio in ethanol in the absence of a base produced complexes **1B** and **1C** in 69 and 55% yield, respectively. The gallium complexes of the ligands **HL^E**–**HL^H** were prepared in methanol or ethanol and isolated as nitrates or in some cases as hexafluorophosphates (**HL^F** and **HL^H**) by addition of excess NH$_4$PF$_6$ to the reaction mixture (60–91% yield).[24] Starting from Fe(NO$_3$)$_3$·9H$_2$O and the ligands **HL^B** and **HL^D**–**HL^H** in methanol or ethanol, the iron(III) complexes were obtained in 66–76% yield (**2E** and **2F** were isolated as hexafluorophosphates).[24] The synthesis of the iron(III) complexes of **HL^A** and **HL^C** was carried out in the presence of *N*-methylmorpholine, because this was found to improve their purity.

Characterization. The positive ion ESI-mass spectra of all complexes showed very strong peaks due to [M(L)$_2$]$^+$ ions. A peak with *m/z* 145, attributed to [PF$_6$]$^-$, was registered in the negative ion mode for the hexafluorophosphates. In line with the UV–vis spectra of gallium(III) complexes of 2-acetylpyridine thiosemicarbazones,[24] **1A**–**1H** display a strong absorption band centered between 389–411 nm associated with intraligand transitions. This band is splitted and shifted to lower energies for **1D** (441 and 459sh nm) and **1H** (451 and 469 nm). In the case of iron(III) complexes, charge transfer bands, intraligand transitions, along with a d-d band centered between 829–977 nm attributed to the ^{2}T$_{2g}$ → ^{2}T$_{1g}$ transition for the d^5 low-spin system were observed.[33] The ^{1}H NMR spectrum of the ligand **HL^H** in DMSO-d_6 indicates the presence of only one isomeric form in solution. In contrast, two and three isomers were found for **HL^E** and **HL^F** in DMSO-d_6.[34,35] Interestingly, a second isomer with chemical

shifts at 9.18 (NH), 8.58 (py), 7.86 (py), 7.45 (py), 6.78 (NH$_2$) and 3.28 (N(CH$_3$)$_2$) ppm (one pyridine proton signal overlaps with a signal of the main species) and ~20% content relative to the main isomer was found for **HL^G** in DMSO-d_6, in contrast to the data reported.[36] The signal intensity of the minor species decreases with time, implying its conversion into the main isomeric form of the ligand. In contrast to the metal-free ligands, the gallium(III) complexes show only one set of signals in the ^{1}H NMR spectra, due to the stabilization of the ligand configuration upon coordination to the metal and the equivalence of both ligands bound to gallium(III) in solution. The most remarkable difference between the ^{1}H NMR spectra of the metal-free ligands and those of the gallium(III) complexes is the absence of the N–H proton signals of the thiosemicarbazide moiety in the latter, indicating deprotonation of the ligands upon coordination.

X-ray Crystallography. X-ray diffraction quality single crystals of Triapine (**HL^D**) were obtained by slow evaporation of the sodium bicarbonate neutralized mother liquor. The result of the X-ray diffraction study of **HL^D** is shown in Figure 1a, along with its gallium(III) (**1D**) and iron(III) (**2D**) complexes (Figures 1b and 1c). Selected bond distances and angels are quoted in the legend to Figure 1. Triapine crystallized in the orthorhombic space group P$na2_1$ with two crystallographically independent molecules in the asymmetric unit. Both adopt the *E*-isomeric form in terms of the nomenclature used for the conformations of α-N-heterocyclic thiosemicarbazones,[37] unlike to the X-ray crystal structure of **HL^E** with a *Z* conformation (see Supporting Information). In the gallium(III) and iron(III) complexes of Triapine (**1D** and **2D**) the coordination polyhedron approaches an octahedron, where the two ligands coordinate to the metal via the pyridine nitrogen atom and the nitrogen and sulfur donors of the thiosemicarbazide moiety. Deprotonation of both ligands is accompanied by an elongation of the carbon-sulfur bonds [**1D**: 1.735(6) and 1.743(7) Å; **2D**: 1.754(5) and 1.750(5) Å] as compared to that in the metal-free ligand **HL^D** at 1.697(2) Å.
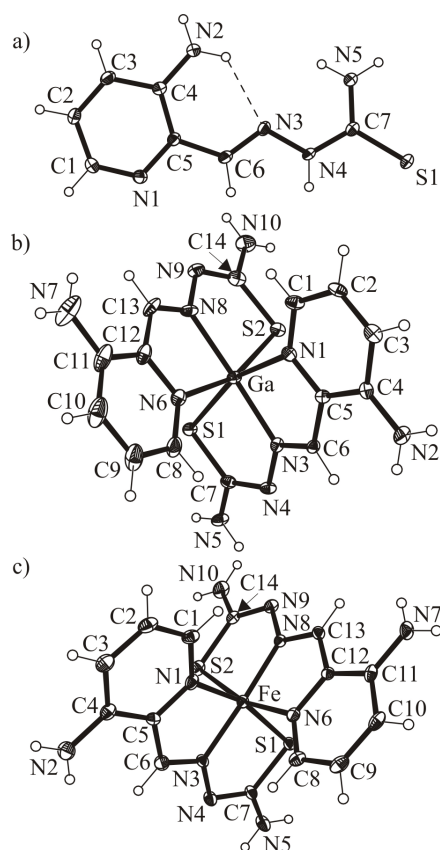
Figure 1. ORTEP plots of the Triapine (**HL^D**) (a), gallium(III) complex (**1D**) (b) and iron(III) complex (**2D**) (c) with atom numbering schemes. The thermal ellipsoids are drawn at 50 (**HL^D** and **2D**) and 30% (**1D**) probability levels, respectively. Selected bond lengths (Å) and bond angles (deg) for **HL^D**: C6−N3 1.283(2), N3−N4 1.384(2), N4−C7 1.344(2), C7−S1 1.697(2), C7−N5 1.325(3) Å; $\Theta_{(N2-C4-C5-C6)}$ 0.1(3), $\Theta_{(C5-C6-N3-N4)}$ 179.48(17), $\Theta_{(N3-N4-C7-S1)}$ 178.92(14)°. **1D**: Ga1−N1 2.130(4), Ga1−N6 2.110(5), Ga1−N3 2.034(4), Ga1−N8 2.040(5), Ga1−S1 2.3722(14), Ga1−S2 2.3563(16), C6−N3 1.301(6), C13−N8 1.279(7), N3−N4 1.362(6), N8−N9 1.379(7), N4−C7 1.339(7), N9−C14 1.332(8), C7−S1 1.735(6), C14−S2 1.743(7) Å; N1−Ga1−N3 77.77(17), N6−Ga1−N8 77.60(19), N3−Ga1−S1 82.56(12), N8−Ga1−S2 82.79(15)°. **2D**: Fe1−N1 1.995(4), Fe1−N6 2.011(4), Fe1−N3 1.922(4), Fe1−N8 1.925(4), Fe1−S1 2.2302(13), Fe1−S2 2.2171(14), C6−N3 1.299(6), C13−N8 1.299(6), N3−N4 1.379(5), N8−N9 1.379(5), N4−C7 1.318(6), N9−C14 1.323(6), C7−S1 1.754(5), C14−S2 1.750(5) Å; N1−Fe1−N3 80.85(17), N6−Fe1−N8 80.97(17), N3−Fe1−S1 83.92(12), N8−Fe1−S2 84.24(12)°.

Electrochemistry. In phase I and II clinical trials, patients treated with Triapine developed methemoglobinemia,[15,38] a disorder characterized by the presence of a higher than normal level of methemoglobin (metHb) in the blood. This side effect was ascribed to the redox activity of the iron complex of Triapine, although its electrochemical behavior was not studied. We investigated the electrochemical properties of all synthesized metal complexes by cyclic voltammetry, and the results are summarized in Table 1.

Table 1. Electrochemical Data[a] for **1A–1H** and **2A–2H**

Gallium complexes			
	$E_{1/2}$ / $^{I}L^{red}$	$E_{1/2}$ / $^{II}L^{red}$	E_p / $^{III}L^{red}$
1A	–0.82	–1.10	–1.63[b,c]
1B	–0.93	–1.21	–1.80[b,c]
1C	–1.21	–1.46	–2.02[b,c]
1D	–0.94	–1.23	–1.78[b,c]
1E	–0.80	–1.09	–1.67[b,c]
1F	–0.92	–1.21	–1.77[b,c]
1G	–1.21	–1.47	–2.02[b,c]
1H	–0.93	–1.22	–1.78[b,c]

Iron complexes			
	$E_{1/2}$ / $Fe^{III/II}$	$E_{1/2}$ / $^{I}L^{red}$	$E_{1/2}$ / $^{II}L^{red}$
2A	0.15	–1.44	–1.80[b]
2B	0.04	–1.58	–1.92[b]
2C	–0.21	–1.63	–2.02[b]
2D	0.01	–1.56	–1.92[b]
2E	0.18	–1.47	–1.78
2F	0.07	–1.60	–1.99[b,c]
2G	–0.22	–1.66	–2.04[b]
2H	0.03	–1.62	–1.92

a) Potentials in V ± 0.01 *vs*. NHE in 0.20 M [*n*-Bu$_4$N][BF$_4$]/DMSO; b) for the irreversible waves, the E$_p$ values are given; c) two electron wave.

In 0.20 M [*n*-Bu$_4$N][BF$_4$]/DMSO solution all iron complexes display a reversible Fe^{III}/Fe^{II} redox couple between –0.21 and +0.18 V *vs*. NHE (normal hydrogen electrode) depending on the ligand identity. A decrease of the redox potential in the order **2A > 2B > 2C** is in line with an increase of the electron donor properties of the corresponding ligands due to the presence of different substituents at the azomethine group (NH$_2$ > CH$_3$ > H). Likewise the electron donating properties of the amino group cause

the redox potential shift of the iron(III) complex of Triapine (**2D**) at 0.01 V as compared to the iron(III) complex of 2-formylpyridine thiosemicarbazone **2A** at +0.15 V *vs.* NHE. Compared to **2A–2D**, the reduction waves for the ^{4}N-dimethyl substituted analogs **2E–2H** are shifted by 10–30 mV to more positive potentials, in contrast to the expected negative shift because of the stronger electron donating properties of dimethylamine as compared to ammonia [pK_a: dimethylamine (10.73); ammonia (9.25)].[39] Beside the metal-centered reductions, the iron complexes display two ligand-centered reduction waves, the first (^{I}L$_{red}$) between –1.44 and –1.66 V (Figure 2) and the second (^{II}L$_{red}$) between –1.80 and –2.04 V *vs.* NHE close to the solvent cut-off. For the corresponding gallium(III) complexes **1A–1H** two reversible reductions (^{I}L$_{red}$ and ^{II}L$_{red}$) from –0.80 to –1.21 and from –1.09 to –1.47 V, correspondingly, and an irreversible two-electron reduction (^{III}L$_{red}$) between –1.63 and –2.02 V *vs.* NHE were observed. In comparison the ligand-centered redox couples ^{I}L$_{red}$ and ^{II}L$_{red}$ of the corresponding iron(III) complexes (which first are reduced to the iron(II) species) are negatively shifted by 400–700 mV. All the ligand-centered redox processes can be attributed to the reduction of the C=N double bond(s) adjacent to the pyridine ring[40] (supplementary data on the electrochemical behavior of the complexes in DMSO and CH$_3$CN can be found in Supporting Information).
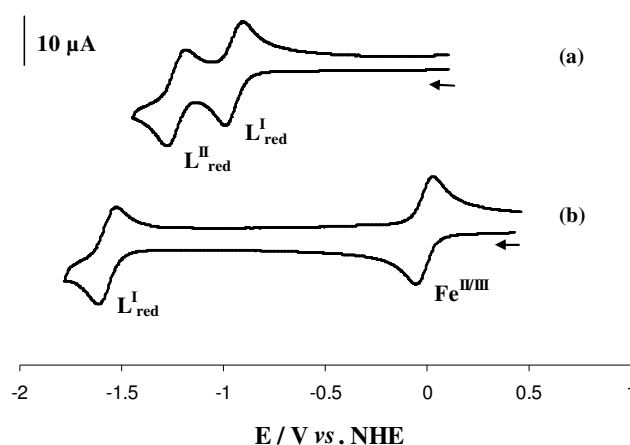

Figure 2. Cyclic voltammograms of complexes **1D** (a) and **2D** (b) in DMSO solution containing 0.20 M [*n*-Bu$_4$N][BF$_4$] at a scan rate of 0.20 V s^{-1} using a glassy carbon working electrode, displaying the ligand (L^{red}) and the Fe^{II}/Fe^{III} redox couple.

The influence of water on the iron redox potentials was studied by cyclic voltammetry measurements in H_2O/DMSO (7:3 v/v) mixtures with 0.2 M $NaClO_4$ as the supporting electrolyte. The low aqueous solubility of the complexes prevented the use of pure aqueous electrolyte solutions. The Fe^{III}/Fe^{II} redox couples remained reversible in H_2O/DMSO solution but were shifted by 10–50 mV to lower redox potentials. Unlike, complexes **2D** (Figure S1) and **2H** showed a positive shift by 30–40 mV.

Our data are in very good agreement with recently reported redox potentials for **2B** and **2F** in CH_3CN/H_2O (7:3) at 0.02 and 0.05 V vs NHE.[41] In cell-free assays Triapine was reported to enhance ascorbate oxidation, benzoate hydroxylation and quenching of purified RR tyrosyl radical in the presence of iron salts.[27] In addition, EPR measurements showed that the iron(II) complex of Triapine is capable of reducing O_2 to reactive oxygen species (ROS).[25] The potential range and the reversibility of the redox couple of the iron complex **2D** in H_2O/DMSO solution provide further evidence that the complex is able to undergo redox cycling and produce ROS under physiological conditions. This conclusion is also valid for the other iron complexes studied in this work, but probably to a lesser extent to complexes **2C** and **2G** with more negative potentials of the Fe^{III}/Fe^{II} redox couples at around –0.2 V vs. NHE.

Cytotoxicity. The cytotoxic potency of the thiosemicarbazones and their corresponding gallium(III) and iron(III) complexes was measured in the human tumor cell lines 41M (ovarian carcinoma) and SK-BR-3 (mammary carcinoma) by means of the colorimetric MTT assay. Generally, the 41M cells were more sensitive to the compounds investigated in this study. The metal-free ligands and the corresponding metal complexes cover a broad range of activity, with IC_{50} values ranging from nanomolar to high micromolar concentrations, depending on the ligand substitutions and the metal ion (Table 2).

Table 2. Cytotoxicity of α-N-heterocyclic thiosemicarbazones (**HL^A**–**HL^H**), their gallium(III) (**1A**–**1H**) and iron(III) complexes (**2A**–**2H**) in two human cancer cell lines.

| | IC$_{50}$ (μM)[a] | |
Compound	41M	SK-BR-3
Ligands		
HL^A	2.9 ± 0.6	3.2 ± 0.6
HL^B	2.5 ± 0.3	3.6 ± 0.2
HL^C	4.9 ± 0.04	5.6 ± 1.1
HL^D	0.45 ± 0.03	0.52 ± 0.08
HL^E	0.0040 ± 0.0009	0.0098 ± 0.0011
HL^G	0.32 ± 0.03	0.29 ± 0.01
HL^H	0.21 ± 0.13	0.29 ± 0.08
Ga(III) Complexes		
1A	1.5 ± 0.1	1.5 ± 0.5
1B	1.2 ± 0.1	1.0 ± 0.1
1C	3.4 ± 1.0	4.6 ± 1.1
1D	0.25 ± 0.05	0.35 ± 0.04
1E	0.0029 ± 0.0001	0.0050 ± 0.0009
1G	0.11 ± 0.05	0.12 ± 0.04
1H	0.020 ± 0.001	0.025 ± 0.004
Fe(III) Complexes		
2A	2.7 ± 0.5	4.9 ± 0.5
2B	28 ± 12	>100
2C	>100	>100
2D	1.5 ± 0.5	1.7 ± 0.4
2E	0.11 ± 0.04	0.15 ± 0.05
2G	1.6 ± 0.7	1.5 ± 0.4
2H	5.2 ± 0.2	6.0 ± 0.9
Ga(NO$_3$)$_3$[b]	70 ± 4	>100
Fe(NO$_3$)$_3$[b]	>100	>100

[a] 50% inhibitory concentrations in 41M and SK-BR-3 cells after exposure for 96 h in the MTT assay. Values are means ± standard deviations obtained from at least three independent experiments, [b] Values taken from reference 24.

Structure-Activity Relationships of the Metal-Free Ligands. Specific structural modifications on the ligand were made to explore the following structure-activity relationships:

(i) The effect of substituents at the carbon atom of the azomethine group. Substitution of the hydrogen atom in **HL^A** by a methyl group does not change the antiproliferative activity. However, the substitution of the hydrogen atom by a NH$_2$ group (**HL^C**) results in about 2-fold decrease of cytotoxicity in both cell lines.

The IC$_{50}$ values for the ligands **HL^A** and **HL^B** were documented in the literature.[42] These are very similar, varying from 1 to 10 μM, depending on the cell line. The first 2-pyridineformamide thiosemicarbazones were synthesized ten years ago with the aim of increasing aqueous solubility.[43] The first results on their cytotoxicity were reported only quite recently. In particular, **HL^C** tested in glioblastoma cell lines showed cytotoxicities in micromolar concentration range (3.6–7.3 μM).[44] In the case of Triapine (**HL^D**) the reported IC$_{50}$ values range from 0.2 to 3.0 μM.[27,45] However, because of the use of different cell lines and conditions, the impact of the structural changes in the ligands **HL^A**–**HL^D** (all containing a terminal NH$_2$ group) remained obscure. Our cytotoxicity data for both cell lines 41M and SK-BR-3 confirm that the antiproliferative activity of **HL^A** is very similar to that of **HL^B**, whereas **HL^C** possesses a slightly lower cytotoxic potency (Table 2). Interestingly, Triapine shows IC$_{50}$ values by a factor 10 lower than **HL^C**, indicating that the effect of the second amino group is dependent on its position.

(ii) Dimethylation of the terminal NH$_2$ group. Terminal dimethylation enhances the activity of the thiosemicarbazones. However, the magnitude of this effect is strongly dependent on the other ligand substitutions. The strongest enhancement was observed when comparing **HL^A** with its dimethylated counterpart **HL^E**. The ^{4}N-dimethylation results in a 725- (41M) and 320-fold (SK-BR-3) increase of cytotoxicity, respectively (Table 2, Figure 3). The same trend but with distinctly smaller differences was observed for the two ligands containing a 2-pyridinecarboxamide moiety (**HL^C** vs. **HL^G**), with an increase of cytotoxicity by a factor of 15–20 as a result of dimethylation. The effect was found to be weakest for Triapine and its dimethylated derivative (**HL^D** vs. **HL^H**). In this case only a 2-fold increase of cytotoxicity was observed.

(iii) The effect of an amino group in terminally dimethylated thiosemicarbazones. The cytotoxicity of the terminally dimethylated Triapine analogue **HL^H** is strongly diminished compared to that of **HL^E**, in which the amino group in position 3 of the pyridine heterocycle is absent. Thus, the addition of a NH$_2$ functionality to **HL^E** results in a 50- and 30-fold decrease of IC$_{50}$ values in 41M and SK-BR-3 cells, respectively. Likewise the presence of the NH$_2$ group at the carbon atom of the azomethine bond in **HL^G**

118

results in 30- to 80-fold decrease of cytotoxicity when compared to that of **HL^E**. Together these data suggest a critical role of the NH$_2$ group on the biological activity of terminally dimethylated α-N-heterocyclic thiosemicarbazones.

Thus, the most striking enhancement in cytotoxic activity (by a factor of ~300 to 700) was achieved by dimethylation of the terminal amino group of **HL^A**. A similar effect was observed when the terminal NH$_2$ group of 2-acetylpyridine thiosemicarbazone was disubstituted.[41,46] On the other hand, our results demonstrate that the enhancement of cytotoxic potency by ^{4}N-dimethylation is nearly annihilated when another NH$_2$ group is present (**HL^H**, **HL^G**). Hence, contrary to what has been assumed in the literature,[46] addition of the terminal methyl groups, while necessary, is not sufficient for the drastic enhancement in cytotoxic activity of this derivatives series. Removal of any NH$_2$ functionality is also needed.
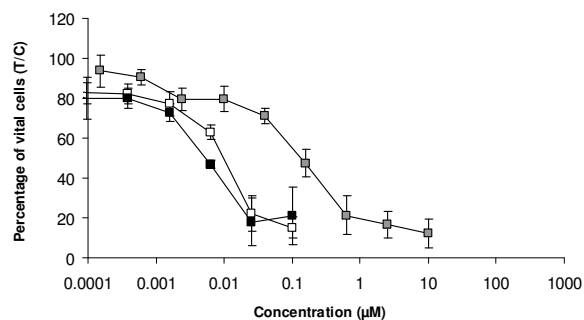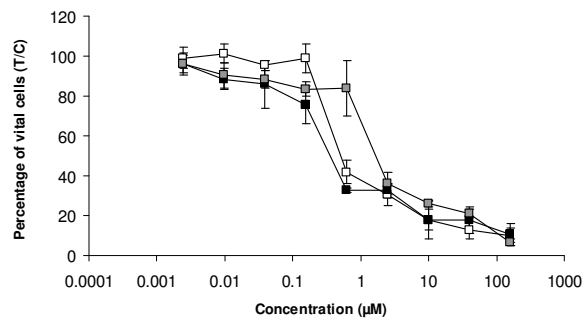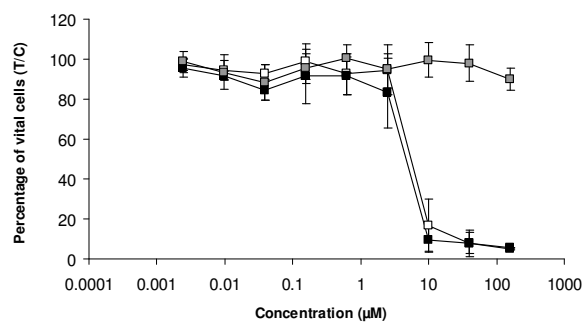
41M

SK-BR-3

A

B

C

D

E

Figure 3. Concentration-effect curves of metal-free thiosemicarbazones (white symbols), their gallium(III) complexes (black symbols) and iron(III) complexes (grey symbols), obtained by the MTT assay in 41M cells (left panels) and SK-BR-3 cells (right panels). (A) **HL^A**, **1A**, **2A**; (B) **HL^B**, **1B**, **2B**; (C) **HL^C**, **1C**, **2C**; (D) **HL^D**, **1D**, **2D** and (E) **HL^E**, **1E**, **2E**. Values are means ± standard deviations from at least three independent experiments.
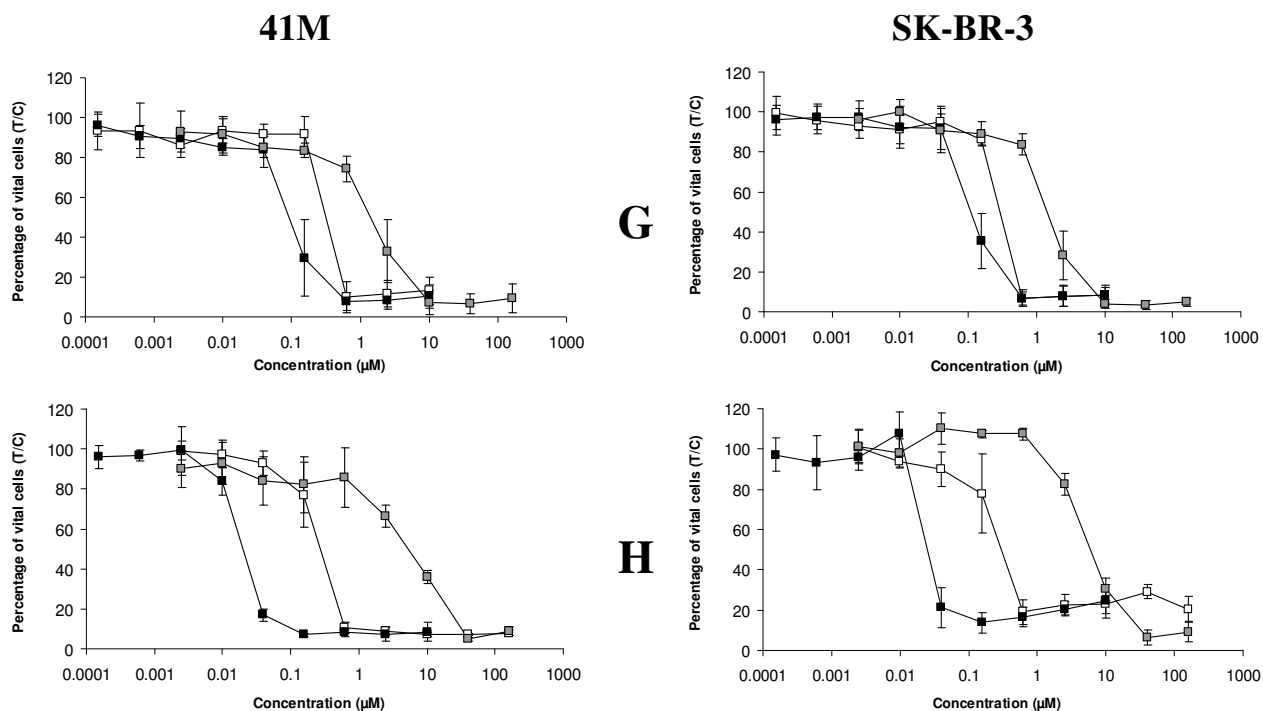
Figure 3 (continued). Concentration-effect curves of metal-free thiosemicarbazones (white symbols), their gallium(III) complexes (black symbols) and iron(III) complexes (grey symbols), obtained by the MTT assay in 41M cells (left panels) and SK-BR-3 cells (right panels). (G) **HL^G**, **1G**, **2G** and (H) **HL^H**, **1H**, **2H**. Values are means ± standard deviations from at least three independent experiments.

Structure-Activity Relationships of the Metal Complexes. The effects of complexation of thiosemicarbazones to gallium(III) and iron(III) are divergent (Table 2, Figure 3), and have been established by comparison of cytotoxicities of metal complexes and metal-free ligands. Generally, the iron(III) complexes show reduced cytotoxicity in comparison to that of the corresponding ligands. The effects vary from 3-fold to >28-fold increased IC$_{50}$ values. In contrast to the iron(III) complexes,

gallium(III) thiosemicarbazonates are 1.2 to 3.6 times more cytotoxic than the corresponding metal-free ligands. The effect is more pronounced only in the case of the gallium complex **1H**, which is 10 times more active than the corresponding uncomplexed ligand **HL^H**.

In all previous studies the effect of Triapine complexation to iron has been determined by simple addition of iron salt to a solution of Triapine, assuming the formation of the desired complex. However, the applied procedure does not guarantee its formation. Given the conditions for complexation reactions are provided, mixtures of complexes with different metal-to-ligand stoichiometries and various co-ligands can be produced. This might explain why the reported effects of Triapine complexation to iron are divergent. On the one hand, an enhancement in cytotoxic activity was observed in murine leukemia cells.[26] On the other hand, a slight decrease was found in neuroblastoma cells,[27] whereas no difference was discernible in neuroephithelioma cells.[47] No marked differences were found between the cytotoxic potencies of iron(II) and iron(III) complexes, presumably due to spontaneous oxidation of iron(II) to iron(III) in cell culture medium.[26,47] Generally, the reported influence of the complexation of Triapine to iron is moderate, in contrast to classic iron chelating agents such as DFO (desferrioxamine), which result in iron complexes that are almost devoid of antiproliferative activity.[47] It is generally assumed that the iron complex of Triapine is the active species. This is based on findings in cell-free assays showing that the iron(II) complex is able to react with dioxygen and generate reactive oxygen species (ROS) and that the preformed iron complex inhibits ribonucleotide reductase (RR) much more effectively than the metal-free ligand.[25]

In this study, the isolated iron(III) complex of Triapine (**2D**) is 3 times less cytotoxic in both cell lines than metal-free Triapine (**HL^D**). Interestingly, this decrease in activity upon complexation with iron(III) is smaller than in the case of **HL^B**, **HL^C** and **HL^E–HL^H**. Iron(III) complexes of these ligands are 5 to 30 times less cytotoxic than the uncomplexed ligands. Only complexation of **HL^A** to iron(III) did not result in a change in cytotoxicity. Taking into account the 1:2 stoichiometry of the iron-thiosemicarbazonate complexes, the decrease in activity is even more pronounced. However, there is no clear correlation

between the cytotoxic potencies of the iron(III) complexes and the uncomplexed ligands, suggesting that the binding strength to iron(III) or another factor has a modulating effect on cytotoxicity.

We have previously noted an enhancement of antiproliferative activity of gallium(III) complexes in comparison to their corresponding ligands.[24] In this study this trend is preserved, with about 2-fold increase of cytotoxic activity as compared to the respective metal-free ligands. One complex (**1H**), however, exhibits a ~10-fold enhancement of activity in both cell lines. These results suggest that the higher activity of the gallium(III) complexes is mainly due to the stoichiometric effect of the 1:2 gallium-to-ligand complexes.

Inhibition of Ribonucleotide Reductase. ^{3}H-cytidine DNA incorporation assays were performed in HL60 cells after 4 h drug incubation for **HL^D**, **HL^E**, **2D** and **2E** in order to ascertain whether the differences in cytotoxicity induced by coordination to iron(III) and/or by terminal dimethylation are related to different capacities of inhibiting RR. As shown in Table 3, the RR inhibitory potential follows the same trends as observed in the cytotoxicity tests, but in detail some differences are obvious. The cytotoxicity data show only a small increase in the IC$_{50}$ values after coordination of **HL^D** to iron(III) (**2D**), whereas in comparison the effect of coordination to iron(III) on RR inhibition is much more pronounced. The magnitudes of these effects are in reversed order for **HL^E** and **2E**. While the ability of **2E** to inhibit RR is only slightly decreased, the cytotoxicity of **2E** is reduced by a factor of 16 as compared to the metal-free ligand **HL^E**. Concerning the terminal dimethylation, a strong increase in cytotoxicity on going from **HL^D** to **HL^E** is not supported to the same extent by their ability to inhibit RR. Notably, in the IC$_{50}$ range even small increases in drug concentration of the metal-free ligands induce strong effects on RR activity (Figure 4). In contrast, the iron complexes show a gradual increase of RR inhibition over a broad drug concentration range.

Table 3. Comparison of the RR inhibitory potency and cytotoxicity of **HL^D**, **HL^E** and their iron(III) complexes **2D** and **2E** in HL60 cells.

Compound	IC$_{50}$ (μM)[a]			
	RR inhibition		cytotoxicity	
HL^D	5.4	± 2.4	0.27	± 0.06
2D	53	± 8.8	0.84	± 0.05
HL^E	0.80	± 0.13	0.0068	± 0.0022
2E	1.5	± 0.8	0.11	± 0.05

[a] 50% inhibitory concentrations in HL60 cells. RR inhibition was determined using ^{3}H-cytidine DNA incorporation assays after 4 h drug incubation. Cytotoxicity was determined after exposure for 96 h by the MTT assay. Values are means ± standard deviations from at least three independent experiments.
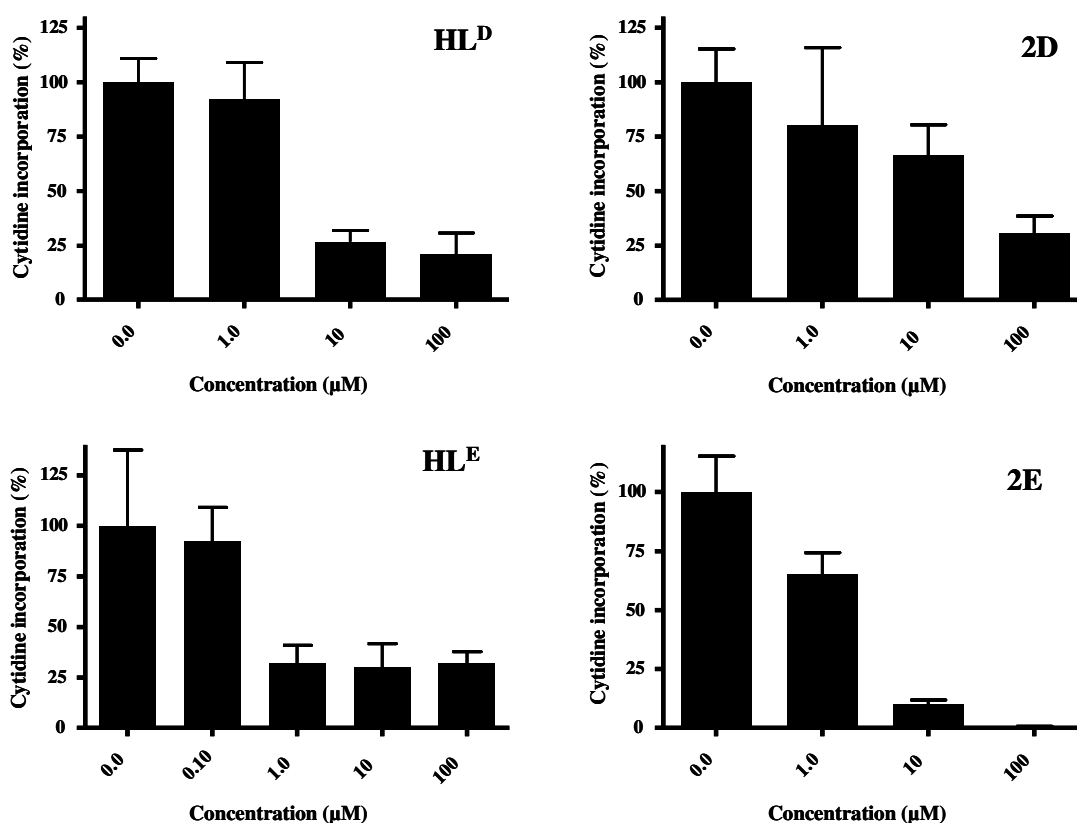
Figure 4. The ability of inhibiting ribonucleotide reductase for **HL^D**, **HL^E** and their iron(III) complexes **2D** and **2E** as determined by ^{3}H-cytidine DNA incorporation assays in HL60 cells.

It should be noted that the RR inhibitory potential of Triapine (**HL^D**) is well documented in the literature. In particular, in cell-free systems short-time treatment of purified prokaryotic or mouse RR by Triapine resulted in reduced ^{3}H-cytidine incorporation into DNA.[25,26] In line with these data, EPR measurements of intact SK-M-MC neuroepithelioma cells after their treatment with 25 μM Triapine for

24 h showed a 39% quenching of the tyrosyl radical.[27] To our knowledge the RR inhibitory activity of the iron(III) complex of Triapine (**2D**) was so far determined exclusively under reducing conditions in cell-free systems.[25,26] Pre-complexation of Triapine to iron was found to strongly enhance RR inhibition. This is in line with our previous report on enhanced tyrosyl radical quenching in isolated mouse R2 subunits by iron(III) [4]N-dimethylated thiosemicarbazonates.[24] In the present study, the ability of **HL^D**, **HL^E** and their iron(III) complexes to inhibit RR was determined in living cells. Here, iron(III) complexes show a reduced RR inhibiting activity as compared to the metal-free ligands – the difference being much more evident between **HL^D** and **2D**. The mechanisms underlying these effects are still not known. A possible explanation is the ionic nature and the reduced lipophilicity of the iron complex, which probably results in lower uptake into the cell. To clarify whether the differences observed between metal-free ligands and the respective iron complexes are based on reduced drug uptake or depend on other yet unknown mechanisms is a matter of ongoing investigations.

With regard to the impact of [4]N-disubstitution on the RR inhibitory potency, only some in vitro tests on 5-hydroxy-2-formylpyridine thiosemicarbazones using purified RR have been reported so far.[48] In contrast to our data in living cells, those studies showed that dimethylation of the terminal amino group markedly decreased the RR inhibitory activity. However, taking into account that different assays for determination of RR inhibitory potencies were performed and the fact that in the earlier study[48] no cytotoxicity data were reported, a direct comparison is not possible. Our data suggest that the enhancement in antiproliferative activity by terminal dimethylation can not be solely dependent on RR inhibition, and that other intracellular targets may be involved.

Conclusions

In this study we developed a novel straightforward three-step synthesis of Triapine, the most promising α-N-heterocyclic thiosemicarbazone for anticancer therapy today. In addition, iron(III) and gallium(III) complexes of Triapine were prepared for the first time. The synthesis of 2-formylpyridine, 2-

acetylpyridine, 2-pyridineformamide thiosemicarbazones and their [4]N-dimethylated analogs as well as the corresponding gallium(III) and iron(III) complexes permitted to establish novel structure-cytotoxicity relationships. In particular, they revealed an increase of cytotoxicity by complexation of Triapine and related ligands to gallium(III), while coordination to iron(III) reduces their activity. Terminal nitrogen dimethylation was found to strongly enhance the cytotoxicity of metal-free ligands as well as their iron(III) and gallium(III) complexes. This is, however, not the case, when a NH_2 functionality is present anywhere at the thiosemicarbazone backbone. ^{3}H-cytidine DNA incorporation assays showed that the increased cytotoxicity upon terminal dimethylation is only partly dependent on the ability of these compounds to inhibit RR, implying that other mechanisms are involved. Taken together, this study indicates the importance of detailed structure-activity-relationship analyses for the understanding of the molecular mechanisms underlying the anticancer activity of thiosemicarbazones and for the creation of more effective chemotherapeutics.

Experimental Section

All solvents and reagents were obtained from commercial suppliers and used without further purification. 2-Acetylpyridine [4]N-dimethylthiosemicarbazone (**HL^F**) and its gallium(III) (**1F**) and iron(III) complexes (**2F**) were prepared as previously reported.[24] 2-Formylpyridine thiosemicarbazone (**HL^A**) was synthesized by refluxing 2-formylpyridine with thiosemicarbazide in EtOH/H$_2$O 3 : 2 for 5 h, and 2-formylpyridine [4]N-dimethylthiosemicarbazone (**HL^E**) by refluxing 2-formylpyridine and [4]N-dimethylthiosemicarbazide[49] in MeOH for 5 h (X-ray diffraction quality crystals of **HL^E** were obtained by recrystallization from methanol). 2-Acetylpyridine thiosemicarbazone (**HL^B·0.5H₂O**) was obtained by refluxing 2-acetylypridine and thiosemicarbazide in EtOH for 5 h, followed by recrystallization in EtOH. The content of water was confirmed by thermogravimetric analysis. 2-Pyridineformamide thiosemicarbazone (**HL^C**) was prepared following the literature protocol.[50] 2-Pyridineformamide [4]N-dimethylthiosemicarbazone (**HL^G**) was synthesized in a similar manner by using [4]N-dimethylthiosemicarbazide instead of thiosemicarbazide, with a 76% yield, in comparison to 25%

reported in the literature.[36] *tert*-Butyl (2-formylpyridin-3-yl)carbamate was obtained using *tert*-butyl (2-bromopyridin-3-yl)carbamate (see below), *n*-butyllithium and *N*-formylpiperidine.[32] The condensation reaction with thiosemicarbazide and deprotection were performed according to the published procedure.[29] Elemental analyses were carried out on a Carlo Erba microanalyzer at the Microanalytical Laboratory of the University of Vienna. Electrospray ionization mass spectrometry was carried out with a Bruker Esquire 3000 instrument (Bruker Daltonic, Bremen, Germany). Expected and experimental isotope distributions were compared. Infrared spectra were obtained from KBr pellets with a Perkin-Elmer FT-IR 2000 instrument (4000–400 cm^{-1}). UV–vis spectra were recorded on a Perkin Elmer Lambda 650 UV–vis spectrophotometer using samples dissolved in methanol (900–210 nm). The iron(III) complexes were in addition measured on a Hewlett-Packard 8453 UV–vis spectrophotometer (1100–210 nm). The content of water in complexes **1C**, **2C** and **2D** was verified by thermogravimetric analysis (TGA) with a Mettler Toledo TGA/SDTA851e apparatus, with a 3 °C/min heating rate under an air atmosphere. ^{1}H and ^{13}C one- and two-dimensional NMR spectra were recorded in DMSO-d_6, with a Bruker Avance III 500 MHz FT-NMR spectrometer. The residual ^{1}H and ^{13}C present in DMSO-d_6 were used as internal references. Abbreviations for NMR data: py = pyridine, $C_{q, py}$ = quaternary carbon of pyridine.

Electrochemistry. Cyclic voltammograms were measured in a three-electrode cell using a 2.0 mm-diameter glassy carbon working electrode, a platinum auxiliary electrode, and an Ag|Ag$^+$ reference electrode containing 0.10 M AgNO$_3$. Measurements were performed at room temperature using an EG & G PARC 273A potentiostat/galvanostat. Deaeration of solutions was accomplished by passing a stream of argon through the solution for 5 min prior to the measurement and then maintaining a blanket atmosphere of argon over the solution during the measurement. The potentials were measured in 0.20 M [*n*-Bu$_4$N][BF$_4$]/DMSO, using [Fe(η^5-C$_5$H$_5$)$_2$] ($E_{\frac{1}{2}}$ = +0.68 V *vs*. NHE)[51] as internal standard, and are quoted relative to the normal hydrogen electrode (NHE). For cyclic voltammetry measurements in 0.20 M NaClO$_4$ DMSO/H$_2$O (3:7 v/v) solutions, a 2.0 mm-diameter glassy carbon working electrode, a platinum auxiliary electrode, and an Ag|Ag$^+$ reference electrode containing 3.0 M NaCl were used.

Synthesis of Ligands and Metal Complexes

***tert*-Butyl-(2-bromopyridin-3-yl)carbamate.** A solution of 3-amino-2-bromopyridine (3.0 g, 17.3 mmol) in dry THF (20 mL) was cooled to 0 °C and treated with 1M solution of sodium bis(trimethylsilyl)amide in THF (35 mL, 35 mmol). After 30 min a solution of di-*tert*-butyl dicarbonate (3.95 g, 18.1 mmol) in dry THF (20 mL) was added, and the mixture was stirred for 1.5 h at room temperature. The reaction mixture was poured into 0.1 M HCl (400 mL) and extracted twice with ethyl acetate (240 mL). The combined organic layers were extracted with brine (200 mL), dried over MgSO$_4$, filtered and evaporated under reduced pressure. The residue was purified by chromatography on silica using ethyl acetate/hexane 1:5 as eluent. Yield: 3.9 g (82%). Anal. Calcd. for C$_{10}$H$_{13}$N$_2$O$_2$Br (M_r = 273.13 g/mol): C, 43.98; H, 4.80; N, 10.26. Found: C, 44.01; H, 4.51; N, 10.21. ^{1}H NMR (500.10 MHz, DMSO-d_6): δ 8.77 (s, 1H, NH), 8.17 (dd, $^3J_{H,H}$ = 4.4 Hz, $^4J_{H,H}$ = 1.9 Hz, 1H, py), 7.92 (dd, $^3J_{H,H}$ = 7.9 Hz, $^4J_{H,H}$ = 1.9 Hz, 1H, py), 7.43 (dd, $^3J_{H,H}$ = 7.9 Hz, $^3J_{H,H}$ = 4.4 Hz, 1H, py), 1.47 (s, 9H, C(CH$_3$)$_3$). ^{13}C NMR (125.81 MHz, DMSO-d_6): δ 153.4 (C=O), 146.3 (C$_{py}$), 138.3 (C$_{q, py}$), 134.8 (C$_{q, py}$), 134.6 (C$_{py}$), 124.1 (C$_{py}$), 80.5 (*C*(CH$_3$)$_3$), 28.5 (C(*C*H$_3$)$_3$).

3-aminopyridine-2-carboxaldehyde ^{4}N-dimethylthiosemicarbazone, (HL^H). To *tert*-butyl (2-formylpyridin-3-yl)carbamate (147 mg, 0.66 mmol) and ^{4}N-dimethylthiosemicarbazide (79 mg, 0.66 mmol) in ethanol (3 mL) and H$_2$O (1 mL) was added conc. HCl (0.3 mL) and the mixture was stirred under reflux for 5 h. After cooling to room temperature 10% (w/w) aqueous NaHCO$_3$ (0.8 mL) was added and the mixture was stirred for further 30 min. The yellow hygroscopic HL^H·HCl was filtered off, washed with cold water, cold ethanol (–20 °C) and diethyl ether and dried *in vacuo*. Yield: 130 mg (76%). ^{1}H NMR (500.10 MHz, DMSO-d_6): δ 12.00 (s, 1H, NH), 8.88 (s, 1H, HC=N), 8.15 (br. s, 2H, NH$_2$), 8.03 (m, 1H, py), 7.69 (d, $^3J_{H,H}$ = 8.2 Hz, 1H, py), 7.57 (m, 1H, py), 3.35 (s, 6H, N(CH$_3$)$_2$). The HL^H·HCl salt (90 mg, 0.35 mmol) was dissolved in H$_2$O (4 mL) at 70 °C and *N*-methylmorpholine (60 μL, 0.55 mmol) was added. The reaction mixture was cooled to room temperature and stirred for 1 h.

The precipitate was filtered off, washed with H_2O, cold ethanol (–20 °C) and diethyl ether, dried *in vacuo* and afterwards over P_2O_5. Yield: 65 mg (84%). Anal. Calcd. for $C_9H_{13}N_5S$ (M_r = 223.30 g/mol): C, 48.41; H, 5.87; N, 31.36; S, 14.36. Found: C, 48.30; H, 5.96; N, 31.18; S, 14.19. ESI-MS in MeOH (negative): *m/z* 222, [HL^H–H]$^-$. IR spectrum in KBr, cm^{-1} (selected bands): 3304 s, 3140s, 1622 s, 1546 s, 1442 s, 1312 s, 1210 s, 1129 m, 1059 m, 910 s, 795 m, 710 m. UV–vis (MeOH), λ_{max}, nm (ε, M^{-1} cm^{-1}): 232 (21180), 262 (16160), 369 (14020), 436 (1920). ^{1}H NMR (500.10 MHz, DMSO-d_6): δ 11.09 (s, 1H, NH), 8.55 (s, 1H, HC=N), 7.83 (dd, $^3J_{H,H}$ = 4.1 Hz, $^4J_{H,H}$ = 1.6 Hz, 1H, py), 7.20 (br. s, 2H, NH$_2$), 7.09 (dd, $^3J_{H,H}$ = 8.2 Hz, $^4J_{H,H}$ = 1.6 Hz, 1H, py), 7.06 (dd, $^3J_{H,H}$ = 8.2 Hz, $^3J_{H,H}$ = 4.1 Hz, 1H, py), 3.31 (s, 6H, N(CH$_3$)$_2$).^{13}C NMR (125.81 MHz, DMSO-d_6): δ 180.0 (C=S), 149.1 (HC=N), 144.1 (C$_{q, py}$), 137.0 (C$_{py}$), 134.4 (C$_{q, py}$), 124.3 (C$_{py}$), 122.3 (C$_{py}$), 41.4 (N(CH$_3$)$_2$).

[Bis(2-formylpyridine thiosemicarbazonato)-*N,N,S*-gallium(III)] nitrate, [Ga(L^A)$_2$]NO$_3$·0.5CH$_3$OH (1A). To 2-formylpyridine thiosemicarbazone (**HL^A**) (140 mg, 0.78 mmol) and NaOCH$_3$ (63 mg, 1.17 mmol) in dry methanol (14 mL) at 70 °C under an argon atmosphere gallium(III) nitrate nonahydrate (162 mg, 0.39 mmol) was added and the mixture was stirred at 70 °C for 3 h, then cooled to room temperature and filtered from undissolved impurities. The clear solution was allowed to stand at +4 °C for 3 days and the crystals formed were filtered off, washed with cold methanol (–20 °C) and dried *in vacuo*. Yield: 54 mg (27%). Anal. Calcd. for $C_{14}H_{14}GaN_9O_3S_2$·0.5CH$_3$OH (M_r = 506.20 g/mol): C, 34.41; H, 3.19; N, 24.90. Found: C, 34.45; H, 3.33; N, 24.63. ESI-MS in MeOH (positive): *m/z* 427, [Ga(L^A)$_2$]$^+$. IR spectrum in KBr, cm^{-1} (selected bands): 3422 w, 3280 w, 3100 br. s, 1607 s, 1429 s, 1384 m, 1314 m, 1234 m, 1174 s, 880 m, 735 m, 628 m. UV–vis (MeOH), λ_{max}, nm (ε, M^{-1} cm^{-1}): 318 (24390), 395 (22240). ^{1}H NMR (500.10 MHz, DMSO-d_6): δ 8.95 (s, 2H, HC=N), 8.26 (br. s, 4H, NH$_2$), 8.20 (dt, $^3J_{H,H}$ = 7.9 Hz, $^4J_{H,H}$ = 1.6 Hz, 2H, py), 7.98 (m, 4H, py), 7.58 (m, 2H, py). ^{13}C NMR (125.81 MHz, DMSO-d_6): δ 178.6 (C–S), 145.2 (C$_q$, py), 144.9 (C$_{py}$), 142.7 (C$_{py}$), 137.8 (HC=N), 127.6 (C$_{py}$), 126.5 (C$_{py}$).

[Bis(2-acetylpyridine thiosemicarbazonato)-*N,N,S*-gallium(III)] nitrate, [Ga(L^B)$_2$]NO$_3$ (1B). To 2-acetylpyridine thiosemicarbazone (**HL^B**) (200 mg, 1.03 mmol) in ethanol (5 mL) at 70 °C gallium(III) nitrate nonahydrate (217 mg, 0.52 mmol) in ethanol (2 mL) was added and the solution was stirred at 50 °C for 2 h. The reaction mixture was cooled to room temperature and allowed to stand at +4 °C for 4 h. The yellow precipitate was filtered off, washed with cold ethanol (–20 °C) and diethyl ether, and dried *in vacuo.* Yield: 185 mg (69%). Anal. Calcd. for C$_{16}$H$_{18}$GaN$_9$O$_3$S$_2$ (M_r = 518.23 g/mol): C, 37.08; H, 3.50; N, 24.33; S, 12.38. Found: C, 37.09; H, 3.42; N, 24.28; S, 12.35. ESI-MS in MeOH (positive): *m/z* 455, [Ga(L^B)$_2$]$^+$. IR spectrum in KBr, cm^{-1} (selected bands): 3386 w, 3260 w, 3158 m, 1601 s, 1432 s, 1373 s, 1294 m, 1188 m, 810 m, 778 m, 720 m. UV–vis (MeOH), λ$_{max}$, nm (ε, M^{-1} cm^{-1}): 295 (20200), 392 (28740). ^{1}H NMR (500.10 MHz, DMSO-*d$_6$*): δ 8.26–8.20 (m, 4H, py), 8.01 (br. s, 4H, NH$_2$), 7.93 (m, 2H, py), 7.60 (m, 2H, py), 2.81 (s, 6H, CH$_3$). ^{13}C NMR (125.81 MHz, DMSO-*d$_6$*): δ 176.8 (C–S), 146.7 (C=N), 145.7 (C$_{q, py}$), 144.7 (C$_{py}$), 142.7 (C$_{py}$), 127.5 (C$_{py}$), 124.3 (C$_{py}$), 14.7 (CH$_3$).

[Bis(2-pyridineformamide thiosemicarbazonato)-*N,N,S*-gallium(III)] nitrate, [Ga(L^C)$_2$]NO$_3$·0.5H$_2$O (1C). To 2-pyridineformamide thiosemicarbazone (**HL^C**) (200 mg, 1.02 mmol) in ethanol (20 mL) at 70 °C gallium(III) nitrate nonahydrate (214 mg, 0.51 mmol) in ethanol (2.5 mL) was added and the mixture was stirred at the same temperature for 1 h. The yellow solid was separated from the hot solution by filtration, washed with ethanol, dried *in vacuo* at 50 °C and then over P$_2$O$_5$. Yield: 148 mg (55%). Anal. Calcd. for C$_{14}$H$_{16}$GaN$_{11}$O$_3$S$_2$·0.5H$_2$O (M_r = 529.21 g/mol): C, 31.77; H, 3.24; N, 29.11; S, 12.12. Found: C, 31.79; H, 3.17; N, 28.75; S, 12.19. ESI-MS in MeOH (positive): *m/z* 457, [Ga(L^C)$_2$]$^+$. ESI-MS in MeOH (negative): *m/z* 455, [Ga(L^C)$_2$ – 2H]$^-$. IR spectrum in KBr, cm^{-1} (selected bands): 3271 br. m, 3163 w, 1648 s, 1605 s, 1515 s, 1470 s, 1384 m, 787 m, 727 m. UV–vis (MeOH), λ$_{max}$, nm (ε, M^{-1} cm^{-1}): 257 (18410), 300 (10820), 389 (17600). ^{1}H NMR (500.10 MHz, DMSO-*d$_6$*): δ 8.43 (d, $^3J_{H,H}$ = 8.2 Hz, 2H, py), 8.27 (dt, $^3J_{H,H}$ = 7.9 Hz, $^4J_{H,H}$ = 1.6 Hz, 2H, py), 8.06 (v. br. s, 4H, N=CNH$_2$), 7.88 (m, 2H, py), 7.71 (m, 2H, py), 6.65 (s, 4H, NH$_2$). ^{13}C NMR (125.81 MHz, DMSO-*d$_6$*): δ 169.4 (C–S), 145.5 (C=N), 144.7 (C$_{py}$), 142.4 (C$_{py}$), 141.6 (C$_{q, py}$), 128.4 (C$_{py}$), 122.1 (C$_{py}$).

[Bis(3-aminopyridine-2-carboxaldehyde thiosemicarbazonato)-*N,N,S*-gallium(III)] nitrate, [Ga(L^D)$_2$]NO$_3$·0.15CH$_3$OH (1D). To a suspension of 3-aminopyridine-2-carboxaldehyde thiosemicarbazone (**HL^D**) (150 mg, 0.77 mmol) in methanol (10 mL) and triethylamine (112 µL, 0.81 mmol) at 50 °C gallium(III) nitrate nonahydrate (166 mg, 0.40 mmol) in methanol (2.5 mL) was added and the mixture was stirred for 20 min at 50 °C and 2.5 h at room temperature. The bright orange precipitate formed was filtered off, washed with cold methanol (–20 °C), dried *in vacuo* and afterwards over P$_2$O$_5$. Yield: 144 mg (72%). Anal. Calcd. for C$_{14}$H$_{16}$GaN$_{11}$O$_3$S$_2$·0.15CH$_3$OH (M_r = 525.01 g/mol): C, 32.37; H, 3.19; N, 29.34; S, 12.22. Found: C, 32.39; H, 3.25; N, 29.13; S, 12.14. ESI-MS in MeOH (positive): *m/z* 457, [Ga(L^D)$_2$]$^+$. ESI-MS in MeOH (negative): *m/z* 455, [Ga(L^D)$_2$ – 2H]$^-$. IR spectrum in KBr, cm^{-1} (selected bands): 3336 s, 3217 s, 1600 s, 1467 s, 1429 s, 1384 m, 1252 m, 1220 m, 1146 s, 849 m, 805 m, 630 s. UV–vis (MeOH), λ_{max}, nm (ε, M^{-1} cm^{-1}): 214sh (42410), 294 (31980), 441 (38830), 459sh (35600). ^{1}H NMR (500.10 MHz, DMSO-d_6): δ 9.14 (s, 2H, HC=N), 7.83 (br. s, 4H, SCNH$_2$), 7.31–7.24 (m, 4H, py), 7.13 (d, $^3J_{H,H}$ = 4.7 Hz, 2H, py), 6.71 (br. s, 4H, NH$_2$). ^{13}C NMR (125.81 MHz, DMSO-d_6): δ 177.1 (C–S), 145.9 (C$_{q, py}$), 135.5 (HC=N), 132.9 (C$_{py}$), 128.1 (C$_{py}$), 127.6 (C$_{q, py}$), 127.3 (C$_{py}$). Crystals suitable for X-ray data collection were obtained by slow evaporation of an ethanolic solution of **1D**.

[Bis(2-formylpyridine ^{4}N-dimethylthiosemicarbazonato)-*N,N,S*-gallium(III)] hexafluorophosphate, [Ga(L^E)$_2$]PF$_6$ (1E). To 2-formylpyridine ^{4}N-dimethylthiosemicarbazone (**HL^E**) (87 mg, 0.42 mmol) in methanol (6 mL) at 40 °C gallium(III) nitrate nonahydrate (87 mg, 0.21 mmol) in methanol (2 mL) was added and the mixture was stirred at room temperature for 3 h. Addition of ammonium hexafluorophosphate (100 mg, 0.61 mmol) to the reaction mixture led to the formation of a yellow solid which was filtered off washed with methanol and dried *in vacuo*. Yield: 92 mg (70%). Anal. Calcd. for C$_{18}$H$_{22}$F$_6$GaN$_8$PS$_2$ (M_r = 629.24 g/mol): C, 34.36; H, 3.52; N, 17.81; S, 10.19. Found: C, 34.18; H, 3.49; N, 17.54; S, 10.23. ESI-MS in MeOH (positive): *m/z* 483, [Ga(L^E)$_2$]$^+$. ESI-MS in MeOH (negative): *m/z* 145, [PF$_6$]$^-$. IR spectrum in KBr, cm^{-1} (selected bands): 1607 m, 1514 s, 1368 s, 1316 m, 1249 s, 1217 m, 1138 s, 914 m, 837 vs, 557 m. UV–vis (MeOH), λ_{max}, nm (ε, M^{-1} cm^{-1}): 252sh

(11190), 301 (17690), 411 (46240). ^{1}H NMR (500.10 MHz, DMSO-d_6): δ 9.04 (s, 2H, HC=N), 8.20 (dt,

$^3J_{H,H}$ = 7.9 Hz, $^4J_{H,H}$ = 1.6 Hz, 2H, py), 7.99 (m, 4H, py), 7.56 (m, 2H, py), 3.30 and 3.23 (br. s, 12H,

N(CH$_3$)$_2$). ^{13}C NMR (125.81 MHz, DMSO-d_6): δ 177.4 (C–S), 145.3 (C$_{q,\ py}$), 145.0 (C$_{py}$), 142.8 (C$_{py}$),

138.2 (HC=N), 127.6 (C$_{py}$), 126.4 (C$_{py}$), 41.3 and 38.8 (N(CH$_3$)$_2$).

[Bis(2-pyridineformamide ^{4}**N-dimethylthiosemicarbazonato)-*N,N,S*-gallium(III)]** **nitrate,**
[Ga(L^G)$_2$]NO$_3$ (1G). To 2-pyridineformamide ^{4}N-dimethylthiosemicarbazone (**HL^G**) (400 mg, 1.79

mmol) in ethanol (20 mL) at 70 °C gallium(III) nitrate nonahydrate (375 mg, 0.90 mmol) in ethanol (5

mL) was added and the mixture was stirred at the same temperature for 2 h. The yellow-orange solid

was separated from the hot solution by filtration, washed with ethanol and dried *in vacuo*. Yield: 380 mg

(74%). Anal. Calcd. for C$_{18}$H$_{24}$GaN$_{11}$O$_3$S$_2$ (M_r = 576.31 g/mol): C, 37.51; H, 4.20; N, 26.73; S, 11.13.

Found: C, 37.47; H, 4.14; N, 26.34; S, 11.19. ESI-MS in MeOH (positive): *m/z* 513, [Ga(L^G)$_2$]$^+$. ESI-

MS in MeOH (negative): *m/z* 511, [Ga(L^G)$_2$ – 2H]$^-$. IR spectrum in KBr, cm^{-1} (selected bands): 1644 s,

1522 s, 1487 m, 1362 br. s, 913 m, 788 m. UV–vis (MeOH), λ$_{max}$, nm (ε, M^{-1} cm^{-1}): 260 (21800), 324

(11900), 409 (22640). ^{1}H NMR (500.10 MHz, DMSO-d_6): δ 8.45 (d, $^3J_{H,H}$ = 8.2 Hz, 2H, py), 8.27 (dt,

$^3J_{H,H}$ = 7.9 Hz, $^4J_{H,H}$ = 1.5 Hz, 2H, py), 8.15 (v. br. s, 4H, NH$_2$), 7.84 (m, 2H, py), 7.69 (m, 2H, py), 3.15

(s, 12H, N(CH$_3$)$_2$). ^{13}C NMR (125.81 MHz, DMSO-d_6): δ 169.7 (C–S), 145.6 (C=N), 144.7 (C$_{py}$), 142.4

(C$_{py}$), 141.7 (C$_{q,\ py}$), 128.3 (C$_{py}$), 122.1 (C$_{py}$), 39.3 (N(CH$_3$)$_2$).

[Bis(3-aminopyridine-2-carboxaldehyde ^{4}**N-dimethylthiosemicarbazonato)-*N,N,S*-gallium(III)]**
hexafluorophosphate, [Ga(L^H)$_2$]PF$_6$ (1H). To a suspension of 3-aminopyridine-2-carboxaldehyde ^{4}N-

dimethylthiosemicarbazone hydrochloride (**HL^H·HCl**) (150 mg, 0.58 mmol) in ethanol (15 mL)

gallium(III) nitrate nonahydrate (130 mg, 0.31 mmol) in ethanol (3 mL) was added and the mixture was

stirred for 1.5 h at room temperature. Subsequently a solution of ammonium hexafluorophosphate (200

mg, 1.23 mmol) in ethanol (2 mL) was added. After 2 h the orange precipitate was filtered off, washed

with cold ethanol (–20 °C) and dried *in vacuo*. Yield: 114 mg (60%). Anal. Calcd. for

C$_{18}$H$_{24}$F$_6$GaN$_{10}$PS$_2$ (M_r = 659.27 g/mol): C, 32.79; H, 3.67; N, 21.25; S, 9.73. Found: C, 33.02; H, 3.83;

N, 21.14; S, 9.70. ESI-MS in MeOH (positive): *m/z* 513, [Ga(L^H)$_2$]$^+$. ESI-MS in MeOH (negative): *m/z*

145, [PF$_6$]$^-$. IR spectrum in KBr, cm^{-1} (selected bands): 3488 w, 3439 w, 3400 m, 3337 w, 1645 m, 1511 s, 1471 s, 1380 s, 1322 s, 1256 s, 1124 s, 913 m, 845 vs, 557 m. UV–vis (MeOH), λ_{max}, nm (ε, M^{-1} cm^{-1}): 226 (28950), 301 (24070), 349sh (6860), 451 (44050), 469 (42720). ^{1}H NMR (500.10 MHz, DMSO-d_6): δ 9.29 (s, 2H, HC=N), 7.29 (dd, $^3J_{H,H}$ = 8.5 Hz, $^4J_{H,H}$ = 1.3 Hz, 2H, py) 7.24 (dd, $^3J_{H,H}$ = 8.5 Hz, $^3J_{H,H}$ = 4.7 Hz, 2H, py), 7.15 (d, $^3J_{H,H}$ = 4.4 Hz, 2H, py), 6.71 (br. s, 4H, NH$_2$), 3.21 (s, 12H, N(CH$_3$)$_2$). ^{13}C NMR (125.81 MHz, DMSO-d_6): δ 176.2 (C–S), 145.9 (C$_{q, py}$), 136.1 (HC=N), 132.9 (C$_{py}$), 128.1 (C$_{py}$), 127.6 (C$_{q, py}$), 127.3 (C$_{py}$), 40.9 and 38.6 (N(CH$_3$)$_2$).

[Bis(2-formylpyridine thiosemicarbazonato)-*N*,*N*,*S*-iron(III)] nitrate, [Fe(L^A)$_2$]NO$_3$ (2A). To 2-formylpyridine thiosemicarbazone (**HL^A**) (200 mg, 1.11 mmol) and *N*-methylmorpholine (120 µL, 1.09 mmol) in methanol (20 mL) at 70 °C iron(III) nitrate nonahydrate (222 mg, 0.55 mmol) in methanol (2 mL) was added dropwise and the reaction mixture was stirred for 3 h at 70 °C. After cooling to room temperature ca. 1/2 of the solvent was removed under reduced pressure and the reaction mixture was allowed to stand at +4 °C overnight. The black crystalline product was filtered off, washed with cold methanol, dried *in vacuo* and afterwards over P$_2$O$_5$. Yield: 195 mg (74%). Anal. Calcd. for C$_{14}$H$_{14}$FeN$_9$O$_3$S$_2$ (M_r = 476.30 g/mol): C, 35.30; H, 2.96; N, 26.47; S, 13.47. Found: C, 35.21; H, 2.91; N, 26.34; S, 13.38. ESI-MS in MeOH (positive): *m/z* 414, [Fe(L^A)$_2$]$^+$. IR spectrum in KBr, cm^{-1} (selected bands): 3295 s, 3100 br. s, 1645 m, 1616 s, 1603 s, 1456 s, 1435 s, 1384 s, 1292 m, 1154 s, 863 m, 767 m, 725 m, 620 m. UV–vis (MeOH), λ_{max}, nm (ε, M^{-1} cm^{-1}): 240sh (29610), 295 (20470), 312sh (20400), 352 (19560), 417sh (11200), 462sh (7220) 585sh (540), 882 (550).

[Bis(2-acetylpyridine thiosemicarbazonato)-*N*,*N*,*S*-iron(III)] nitrate, [Fe(L^B)$_2$]NO$_3$ (2B). To 2-acetylpyridine thiosemicarbazone (**HL^B**) (200 mg, 1.03 mmol) in methanol (10 mL) at room temperature iron(III) nitrate nonahydrate (208 mg, 0.51 mmol) in methanol (2 mL) was added dropwise and the reaction mixture was stirred for 3 h. The black product formed was filtered off, washed with methanol, dried *in vacuo* and then over P$_2$O$_5$. Yield: 198 mg (74%). Anal. Calcd. for C$_{16}$H$_{18}$FeN$_9$O$_3$S$_2$ (M_r = 504.35 g/mol): C, 38.10; H, 3.60; N, 24.99; S, 12.72. Found: C, 38.14; H, 3.56; N, 24.82; S, 12.83. ESI-MS in

MeOH (positive): m/z 442, $[Fe(L^B)_2]^+$. IR spectrum in KBr, cm^{-1} (selected bands): 3272 m, 3108 br. s, 1638 m, 1598 s, 1497 m, 1446 s, 1384 s, 1170 m, 767 m. UV–vis (MeOH), λ_{max}, nm (ε, M^{-1} cm^{-1}): 242sh (31940), 299 (22870), 319 (22700), 354 (18900), 412 (11930), 456sh (8950), 578sh (540), 865 (670).

[Bis(2-pyridineformamide thiosemicarbazonato)-*N,N,S*-iron(III)] nitrate, [Fe(L^C)$_2$]NO$_3$·1.5H$_2$O (2C). To 2-pyridineformamide thiosemicarbazone (**HL^C**) (200 mg, 1.02 mmol) and *N*-methylmorpholine (111 µL, 1.01 mmol) in methanol (10 mL) at 50 °C iron(III) nitrate nonahydrate (205 mg, 0.51 mmol) in methanol (2 mL) was added and the mixture was stirred at 50 °C for 2 h. After cooling to room temperature ca. 1/2 of the solvent was removed under reduced pressure and the reaction mixture was allowed to stand at +4 °C overnight. The black crystals were filtered off, washed with cold methanol and dried *in vacuo*. Yield: 213 mg (78%). Anal. Calcd. for C$_{14}$H$_{16}$FeN$_{11}$O$_3$S$_2$·1.5H$_2$O (M_r = 533.35 g/mol): C, 31.53; H, 3.59; N, 28.89; S, 12.02. Found: C, 31.42; H, 3.35; N, 28.69; S, 11.85. ESI-MS in MeOH (positive): m/z 444, $[Fe(L^C)_2]^+$. IR spectrum in KBr, cm^{-1} (selected bands): 3279 s, 3161 s, 1622 br. s, 1550 m, 1515 m, 1463 s, 1384 s, 1193 m, 784 m. UV–vis (MeOH), λ_{max}, nm (ε, M^{-1} cm^{-1}): 245sh (33110), 299 (15250), 355sh (11730), 460 (10280), 829 (990).

[Bis(3-aminopyridine-2-carboxaldehyde thiosemicarbazonato)-*N,N,S*-iron(III)] nitrate, [Fe(L^D)$_2$]NO$_3$·H$_2$O (2D). To a suspension of 3-aminopyridine-2-carboxaldehyde thiosemicarbazone (**HL^D**) (150 mg, 0.77 mmol) in ethanol (24 mL) at 50 °C iron(III) nitrate nonahydrate (157 mg, 0.39 mmol) in ethanol (2 mL) was added dropwise and the mixture was stirred for 10 min at 50 °C and 3 h at room temperature. The black-green precipitate was filtered off, washed with cold ethanol (–20 °C) and diethyl ether, dried *in vacuo* and afterwards over P$_2$O$_5$. Yield: 132 mg (66%). Anal. Calcd. for C$_{14}$H$_{16}$FeN$_{11}$O$_3$S$_2$·H$_2$O (M_r = 524.34 g/mol): C, 32.07; H, 3.46; N, 29.38; S, 12.23. Found: C, 32.34; H, 3.18; N, 29.51; S, 12.48. ESI-MS in MeOH (positive): m/z 444, $[Fe(L^D)_2]^+$. IR spectrum in KBr, cm^{-1} (selected bands): 3298 m, 3149 br. m, 1629 s, 1583 s, 1469 s, 1439 s, 1384 m, 1272 s, 1245 m, 1140 s, 794 m, 631 m. UV–vis (MeOH), λ_{max}, nm (ε, M^{-1} cm^{-1}): 267 (26320), 303 (25340), 410sh (19655), 441

(21530), 483sh (15960), 606 (840), 912 (490). Crystals suitable for X-ray data collection were obtained by slow evaporation of a methanolic solution of **2D**.

[Bis(2-formylpyridine ^{4}N-dimethylthiosemicarbazonato)-*N,N,S*-iron(III)] hexafluorophosphate, [Fe(L^E)$_2$]PF$_6$ (2E). To 2-formylpyridine ^{4}N-dimethylthiosemicarbazone (**HL^E**) (70 mg, 0.34 mmol) dissolved in ethanol (7 mL) at 40 °C iron(III) nitrate nonahydrate (68 mg, 0.17 mmol) in ethanol (2 mL) was added and the mixture was stirred at room temperature for 1.5 h. After addition of ammonium hexafluorophosphate (90 mg, 0.55 mmol) the reaction mixture was stirred further for 1 h. The solid was filtered off, washed three times with cold ethanol (–20 °C) and dried *in vacuo* and then over P$_2$O$_5$. Yield: 79 mg (76%). Anal. Calcd. for C$_{18}$H$_{22}$F$_6$FeN$_8$PS$_2$ (M_r = 615.36 g/mol): C, 35.13; H, 3.60; N, 18.21; S, 10.42. Found: C, 35.30; H, 3.89; N, 17.84; S, 10.20. ESI-MS in MeOH (positive): *m/z* 470, [Fe(L^E)$_2$]$^+$. ESI-MS in MeOH (negative): *m/z* 145, [PF$_6$]$^-$. IR spectrum in KBr, cm^{-1} (selected bands): 1557 s, 1500 s, 1400 s, 1372 s, 1319 m, 1252 m, 1127 s, 839 vs, 558 m. UV–vis (MeOH), λ_{max}, nm (ε, M^{-1} cm^{-1}): 218sh (37940), 248 (26930), 299 (17690), 319sh (25100), 382 (25820), 624 (783), 905 (470).

[Bis(2-pyridineformamide ^{4}N-dimethylthiosemicarbazonato)-*N,N,S*-iron(III)] nitrate, [Fe(L^G)$_2$]NO$_3$ (2G). To 2-pyridineformamide ^{4}N-dimethylthiosemicarbazone (**HL^G**) (400 mg, 1.79 mmol) in methanol (30 mL) at 50 °C iron(III) nitrate nonahydrate (362 mg, 0.90 mmol) in methanol (3 mL) was added and the mixture was stirred at the same temperature for 2 h. After cooling to room temperature ca. 1/2 of the solvent was removed under reduced pressure and the reaction mixture was allowed to stand at +4 °C overnight. The precipitate was filtered off, washed with ethanol and dried *in vacuo* at 50 °C. Yield: 340 mg (68%). Anal. Calcd. for C$_{18}$H$_{24}$FeN$_{11}$O$_3$S$_2$ (M_r = 562.43 g/mol): C, 38.44; H, 4.30; N, 27.39; S, 11.40. Found: C, 38.24; H, 4.52; N, 26.94; S, 11.03. ESI-MS in MeOH (positive): *m/z* 500, [Fe(L^G)$_2$]$^+$. ESI-MS in MeOH (negative): *m/z* 498, [Fe(L^G)$_2$ – 2H]$^-$. IR spectrum in KBr, cm^{-1} (selected bands): 3268 w, 1619 s, 1552 s, 1532 s, 1479 s, 1385 s, 1254 m, 911 m, 780 s, 752 m. UV–vis (MeOH), λ_{max}, nm (ε, M^{-1} cm^{-1}): 248sh (31850), 300 (14490), 370 (13960), 464 (11730), 869 (980).

[Bis(3-aminopyridine-2-carboxaldehyde ^{4}N-dimethylthiosemicarbazonato)-*N,N,S*-iron(III)] nitrate, [Fe(L^H)$_2$]NO$_3$ (2H). To a suspension of 3-aminopyridine-2-carboxaldehyde ^{4}N-dimethylthiosemicarbazone hydrochloride (**HL^H·HCl**) (120 mg, 0.46 mmol) in ethanol (12 mL) iron(III) nitrate nonahydrate (100 mg, 0.25 mmol) in ethanol (1 mL) was added dropwise and the mixture was stirred for 3 h at room temperature. The brown precipitate was filtered off, washed with cold ethanol (–20 °C) and diethyl ether, dried *in vacuo* at 50 °C and then over P$_2$O$_5$. Yield: 95 mg (73%). Anal. Calcd. for C$_{18}$H$_{24}$FeN$_{11}$O$_3$S$_2$ (M_r = 562.43 g/mol): C, 38.44; H, 4.30; N, 27.39; S, 11.40. Found: C, 38.54; H, 4.27; N, 27.11; S, 11.35. ESI-MS in MeOH (positive): m/z 500, [Fe(L^H)$_2$]$^+$. IR spectrum in KBr, cm^{-1} (selected bands): 3331 w, 3207 w, 1647 m, 1582 s, 1553 s, 1500 s, 1468 s, 1384 s, 1324 m, 1256 s, 1112 s, 913 m, 796 m, 618 m. UV–vis (MeOH), λ_{max}, nm (ε, M^{-1} cm^{-1}): 226sh (28950), 270 (27460), 308 (27070), 438 (31030), 487sh (22370), 642 (980), 977 (510)

Crystallographic Structure Determination. X-ray diffraction measurements were performed on a Bruker X8 APEX II CCD-diffractometer. Crystal data, data collection parameters, and structure refinement details for **HL^D**, **HL^E**, **1D** and **2D** are given in Tables S1 and S2. The structures were solved by direct methods and refined by full-matrix least-squares techniques. Non-hydrogen atoms were refined with anisotropic displacement parameters. H atoms were placed at calculated positions and refined as riding atoms in the subsequent least squares model refinements. The isotropic thermal parameters were estimated to be 1.2 times the values of the equivalent isotropic thermal parameters of the atoms to which hydrogens were bonded. The following computer programs were used: structure solution, SHELXS-97;[52] refinement, SHELXL-97;[53] molecular diagrams, ORTEP;[54] computer: Pentium IV; scattering factors.[55] Crystallographic data have been deposited at the Cambridge Crystallographic Data Center with numbers CCDC729370–729373. Copies of data can be obtained, free of charge, on application to CCDC, 12 Union Road, Cambridge CB2 1EZ, UK (deposit@ccdc.com.ac.uk).

Cell lines and Culture Conditions. Human 41M (ovarian carcinoma) and SK-BR-3 (mammary carcinoma) cells were kindly provided by Lloyd R. Kelland (CRC Centre for Cancer Therapeutics, Institute of Cancer Research, Sutton, UK) and Evelyn Dittrich (Department of Medicine I, Medical University of Vienna, Austria), respectively. Cells were grown in 75 cm² culture flasks (Iwaki/Asahi Technoglass, Gyouda, Japan) as adherent monolayer cultures in Minimal Essential Medium (MEM) supplemented with 10% heat-inactivated fetal bovine serum, 1 mM sodium pyruvate, 4 mM L-glutamine and 1% non-essential amino acids (100×) (all purchased from Sigma-Aldrich, Vienna, Austria). Cultures were maintained at 37 °C in a humidified atmosphere containing 5% CO_2.

Cytotoxicity Tests in Cancer Cell Lines. Antiproliferative effects were determined by means of a colorimetric microculture assay (MTT assay, MTT = 3-(4,5-dimethyl-2-thiazolyl)-2,5-diphenyl-2H-tetrazolium bromide). Cells were harvested from culture flasks by trypsinization and seeded in 100 µL aliquots into 96-well microculture plates (Iwaki/Asahi Technoglass, Gyouda, Japan) in densities of 4×10^3 cells/well, in order to ensure exponential growth of untreated controls throughout the experiment. After a 24 h pre-incubation, dilutions of the test compounds in 100 µL/well complete culture medium were added. Because of low aqueous solubility, the test compounds were dissolved in DMSO first and then serially diluted in complete culture medium such that the effective DMSO content did not exceed 0.5%. After exposure for 96 h, all media were replaced by 100 µL/well RPMI 1640 medium (supplemented with 10% heat-inactivated fetal bovine serum and 2 mM L-glutamine) plus 20 µL/well MTT solution in phosphate-buffered saline (5 mg/ml). After incubation for 4 h, the medium/MTT mixtures were removed, and the formazan crystals formed by vital cells were dissolved in 150 µL DMSO per well. Optical densities at 550 nm were measured with a microplate reader (Tecan Spectra Classic), using a reference wavelength of 690 nm to correct for unspecific absorption. The quantity of vital cells was expressed in terms of T/C values by comparison to untreated control microcultures, and 50% inhibitory concentrations (IC_{50}) were calculated from concentration-effect curves by interpolation. Evaluation is based on means from at least three independent experiments, each comprising at least three microcultures per concentration level.

Ribonucleotide Reductase Inhibition. To compare the RR inhibitory potential of **HL**^D and **HL**^E with that of their corresponding iron complexes **2D** and **2E**, ^{3}H-cytidine incorporation assays were performed.[56] For this purpose, exponentially growing HL60 cells (5×10^6) were incubated with the test substances for 4 h. After the incubation period, the cells were pulsed with ^{3}H-cytidine (0.3125 μCi, 5 nM) for 1 h at 37 °C. Then cells were collected and washed with PBS. For cell lysis, the cell pellets were resuspended in a lysis buffer containing 10 mM EDTA, 50 mM Tris (pH 8.0), and 0.5% sodium lauryl sarcosine and frozen at –20 °C. For DNA extraction, the cell lysate was incubated with 20 units RNAse at 37 °C for 1 h followed by 24 h treatment with 150 μg proteinase K. Subsequently DNA was extracted using standard procedures. After precipitation with ethanol, DNA was resuspended in water, DNA content measured, and radioactivity was determined.[57]

Supporting Information Available: Reaction pathways to Triapine; cyclic voltammogram of the iron(III) complex **2D** in H$_2$O/DMSO, supplementary data on the electrochemical behavior of the complexes in DMSO and CH$_3$CN, crystallographic data in CIF format, details of X-ray data collection and refinement and the results of X-ray diffraction studies of **HL**^E. This material is available free of charge via the Internet at http://pubs.acs.org.

References

[1] Casas, J. S.; Garcia-Tasende, M. S.; Sordo, J. Main group metal complexes of semicarbazones and thiosemicarbazones. A structural review. *Coord. Chem. Rev.* **2000**, *209*, 197–261.

[2] Lobana, T. S.; Rekha; Butcher, R. J.; Castineiras, A.; Bermejo, E.; Bharatam, P. V. Bonding Trends of Thiosemicarbazones in Mononuclear and Dinuclear Copper(I) Complexes: Syntheses, Structures, and Theoretical Aspects. *Inorg. Chem.* **2006**, *45*, 1535–1542.

[3] Barbazan, P.; Carballo, R.; Casas, J. S.; Garcia-Martinez, E.; Pereiras-Gabian, G.; Sanchez, A.; Vazquez-Lopez, E. M. Synthesis and Characterization of New Trimeric Rhenium(I) Complexes. The Influence of Steric Factors on the Size of Pyrazolonaterhenium(I) Metallomacrocycles. *Inorg. Chem.* **2006**, *45*, 7323–7330.

[4] Pedrido, R.; Romero, M. J.; Bermejo, M. R.; Gonzalez-Noya, A. M.; Garcia-Lema, I.; Zaragoza, G. Metal-catalyzed oxidation processes in thiosemicarbazones: new complexes with the ligand N-{2-([4-N-ethylthiosemicarbazone]-methyl)phenyl}-p-toluenesulfonamide. *Chem. Eur. J.* **2008**, *14*, 500–512.

[5] West, D. X.; Padhye, S. B.; Sonawane, P. B. Structural and physical correlations in the biological properties of transition metal heterocyclic thiosemicarbazone and S-alkyl dithiocarbazate complexes. *Struct. Bond.* **1991**, *76*, 1–50.

[6] Bonnitcha, P. D.; Vavere, A. L.; Lewis, J. S.; Dilworth, J. R. In vitro and in vivo evaluation of bifunctional bisthiosemicarbazone ^{64}Cu-complexes for the positron emission tomography imaging of hypoxia. *J. Med. Chem.* **2008**, *51*, 2985–2991.

[7] Brockman, R. W.; Thomson, J. R.; Bell, M. J.; Skipper, H. E. Observations on the antileukemic activity of pyridine-2-carboxaldehyde thiosemicarbazone and thiocarbohydrazone. *Cancer Res*. **1956**, *16*, 167–170.

[8] French, F. A.; Blanz, E. J., Jr. The carcinostatic activity of thiosemicarbazones of formyl heteroaromatic compounds. III. Primary correlation. *J. Med. Chem*. **1966**, *9*, 585–589.

[9] DeConti, R. C.; Toftness, B. R.; Agrawal, K. C.; Tomchick, R.; Mead, J. A. R.; Bertino, J. R.; Sartorelli, A. C.; Creasey, W. A. Clinical and pharmacological studies with 5-hydroxy-2-formylpyridine thiosemicarbazone. *Cancer Res*. **1972**, *32*, 1455–1462.

[10] Krakoff, I. H.; Etcubanas, E.; Tan, C.; Mayer, K.; Bethune, V.; Burchenal, J. H. Clinical trial of 5-hydroxypicolinaldehyde thiosemicarbazone (5-HP; NSC-107392), with special reference to its iron-chelating properties. *Cancer Chemother. Rep*. **1974**, *58*, 207–212.

[11] Yu, Y.; Wong, J.; Lovejoy, D. B.; Kalinowski, D. S.; Richardson, D. R. Chelators at the Cancer Coalface: Desferrioxamine to Triapine and Beyond. *Clin. Cancer Res.* **2006**, *12*, 6876–6883.

[12] Ma, B.; Goh, B. C.; Tan, E. H.; Lam, K. C.; Soo, R.; Leong, S. S.; Wang, L. Z.; Mo, F.; Chan, A. T. C.; Zee, B.; Mok, T. A multicenter phase II trial of 3-aminopyridine-2-carboxaldehyde thiosemicarbazone (3-AP, Triapine) and gemcitabine in advanced non-small-cell lung cancer with pharmacokinetic evaluation using peripheral blood mononuclear cells. *Invest. New Drugs* **2008**, *26*, 169–173.

[13] Karp, J. E.; Giles, F. J.; Gojo, I.; Morris, L.; Greer, J.; Johnson, B.; Thein, M.; Sznol, M.; Low, J. A Phase I study of the novel ribonucleotide reductase inhibitor 3-aminopyridine-2-carboxaldehyde thiosemicarbazone (3-AP, Triapine) in combination with the nucleoside analog fludarabine for patients

with refractory acute leukemias and aggressive myeloproliferative disorders. *Leuk. Res.* **2008**, *32*, 71–77.

[14] Mackenzie, M. J.; Saltman, D.; Hirte, H.; Low, J.; Johnson, C.; Pond, G.; Moore, M. J. A Phase II study of 3-aminopyridine-2-carboxaldehyde thiosemicarbazone (3-AP) and gemcitabine in advanced pancreatic carcinoma. A trial of the Princess Margaret Hospital Phase II consortium. *Invest. New Drugs* **2007**, *25*, 553–558.

[15] Knox, J. J.; Hotte, S. J.; Kollmannsberger, C.; Winquist, E.; Fisher, B.; Eisenhauer, E. A. Phase II study of Triapine in patients with metastatic renal cell carcinoma: a trial of the National Cancer Institute of Canada Clinical Trials Group (NCIC IND.161). *Invest. New Drugs* **2007**, 25, 471–477.

[16] Moore, E. C.; Zedeck, M. S.; Agrawal, K. C.; Sartorelli, A. C. Inhibition of ribonucleoside diphosphate reductase by 1-formylisoquinoline thiosemicarbazone and related compounds. *Biochemistry* **1970**, *9*, 4492–4498.

[17] French, F. A.; Blanz, E. J., Jr.; Shaddix, S. C.; Brockman, R. W. α-(*N*)-Formylheteroaromatic thiosemicarbazones. Inhibition of tumor-derived ribunucleoside diphosphate reductase and correlation with in vivo antitumor activity. *J. Med. Chem.* **1974**, *17*, 172–181.

[18] Moore, E. C.; Sartorelli, A. C. Inhibition of ribonucleotide reductase by α-(N)-heterocyclic carboxaldehyde thiosemicarbazones. *Pharm. Ther.* **1984**, *24*, 439–447.

[19] Liu, M.-C.; Lin, T.-S.; Sartorelli, A. C. Chemical and biological properties of cytotoxic α-(N)-heterocyclic carboxaldehyde thiosemicarbazones. *Prog. Med. Chem.* **1995**, *32*, 1–35.

[20] Shao, J.; Zhou, B.; Chu, B.; Yen, Y. Ribonucleotide reductase inhibitors and future drug design. *Curr. Cancer Drug Targets* **2006**, *6*, 409–431.

[21] Kolberg, M.; Strand, K. R.; Graff, P.; Andersson, K. K. Structure, function, and mechanism of ribonucleotide reductases. *Biochim. Biophys. Acta* **2004**, *1699*, 1–34.

[22] Tanaka, H.; Arakawa, H.; Yamaguchi, T.; Shlralsh, K.; Fukuda, S.; Matsui, K.; Take, Y.; Nakamura, Y. A ribonucleotide reductase gene involved in a p53-dependent cell-cycle checkpoint for DNA damage. *Nature* **2000**, *404*, 42–49.

[23] Nakano, K.; Balint, E.; Ashcroft, M.; Vousden, K. H. A ribonucleotide reductase gene is a transcriptional target of p53 and p73. *Oncogene* **2000**, *19*, 4283–4289.

[24] Kowol, C. R.; Berger, R.; Eichinger, R.; Roller, A.; Jakupec, M. A.; Schmidt, P. P.; Arion, V. B.; Keppler, B. K. Gallium(III) and Iron(III) Complexes of α-N-Heterocyclic Thiosemicarbazones: Synthesis, Characterization, Cytotoxicity, and Interaction with Ribonucleotide Reductase. *J. Med. Chem.* **2007**, *50*, 1254–1265.

[25] Shao, J.; Zhou, B.; Di Bilio, A. J.; Zhu, L.; Wang, T.; Qi, C.; Shih, J.; Yen, Y. A Ferrous-triapine complex mediates formation of reactive oxygen species that inactivate human ribonucleotide reductase. *Mol. Cancer Ther.* **2006**, *5*, 586–592.

[26] Finch, R. A.; Liu, M.-C.; Cory, A. H.; Cory, J. G.; Sartorelli, A. C. Triapine (3-aminopyridine-2-carboxaldehyde thiosemicarbazone; 3-AP). An inhibitor of ribonucleotide reductase with antineoplastic activity. *Adv. Enzyme Regul.* **1999**, *39*, 3–12.

[27] Chaston, T. B.; Lovejoy, D. B.; Watts, R. N.; Richardson, D. R. Examination of the Antiproliferative Activity of Iron Chelators: Multiple Cellular Targets and the Different Mechanism of Action of Triapine Compared with Desferrioxamine and the Potent Pyridoxal Isonicotinoyl Hydrazone Analogue 311. *Clin. Cancer Res.* **2003**, *9*, 402–414.

[28] Wang, Y.; Liu, M.-C.; Lin, T.-S.; Sartorelli, A. C. Synthesis and antitumor activity of 3- and 5-hydroxy-4-methylpyridine-2-carboxaldehyde thiosemicarbazones. *J. Med. Chem.* **1992**, *35*, 3667–71.

[29] Niu, C.; Li, J.; Doyle, T. W.; Chen, S.-H. Synthesis of 3-amino-2-pyridinecarboxaldehyde thiosemicarbazone (3-AP). *Tetrahedron* **1998**, *54*, 6311–6318.

[30] Li, J.; Zheng, L.-M.; King, I.; Doyle, T. W.; Chen, S.-H. Syntheses and antitumor activities of potent inhibitors of ribonucleotide reductase: 3-amino-4-methylpyridine-2-carboxaldehyde-thiosemicarbazone (3-AMP), 3-amino-pyridine-2-carboxaldehyde-thiosemicarbazone (3-AP) and its water-soluble prodrugs. *Curr. Med. Chem.* **2001**, *8*, 121–133.

[31] Kelly, T. A.; McNeil, D. W. A simple method for the protection of aryl amines as their t-butylcarbamoyl (Boc) derivatives. *Tetrahedron Lett.* **1994**, *35*, 9003–9006.

[32] Venuti, M. C.; Stephenson, R. A.; Alvarez, R.; Bruno, J. J.; Strosberg, A. M. Inhibitors of cyclic AMP phosphodiesterase. 3. Synthesis and biological evaluation of pyrido and imidazolyl analogs of 1,2,3,5-tetrahydro-2-oxoimidazo[2,1-b]quinazoline. *J. Med. Chem.* **1988**, *31*, 2136–2145.

[33] Sreekanth, A.; Fun, H.-K.; Kurup, M. R. P. Structural and spectral studies of an iron(III) complex [Fe(Pranthas)$_2$][FeCl$_4$] derived from 2-acetylpyridine-N(4),N(4)-(butane-1,4-diyl) thiosemicarbazone (HPranthas). *J. Mol. Struct.* **2005**, *737*, 61–67.

[34] Kowol, C. R.; Eichinger, R.; Jakupec, M. A.; Galanski, M.; Arion, V. B.; Keppler, B. K. Effect of metal ion complexation and chalcogen donor identity on the antiproliferative activity of 2-acetylpyridine N,N-dimethyl(chalcogen)semicarbazones. *J. Inorg. Biochem.* **2007**, *101*, 1946–1957.

[35] Pessoa, M. M. B.; Andrade, G. F. S.; Paoli Monteiro, V. R.; Temperini, M. L. A. 2-Formylpyridinethiosemicarbazone and methyl derivatives: spectroscopic studies. *Polyhedron* **2001**, *20*, 3133–3141.

[36] Bermejo, E.; Castifieiras, A.; Fostiak, L. M.; Garcia, I.; Llamas-Saiz, A. L.; Swearingen, J. K.; West, D. X. Synthesis; characterization and molecular structure of 2-pyridylformamide N(4)-dimethylthiosemicarbazone and some five-coordinated zinc(II) and cadmium(II) complexes. *Z. Naturforsch., B: Chem. Sci.* **2001**, *56*, 1297–1305.

[37] West, D. X.; Bain, G. A.; Butcher, R. J.; Jasinski, J. P.; Li, Y.; Pozdniakiv, R. Y. Structural studies of three isomeric forms of heterocyclic N(4)-substituted thiosemicarbazones and two nickel(II) complexes. *Polyhedron* **1996**, *15*, 665–674.

[38] Odenike, O. M.; Larson, R. A.; Gajria, D.; Dolan, M. E.; Delaney, S. M.; Karrison, T. G.; Ratain, M. J.; Stock, W. Phase I study of the ribonucleotide reductase inhibitor 3-aminopyridine-2-carboxaldehyde-thiosemicarbazone (3-AP) in combination with high dose cytarabine in patients with advanced myeloid leukemia. *Invest. New Drugs* **2008**, *26*, 233–239.

[39] *CRC Handbook of Chemistry and Physics*; Lide, D. R., Ed.; CRC Press: Boca Raton, FL, 2004.

[40] Kowol, C. R.; Reisner, E.; Chiorescu, I.; Arion, V. B.; Galanski, M.; Deubel, D. V.; Keppler B. K. An electrochemical study of antineoplastic gallium, iron and ruthenium complexes with redox non-innocent α-N-heterocyclic chalcogensemicarbazones. *Inorg. Chem.* **2008**, *47*, 11032–11047.

[41] Richardson, D. R.; Kalinowski, D. S.; Richardson, V.; Sharpe, P. C.; Lovejoy, D. B.; Islam, M.; Bernhardt, P. V. 2-Acetylpyridine Thiosemicarbazones are Potent Iron Chelators and Antiproliferative Agents: Redox Activity, Iron Complexation and Characterization of their Antitumor Activity. *J. Med. Chem.* **2009**, *52*, 1459–1470.

[42] Easmon, J.; Heinisch, G.; Hofmann, J.; Langer, T.; Grunicke, H. H.; Fink, J.; Purstinger, G. Thiazolyl and benzothiazolyl hydrazones derived from α-(N)-acetylpyridines and diazines: synthesis, antiproliferative activity and CoMFA studies. *Eur. J. Med. Chem.* **1997**, *32*, 397–408.

[43] West, D. X.; Swearingen, J. K.; Valdes-Martinez, J.; Hernandez-Ortega, S.; El-Sawaf, A. K.; Van Meurs, F.; Castineiras, A.; Garcia, I.; Bermejo, E. Spectral and structural studies of iron(III), cobalt(II,III) and nickel(II) complexes of 2-pyridineformamide N(4)-methylthiosemicarbazone. *Polyhedron* **1999**, *18*, 2919–2929.

[44] Mendes, I. C.; Soares, M. A.; dos Santos, R. G.; Pinheiro, C.; Beraldo, H. Gallium(III) complexes of 2-pyridineformamide thiosemicarbazones: Cytotoxic activity against malignant glioblastoma *Eur. J. Med. Chem.* **2009,** *44*, 1870–1877.

[45] Yuan, J.; Lovejoy, D. B.; Richardson, D. R. Novel di-2-pyridyl-derived iron chelators with marked and selective antitumor activity: In vitro and in vivo assessment. *Blood* **2004**, *104*, 1450–1458.

[46] Easmon, J.; Heinisch, G.; Holzer, W.; Rosenwirth, B. Novel thiosemicarbazones derived from formyl- and acyldiazines: synthesis, effects on cell proliferation, and synergism with antiviral agents. *J. Med. Chem.* **1992**, *35*, 3288–3296.

[47] Richardson, D. R.; Sharpe, P. C.; Lovejoy, D. B.; Senaratne, D.; Kalinowski, D. S.; Islam, M.; Bernhardt, P. V. Dipyridyl Thiosemicarbazone Chelators with Potent and Selective Antitumor Activity Form Iron Complexes with Redox Activity. *J. Med. Chem.* **2006**, 49, 6510–6521.

[48] Agrawal, K. C.; Lee, M. H.; Booth, B. A.; Moore, E. C.; Sartorelli, A. C. Potential antitumor agents. 11. Inhibitors of alkaline phosphatase, an enzyme involved in the resistance of neoplastic cells to 6-thiopurines. *J. Med. Chem.* **1974**, *17*, 934–938.

[49] McElhinney, R. S. Derivatives of thiocarbamic acid. I. Preparation of 4-substituted thiosemicarbazides. *J. Chem. Soc.* **1966**, *10*, 950–955.

[50] Castineiras, A.; Garcia, I.; Bermejo, E.; West, D. X. Structural and spectral studies of 2-pyridineformamide thiosemicarbazone and its complexes prepared with zinc halides. *Z. Naturforsch., B: Chem. Sci.* **2000**, *55*, 511–518.

[51] Barette, W. C., Jr.; Johnson, H. W., Jr.; Sawyer, D. T. Voltammetric evaluation of the effective acidities (pKa') for Broensted acids in aprotic solvents. *Anal. Chem.* **1984**, *56*, 1890–1898.

[52] Sheldrick, G. M. *SHELXS-97, Program for Crystal Structure Solution;* University Göttingen: Göttingen, Germany, **1997**.

[53] Sheldrick, G. M. *SHELXL-97, Program for Crystal Structure Refinement;* University Göttingen: Göttingen, Germany, **1997**.

[54] Johnson, G. K. Report ORNL-5138; Oak Ridge National Laboratory; Oak Ridge, TN, **1976**.

[55] International Tables for X-ray Crystallography; Kluwer Academic Press: Dodrecht, The Netherlands, **1992**; Vol. C, Tables 4.2.6.8 and 6.1.1.4.

[56] Heffeter, P.; Jakupec, M. A.; Korner, W.; Wild, S.; von Keyserlingk, N. G.; Elbling, L.; Zorbas, H.; Korynevska, A.; Knasmuller, S.; Sutterluty, H.; Micksche, M.; Keppler, B. K.; Berger, W. Anticancer activity of the lanthanum compound [tris(1,10-phenanthroline)lanthanum(III)]trithiocyanate (KP772; FFC24). *Biochem. Pharmacol.* **2006**, *71*, 426–440.

[57] Szekeres, T.; Gharehbaghi, K.; Fritzer, M.; Woody, M.; Srivastava, A.; van't Riet, B.; Jayaram, H. N.; Elford, H. L. Biochemical and antitumor activity of trimidox, a new inhibitor of ribonucleotide reductase. *Cancer Chemother. Pharmacol.* **1994**, *34*, 63–6.

Table of Contents graphic

Impact of Metal Coordination on Cytotoxicity of 3-Aminopyridine-2-carboxaldehyde Thiosemicarbazone (Triapine) and Novel Insights into Terminal Dimethylation
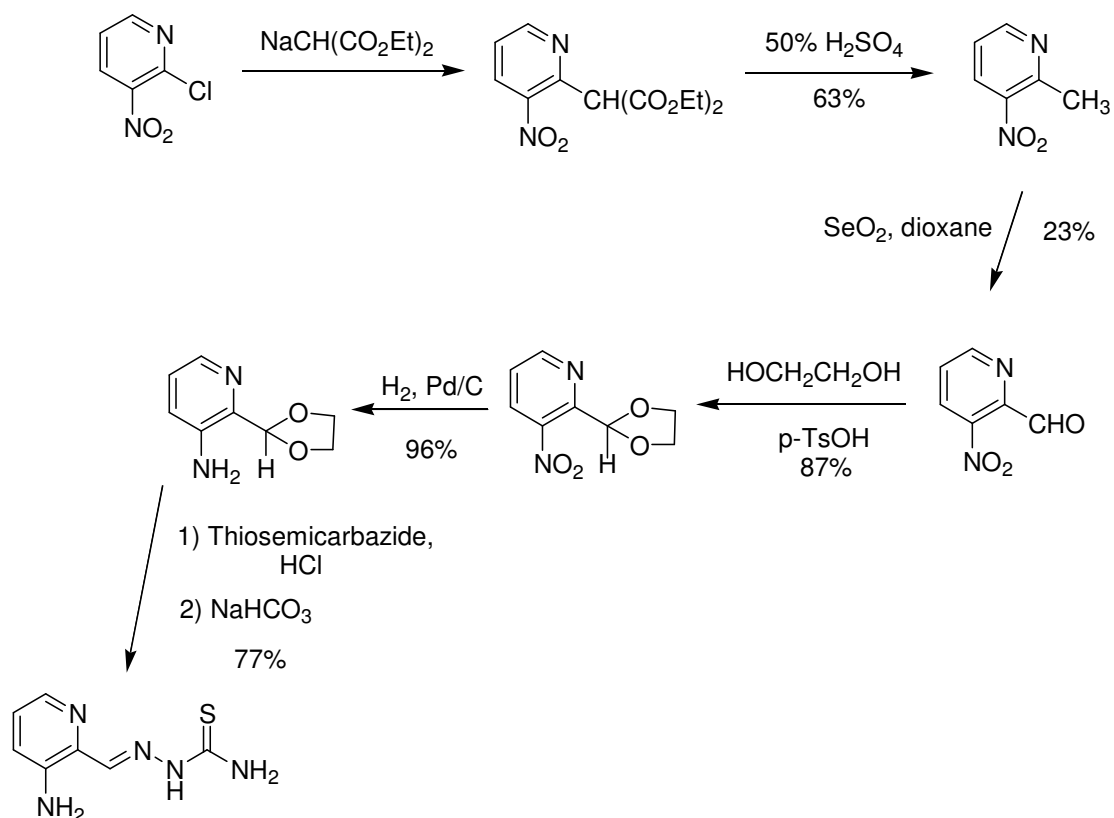
Christian R. Kowol, Robert Trondl, Petra Heffeter, Vladimir B. Arion, Michael A. Jakupec, Alexander Roller, Markus Galanski, Walter Berger, Bernhard K. Keppler.
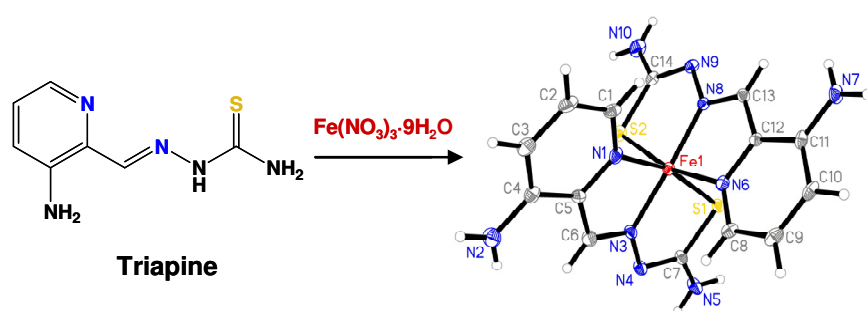
Supporting Information

Impact of Metal Coordination on Cytotoxicity of 3-Aminopyridine-2-carboxaldehyde Thiosemicarbazone (Triapine) and Novel Insights into Terminal Dimethylation

Christian R. Kowol,[†] Robert Trondl,[†] Petra Heffeter,[‡] Vladimir B. Arion,[†,] Michael A. Jakupec,[†] Alexander Roller,[†] Markus Galanski,[†] Walter Berger,[‡] Bernhard K. Keppler[†,]**

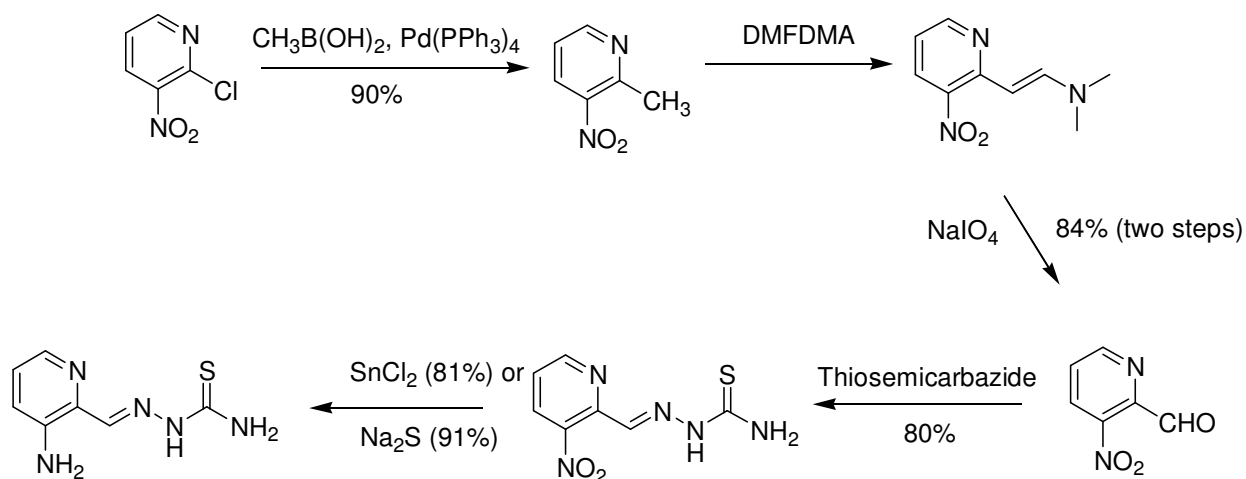[†] University of Vienna, Institute of Inorganic Chemistry, Währingerstr. 42, A-1090 Vienna, Austria

[‡] Medical University of Vienna, Institute of Cancer Research, Borschkeg. 8a, A-1090 Vienna, Austria
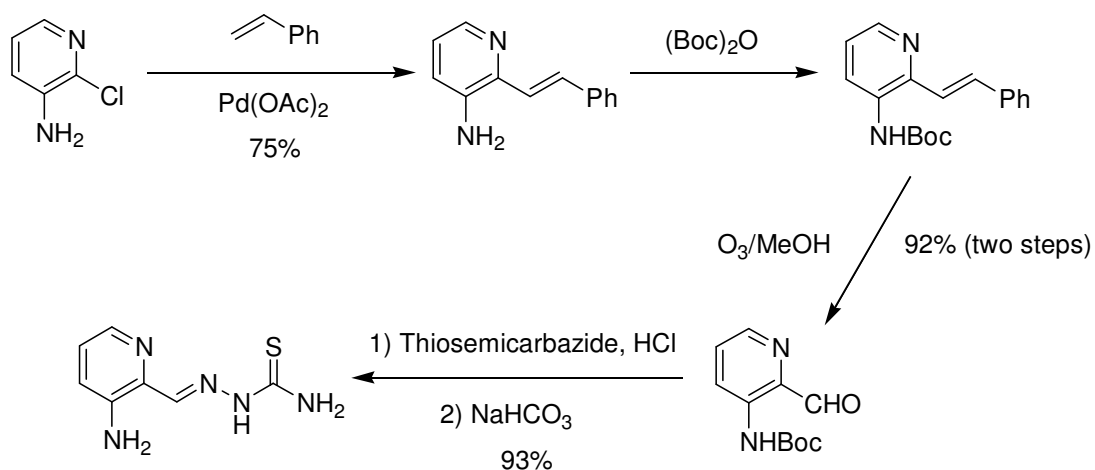
Table of contents

Scheme S1. The original six step synthesis of Triapine (**HL^D**) with an overall yield of 9%.

Scheme S2. Improved five step synthesis of Triapine (**HL^D**) with an overall yield of 55%.

Scheme S3. Four step synthesis of Triapine (**HL^D**) with an overall yield of 64%.
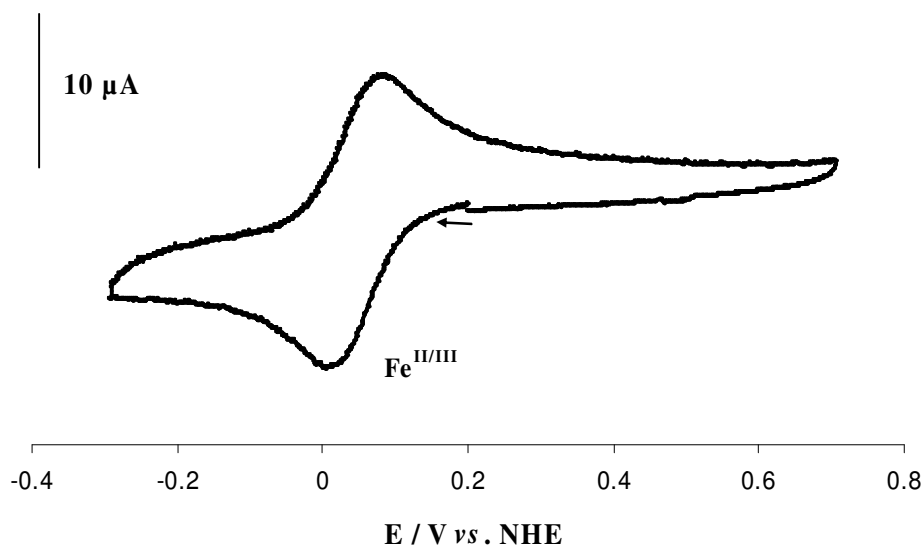

Figure S1. Cyclic voltammogram of the Triapine iron(III) complex **2D** in H_2O/DMSO (7:3 v/v) solution containing 0.20 M $NaClO_4$ at a scan rate of 0.20 V s^{-1} using a glassy carbon working electrode.

Discussion of the electrochemical behavior of the metal complexes in DMSO and CH$_3$CN solution

In our previously reported study of the electrochemical behavior of 2-acetylpyridine ^{4}N- disubstituted thiosemicarbazones[1] (pyrrolidine, piperidine, dimethylamine, aniline and *p*-nitroaniline) and their gallium(III), iron(III) and ruthenium(III) complexes in CH$_3$CN solution we found a perfect correlation between the pK_a value of the terminal amine and the redox potentials of the metal and ligand centered redox couples. Using the resultant linear equations and the pK_a value of ammonia at 9.25[2] the redox potentials of the 2-acetylpyridine thiosemicarbazone complexes **1B** and **2B** in CH$_3$CN solution can be predicted (linear equations for the gallium complexe ^{I}L^{red}: E$_{1/2}$ (V) = –0.673 – 0.0247·pK_a; ^{II}L^{red} : E$_{1/2}$ (V) = –0.902 – 0.0302·pK_a; iron complexe: Fe^{III}/Fe^{II}: E$_{1/2}$ (V) = 0.285 – 0.0197·pK_a; ^{I}L^{red}: E$_{1/2}$ (V) = –1.302 – 0.0284·pK_a).

Table S1. Predicted and experimental redox potentials of **1B** and **2B** in CH$_3$CN solution.

	1B		2B	
	^{I}L^{red}	^{II}L^{red}	Fe^{III}/Fe^{II}	^{I}L^{red}
E$_{1/2}$ predicted (V vs NHE)	–0.90	–1.18	+0.10	–1.56
E$_{1/2}$ experimental (V vs. NHE)^a	–0.88	–1.16	+0.11	–1.54

^{a} 0.20 M [*n*-Bu$_4$N][BF$_4$]/CH$_3$CN using a glassy carbon electrode

This shows an excellent agreement between the predicted and experimental redox potentials in CH$_3$CN. Interestingly compared to CH$_3$CN, in DMSO solution the redox potentials of **1B** and **2B** are shifted 50–70 mV to lower values, whereas for the analogous ^{4}N-dimethylated complexes **1F** and **2F** no shift between CH$_3$CN and DMSO can be observed (≤10 mV).

X-Ray crystallographic data

Table S1. Details of data collection for $\mathbf{HL^D}$, $\mathbf{HL^E}$, **1D** and **2D**.

Compound	$\mathbf{HL^D}$	$\mathbf{HL^E}$	**1D**	**2D**
Number of frames	1803	1628	1489	1170
Seconds/frame	80	40	60	30
Scan width	1	1	1	1
Distance from the detector	40	40	40	40

Table S2. Crystal Data for $\mathbf{HL^D}$, $\mathbf{HL^E}$, **1D** and **2D**.

	$\mathbf{HL^D}$	$\mathbf{HL^E}$	**1D**	**2D**
Empirical	$C_7H_9N_5S$	$C_9H_{12}N_4S$	$C_{16}H_{22}GaN_{11}O_4S_2$	$C_{14}H_{23}FeN_{11}O_{6.5}S_2$
Formula weight	195.25	208.29	566.29	569.40
Space group	$Pna2_1$	P-1	P-1	$C2/c$
a [Å]	18.5732(8)	7.3747(2)	9.3441(7)	9.2033(4)
b [Å]	5.5273(2)	7.4532(2)	18.7491(10)	23.0998(11)
c [Å]	17.2799(7)	9.6324(3)	12.9501(13)	21.2104(8)
α [deg]			102.437(6)	
β [deg]		109.630(2)	95.239(5)	92.473(3)
γ [deg]			96.569(5)	
V [Å^3]	1773.95(12)	489.97(2)	1136.26(18)	4505.0(3)
Z	8	2	2	8
λ [Å]	0.71073	0.71073	0.71073	0.71073
ρ_{calcd} [g cm^{-3}]	1.462	1.412	1.655	1.679
Crystal size [mm]	$0.30 \times 0.15 \times 0.04$	$0.40 \times 0.30 \times 0.10$	$0.06 \times 0.05 \times 0.02$	$0.30 \times 0.20 \times 0.01$
T [K]	100	100	296	100
μ [mm^{-1}]	0.323	0.294	1.445	0.916
$R_1^{[a]}$	0.0364	0.0337	0.0577	0.0615
$wR_2^{[b]}$	0.0893	0.0990	0.1526	0.1446
GOF$^{[c]}$	1.012	1.069	1.000	1.003

[a] $R_1 = \Sigma||F_o| - |F_c||/\Sigma|F_o|$. [b] $wR_2 = \{\Sigma[w(F_o^2 - F_c^2)^2]/\Sigma[w(F_o^2)^2]\}^{1/2}$. [c] $\text{GOF} = \{\Sigma[w(F_o^2 - F_c^2)^2]/(n - p)\}^{1/2}$, where n is the number of reflections and p is the total number of parameters refined.
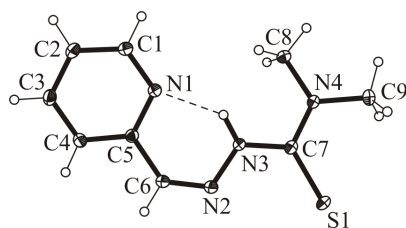
ORTEP plot of **HL^E** with atom numbering schemes. The thermal ellipsoids are drawn at 50% probability level. Selected bond lengths (Å) and bond angles (deg): C6–N2 = 1.2933(16), N2–N3 = 1.3595(15), N3–C7 = 1.3726(15), C7–S1 = 1.6855(13), C7–N4 = 1.3419(16); N1–C5–C6–N2 = −1.2(2), C6–N2–N3–C7 = 177.67(12), N2–N3–C7–S1 = −4.94(17).

[1] Kowol, C. R.; Reisner, E.; Chiorescu, I.; Arion, V. B.; Galanski, M.; Deubel, D. V.; Keppler B. K. An electrochemical study of antineoplastic gallium, iron and ruthenium complexes with redox non-innocent α-N-heterocyclic chalcogensemicarbazones. *Inorg. Chem.* **2008**, *47*, 11032–11047.

[2] *CRC Handbook of Chemistry and Physics*; Lide, D. R., Ed.; CRC Press: Boca Raton, FL, 2004.

2.5 Fluorescence Properties and Cellular Distribution of the Investigational Anti-cancer Drug Triapine (3-Aminopyridine-2-carboxaldehyde Thiosemicarbazone) and its Zinc(II) Complex
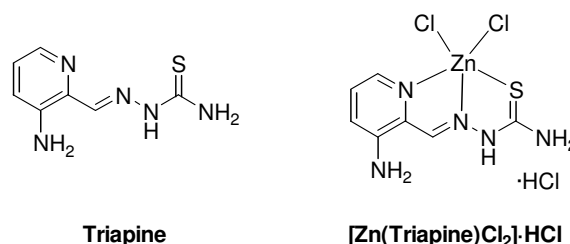
Fluorescent Anti-cancer Drug

Fluorescence Properties and Cellular Distribution of the Investigational Anti-cancer Drug Triapine (3-Aminopyridine-2-carboxaldehyde Thiosemicarbazone) and its Zinc(II) Complex

Christian R. Kowol, Robert Trondl, Vladimir B. Arion, * *Michael A. Jakupec, Irene Lichtscheidl, Bernhard K. Keppler* *

The antineoplastic activity of α-*N*-heterocyclic thiosemicarbazones was discovered several decades ago.[1] Currently the most promising drug candidate of this class of compounds is Triapine (3-aminopyridine-2-carboxaldehyde thiosemicarbazone, 3-AP), which entered several phase I and II clinical trials as an antitumor chemotherapeutic agent.[2] Triapine is a potent inhibitor of the enzyme ribonucleotide reductase, which catalyzes the reduction of ribonucleotides to deoxyribonucleotides and is essential for cell proliferation.[3] The enzyme consists of two homodimeric subunits R1 and R2. The latter contains a diiron center and a tyrosyl radical.[4] Although the mechanism of action of Triapine is not fully understood, at least at the molecular level, the active species of Triapine is presumed to be an iron complex which is able to generate reactive oxygen species (ROS) and subsequently destroy the tyrosyl radical in the R2 subunit of ribonucleotide reductase.[5] It should also be noted that nothing is known about the cellular distribution of this investigational anti-cancer drug.

We discovered that Triapine possesses intrinsic fluorescence when light-irradiated at around λ = 360 nm. This enabled us to monitor for the first time the uptake and intra-cellular distribution of an α-*N*-heterocyclic thiosemicarbazone in living human cancer cells by fluorescence microscopy. The results of this study are reported herein. In addition we synthesized the first zinc(II) complex of Triapine (Scheme 1), considering that coordination of α-*N*-heterocyclic thiosemicarbazones to zinc can increase the antineoplastic activity both in vitro[6] and in vivo,[7] and compared its properties with those of the metal-free Triapine.

[*]   C. R. Kowol, R. Trondl, Prof. V. B. Arion, Dr. M. A. Jakupec,
        Prof. B. K. Keppler
        Institute of Inorganic Chemistry
        University of Vienna
        Waehringer Str. 42, A-1090 Vienna, Austria
        Fax: (+43) 1-42779526
        E-mail: vladimir.arion@univie.ac.at,
        bernhard.keppler@univie.ac.at

        Prof. I. Lichtscheidl
        Institution of Cell Imaging and Ultrastructure Research
        University of Vienna
        Althanstr. 14, A-1090 Vienna, Austria

Supporting information for this article is available on the WWW under http://www.angewandte.org or from the author.

Triapine   **[Zn(Triapine)Cl₂]·HCl**

Scheme 1.

The yellow complex [Zn(Triapine)Cl₂]·HCl was prepared by reaction of ZnCl₂ with Triapine in 1:1 molar ratio in methanol in the presence of 2 equiv of 12 M HCl. In the absence of hydrochloric acid in ethanol, [Zn(Triapine)Cl₂] precipitated with a small amount (<5%) of unidentified by-product. The mother liquor generated single crystals of [Zn(Triapine)Cl₂]·EtOH. The results of an X-ray crystallographic study[8] of the latter are shown in Figure 1, along with selected bond lengths and angles. The geometry around the five-coordinate zinc(II) bound to the neutral tridentate Triapine via *NNS* donor atoms and two chlorido ligands is intermediate between square-pyramidal and trigonal-bipyramidal ($\tau = 0.34$).[9]
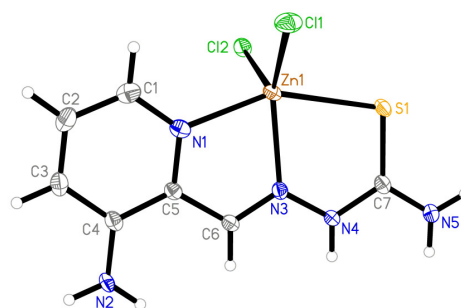

Figure 1. ORTEP plot of the complex [Zn(Triapine)Cl₂] with thermal ellipsoids at 50% probability level. Selected bond distances (Å) and angles (deg): Zn–Cl1, 2.2657(5); Zn–Cl2, 2.3038(5); Zn–S, 2.5016(5); Zn–N1, 2.1486(16); Zn–N3, 2.1378(15); N1–Zn–S, 151.46(4); N3–Zn–Cl1, 131.02(4); N3–Zn–Cl2, 113.60(4).

The UV/vis spectrum of Triapine in H₂O exhibits an absorption band of the lowest energy at 359 nm, which is 6 nm bathochromically shifted in the spectrum of the [Zn(Triapine)Cl₂]·HCl complex (Figure 2). Both compounds show very similar emission spectra with a maximum at 457 nm when irradiated at $\lambda_{ex} = 360$ nm (Figure 2). The quantum yields of Triapine and [Zn(Triapine)Cl₂]·HCl in H₂O are 0.018 and 0.021

(each value ± 15%), respectively, with quinine sulfate dihydrate in 0.1 M $HClO_4$ as the standard.

In the literature, several intrinsically fluorescent mono-thiosemicarbazones were documented as sensors for metal ion detection.[10] Zinc(II) complexes of biologically active bis(thiosemicarbazones) were reported with quantum yields in DMSO in the same range as the compounds studied herein.[11]
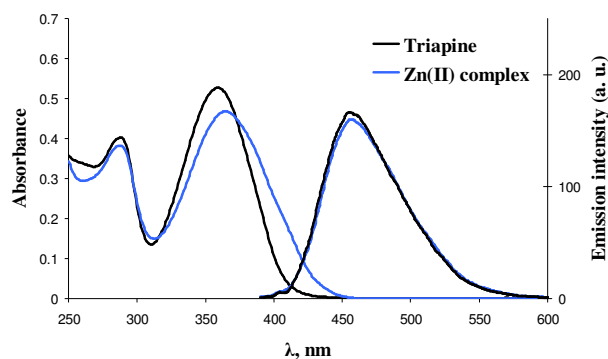

Figure 2. UV/vis (30 µM) and fluorescence (5 µM, λ_{ex} = 360 nm) spectra of Triapine (black) and [Zn(Triapine)Cl$_2$]·HCl (blue) in H$_2$O (maximum content of DMSO = 0.5%).

The cellular distribution of both compounds was studied by fluorescence microscopy in living SW480 cells (colon carcinoma, human). Bright-field images of SW480 cells treated with Triapine (0.25 mM in 0.5% DMSO/PBS) or [Zn(Triapine)Cl$_2$]·HCl (0.50 mM in PBS) (Figures 3A, B) were taken prior to fluorescence imaging to ensure that the studied cells were morphologically intact. Fluorescence images (Figures 3C, D) showed that both compounds are taken up by cells within minutes and that cellular distribution of the compounds can be visualized. Both Triapine and its zinc complex have a striking affinity to the nuclear membrane and to a more diffuse structure in the cytoplasm. Fluorescence images were scaled in pseudocolors to highlight cellular regions with particularly high affinity to the substances (Figures 3E, F). Remarkably, the zinc complex binds to a substructure within the nucleus, suggestive of nucleoli. Immunostaining of the nucleolar protein fibrillarin and co-staining with [Zn(Triapine)Cl$_2$]·HCl unequivocally proved that these substructures are indeed nucleoli (Figures 3G, H). In contrast, a strong affinity of Triapine to the nucleoli was not discernible. Nevertheless, the distinct differences in the distribution of the two substances suggests that zinc(II) remains coordinated to Triapine within the cell.

The cytotoxic potencies of Triapine and [Zn(Triapine)Cl$_2$]·HCl were determined in SW480 (colon carcinoma) and 41M (ovarian carcinoma) cells by means of the colorimetric MTT assay. Comparison of the two compounds did not reveal meaningful differences. The IC$_{50}$ values of Triapine in SW480 and 41M cells are 0.55±0.2 and 0.45±0.03 µM, respectively, whereas [Zn(Triapine)Cl$_2$]·HCl shows IC$_{50}$ values of 0.54±0.02 and 0.52±0.02 µM, respectively.

In accordance with our findings, other groups suggested considerable uptake of zinc bis(thiosemicarbazone) complexes into the nucleolus.[12] Furthermore, the affinity of nucleoli for exogenous zinc bound to diphenylthiocarbazone was observed in HeLa cells.[13] In literature the presence of physiological zinc in nucleoli of oocytes of starfish was reported, suggesting that zinc(II) mediates the affinity of the complexes to nucleoli.[14]

Our results demonstrate that Triapine can be visualized with fluorescence microscopy in living cells without any conjugation of fluorophores. Although the cytotoxicities of metal-free Triapine and its zinc(II) complex are very similar in vitro, the cellular distributions, especially with regard to the nucleus are distinctly different.
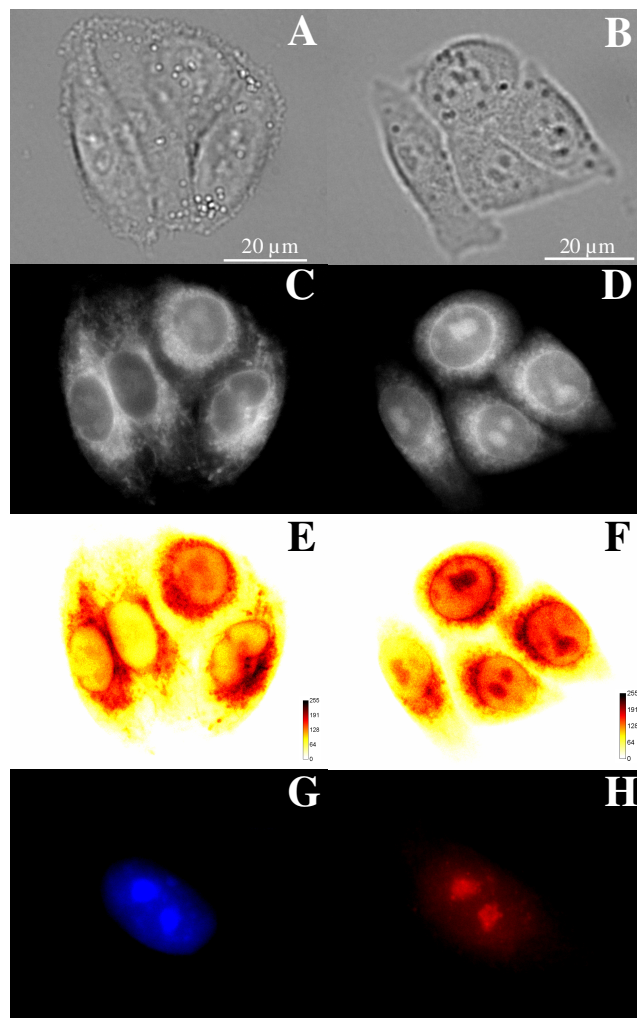

Figure 3. Live-cell images of SW480 colon carcinoma cells incubated with Triapine (A, C, E) or [Zn(Triapine)Cl$_2$]·HCl (B, D, F). (A, B) Bright-field images; (C, D) fluorescence images; (E, F) pseudocolor fluorescence images. Co-staining with [Zn(Triapine)Cl$_2$]·HCl (G) and immunofluorescence of the nucleolar protein fibrillarin (H), confirming the localization of the compound in nucleoli.

Experimental Section

All solvents and reagents were obtained from commercial suppliers and used without further purification. Triapine was synthesized by a three-step synthesis in 64% overall yield. In the first step the amino group of commercially available 3-amino-2-bromopyridine was protected with di-*tert*-butyl dicarbonate using sodium bis(trimethylsilyl)amide as the base.[15] Treatment of the *tert*-Boc protected 3-amino-2-bromopyridine with *n*-BuLi in dry THF and subsequent reaction with *N*-formylpiperidine gives the carboxaldehyde.[16] Finally, the condensation reaction with thiosemicarbazide in ethanol in the presence of concentrated HCl afforded Triapine hydrochloride, which was converted into the free base by treatment with sodium bicarbonate.[17]

158

[Zn(Triapine)Cl₂]·HCl: Triapine (50 mg, 0.26 mmol) dissolved in boiling methanol (10 mL) was slowly added to a mixture of zinc(II) chloride (35 mg, 0.26 mmol) and conc. HCl (43 µL) in methanol (5 mL) at 50 °C. The mixture was stirred for 10 min at 50 °C. The yellow precipitate was filtered off, washed with methanol, diethyl ether, dried *in vacuo* and over P_2O_5. Yield: 62 mg, 66%. Elemental analysis (%): calcd for $C_7H_9Cl_2N_5SZn\cdot HCl$ (M_r = 368.00 g/mol): C 22.85, H 2.74, N 19.03, S 8.71, found: C 23.11, H 2.71, N 18.87, S 8.77. ESI-MS in MeOH (negative): m/z 292, [Zn(Triapine)Cl₂ – H – Cl]⁻. IR (KBr) (selected bands): υ = 3439 (m), 3351 (s), 3275 (m), 3195 (m), 1640 (s), 1619 (s), 1542 (s), 1471 (s), 1387 (m), 1269 (s), 1099 (m), 947 (m), 919 (m), 834 (m), 782 (s), 562 (br. m), 482 (m) cm⁻¹; UV/vis (H_2O): λ_{max} (ε): 365 (15440), 288 (12630), 234sh (16500), 216 (17840); ¹H NMR (500.10 MHz, [D₆]DMSO): δ = 11.91 (s, 1H, NH), 8.54 (s, 1H, NH₂), 8.33 (s, 1H, HC=N), 8.30 (s, 1H, NH₂), 8.04 (d, ^3J(H,H) = 4.4 Hz, 1H, py), 7.68 (d, ^3J(H,H) = 8.5 Hz, 1H, py), 7.56 (s, 1H, py), 7.06 (v. br. s, 2H, NH₂) ppm; ¹³C NMR (125.81 MHz, [D₆]DMSO): δ = 178.6 (C=S), 146.0 ($C_{q,py}$), 137.0 (HC=N), 131.3 (C_{py}), 130.2 (C_{py}), 127.0 ($C_{q,py}$), 126.5 (C_{py}) ppm.

Fluorescence Microscopy. Fluorescence properties of Triapine and [Zn(Triapine)Cl₂]·HCl were observed under UV irradiation (360–370 nm) with an Olympus BX41 microscope equipped with 60x and 100x planapochromate oil-immersion objectives and a ColorViewIII camera. Images were taken with several concentrations and always resulted in the same distribution within the cells. Exposure time was adjusted so that almost all auto-fluorescence of cells could be excluded, and excitation time was kept as short as possible to minimize irradiation impact on cells.

Details of analytical characterization, X-ray data collection and refinement, cell culture, cytotoxicity tests and immunostaining are provided in the Supporting Information.

[1] R. W. Brockman, J. R. Thomson, M. J. Bell, H. E. Skipper, *Cancer Res.* **1956**, *16*, 167–170.

[2] a) Y. Yu, J. Wong, D. B. Lovejoy, D. S. Kalinowski, D. R. Richardson, *Clin. Cancer Res.* **2006**, *12*, 6876–6883; b) B. Ma, B. C. Goh, E. H. Tan, K. C. Lam, R. Soo, S. S. Leong, L. Z. Wang, F. Mo, A. T. C. Chan, B. Zee, T. Mok, *Invest. New Drugs* **2008**, *26*, 169–173; c) M. J. Mackenzie, D. Saltman, H. Hirte, J. Low, C. Johnson, G. Pond, M. J. Moore, *Invest. New Drugs* **2007**, *25*, 553–558; d) J. J. Knox, S. J. Hotte, C. Kollmannsberger, E. Winquist, B. Fisher, E. A. Eisenhauer, *Invest. New Drugs* **2007**, *25*, 471–477; e) J. E. Karp, F. J. Giles, I. Gojo, L. Morris, J. Greer, B. Johnson, M. Thein, M. Sznol, J. Low, *Leuk. Res.* **2008**, *32*, 71–77.

[3] R. A. Finch, M.-C. Liu, A. H. Cory, J. G. Cory, A. C. Sartorelli, *Adv. Enzyme Regul.* **1999**, *39*, 3–12.

[4] M. Kolberg, K. R. Strand, P. Graff, K. K. Andersson, *Biochim. Biophys. Acta* **2004**, *1699*, 1–34.

[5] J. Shao, B. Zhou, A. J. Di Bilio, L. Zhu, T. Wang, C. Qi, J. Shih, Y. Yen, *Mol. Cancer Ther.* **2006**, *5*, 586–592.

[6] a) D. Kovala-Demertzi, P. N. Yadav, J. Wiecek, S. Skoulika, T. Varadinova, M. A. Demertzis, *J. Inorg. Biochem.* **2006**, *100*, 1558–1567; b) J. M. Perez, A. I. Matesanz, A. Martin-Ambite, P. Navarro, C. Alonso, P. Souza, *J. Inorg. Biochem.* **1999**, *75*, 255–261.

[7] a) G. Atassi, P. Dumont, J. C. E. Harteel, *Eur. J. Cancer* **1979**, *15*, 451–459; b) D. Kovala-Demertzi, A. Alexandratos, A. Papageorgiou, P. N. Yadav, P. Dalezis, M. A. Demertzis, *Polyhedron* **2008**, *27*, 2731–2738.

[8] Crystal data for [Zn(Triapine)Cl₂]·EtOH: $C_9H_{15}Cl_2N_5OSZn$, M_r = 377.61 g mol⁻¹, crystal size 0.20×0.10×0.03 mm, monoclinic, space group $P2_1/c$, a = 11.4639(7), b = 10.2716(5), c = 12.7509(7) Å, β = 99.422(4)°, V = 1481.20(4) Å³, Z = 4, ρ_{calcd} = 1.693 g cm⁻³, μ = 2.158 mm⁻¹, Mo$_{K\alpha}$ radiation λ = 0.71073 Å, T = 100 K, $2\theta_{max}$ = 30.10, 61508 reflections measured, 4342 independent reflections, R_{int} = 0.0692, R_1[(I) > 2σ(I)] = 0.0274, wR_2 (all data) = 0.0642. CCDC 732708 contains the supplementary crystallographic data for this paper. These data can be obtained free of charge from The Cambridge Crystallographic Data Centre via www.ccdc.cam.ac.uk/data_request/cif.

[9] A. W. Addison, T. N. Rao, J. Reedijk, J. Van Rijn, G. C. Verschoor, *J. Chem. Soc., Dalton Trans.* **1984**, 1349–1356.

[10] a) Y. Yu, L.-R. Lin, K.-B. Yang, X. Zhong, R.-B. Huang, L.-S. Zheng, *Talanta* **2006**, *69*, 103–106; b) J. Vazquez Ruiz, A. Garcia de Torres, J. M. Cano-Pavon, *Talanta* **1984**, *31*, 29–32.

[11] J. P. Holland, F. I. Aigbirhio, H. M. Betts, P. D. Bonnitcha, P. Burke, M. Christlieb, G. C. Churchill, A. R. Cowley, J. R. Dilworth, P. S. Donnelly, J. C. Green, J. M. Peach, S. R. Vasudevan, J. E. Warren, *Inorg. Chem.* **2007**, *46*, 465–485.

[12] A. R. Cowley, J. Davis, J. R. Dilworth, P. S. Donnelly, R. Dobson, A. Nightingale, J. M. Peach, B. Shore, D. Kerr, L. Seymour, *Chem. Comm.* **2005**, 845–847.

[13] G. P. Studzinski, *J. Histochem. Cytochem.* **1965**, *13*, 365–375.

[14] T. Fujii, *Nature* **1954**, *174*, 1108–1109.

[15] T. A. Kelly, D. W. McNeil, *Tetrahedron Lett.* **1994**, *35*, 9003–9006.

[16] M. C. Venuti, R. A. Stephenson, R. Alvarez, J. J. Bruno, A. M. Strosberg, *J. Med. Chem.* **1988**, *31*, 2136–2145.

[17] C. Niu, J. Li, T. W. Doyle, S.-H. Chen, *Tetrahedron* **1998**, *54*, 6311–6318.

Entry for the Table of Contents

Fluorescent Anti-cancer drug

Christian R. Kowol, Robert Trondl,
Vladimir B. Arion, Michael A. Jakupec,
Irene Lichtscheidl, Bernhard K. Keppler
_____ **Page – Page**

Fluorescence Properties and Cellular
Distribution of the Investigational Anti-
cancer Drug Triapine (3-Aminopyridine-
2-carboxaldehyde Thiosemicarbazone)
and its Zinc(II) Complex

Triapine

Fluorescence
microscopy
$\lambda_{ex} = 360$ nm
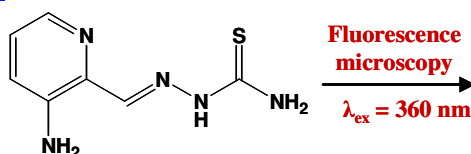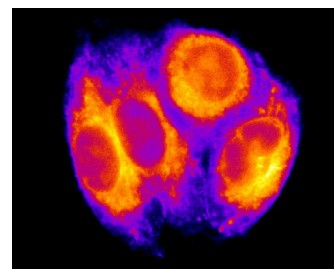
We discovered that Triapine (3-aminopyridine-2-carboxaldehyde
thiosemicarbazone), which entered several phase I and II clinical trials as an
antitumor chemotherapeutic agent, possesses intrinsic fluorescence properties (λ_{ex}
= 360 nm). This observation enabled us to monitor for the first time the uptake and
intra-cellular distribution of an α-N-heterocyclic thiosemicarbazone in living human
cancer cells by fluorescence microscopy.

Supporting Information

Fluorescence Properties and Cellular Distribution of the Investigational Anti-cancer Drug Triapine (3-Aminopyridine-2-carboxaldehyde Thiosemicarbazone) and its Zinc(II) Complex

Christian R. Kowol,[1] Robert Trondl,[1] Vladimir B. Arion,[1,*] Michael A. Jakupec,[1] Irene Lichtscheidl,[2] Bernhard K. Keppler[1,*]

[1]University of Vienna, Institute of Inorganic Chemistry, Währingerstr. 42, A-1090 Vienna, Austria

[2]University of Vienna, Institution of Cell Imaging and Ultrastructure Research, Althanstr. 14, A-1090 Vienna, Austria

Experimental Section

Elemental analyses were carried out on a Carlo Erba microanalyzer at the Microanalytical Laboratory of the University of Vienna. Electrospray ionization mass spectrometry was carried out with a Bruker Esquire 3000 instrument (Bruker Daltonic, Bremen, Germany). Expected and experimental isotope distributions were compared. Infrared spectra were obtained from KBr pellets with a Perkin-Elmer FT-IR 2000 instrument (4000–400 cm^{-1}). UV–vis spectra were recorded on a Perkin Elmer Lambda 650 UV–vis spectrophotometer. Fluorescence emission spectra were recorded on a Perkin-Elmer LS 55 fluorescence spectrophotometer. Emission spectra were corrected using the published data from NIST for quinine sulfate dihydrate in 0.1 M $HClO_4$.[1] The fluorescence quantum yields were determined using the formula:

$$\phi_{sample} = \frac{A_{ref} \cdot I \cdot n^2}{A \cdot I_{ref} \cdot n_{ref}^2} \phi_{ref}$$

where quinine sulfate dihydrate in 0.1 M $HClO_4$ is the reference ($\phi_{ref} = 0.59$)[1], A the integrated area under the emission spectrum, I the absorbance at the excitation wavelength and n the refractive index of the solvent. The highest concentration of the samples was 5 μM so that the absorbance at the excitation wavelength (360 nm) did not exceed 0.1. ^{1}H and ^{13}C one- and two-dimensional NMR spectra were recorded in DMSO-d_6 with a Bruker Avance III 500 MHz FT-NMR spectrometer. The residual ^{1}H and ^{13}C present in DMSO-d_6 were used as internal references. Abbreviations for NMR data: py = pyridine, $C_{q, py}$ = quaternary carbon of pyridine.

Details of X-ray data collection and refinement. X-ray diffraction measurements were performed on a Bruker X8 APPEXII CCD diffractometer. A single crystal of suitable size was coated with Paratone-N oil, mounted at room temperature on the tip of a glass fiber and cooled under a stream of cold N_2 maintained by a KRYOFLEX low-temperature apparatus. The crystal was positioned at 40 mm from the detector, and 2667 frames were measured, each for 20 s over 1° scan width. The data were processed using SAINT software.[2] The structures were solved by direct methods and refined by full-matrix least-

squares techniques. Non-hydrogen atoms were refined with anisotropic displacement parameters. H atoms were placed at calculated positions and refined as riding atoms in the subsequent least squares model refinements. The isotropic thermal parameters were estimated to be 1.2 times the values of the equivalent isotropic thermal parameters of the atoms to which hydrogens were bound. The following computer programs were used: structure solution, SHELXS-97;[3] refinement, SHELXL-97;[4] molecular diagrams, ORTEP;[5] computer: Pentium IV; scattering factors.[6]

Cell Culture. Human 41M (ovarian carcinoma) and SW480 (colon carcinoma) cells were kindly provided by Lloyd R. Kelland (CRC Centre for Cancer Therapeutics, Institute of Cancer Research, Sutton, UK) and Brigitte Marian (Institute of Cancer Research, Department of Medicine I, Medical University of Vienna, Austria), respectively. Cells were grown in 75 cm² culture flasks (Iwaki/Asahi Technoglass, Gyouda, Japan) as adherent monolayer cultures in complete culture medium, i. e. Minimal Essential Medium (MEM) supplemented with 10% heat-inactivated fetal bovine serum, 1 mM sodium pyruvate, 4 mM L-glutamine and 1% non-essential amino acids (100×) (all purchased from Sigma-Aldrich, Vienna, Austria) without antibiotics. For fluorescence microscopy, cells were grown in 6-well plates on sterile cover slips. Cultures were maintained at 37 °C in a humidified atmosphere containing 5% CO_2 and 95% air.

Cytotoxicity Tests in Cancer Cell Lines. Antiproliferative effects were determined by means of a colorimetric microculture assay (MTT assay, MTT = 3-(4,5-dimethyl-2-thiazolyl)-2,5-diphenyl-2H-tetrazolium bromide). Cells were harvested from culture flasks by trypsinization and seeded in 100 µL aliquots into 96-well microculture plates (Iwaki/Asahi Technoglass, Gyouda, Japan) in densities of 4×10^3 cells/well (41M) and 2.5×10^3 cells/well (SW480), respectively in order to ensure exponential growth of untreated controls throughout the experiment. After a 24 h pre-incubation, dilutions of the test compounds in 100 µL/well complete culture medium were added. Because of low aqueous solubility, the test compounds were dissolved in DMSO first and then serially diluted in complete culture medium

S3

such that the effective DMSO content did not exceed 0.5%. After exposure for 96 h, all media were replaced by 100 µL/well RPMI 1640 medium (supplemented with 10% heat-inactivated fetal bovine serum and 2 mM L-glutamine) plus 20 µL/well MTT solution in phosphate-buffered saline (5 mg/ml). After incubation for 4 h, the medium/MTT mixtures were removed, and the formazan crystals formed by vital cells were dissolved in 150 µL DMSO per well. Optical densities at 550 nm were measured with a microplate reader (Tecan Spectra Classic), using a reference wavelength of 690 nm to correct for unspecific absorption. The quantity of vital cells was expressed in terms of T/C values by comparison to untreated control microcultures, and 50% inhibitory concentrations (IC_{50}) were calculated from concentration-effect curves by interpolation. Evaluation is based on means from at least three independent experiments, each comprising at least three replicates per concentration level.

Immunostaining. Cells were cultured on cover slides and fixed with 4% formaldehyde. After fixation, cells were permeabilized with 0.3% Triton X-100 solution and then treated for 1 h with 5% serum diluted in PBS to block non-specific binding. The primary antibody against fibrillarin (1:400, monoclonal Rabbit, New England Biolabs GmbH, Frankfurt am Main, Germany) bound overnight at 4 °C. After washing with PBS, cells were incubated with the secondary fluorochrome conjugated antibody (1:500, Alexa Fluor 594 goat anti-rat IgG, Invitrogen, Karlsruhe, Germany) for 1 h at room temperature. Cells were washed, and the secondary antibody was localized by fluorescence microscopy (Olympus CKX41, Tokyo, Japan).

[1] Velapoldi R. A.; Mielenz, K. D. National Bureau of Standards (now the National Institute of Standards and Technology, NIST) Special Publication 260-64, 1980, U.S. Government Printing Office, Washington, DC 20402.

[2] SAINT-Plus (Version 7.06a) and APEX2. Bruker-Nonius AXS Inc. 2004, Madison, Wisconsin, USA.

[3] Sheldrick, G. M. *SHELXS-97, Program for Crystal Structure Solution;* University Göttingen: Göttingen, Germany, 1997.

[4] Sheldrick, G. M. *SHELXL-97, Program for Crystal Structure Refinement;* University Göttingen: Göttingen, Germany, 1997.

[5] Johnson, G. K. Report ORNL-5138; Oak Ridge National Laboratory; Oak Ridge, TN, 1976.

[6] International Tables for X-ray Crystallography; Kluwer Academic Press: Dodrecht, The Netherlands, 1992; Vol. C, Tables 4.2.6.8 and 6.1.1.4.

<div align="right">

Curriculum Vitae
May 2009

</div>

Mag. Christian Kowol

eMail: christian.kowol@univie.ac.at

Nationality: Austria
Date of birth: 03/02/1979
Marital status: single

Education

2006 –   Teaching Assistant (Assistent in Ausbildung) at the
             Institute of Inorganic Chemistry, University of Vienna

2006 –   Ph.D. Research at the Institute of Inorganic Chemistry,
             University of Vienna

December 2005   Graduation with Master of Science, First Class with
             Distinction

2000 – 2005   Chemistry studies, University of Vienna

1999 – 2000   Civilian service

July 1999   High-school graduation at Hegelgasse 14, 1010, Vienna

1986 – 1998   Waldorf school Vienna (Mauer)

Grants

2007   Grant for academic excellence (Leistungsstipendium)
             from the University of Vienna

2005   Grant for academic excellence (Leistungsstipendium aus
             Stiftung und Sondervermögen) from the University of
             Vienna

2005   Grant for academic excellence (Leistungsstipendium)
             from the University of Vienna

2002   Grant for academic excellence (Leistungsstipendium)
             from the University of Vienna

Professional Experience

Practical vacation work at the Institute of Inorganic Chemistry, University of Vienna, from July - September 2002

Research in the field of syntheses and characterization of novel anticancer agents at the Institute of Inorganic Chemistry, University of Vienna, July/August 2003 and November-January 2004/2005

Tutor at the Institute of Inorganic Chemistry, University of Vienna: summer term 2004, winter term 2004, summer term 2005 and winter term 2005

Publications

Kowol, C. R.; Reisner, E.; Chiorescu, I.; Arion, V. B.; Galanski, M.; Deubel, D. V.; Keppler, B. K. An Electrochemical Study of Antineoplastic Gallium, Iron and Ruthenium Complexes with Redox Noninnocent α-N-Heterocyclic Chalcogensemicarbazones. *Inorg. Chem.* **2008**, *47*, 11032–11047.

Cebrian-Losantos, B.; Reisner, E.; Kowol, C. R.; Roller, A.; Shova, S.; Arion, V. B.; Keppler, B. K. Synthesis and Reactivity of the Aquation Product of the Antitumor Complex trans-[$Ru^{III}Cl_4(indazole)_2$]⁻. *Inorg. Chem.* **2008**, *47*, 6513–6523.

Kowol, C. R.; Eichinger, R.; Jakupec, M. A.; Galanski, M.; Arion, V. B.; Keppler, B. K. Effect of metal ion complexation and chalcogen donor identity on the antiproliferative activity of 2-acetylpyridine N,N-dimethyl(chalcogen)semicarbazones. *J. Inorg. Biochem.* **2007**, *101*, 1946–1957.

Grguric-Sipka, S.; Kowol, C. R.; Valiahdi, S-M.; Eichinger, R.; Jakupec, M. A.; Roller, A.; Shova, S.; Arion, V. B.; Keppler, B. K. Ruthenium(II) complexes of thiosemicarbazones: the first water-soluble complex with pH-dependent antiproliferative activity. *Eur. J. Inorg. Chem.* **2007**, 2870–2878.

Kowol, C. R.; Berger, R.; Eichinger, R.; Roller, A.; Jakupec, M. A.; Schmidt, P. P.; Arion, V. B.; Keppler, B. K. Gallium(III) and Iron(III) Complexes of α-N-Heterocyclic Thiosemicarbazones: Synthesis, Characterization, Cytotoxicity, and Interaction with Ribonucleotide Reductase. *J. Med. Chem.* **2007**, *50*, 1254–1265.

Rudnev, A. V.; Foteeva, L. S.; Kowol, C.; Berger, R.; Jakupec, M. A.; Arion, V. B.; Timerbaev, A. R.; Keppler, B. K. Preclinical characterization of anticancer gallium(III) complexes: Solubility, stability, lipophilicity and binding to serum proteins. *J. Inorg. Biochem.* **2006**, *100*, 1819–1826.

Eichinger, R.; Kowol, C. R.; Arion, V. B.; Jakupec, M. A.; Keppler, B. K. Divergent effects of complexation with gallium(III) or iron(III) on the antitumor potency of 2-acetylpyridine-[4]N-dimethylthiosemicarbazone. *Met. Ions Biol. Med.* **2006**, *9*, 30–34.

Dobrov, A.; Arion, V. B.; Kandler, N.; Ginzinger, W.; Jakupec, M. A.; Rufinska, A.; Graf von Keyserlingk, N.; Galanski, M.; Kowol, C.; Keppler, B. K. The First Metal-Based Paullone Derivative with High Antiproliferative Activity in Vitro. *Inorg. Chem.* **2006**, *45*, 1945–1950.

Presentations at Conferences

<u>Kowol, C. R.;</u> Grguric-Sipka, S.; Valiahdi, S-M.; Eichinger, R.; Jakupec, M. A.; Arion, V. B.; Keppler, B. K. "The first ruthenium(II) thiosemicarbazone complex with pH-dependent antiproliferative activity"
13th International Conference on Biological Inorganic Chemistry (ICBIC XIII), Vienna, Austria, 2007. Poster presentation

<u>Kowol, C. R.;</u> Berger, R.; Eichinger, R.; Jakupec, M. A.; Arion, V. B.; Keppler, B. K. "Cytotoxicity Study of Novel Gallium(III) and Iron(III) Thiosemicarbazonate Complexes"
COST D20 final meeting, Brno, Czech Republic 2006. Poster presentation

<u>Eichinger, R.;</u> Kowol, C. R.; Arion, V. B.; Jakupec, M. A.; Keppler, B. K. "Divergent effects of complexation with gallium(III) and iron(III) on the antitumor potency of 2-acetylpyridine 4N-dimethylthiosemicarbazone"
9th International Symposium on Metal Ions in Biology and Medicine, Lisbon, Portugal 2006. Poster presentation

<u>Kowol, C. R.</u> "Antineoplastic gallium(III) and iron(III) thiosemicarbazonate complexes"
Workshop of Inorganic Chemitry in Austria (4. WACÖ), Eisenstadt, Austria, 2006. Oral communication

<u>Ginzinger W.;</u> Schmid W. F.; Kandler N.; Jakupec M. A., Graf v. Keyserlingk N.; Galanski M.; Kowol C.; Arion V.B.; Keppler B. K. "Gallium and Iron Complexes of a Paullone Derivative: Synthesis, Characterization and Antiproliferative Activity"
Novel Approaches for the Discovery and the Development of Anticancer Agents, CESAR, Vienna, Austria, 2005. Poster presentation